INFLUENCE OF MOISTURE DAMAGE AND HYDRATED LIME ON THE FATIGUE LIFE OF HOT MIX ASPHALT AND WARM MIX ASPHALT

Submitted in partial fulfilment of the requirements
for the award of the degree of

Doctor of Philosophy

By

Utsav Vishal
701333

Department of Civil Engineering
NATIONAL INSTITUTE OF TECHNOLOGY
WARANGAL

NOVEMBER 2021

INFLUENCE OF MOISTURE DAMAGE AND HYDRATED LIME ON THE FATIGUE LIFE OF HOT MIX ASPHALT AND WARM MIX ASPHALT

Submitted in partial fulfilment of the requirements
for the award of the degree of

Doctor of Philosophy

By

Utsav Vishal

701333

Supervisor

Dr. Venkaiah Chowdary

Associate Professor

Department of Civil Engineering

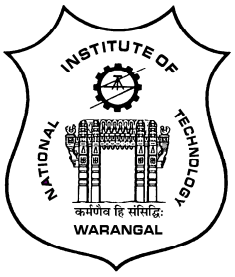

Department of Civil Engineering

NATIONAL INSTITUTE OF TECHNOLOGY

WARANGAL

NOVEMBER 2021

NATIONAL INSTITUTE OF TECHNOLOGY

WARANGAL

CERTIFICATE

This is to certify that the thesis entitled **"INFLUENCE OF MOISTURE DAMAGE AND HYDRATED LIME ON THE FATIGUE LIFE OF HOT MIX ASPHALT AND WARM MIX ASPHALT"** being submitted by **Mr. Utsav Vishal** for the award of the degree of **DOCTOR OF PHILOSOPHY** to the **Department of Civil Engineering** of **NATIONAL INSTITUTE OF TECHNOLOGY, WARANGAL** is a record of bonafide research work carried out by him under my supervision and it has not been submitted elsewhere for the award of any degree.

Dr. VENKAIAH CHOWDARY
Thesis Supervisor
Associate Professor
Department of Civil Engineering
National Institute of Technology, Warangal
Telangana, India

APPROVAL SHEET

This thesis entitled **"Influence of Moisture Damage and Hydrated Lime on the Fatigue Life of Hot Mix Asphalt and Warm Mix Asphalt"** by **Mr. Utsav Vishal** is approved for the degree of **Doctor of Philosophy**.

Examiners

_____

_____

_____

Supervisor

_____

_____

Chairman

_____

Date: _____

Declaration

This is to certify that the work presented in the thesis entitled **Influence of Moisture Damage and Hydrated Lime on the Fatigue Life of Hot Mix Asphalt and Warm Mix Asphalt** is a bonafide work done by me under the supervision of **Dr. Venkaiah Chowdary** and was not submitted elsewhere for the award of any degree.

I declare that this written submission represents my ideas in my own words and where others' ideas or words have been included, I have adequately cited and referenced the original sources. I also declare that I have adhered to all principles of academic honesty and integrity and have not misrepresented or fabricated or falsified any idea/data/fact/source in my submission. I understand that any violation of the above will be a cause for disciplinary action by the Institute and can also evoke penal action from the sources which have thus not been properly cited or from whom proper permission has not been taken when needed.

_____

(Signature)

Utsav Vishal

Roll No.: 701333

Date: _____

Dedicated to

My

Mother

ACKNOWLEDGEMENTS

I take this opportunity to express my deep sense of gratitude to my supervisor **Dr. Venkaiah Chowdary** for his invaluable guidance, support and constant encouragement throughout my research work. I regard him as a respected mentor who have been so kind as to give me his valuable assistance in various ways.

I wish to take this opportunity to express my best thanks to **Prof. C.S.R.K. Prasad**, Transportation Division, Department of Civil Engineering, National Institute of Technology, Warangal for his valuable suggestions and constant encouragement throughout the course of my thesis work. I wish to take this opportunity to express my sincere thanks to **Dr. K.V.R. Ravi Shankar, Dr. S. Shankar, Dr. Arpan Mehar, Dr. Vishnu R., and Dr. K.B. Raghuram,** Assistant Professors, Transportation Division, Department of Civil Engineering, National Institute of Technology, Warangal for helping me during the course of my research work with their valuable suggestions and encouragement.

I wish to express my gratitude to the Head of Civil Engineering Department **Prof. P. Rathish Kumar** and the former Heads of the Civil Engineering Department, **Prof. M. Chandrasekhar, Prof. Deva Pratap, Prof. D. Rama Seshu and Prof. G. Rajesh Kumar** for the support provided in completing my doctoral research. Also, I express my sincere gratitude for the support and suggestions provided to me by my Doctoral Committee members **Dr. C.S.R.K. Prasad**, Professor, Department of Civil Engineering, **Dr. A. Venu Gopal**, Professor, Department of Mechanical Engineering and **Dr. V. Ramana Murthy**, Professor, Department of Civil Engineering.

I am grateful to **Prof. N.V. Ramana Rao,** Director, National Institute of Technology, Warangal for extending every possible help during the course of the study.

My best thanks are due to **Prof. J. Murali Krishnan**, Department of Civil Engineering, Indian Institute of Technology Madras for his indispensable guidance, support and, his valuable suggestions in course of experimentation and preparation of my thesis. I consider it a privilege that I got the opportunity to work with him.

I wish to express my gratitude to **Dr. A. Padmarekha**, Associate Professor, Department of Civil Engineering, SRM Institute of Science and Technology for valuable suggestions and support.

I wish to thank all the **Research Scholars** for their friendly and sincere advice and constant encouragement. Special thanks to **Dr. J. Jaya Krishna**, **Dr. Syed Mubashirhussain, T. Arjun Kumar, Kakara Srikanth, and Prashanth Shekar Lokku** for their friendly advice and timely help. I would also like to thank **Dr. Eshwar Sala**, **Dr. D. Abhigna**, **K.M. Peera, Khalil Kakar, Dr. K. Adiya, and G. Pallavi** for all the help provided during my research tenure.

I express my sincere gratitude for the help provided by **Md. Abdul Gaffer**, **K. Ramesh**, **K. Purushotham** and **Amjad Pasha** during the course of my experimentation. Also, I wish to thank the teaching and non-teaching staff of the Civil Engineering Department, NIT Warangal for their cooperation during the research.

I express my deepest gratitude to **Mr. A. Pugazhenthi** and all the students and staff for the help provided at Asphalt Laboratory and Pavement Laboratory during my stay and experimentation at IIT Madras. Special thanks to **Atanu, Arbin, and Sandeep, Abhijith** for their friendly companionship during my stay at IIT Madras.

My deepest gratitude is due to my parents and sisters for their love and relentless support and encouragement during my research tenure.

Utsav Vishal

ABSTRACT

The total road network in India is 64 lakh km, out of which about 90% are bituminous (asphalt) roads. Bituminous concrete, a dense-graded asphalt mixture is widely used in the construction of wearing courses in flexible pavements. Moisture sensitivity of asphalt mixture is the major cause of premature failure. Various additives are used to increase the service life of asphalt pavements and to mitigate moisture damage. Warm mix additives and hydrated lime are two well-accepted additives. The use of warm mix additives in asphalt mixtures reduces emissions during production and maintains required workability at reduced temperatures. Due to the reduced rate of aging of warm mix asphalt binder, warm mix asphalt mixtures are expected to exhibit enhanced fatigue resistance compared to hot mix asphalt. However, the fatigue life of warm mix asphalt can reduce due to the potential for increased moisture damage. Traditionally, hydrated lime has been used as an antistripping additive. Hydrated lime is a non-commercial additive which is widely used in hot mix asphalt as filler and an anti-stripping agent due to its availability and cost-effectiveness over other additives. Hydrated lime changes the surface chemistry of the aggregates and thus results in stronger adhesion between aggregate and binder. Thus, the presence of hydrated lime in asphalt mixtures enhances its moisture resistance apart from reducing the aging. However, due to the filler effect of lime, the increase in stiffness is expected to reduce the fatigue life of the asphalt mixture. The fatigue performance of asphalt mixtures consisting of such a combination of additives especially when subjected to moisture conditioning process is not well understood. Thus, there is a need to quantify the precise role of hydrated lime on the fatigue life of unconditioned and moisture conditioned hot mix asphalt and warm mix asphalt.

This study quantifies the influence of moisture damage and hydrated lime on the fatigue life of large-sized prismatic beam specimens of hot mix asphalt and warm mix asphalt. To moisture condition large-sized prismatic beam specimens, a moisture conditioning process is initially established. Such beams are required for evaluating the fatigue characteristics of asphalt mixtures in a four-point beam bending test. The current moisture conditioning protocols are aimed at cylindrical specimens alone and no guidelines are available for prismatic beams; especially when these beams are compacted to lower air void content. In this study, prismatic beam specimens of bituminous concrete mixed with VG-30 binder were prepared. Warm mix asphalt was produced using a surfactant based warm mix additive.

Hydrated lime was added to both hot mix asphalt and warm mix asphalt. Prismatic beams with target air voids of 4 ± 0.5% and with dimensions of 0.38 ± 0.006 m (length) × 0.050 ± 0.002 m (width) × 0.063 ± 0.002 m (height) were produced. These specimens were subjected to partial vacuum saturation by submerging completely in water. The vacuum pressures and durations were adjusted such that the desired saturation could be achieved. The saturated bituminous concrete beam specimens were mechanically weakened through the freeze-thaw conditioning. It is observed that the influence of additives is negligible on the degree of saturation. Both unconditioned and moisture conditioned specimens of hot mix asphalt and warm mix asphalt with and without hydrated lime were subjected to fatigue testing using four-point beam bending at three strain levels (400, 600, and 800 microstrain). The collected data was analyzed appealing to various post-processing methods, and it was seen based on the evolution of flexural stiffness and energy dissipation that the beneficial effect of warm mix additives or hydrated lime was witnessed at lower strain level (400 microstrain) and not at higher strain levels (600 and 800 microstrain).

This study also quantifies the effects of moisture and hydrated lime on viscoelastic dissipation and dissipation due to damage in both hot mix asphalt and warm mix asphalt. Three models are used to separate damage dissipation from total dissipation. The pseudo-strain concept, constitutive assumption approach, and a linear viscoelastic model (Burger's model) are used to compute damage dissipation. The sensitivity of the three approaches on moisture damage, the addition of warm mix asphalt additive and hydrated lime, and the effect of three strain levels (400, 600, and 800 microstrain) are analysed based on the proportion of damage dissipation. The Burgers model is found to be sensitive to moisture damage, warm mix asphalt additive, and hydrated lime at all strain levels. In summary, moisture conditioning process to saturate large-sized prismatic beam specimen to be tested for fatigue is established initially. Subsequently, the influence of moisture damage and hydrated lime on fatigue life of hot mix asphalt and warm mix asphalt is quantified based on the evolution of flexural stiffness and energy dissipation. Finally, the total energy dissipated is apportioned into viscous dissipation and dissipation due to damage using three approaches.

KEYWORDS: damage dissipation, energy dissipation, fatigue life, flexural stiffness, four-point beam bending, hydrated lime, moisture susceptibility, viscoelastic dissipation, warm mix asphalt.

TABLE OF CONTENTS

LIST OF TABLES

LIST OF FIGURES

LIST OF ABBREVIATIONS

AASHTO	American Association of State Highway and Transportation Officials
ASTM	American Society of Testing and Materials
BC	Bituminous Concrete
FHWA	Federal Highway Administration
HMA	Hot Mix Asphalt
HL	Hydrated lime
IRC	Indian Roads Congress
IS	Indian Standard
ITS	Indirect Tensile Strength
MID	Moisture Induced Damage
MoRTH	Ministry of Road Transport and Highways
NHAI	National Highways Authority of India
NCHRP	National Cooperative Highway Research Program
NM	Normalized Modulus
PID	Proportional – Integral - Derivative
RDEC	Ratio of Dissipated Energy Change
RMSE	Root Mean Square Error
TSR	Tensile Strength Ratio
UTS	Universal Testing Software
WMA	Warm Mix Asphalt

NOTATIONS

G_{mb}	Bulk Specific Gravity
G_{mm}	Theoretical Maximum Specific Gravity
R^2	Coefficient of Correlation
°C	Degree Centigrade
S	Degree of Saturation
W_{sat}	Saturated Surface Dry Weight
W_d	Weight of Dry Specimen
V_a	Air Voids
Vol_{air}	Volume of Air Voids
V_{beam}	Volume of the Beam
ITS_{wet}	Indirect Tensile Strength of Wet Specimen
ITS_{dry}	Indirect Tensile Strength of Unconditioned Specimen
με	Microstrain
δ	Phase Angle
n	Number of Cycles
S_i	Flexural Stiffness at i^{th} cycle
σ_t	Maximum Tensile Stress
ε_t	Maximum Tensile Strain
W_n	Energy Ratio
w_n	Energy Dissipated at the n^{th} Cycle
w_0	Energy Dissipated at the Initial Cycle
Δ DE	Change in Dissipated Energy between Cycles n and n+1
DE	Total Dissipated Energy at n Cycles
ϵ_0	Strain Amplitude

$\boldsymbol{\omega}$	Frequency
$\mathbf{E_n}$	Dynamic Modulus
$\mathbf{W_T}$	Total Energy Dissipation
$\mathbf{W_{ve}}$	Dissipation due to the Viscoelastic Behaviour
$\mathbf{W_d}$	Dissipation due to Damage
$\boldsymbol{\sigma_{ve}}$	Viscoelastic Stress
$\boldsymbol{\epsilon_R}$	Strain-like Quantity
$\mathbf{E_R}$	Reference Modulus
$\boldsymbol{\delta_{ve}}$	Viscoelastic Phase Angle
$\dot{\boldsymbol{\sigma}}$	First Order Time Derivative of Stress
$\ddot{\boldsymbol{\sigma}}$	Second Order Time Derivative of Stress
$\dot{\boldsymbol{\varepsilon}}$	First Order Time Derivative of Strain
$\ddot{\boldsymbol{\varepsilon}}$	Second Order Time Derivative of Strain
$\mathbf{R_1}$, $\mathbf{R_2}$	Spring Constant
$\boldsymbol{\eta_1}, \boldsymbol{\eta_2}$	Dashpot Constant
$\mathbf{t}$	Time

CHAPTER 1

INTRODUCTION

1.1 A General Understanding of Moisture Damage

The total road network in India is about 64 lakh km, out of which 90 % are asphalt pavements. Even though the national highways network is about 1.42 lakh km which is 2.21 % of the total road network, it shares 40 % of the total road traffic (MoRTH 2020). State highways has a road network of 2.21 lakh km and other roads consist of 60.37 lakh km. Bituminous concrete (BC), a dense mixture is widely used in the construction of wearing courses of high-volume roads, typically in the construction of expressways, national highways and state highways apart from the urban roads and other major roads. To keep this road network serviceable has always been the prime challenge. Numerous factors are involved in the deterioration of the bituminous or asphalt pavements. Moisture resistance of asphalt mixtures plays a vital role in the performance of the asphalt pavement where the premature failure reduces its service life. One of the dominant reasons for premature failure is the surplus water present in the pavement (Elsayed and Lindly 1996). Thus, moisture damage in asphalt pavements is observed to be a worldwide concern (Yilmaz and Sargin 2012). Various additives are being used in asphalt binders and mixtures in an attempt to improve the overall performance of the asphalt mixtures. The moisture damage in asphalt mixtures as defined by various researchers are presented below:

- *"The phenomenon is referred to as stripping and results when moisture causes loss of bond between the aggregate and the asphalt binder" (Asphalt Institute 1981).*
- *"The progressive functional deterioration of a pavement mixture by loss of the adhesive bond between the asphalt cement and the aggregate surface and/or loss of the cohesive resistance within the asphalt cement principally from the action of water" (Kiggundu and Roberts 1988).*
- *"Moisture-induced damage in asphalt mixtures may be defined as the degradation of the mechanical properties of the mix due to the action of moisture" (Bhasin et al. 2007).*
- *"Moisture induced damage (MID) can be defined as the loss of strength and durability caused by the presence of water within the asphalt mixtures. Continuing*

action of moisture-induced weakening and mechanical damage caused by traffic load, which results in gradual dislodgement of aggregate and becomes a dominant mode of failure" (Kringos and Scarpas 2008).

- *"A generalised definition of the term damage is the degree of loss of functionality of a system. Within this context, moisture damage in asphalt mixtures is broadly defined as the degradation of mechanical properties of the material due to the presence of moisture in a liquid or vapour state. Adhesive and cohesive failures are the last step in a process that starts with different modes of moisture transport and results in the generation of moisture damage" (Caro et al. 2008).*
- *"Moisture damage is the degradation of the mechanical properties of the pavement material caused by the presence of moisture in its microstructure" (Kumar and Anand 2012).*

The above definitions clearly reveal that the presence of moisture in asphalt mixtures degrades its mechanical properties due to traffic loads resulting in progressive dislodgement of aggregates because of the adhesive and cohesive failures. Even without the application of mechanical loading and the presence of moisture itself has an adverse effect on material property, the asphalt mixture will be subjected to moisture induced damage with time irrespective of mixture composition. Without the presence of water, the distress may not have developed or might have surfaced at the later stage of service life (Kringos and Scarpas 2008). To provide road safety at the earliest, countries that experience heavy rainfall prefer to use the high permeable wearing course to drain out water. Due to the high water flow rate, asphalt bonds experience weakening and material characteristics deteriorate (Kringos and Scarpas 2005). It was also observed that the high permeable wearing course if holds moisture, strips immediately thereby discouraging the use of high permeable wearing courses by the road agencies (Lippert et al. 2015).

In spite of design efforts to prevent water from entering the pavement system, the fact remains that water infiltrates into the system. Figure 1.1 shows the possible sources of water entering the pavement system. The permeability within the asphalt mixture allows the flow of water through the voids path (Lottman 1971; Krishnan and Rao 2001). The cause for the occurrence of water in the pavement system is ingress through the surface and shoulders, upward capillary movement, freeze/thaw cycles, and changes in water table level. Water penetrates in liquid or vapour state through asphalt mixture microstructure and follows the path of interconnected air voids and cracks (Shakiba et al. 2017). Moreover, when the asphalt

pavement is opened for vehicular movement after construction/overlay, the percentage of air voids is at its maximum, which could make it easier for the infiltration of water. Poor compaction, inadequately dried aggregate, dirty aggregate, poor drainage, and poor aggregate-binder chemistry may lead to the presence of moisture in the asphalt mixtures. Moisture is the major source for the initiation and propagation of several distresses in asphalt mixtures. In addition, the rate of deterioration in asphalt pavement accelerates in the presence of moisture and can result in various distresses including rutting, fatigue, ravelling, or any interaction between them. This weakening, if severe enough, can result in stripping. The probable factors which contribute to the moisture-induced distress in the flexible pavement are listed in Table 1.1.

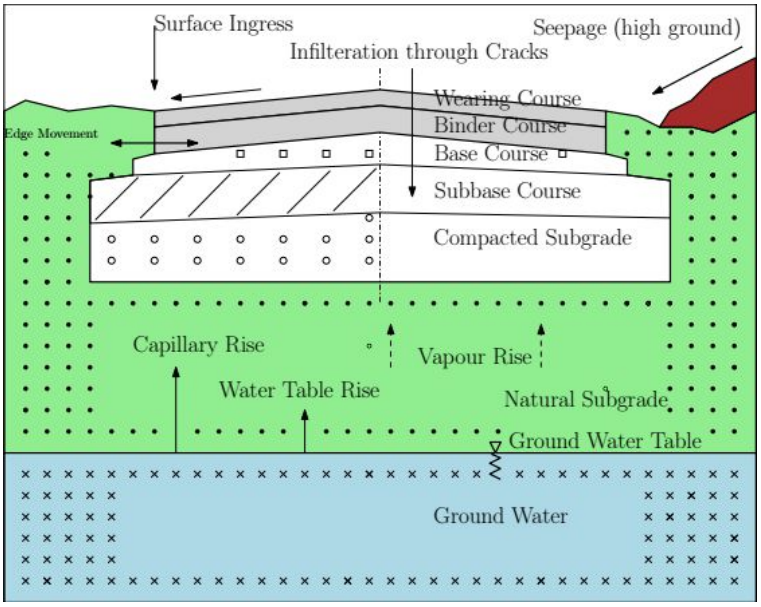

Fig. 1.1: Possible sources of water entering the pavement

The moisture susceptibility of asphalt mixtures are evaluated in the laboratory through various moisture sensitivity tests since 1930 (Terrel and Shute 1989). To date, the moisture induced damage in asphalt mixtures remains an unsolved problem though it had been studied for over 70 years (Tarefder and Zaman 2009). Moisture damage in the asphalt pavement can be reduced by two methods. Either moisture can be prevented from entering the pavement system by sealing the joints and by making the surface layer impervious. This method becomes highly impractical and expensive, as cracks progress and pavement ages. Alternatively, the water entering the pavement system shall be drained as soon as possible (Elsayed and Lindly 1996). Both these methods are not fully effective and researchers across the world are exploring other effective means to minimize the moisture induced damage in asphalt mixtures.

Table 1.1: Factors contributing to moisture induced distresses (Hicks et al. 2003)

Mix design	• Binder and aggregate chemistry • Binder content • Air voids • Additives
Production	• Aggregate coating and quality of aggregate passing 75 μm sieve • Temperature at plant • Excess moisture content in aggregate • Presence of clay
Construction	• Compaction: high air voids • High permeability • Mix segregation • Changes from mix design (field variability)
Climate	• High-rainfall areas • Freeze-thaw cycles • Steam stripping
Other factors	• Surface drainage • Subsurface drainage • Rehabilitation strategies including chip seals over marginal HMA materials • Average daily traffic

In the next section, the mechanisms that explain the occurrence of moisture damage in the asphalt mixture are discussed.

1.2 Moisture Damage Mechanisms

Moisture damage in asphalt mixtures can be divided into two sections, the physical process and the mechanical process. The physical process is described as weakening of mastic and bond between aggregate and asphalt due to erosion. The mechanical process is the existence of pore water pressure under traffic loading (Kringos and Scarpas 2008). The mechanism that drives the stripping process is detachment, displacement, spontaneous emulsification, pore pressure, hydraulic scouring, pH instability, and the effect of the environment. The possibility of adhesive or cohesive failure is summarized in Table 1.2. Damage due to moisture is not the effect of any individual mechanism but is the overall effect of simultaneously and progressive occurrence of these mechanisms. Application of wheel loads pressurizes the moisture present inside the voids, which in turn exerts excessively high pressure. Repeated application of

wheel loads leads to stripping. The moisture damage in asphalt mixtures is attributed either to "adhesion", loss of bond strength between the aggregate surface and the asphalt film, or "cohesion", loss in strength within the asphalt. The theories that explain the moisture damage mechanism are listed in Table 1.3 whereas the recent research works which explain the moisture-induced damage mechanism are listed in Table 1.4.

Table 1.2: Mechanisms related to adhesive and cohesive failure (Little and Jones 2003)

Mechanism	Adhesive failure	Cohesive failure
Detachment	●	
Displacement	●	
Spontaneous emulsification		●
Pore pressure	●	●
Hydraulic scouring	●	
pH instability	●	
Effect of environment	●	●

Table 1.3: Theories explaining moisture damage mechanisms (Kanitpong and Bahia 2003)

Theories	General Principles
Contact angle	Asphalt is displaced because the contact angle of water is less than the asphalt (Taylor et al. 1983, Stuart et al. 1990, Hicks et al. 1991).
Interfacial energy or molecular orientation	Asphalt is displaced because the surface energy of water is less than asphalt (Taylor et al. 1983, Stuart et al. 1990, Hicks et al. 1991).
Chemical reaction theory	Changes in water pH around aggregates affect the microscopic water at the mineral surface, leading to a build-up of opposing, negatively charged, electrical double layers on the aggregate and asphalt surfaces (Taylor et al. 1983, Hicks et al. 1991).
Pore pressure or hydraulic scouring	Pore pressure of water entrapped due to mix densification under traffic results in increased pore pressure on asphalt film, leading to its rupture (Taylor et al. 1983, Hicks et al. 1991, Kandhal et al. 1994).
Spontaneous emulsification	Adhesion between the asphalt and aggregates is lost due to the formation of an inverted emulsion (Taylor et al. 1983, Hicks et al. 1991).

The thickness of the binder coating on the aggregate affects the mode of failure where adhesive strength plays an important role for thin-film coating whereas, for thicker layer, cohesive strength is responsible for moisture-induced damage (Little and Jones 2003).

Table 1.4: Recent literature related to moisture damage mechanisms

Theories	General Principles
Vapour diffusion	Even in the case of continuous coverage of the aggregates by the binder, water vapour can reach the aggregate surface (Cheng 2003, Kringos 2007).
Advective flow	The high rate of water flow causes erosion of the mastic layer in porous mixtures (Kringos and Scarpas 2005).
Supramolecular and colloidal systems	The presence of water in the asphalt-aggregate interface will change the asphalt-aggregate interface to show more complex behaviour than in dry conditions because water causes asphalt and mineral to be solvated. The colloidal structure exists in the adhesion region where asphalt, aggregates, and water coexist at the same time and place (Cho and Kim 2010).
Residual moisture	Residual moisture present inside aggregate that may not have been removed during the drying process (Pine 2015).

Stripping is a complicated problem that depends on numerous factors such as type and use of asphalt mixture, binder characteristics, aggregate characteristics, environment, traffic, construction practices, and application of suitable antistripping agent (Taylor and Khosla 1983). Hydraulic scouring is the prime cause of stripping (Pinkham et al. 2012). Few researchers explain moisture damage as an asphalt-aggregate interaction problem, which is dependent on asphalt chemistry, asphalt rheology, aggregate surface chemistry, and physical properties (Kanitpong and Bahia 2003). Through experiments and modelling it was suggested that, even if the binder is covering the aggregate surface completely, water can diffuse in and reach the aggregate surface (Kringos 2007). It was also shown that this diffusion is binder dependent (Cheng et al. 2003). Carboxylic acids and 2-Quinolone type compounds (responsible for adhesion property of asphalt binder) are most strongly adsorbed on the surface of the aggregate and these compounds are most easily displaced by water from most aggregates. Sulfoxides are found to be adsorbed in high concentrations on the aggregate surface and are easily displaced by water (Huang et al. 2005a).

1.3 Anti-Stripping Additives

Asphalt mixtures are highly moisture susceptible as water has more affinity towards aggregate than asphalt. The use of an anti-stripping additive is desirable to the moisture-sensitive asphalt mixture. Liquid anti stripping additives (liquid amines and diamines, liquid polymers), solid anti stripping additives (Portland cement and fly-ash), polyphosphoric acid and hydrated lime are the few anti stripping additives used with asphalt mixtures. Traditionally, lime has been used as an antistripping additive. The use of lime as an antistripping additive in asphalt mixture to reduce moisture susceptibility is well known (Boyes 2011, Huang et al. 2005a). Hydrated lime has a low molecular weight and is a highly reactive chemical, which results in a high relative concentration of reactive chemical functionality compared to other mineral fillers. Hydrated lime is a strong base and reacts irreversibly with carboxylic acid and similar functional groups in asphalt to form insoluble calcium salt. The adsorption of these acidic components (5 % of total asphalt) onto the surface of hydrated lime removes them from the asphalt phase (Little and Petersen 2005). These components that are adsorbed by hydrated lime and responsible for moisture damage in asphalt mixtures are thus restrained from reacting with water. The addition of hydrated lime improves resistance to moisture damage by reacting with carboxylic acids and 2-quinolones so that there is no moisture-sensitive hydrogen bonding on the aggregate surface (Little and Jones 2004). The effect of hydrated lime is also dependent on the type of asphalt (Little and Petersen 2005, Lesueur and Little 1999). Even though these interactions of hydrated lime results in beneficial effects such as reduction in stripping, stiffening of the binder which in turn increases resistance to rutting, at the same time has negative effect in terms of reduction in fatigue resistance. Hydrated lime increases resistance against moisture in asphalt mixtures by increasing bond strength between asphalt and aggregate. The addition of lime to HMA reduces the rate of oxidation and also reduces the negative effect of products formed due to oxidation (Little et al. 2006).

1.4 Warm Mix Asphalt Additives

Warm Mix Asphalt (WMA) is being widely used globally as these mixtures can achieve the required workability for mixing and compaction even at reduced temperatures compared to Hot Mix Asphalt (HMA). The WMA technologies are broadly classified into three categories including organic additives, chemical additives, and foaming technologies. Organic additives lower the binder viscosity thereby reduces the mixing temperature of asphalt with aggregate. Similarly, various types of foaming technologies do reduce the viscosity of the binder by

increasing its volume. However, chemical additives do not significantly affect the viscosity, but acts as a surfactant, reducing the frictional forces at the interface of aggregate and asphalt thereby reducing the mixing temperature of asphalt with aggregate by approximately 20 to 40 °C compared to the hot mix temperatures. As of 2011, the number of WMA additives available in the United States is close to 20 (Bonaquist 2011). Several nations across the world are working towards reducing greenhouse gas emissions especially after signing the Paris agreement (UNFCCC 2017). Five major WMA technologies that evolved and are used for construction around the world are WMA-Foam, Aspha-min, Sasobit wax, Advera WMA, and Evotherm (Kuang 2012).

Even though the use of warm mix additives, in general, reduce the mixing and compaction temperatures, chemical warm mix additives have been widely preferred by several researchers across the world as these additives do not significantly alter the binder viscosity unlike the organic additives and foaming technologies. In general, chemical additives reduce the internal friction between the aggregate and binder thereby improving the binder coating over the aggregates as they are emulsifiers and surfactants (Li et al. 2016, Pereira et al. 2018). Chemical additives are also termed as tensioactive additives as these additives reduce the binder surface tension without theoretically affecting the rheological properties (Morea et al. 2012). Several chemical additives are being used globally and the relative performance of binders and mixtures depends on the type of chemical additive, its dosage and the choice of binder (Pereira et al. 2018) apart from the type of aggregates (Kakar et al. 2016) due to their diverse range of mechanisms (Caputo et al. 2020). Similar to the organic additives, some of the chemical additives reduce the binder viscosity due to the presence of rheology modifiers in addition to the surfactants. The surfactant-based chemical additives reduces the surface tension of the binder thereby improves its wetting ability due to reduced contact angles (Li et al. 2016, Pereira et al. 2018). Apart from altering the contact angles, the chemical additives also improves the surface free energy values. The contact angle and surface free energy parameters are widely being used to evaluate the moisture resistance of asphalt mixtures.

1.5 Moisture Susceptibility Tests

In order to evaluate the moisture sensitivity of various asphalt mixtures, moisture susceptibility tests are performed. Moisture susceptibility test results may be used to predict the potential for long-term stripping and to evaluate anti-stripping additives, which are added to the asphalt binder, aggregate, or asphalt mixture to help prevent stripping. Over the years,

numerous different tests have been used to evaluate the asphalt mixture susceptibility to moisture damage. An idea was developed that the moisture damage was produced either by the development of pore pressure within the specimen, or by the reaction of water at an elevated temperature at the asphalt-aggregate interface, or by both (Lottman 1978). At moderate or higher temperatures, water removes asphalt from the asphalt mixture (Lottman 1982). Moisture damage occurs on all size of aggregates; however, stripping caused to fine aggregates, which represent the basic matrix of the asphalt mixture, are of primary concern (Kennedy et al. 1982). The severity of moisture damage was found to be independent of air voids and degree of saturation when quantified with the indirect tension test (Tunnicliff and Root 1984). Extreme damage due to the action of water and its freeze-thaw effect was witnessed on the asphalt mixtures. For moisture conditioning, several procedures have been evolved: Nottingham asphalt test equipment, Hamburg wheel test, AASHTO T 283, Moisture Induced Sensitivity Test (MIST), etc. (Ahmad et al. 2018). AASHTO T283 (2014) is used as the moisture susceptibility test in India (MoRTH 2013) to quantify the damaging effect of moisture on the asphalt mixtures. The moisture sensitivity test developed over the years for loose or compacted asphalt mixtures (Table 1.5) measures the overall impact of damage caused and does not isolate the factors that might have occurred during the progression of damage. These tests provide composite test results that are comparable between given sets of conditions.

Table 1.5: Tests conducted on loose and compacted asphalt mixtures

Loose Asphalt Mixtures	**Compacted Asphalt Mixtures**
1. Rolling bottle method (EN 12697-11)	1. Texas freeze-thaw pedestal test (Kennedy and Anagnos (1984)
2. Boiling test/ Texas boiling test (ASTM 3625)	2. Cantabro abrasion test (ASTM D7064/D7064M)
3. Quick bottle test (Maupin Jr. 1980)	3. Marshall immersion test
4. Chemical immersion test	4. Lottman test (NCHRP 246)
5. Net adsorption test (NAT) - SHRP-A-341	5. Modified Lottman (AASHTO T-283)
Other Tests to Evaluate MID	6. Tunnicliff and Root conditioning (ASTM D4867)
1. Pneumatic adhesion tensile testing equipment (PATTI)	7. Immersion-compression (AASHTO T-165) (ASTM D1075)
2. Universal Sorption Device (USD)	8. Hamburg wheel-tracking device

3. Dynamic Wilhelmy plate method (DWPM)	9. Saturation aging tensile test (SATS)
4. Static contact angle measurements	10. Model mobile load simulator (MMLS3)
5. DSR modified (Cho and Bahia 2010)	11. Moisture induced sensitivity test (MIST) (ASTM D7870)

The other tests to evaluate moisture damage in asphalt mixtures that evolved over years are discussed here. The Pneumatic Adhesion Tensile Testing Equipment is used to find cohesive strength within the binder as well as adhesive strength between aggregate and binder. The specimens are fixed to the metal plates, and a pulling force is applied, the amount of force required for separation is tabulated. Other methods to determine moisture susceptibility of asphalt mixtures is to find surface free energy of aggregate and binder. The Universal Sorption Device (USD) is used to find the surface free energy of aggregate. The microcalorimeter in USD is used to measure the heat of immersion of the previously selected aggregates in water whereas the Dynamic Wilhelmy Plate Method (DWPM) is used to compute the surface free energy of asphalt. In this method, a thin glass coated with asphalt is immersed and pulled out of a probe liquid to determine the contact angle between the plate and probe liquid. The static contact angle measurement device measures the contact angle for binder and aggregate using an optical contact angle analyzer and the surface free energy is computed.

1.6 Motivation for the Study

Tarfeder and Zaman (2010) raised two fundamental questions that remain unanswered:

(i) Can the conditions that cause moisture-induced damage be accurately predicted?

(ii) How can moisture-induced damage be mitigated?

The pavement is subjected to vehicular movement after completion of the construction which requires a fundamental understanding of the behaviour of asphalt mixtures under repeated wheel loads. That is, the wearing course of asphalt pavement is directly exposed to repeated loading. Bituminous concrete (BC), a dense-graded asphalt mixture is the most commonly used wearing course in India especially for the high volume traffic corridors. As the wearing course is directly subjected to wheel loading in the presence of moisture during monsoon, it is crucial to understand the fatigue response of asphalt mixtures after the compacted specimen is subjected to moisture damage. Though the indirect tensile strength test on cylindrical asphalt mixture specimen is widely used and tensile strength ratio (TSR) is computed as the

ratio of conditioned ITS to unconditioned ITS, the results were found to be highly inconsistent (Varveri et al. 2014). AASHTO T283 (2014) test protocol is recommended by the Indian Ministry of Road Transport and Highways (2013) to evaluate moisture susceptibility of asphalt mixtures which is based on ITS. ITS test only captures the peak failure load and gives a pass/fail result while it completely overlooks the evolution of deterioration of asphalt mixture during and after moisture damage. Moreover, the ITS test has a very high rate of loading (51 mm per minute), which may not be realistically simulating the field environment.

Asphalt mixture with the same constituents but with a higher level of accessibility to moisture should exhibit higher damage. Even though the specimen is compacted at similar air voids, a variation in TSR is observed and may not exhibit similar damage, and that the increase in moisture accessibility may not always increase the damage (Tarefder and Ahmad 2015a, Tarefder and Ahmad 2015b, Ahmad et al. 2018). Due to chemical changes during freeze-thaw cycles or pore pressure cycles at elevated temperatures, there might be inconsistencies in ITS measurement. The binder might get stiffened due to certain chemical changes but with low stripping, TSR in such a case shall exhibit higher value (Ahmad et al. 2018).

The production of HMA is a high energy consumption technique to produce a workable asphalt mixture, which requires heating aggregate and asphalt to about 160 °C. In this process the binder experiences loss of volatile factions which causes the short-term ageing of the binder. In order to save energy consumption to produce workable asphalt mixtures at reduced temperature, the WMA technology is used. WMA mixtures are produced at about 20 to 40 °C lower than HMA. WMA shall, therefore, be less prone to aging and shall have reduced hardening compared to HMA. Successively WMA is expected to have higher fatigue life than HMA. However, in the presence of moisture, WMA is more prone to experience higher moisture damage than HMA.

In an attempt to curb moisture damage in HMA and WMA hydrated lime was used in the past. Hydrated lime also being active filler will increase the stiffness of the unconditioned asphalt mixture. It can be anticipated that the addition of hydrated lime shall increase the fatigue life of HMA and WMA at lower strain compared to HMA without lime and WMA without lime, respectively. However, at higher strain it is likely that the fatigue life of HMA with hydrated lime and WMA with hydrated lime shall decrease due to increase in stiffness. Although, it would be awaited to see how the increased fatigue life due to warm mix additive shall be affected with the addition of hydrated lime. It would also be awaited to see if the

increase in fatigue life due to warm mix additive counters the reduction in fatigue life due to the filler effect of hydrated lime, with approximately no variation to that of HMA. In the presence of water, hydrated lime shall also perform as an anti-stripping additive. It is thus expected that the moisture conditioned asphalt mixtures with hydrated lime shall perform better than the unconditioned counterparts at all strains. It is also awaited to see how the moisture conditioned HMA with lime and WMA with lime perform during fatigue.

1.7 Objectives

The objectives of the research work are as follows:

1. To evaluate the efficacy of indirect tensile strength ratio test in evaluating the moisture sensitivity of asphalt mixtures.
2. To evaluate the influence of warm mix additive, hydrated lime, and moisture conditioning on the evolution of flexural stiffness and energy dissipation.
3. To quantify the influence of moisture and hydrated lime on the fatigue life of hot mix asphalt and warm mix asphalt.
4. To evaluate the effect of moisture on viscoelastic dissipation and dissipation due to damage on the addition of hydrated lime in hot mix asphalt and warm mix asphalt.

1.8 Scope

The scope of the current research work is limited to the following:

1. All the experiments performed in this study are limited only one dense gradation, i.e., bituminous concrete grading II.
2. Two types of additives, hydrated lime a conventional antistripping additive, and Evotherm a commercial warm mix additive are used in the present investigation.
3. One type of asphalt binder, VG30, an unmodified binder is used in this study.
4. The performance tests considered in this study includes indirect tension test and four-point beam bending fatigue test.

1.9 Organization of the Thesis

The thesis titled “influence of moisture damage and hydrated lime on the fatigue life of hot mix asphalt and warm mix asphalt” is organised in eight chapters. In Chapter 1, an introduction in general about the understanding of moisture damage in the asphalt mixture is discussed. The requirement of warm mix additive and anti-stripping additive is dealt with along with their effect due to moisture damage on fatigue life. The tests to measure moisture-

induced damage that evolved and the nature of their measurement are also reviewed. The motivation to carry out this work, the objectives of the study, and the scope are also put forward.

The second chapter discusses the literature review related to the moisture influence on the asphalt mixture and the details about the gaps in the literature.

The third chapter discusses in detail the properties of aggregate, asphalt, Evotherm, and hydrated lime used in the study. The determination of mixing and compaction temperature, calculation of theoretical maximum specific gravity, Marshall mix design, and compaction of asphalt mixture using Marshall and shear box compactor are discussed in detail. Also, the production of prismatic fatigue beam from shear box beam is methodically discussed.

The fourth chapter includes the complete methodology adopted to proceed with the experimentation to fulfil the set of objectives. Further, the AASHTO T283 conditioning and prismatic beam conditioning process are discussed. The chapter then details the indirect tensile strength test procedure and the test matrix used in the study. Further, the four point beam bending jig used to test prismatic fatigue beam and the UTS15 software used to operate the four point beam bending equipment is discussed. PID tuning to attain smooth sinusoidal waveform of 10 Hz frequency during fatigue test and the four point beam bending test procedure is also discussed. The test matrix and the data collected for the fatigue test are also explained in this chapter.

The fifth chapter includes the results obtained from the indirect tensile strength test on asphalt mixtures and their moisture susceptibility based on tensile strength ratio. The chapter further includes the issues related to the indirect tensile strength test.

The sixth chapter illustrates the influence of moisture damage on the fatigue response of asphalt mixture. The evolution of flexural stiffness and energy dissipated with the number of cycles are discussed concerning the unconditioned and moisture conditioned specimens. Further, the influence of warm mix additive and hydrated lime on the moisture-damaged specimen is discussed. The fatigue life of unconditioned and moisture damaged specimen was determined using AASHTO, ASTM, energy ratio, and the ratio of dissipated energy change and the corresponding test results are discussed in detail. The ranking of the mixtures based on fatigue life are also discussed.

The seventh chapter uses three modelling approaches namely pseudo strain concept, constitutive assumption approach, and a linear viscoelastic rate type model to separate viscous dissipation from total energy dissipation. The chapter further explores the dissipation due to damage and dissipation due to viscous property of asphalt mixtures and the variation caused due to warm mix additive, hydrated lime, and moisture damage on the proportion of damage dissipation to verify five hypotheses to characterize asphalt mixtures are discussed in detail.

The eighth chapter provides an overview of the complete experimental work carried out through the summary and the conclusions. The chapter also indicate the prospective of further research.

1.10 Summary

A large proportion of the roads in India is constructed using bituminous (asphalt) concrete. The major complication faced is the behaviour of asphalt concrete is the presence of water. Moisture damage can augment various distresses including stripping, ravelling, fatigue, and rutting. Various mechanisms causing moisture damage were reported including detachment, displacement, spontaneous emulsification, pore pressure, hydraulic scour, and pH instability (Little and Jones 2003). Numerous tests and moisture conditioning protocols have evolved to simulate the field conditions in the laboratory. The moisture sensitivity tests on asphalt mixtures are performed either on loose specimens or compacted specimens. Modified Lottman indirect tension test procedure also known as AASHTO T283 is the most widely used procedure for determining the moisture susceptibility of asphalt mixtures (Solaimanian et al. 2003). The antistripping additives such as hydrated lime and surfactants are expected to improve the bond between the asphalt binder and the aggregates (Das et al. 2015). However, the fatigue performance of asphalt mixtures consisting of such a combination of additives especially when subjected to moisture conditioning process is not well understood. Further, the fatigue damage occurring in asphalt mixtures due to complex interactions occurring between various constituents including lime, WMA additives, asphalt, and aggregate in the presence of moisture needs to be quantified.

CHAPTER 2

LITERATURE REVIEW

2.1 General

This chapter provides a comprehensive review of the literature in a sequential manner. The literature pertaining to the role of warm mix additives is initially presented followed by the details related to a specific surfactant based warm mix additive. This is followed by the discussion on literature pertaining to moisture damage in asphalt mixtures including both hot mix asphalt and warm mix asphalt. Subsequently, the literature related to antistripping additives in general and lime in particular is presented. The test protocols available to quantify moisture damage on compacted asphalt mixtures are presented followed by the background information on indirect tensile strength test and fatigue tests. Also, the literature pertaining to the usage of fatigue test to quantify moisture damage in asphalt mixtures is presented. Finally, the past research works are summarized to highlight the research gaps.

2.2 Role of Warm Mix Additives

The usage of WMA binders has been increasing globally in pavement construction due to inherent advantages such as reduced working temperatures at the time of mixing, laying, and compaction due to improved asphalt mixture workability. Various studies quantified the beneficial effect of WMA binder compared to hot mix asphalt (HMA) binder in terms of reduced binder aging (Hurley and Prowell 2006) resulting in enhanced fatigue life (Roja and Krishnan 2016). However, lower mixing and compaction temperatures increase the potential for moisture damage due to retained residual moisture in the aggregates (Prowell et al. 2007). Thus, the presence of WMA additive in asphalt mixture reduces the binder aging and increases moisture susceptibility. This shows the need to understand and quantify the effects of WMA additives on the performance of asphalt mixtures. Even though several warm mix technologies are available, the chemical additives will not affect the viscosity of the binder as observed in the case of organic additives and foaming technologies. Thus, Evotherm, a surfactant based warm mix additive has been selected for the current study.

2.3 Evotherm – A Surfactant Based Warm Mix Additive

Evotherm was first introduced in 2005 as Evotherm ET based on emulsion technology. Evotherm ET technology is a high residue emulsion containing 70 % asphalt by total weight. When mixed with hot aggregate, the residual asphalt binder and chemical additive get adhered to the aggregate after the evaporation of water. Evotherm DAT, dispersed additive technology was then introduced. This process used lesser amount of water as compared to emulsion process. In this process, the chemical additive solution was directly injected to asphalt pipeline at the mixing plant. Third generation Evotherm was then introduced as Evotherm 3G. Water was not used in this technology, and the chemical additive was directly added to asphalt. This process was much more convenient to use (NCHRP 691 2011). Surfactant based warm mix additives maintain required workability even at reduced temperatures in the order of approximately 30 ºC lower than the conventional asphalt mixtures, providing safer environment for the workers at construction sites. WMA allows the wetting of aggregate to happen, increases workability at lower temperature, improves adhesion and compaction of the asphalt mixtures. Evotherm® saves 55 percent of energy at plant; reducing CO_2 and SO_2 emission by 45 %, NOX by 60 %, and total organic material by 41 % (FHWA 2021). Fatigue cracking is a well-known cause of affecting the structural and functional performance of the asphalt pavement. Though WMA saves energy, the moisture if present, may not completely evaporate from aggregate, increasing its moisture susceptibility. For this reason, it is vital to evaluate the fatigue characteristics of moisture conditioned WMA. Susceptibility to moisture damage has been a crucial aspect of both HMA and WMA mixtures (Kuang 2012). Though WMA is prepared at a lower temperature than HMA, factors influencing the deterioration of a flexible pavement are similar for both these mixtures.

2.4 Moisture Damage in Asphalt Mixtures

Moisture transport into asphalt mixture can be in the form of liquid and/or vapour. The moisture transport in liquid form is significantly affected by the air void structure (Chen et al. 2004, Masad et al. 2006a, Arambula et al. 2007) whereas, in vapour form, the relative humidity differential plays a major role (Luo et al. 2017). In contrast to the general notion that moisture-related damages occur during monsoon, blisters occurring during summer are attributed to vapour diffusion even through the impermeable dense-grade asphalt mixtures which essentially depend on air temperature and humidity (Sasaki et al. 2006). In such cases, moisture diffuses through the asphalt binder and affects the bond between asphalt binder and

aggregate (Hung et al. 2017). The asphalt binder film thickness and the moisture diffusion coefficient of the asphalt binder greatly affect the moisture transport through the asphalt binder. Combinations of experimental and analytical techniques are used to measure the moisture diffusion through the asphalt binders (Vasconcelos et al. 2010) and fine aggregate mixtures (Vasconcelos et al. 2011). Upon infiltrating through the asphalt mixture, moisture reaches the interface of the aggregate-asphalt. Even though the term asphalt is used to represent the coating over the aggregates, in real sense, it is the asphalt mastic that binds the aggregate particles together. Various studies characterized the moisture transport and moisture damage mechanisms in an attempt to verify the moisture susceptibility of asphalt mixtures (Caro et al. 2008a, Caro et al. 2008b), and comprehensive state-of-the-art reviews are available covering various moisture sensitivity test methods (Airey and Choi 2002, Kakar et al. 2015, Chakravarty and Sinha 2020), mechanisms of moisture damage (Kakar et al. 2015, Chakravarty and Sinha 2020), approaches to predict moisture damage (Kakar et al. 2015, Soenen et al. 2020), and usage of antistripping agents (Kakar et al. 2015, Chakravarty and Sinha 2020). The mechanism of moisture-induced damage in asphalt mixture due to cohesive and adhesive failures is well documented by several researchers (Masad et al. 2006b, Kringos et al. 2008a, Kringos et al. 2008b). The diffusion of vapour through the asphalt binder softens the binder and results in cohesive failure (Arambula et al. 2010a). Adhesive failure occurs when moisture diffuses into the asphalt-aggregate interface (Arambula et al. 2010b) and also when the asphalt mixtures are exposed to moisture for prolonged duration (Das et al. 2015).

The constituent materials of asphalt mixture play a significant role in resisting the moisture damage due to interactions of moisture with various asphalt mixture constituents. One such interaction is between moisture and various constituents of the asphalt binder. These interactions increase at higher temperatures and prolonged contact durations resulting in increased polar compounds on the asphalt surface (Hung et al. 2017). The characteristics of the binder play a major role in moisture damage of asphalt mixture. The presence of moisture in asphalt mixture accelerates the asphalt binder age hardening which in turn reduces the fatigue life of asphalt mixture (Krishnan and Rao 2001). The strong interlink between aging and moisture damage is quantified experimentally through atomic force microscopy (Das et al. 2015) where it was observed that water soluble polar products are formed during the aging process which are subsequently dissolved/washed with moisture flow thereby exposing the original asphalt and reducing the asphalt mastic thickness. Considering the fact that the

WMA additives reduce the binder aging, the possible damages due to moisture are expected to be minimized. Further, taking into account the wide range of WMA additives, the surfactant based WMA additives stabilizes the water-asphalt interface and are expected to result in improved performance towards moisture-induced damages.

Apart from the asphalt and asphalt mastic, the type of aggregates also plays an important role in resisting moisture damage (Ghabchi et al. 2013, Sebaaly et al. 2015). The role of aggregates is normally quantified by selecting different types of aggregates and a single type of asphalt mastic (Apeagyei et al. 2015). It has been observed that the moisture-induced damage increased with the presence of higher retained moisture in the aggregates (Yang et al. 2020). As discussed above, the use of WMA additives reduces the construction temperatures wherein the moisture present in the aggregates can affect the bond between the aggregates and the asphalt mastic. At the same time, the reduced aging of WMA binders due to lower compaction temperatures can enhance the moisture resistance of the asphalt mixture. To overcome the drawback of WMA, the production temperature can be slightly increased (Sanchez-Alonso et al. 2011). Even though the recommendation is to increase the production temperature slightly, such a practice is against the fundamental principle of the WMA and is likely to increase the binder aging. Thus, it is highly desirable that the antistripping additives should be incorporated into the WMA to improve its moisture resistance.

2.5 Lime as an Antistripping Additive

Several types of antistripping additives in liquid form and powder form are being used to minimize moisture damage in asphalt mixtures. A comprehensive review of all such antistripping additives (Chakravarty and Sinha 2020) is available in the literature. In the past, hydrated lime was successfully used to improve the WMA resistance towards moisture damage especially for moist aggregates (Xiao et al. 2009, Hasan et al. 2015). Various mechanisms involving hydrated lime in the modification of asphalt mixtures are well documented in the literature and a comprehensive review of all such mechanisms (Lesueur et al. 2013) is available.

The antistripping additives such as hydrated lime and surfactants are expected to improve the bond between the asphalt binder and the aggregates (Das et al. 2015). It was observed that not only hydrated lime show filler effect, but also reacts chemically and changes physical state of asphalt related to asphaltene, and component compatibility of asphalt. These changes in asphalt due to hydrated lime, changes the flow property of asphalt as the stiffness increases.

The resistance on flow is created as hydrated lime interacts with weak bonds within microstructural units. Hydrated lime reduces the rate of decrease of dissipated energy, hence increasing the fatigue life of asphalt mixtures. Specimens prepared with hydrated lime can accumulate more damage compared to asphalt mixtures without hydrated lime. Lime increases resistance against moisture in asphalt mixtures by increasing bond strength between asphalt and aggregate and a 38 % increase in expected pavement life was observed on addition of hydrated lime (Little et al. 2006). Hydrated lime shall be added to the aggregate just before the application of asphalt, before mixing. Hydrated lime being a strong base, reacts irreversibly with carboxylic acid and other functional group in asphalt to form insoluble calcium salt. The adsorption of these acidic components onto the surface of hydrated lime removes them from asphalt phase (Little and Petersen 2005). The addition of hydrated lime improves resistance to moisture damage by allowing reaction between carboxylic acids and 2-quinolones, so that there is no hydrogen bonding on aggregate surface (Little and Jones 2004). Addition of hydrated lime to the asphalt mixture has various benefits and was found to be more than just active filler. It also acts as an antioxidant and reacts with clay fine in the asphalt mixture. This interaction of hydrated lime reduces stripping, increase resistance to fracture growth at low temperatures and rutting, stiffens the binder, reacts with the oxidised product to reduce its adverse effect and improves the plastic property of clay to increase moisture stability (Little et al. 2006, Rasouli et al. 2018). The addition of hydrated lime increases the flexural stiffness of asphalt mixture signifying the physical and chemical interactions between asphalt and hydrated lime (Rasouli et al. 2018). The effect of hydrated lime is dependent on type of asphalt (Little and Petersen 2005, Lesueur and Little 1999).

2.6 Moisture Conditioning Process

The permeability within the asphalt mixture allows the flow of water through the voids path (Lottman 1971). An idea was developed that the moisture damage was produced either by the development of pore pressure within the specimen, or by the reaction of water at an elevated temperature at the asphalt-aggregate interface, or by both (Lottman 1978). At moderate or higher temperature, water removes asphalt from the asphalt mixture (Lottman 1982). Moisture damage occurs on all size of aggregates. However, stripping caused to fine aggregates, which represent the basic matrix of the asphalt mixture, are of primary concern (Kennedy et al. 1982). Extreme damage due to the action of water and its freeze-thaw effect was witnessed on the asphalt mixture. Several methods to quantify moisture-induced damage in the compacted asphalt mixture are presented in Table 2.1.

Table 2.1: Tests to quantify moisture induced damage on compacted asphalt mixtures

Test Method	Speciment Dimension	Conditioning Process	Mechanical Test	Remarks	Reference	Relevant Standards
Texas freeze-thaw pedestal test	41.33 mm diameter, 19.05 mm height cylindrical specimen	-12 °C for 12 h, 23 °C for 45 min and 49 °C for 12 h	Number of freeze-thaw cycles required to crack the briquet	Visual inspection	Kennedy et al. (1982)	
Modified Texas freeze-thaw pedestal test	41.33 mm diameter, 19.05 mm height cylindrical specimen	-12 °C for 15 h, 23 °C for 45 min and 49 °C for 9 h	Number of freeze-thaw cycles required to crack the briquet	Visual inspection	Kennedy and Anagnos (1984)	
Immersion compression test	101.6 mm diameter, 101.6 mm height cylindrical specimen	60 °C for 24 h or 49 °C for 4 days	Axial compression without lateral support at 25 °C	Wet to dry ratio-maximum vertical load by the cross-sectional area	Godde (1959), ASTM STP 252	AASHTO T165, ASTM D1075
Marshall immersion test	101.6 mm diameter, 101.6 mm height cylindrical specimen	60 °C for 24 h or 49 °C for 4 days	Marshall stability	Retained Marshall stability	Stuart (1986)	
Marshall stability test	101.6 mm diameter, 63.5 mm height, cylindrical specimen	60 °C for 24 h	Marshall stability	Retained Marshall stability		AASHTO T245
Lottman procedure	101.6 mm diameter, 63.5 mm height, cylindrical specimen	Partial vacuum of 600 mm Hg for 30 min, -18 °C to -12 °C for 15 h, 60 °C for 24 h	Indirect tensile strength test		Lottman 1982	

Test Method	Specimen Dimension	Conditioning Process	Mechanical Test	Remarks	Reference	Relevant Standards
Tunnicliff and Root procedure	101.6 mm diameter, 63.5 mm height, cylindrical specimen	Partial vacuum of 508 mm Hg until 55 % to 80 % saturation, 60 °C for 24 h.	Indirect tensile strength		Tunnicliff and Root 1984	
Modified Lottman procedure	100 mm and 150 mm diameter, 63.5 mm and 95 mm height, cylindrical specimen	Partial vacuum of 245-660 mm Hg, 70 % to 80 % saturation, -15 °C to -21 °C for minimum 16 h, 60 °C for 24 h	Indirect tensile strength			AASHTO T283-14
Hamburg wheel tracking device	Slab (or) two 150 mm diameter specimen	Submerged in the water while test at 25 to 70 °C	Wheel tracking at 50 passes/min			AASHTO T 324
Environmental conditioning system (ECS)	101.6 mm diameter, 101.6 mm height, cylindrical specimen	Partial vacuum of 254 mm Hg or 508 mm Hg for 30 min, 3 cycles at 60 °C for 6 h, one freeze at -18 °C for 6 h	Resilient modulus (after each conditioning at 60 °C)		SHRP-A-403	
Moisture induced sensitivty test (MIST) conditioning	Cylindrical specimen, 100 (or) 150 mm diameter, cylindrical specimen	40 to 60 °C, 40 to 70 psi (276 to 483 kPa) pressure under water	Indirect tensile strength, resilient modulus			ASTM D7870

2.7 Background of Indirect Tensile Strength Test

Carneiro and Barcellos (1953) in Brazil and Akazawa (1953) in Japan simultaneously but independently developed indirect tension test. The indirect tension test date back to the year 1953 when it was developed for tests on cement concrete. The indirect tension test does not represent the type of loading experienced by the pavement. Nevertheless, since it was relatively simple to use and the type of specimen and equipment used were the same as for cement concrete, the Indirect Tensile Strength (ITS) test was proposed to be used for asphaltic materials (Hudson and Kennedy 1968, Kennedy and Anagnos 1983). The theory for indirect tensile test stress distribution was first developed by Hertz in 1883. Later, A. Foppl and L. Foppl in 1941, Timoshenko and Goodier in 1951, Frocht in 1957, and Peltier in 1954 considered the theory (Thaulow 1957, Hudson and Kennedy 1968). The stress distribution based on Frocht's equation along the x-axis and y-axis for a cylindrical specimen of diameter (d) and thickness (t) during the ITS test are shown in Figure 2.1 and Figure 2.2 respectively.

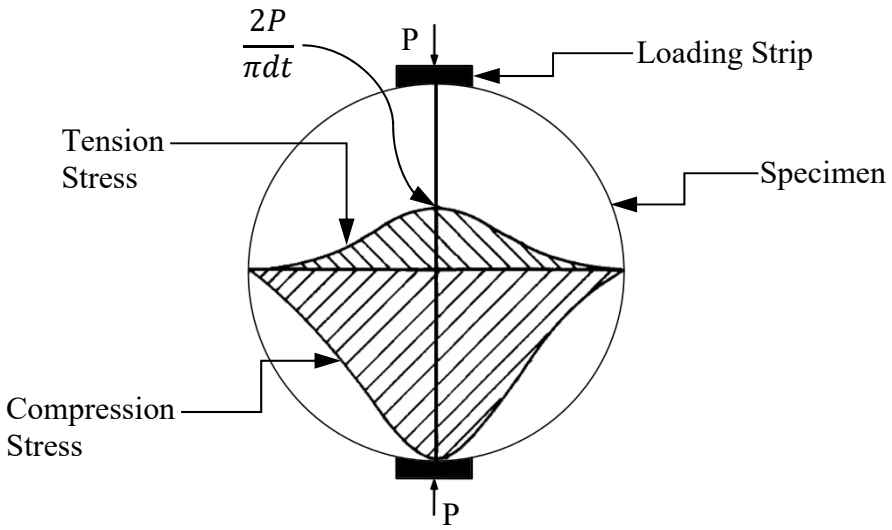

Fig. 2.1: Stress distribution along the x-axis in the ITS specimen (Hudson and Kennedy 1968)

The first use of ITS test to investigate asphalt concrete was carried out by Messina in 1966, and by Breen and Stephens in 1966 (as cited in Hudson and Kennedy 1968). The use of ITS test to measure the moisture damage was proposed by Kandhal and adopted by AASHTO in 1985 (as cited in Brown et al. 2001). AASHTO T283 is also adopted by the Superpave system to evaluate moisture damage in asphalt mixtures (Vargas-Nordcbeck et al. 2016). Indirect tension test (AASHTO T283) is the most widely used test to assess moisture-induced damage in asphalt mixture by calculating retained tensile strength (Brown et al. 2001, Solaimanian et al. 2003, Tarefder and Ahmad 2015a).

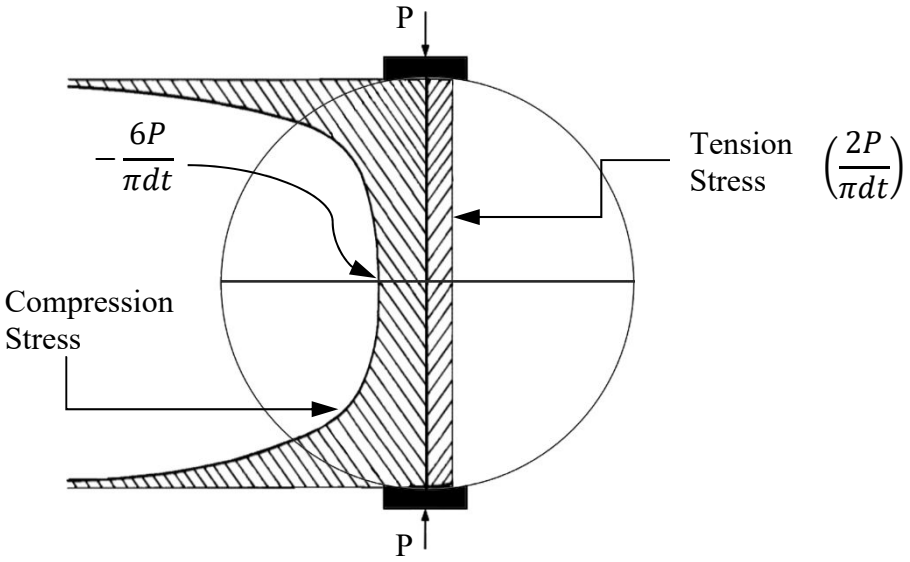

Fig. 2.2: Stress distribution along the y-axis in the ITS specimen (Hudson and Kennedy 1968)

2.8 Background of Fatigue Tests

Matthews et al. (1993) defined fatigue as the cracking resulting from repeated traffic loading but not due to thermal stresses. The available fatigue tests are classified as simple flexure (two-point, three-point, and four-point bending), supported flexure, direct axial, diametral (indirect tension), triaxial, semi-circular bending test, and wheel-track testing (Matthews et al. 1993, Hartman and Gilchrist 2004). The test geometries and characteristics of fatigue tests used for asphalt concrete are shown in Table 2.2 (Benedetto et al. 2004). Out of these test methods, repeated simple flexure, direct tension, and diametral fatigue test were ranked as the top three fatigue test methods (Matthews et al. 1993). The most suitable and frequently used method to simulate fatigue damage at the bottom of the asphalt layer is the simple flexure test (Hartman and Gilchrist 2004). The factors affecting fatigue are load history, mode of loading, rate of applied load, waveform type, test geometry, asphalt property, aggregate property, mixture property, test temperature, presence of moisture, and alteration of material property during fatigue (Epps and Monismith 1972).

The fatigue tests are carried out at either stress controlled mode or strain-controlled mode as shown in Figure 2.3. In a stress-controlled mode, as the stress amplitude is fixed, the strain amplitude increases with a decrease in stiffness to attain the given stress level, and the dissipated energy per cycle increases (Benedetto et al. 1996). The failure in stress-controlled mode is defined as the cracking of the specimen at the end of the experiment. Whereas, in the strain-controlled mode of loading, the strain amplitude is held constant during fatigue, while the stress required to deform the beam to given strain reduces as the asphalt concrete

accumulates damage and the dissipated energy per cycle decreases with the progress of fatigue. The failure in strain-controlled mode is defined as 50 % reduction in the flexural stiffness.

Table 2.2: Characteristics of fatigue tests (Benedetto et al. 2004)

Type	Test Geometry	Type of loading	Strain Amplitude (με)	Max. Stress
T/C	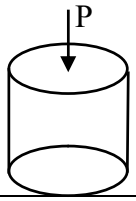	Tension/ compression	Strain: 140, 180, 220	Stress: 0.9 MPa
2PB	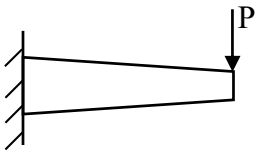	Two-point bending	Strain: 140, 180, 220	Stress: 1.4 MPa
3PB	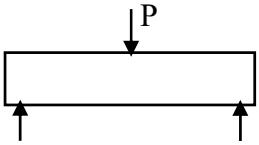	Three-point bending	Strain: 140, 180, 220	Stress: 1.4 MPa
4PB	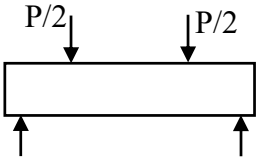	Four-point bending	Strain: 140, 180, 220	Stress: 1.4 MPa
ITT	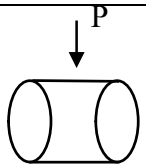	Indirect tension	Strain: 25, 40, 65	-

The fatigue life of prismatic beam can be determined by various post-processing methods based on various standard protocols such as AASHTO T321 (2014), ASTM 7476 (2010), and EN 12697-24 (2012) and are tabulated in Table 2.3.

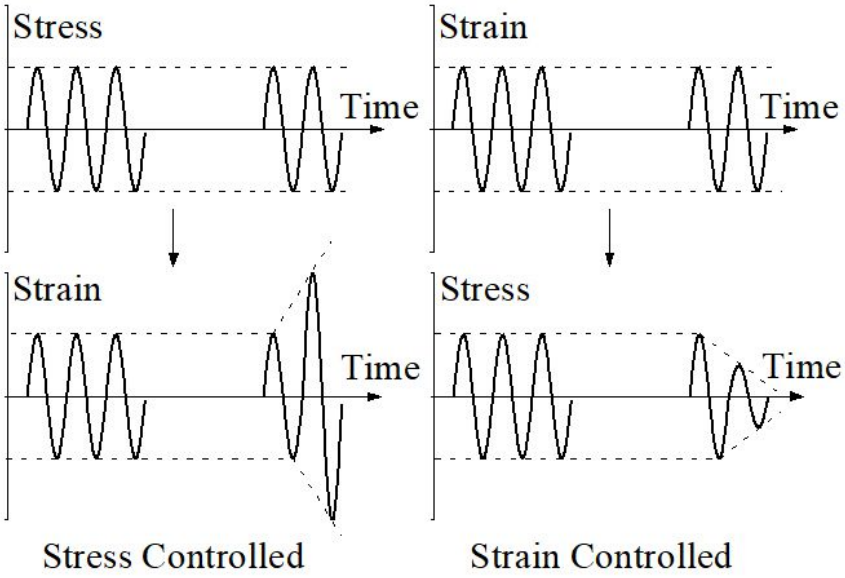

Fig. 2.3: Modes of fatigue test

Table 2.3: Comparison of the fatigue test protocols

Parameters	**AASHTO T 321 (2007)**	**AASHTO T 321 (2014)**	**ASTM 7460 (2010)**	**EN: 12697-24 (2012)**
Frequency range, Hz	5 to 10	5 to 10	5 to 10	0 to 60
Test temperature, ^{o}C	-10 to 25	-10 to 25	20	0 and 20
Loading waveform	Sinusoidal	Sinusoidal	Haversine	Sinusoidal
Initial stiffness determined at	50^{th} cycle	50^{th} cycle	50^{th} cycle	100^{th} cycle
Specimen size	380±6 mm × 50±6 mm × 63±6 mm	380±6 mm × 50±6 mm × 63±6 mm	380±6 mm × 50±2 mm × 63±2 mm	-
Peak to peak tensile micro-strain (με)	250 to 750	250 to 750	50 to 3000	-
Cycles to failure	50 % reduction in stiffness	Max. specimen stiffness × cycle	Peak normalized modulus × cycles	-

2.9 Usage of Fatigue Test to Quantify Moisture Damage

Fatigue test on asphalt mixtures is broadly categorized into two modes, strain control and stress control. A strain controlled test is the one in which the beam is subjected to repeated loading for a given deformation. In a strain controlled mode the beam gradually weaken as

the flexural stiffness reduces and the force required to attain the given deformation also reduces. In a stress controlled mode, the beam is subjected to constant loading, and strain increases with reduction in stiffness until failure. The repeated loading applied to the beam can be either sinusoidal, haversine or trapezoidal and with or without rest period. A four-point beam bending setup ensures pure flexural bending of the test beam in between the two inner clamps. The four-point beam bend test is a long-run performance-based test and shall provide the complete evolution of changes taking place during fatigue of asphalt mixture before and after moisture conditioning. Unlike the ITS test, the fatigue test results shall provide the evolution of flexural stiffness and total energy dissipated for every cycle, until the material fails due to fatigue.

As moisture damage is extremely significant on the flexible pavement, assessment of fatigue response of dense asphalt mixtures after moisture conditioning is obligatory. It was found that the fatigue response was influenced by fine content in the mixture, mixing and compaction temperature (Harvey and Monismith 1993). The fatigue life and total energy dissipated are related parameters (Harvey and Monismith 1993, Dijk 1975). The conditioning of vacuum saturated beams is achieved in three cycles of 5 h at 60 °C followed by 4 h at 25 °C and then one 5 h cycle at - l 8 °C (Shatnawi et al. 1995). Results obtained from strain controlled flexural beam bend test on moisture-conditioned specimens indicate that the flexural beam bend test is sensitive to unconditioned and moisture-conditioned asphalt mixtures (Shatnawi et al. 1995, Lu and Harvey 2006). Fatigue test can identify asphalt mixtures with varying moisture sensitivity (Lu and Harvey 2008). It was also observed that the fatigue life and total dissipated energy are similarly sensitive to binder, aggregate, asphalt content, air voids and mixing and compaction viscosities whereas flexural stiffness was sensitive to binder, air voids and mixing viscosity (Harvey and Monismith 1993).

2.10 Summary

This chapter discussed in detail about the moisture conditioning process and the tests conducted on asphalt mixture. The use of warm mix additive and hydrated lime, their interaction with asphalt, and their effect on moisture sensitivity of asphalt mixtures are also discussed. The chapter also presents the theory of ITS test and fatigue test. The ITS test is used widely to investigate moisture damage in asphalt mixtures whereas the use of fatigue test in assessing moisture damage is limited. The gaps in the literature are elaborated below.

With the reduction in mixing and compaction temperature, WMA binders are less prone to aging compared to HMA binder and this influences the performance of the asphalt mixtures. Due to the reduced rate of ageing of WMA binder, WMA mixtures are expected to exhibit enhanced fatigue damage characteristics compared to the HMA mixture. However, conflicting observations about the fatigue performance of WMA mixtures are reported in various studies. While some studies reported poor fatigue performance of WMA with respect to HMA (Silva et al. 2010), few other studies have reported improved performance of WMA vis-à-vis HMA (Xiao et al. 2015). Few other studies have also reported identical performance of WMA and HMA (Haggag et al. 2011). WMA mixtures were also reported to exhibit an increased tendency to damage due to the presence of moisture (Xiao et al. 2010). At the same time, it was also observed that the moisture susceptibility of asphalt mixtures increased with the addition of warm mix additive (Cheng et al. 2011, Alavi et al. 2013). At this juncture, it is not clear how the enhanced fatigue performance of the WMA mixture, if any, will be influenced by the presence of moisture.

Hydrated lime was also used successfully in the past to improve the WMA resistance towards moisture damage especially for moist aggregates (Hasan et al. 2015). Lime increases the resistance against moisture in asphalt mixtures by increasing the bond strength between asphalt and aggregate. In addition, lime-treated asphalt mixtures are less susceptible to aging compared to asphalt mixtures without lime (Little and Petersen 2005). This reduced rate of aging beneficially increases the fatigue life of asphalt mixture. Thus, the addition of hydrated lime is found to increase the pavement life by 38 % (Little et al. 2006). It was observed that hydrated lime also exhibits the filler effect. In addition, it reacts chemically and changes the physical state of the asphalt binder related to asphaltene, and component compatibility of asphalt (Lesueur et al. 2013). Hydrated lime as a filler in asphalt increases the stiffness of the asphalt mastic compared to mastic with the normal mineral filler (Kim et al. 2008). This increase in stiffness is expected to reduce the fatigue life of the asphalt mixture. The condition at which the filler effect dominates the aging effect on fatigue has not been understood to the required rigor. The filler effect was observed to be more dominant above room temperature. Thus, there is a need to quantify the precise role of hydrated lime on the fatigue life of both the HMA and WMA mixtures.

Next chapter includes the discussion related to the materials used in the study and fabrication of compacted asphalt mixtures.

CHAPTER 3

MATERIALS AND FABRICATION OF SPECIMEN

3.1 Introduction

The present chapter discusses the materials used for the study and fabrication of compacted asphalt mixtures. VG30 grade asphalt and aggregate from two sources are used in the study. Two additives, a surfactant based warm mix additive is used to produce warm mix asphalt, and hydrated lime is added to improve moisture resistance. Bituminous concrete grade 2 (BC gradation-2) mixtures was produced through Marshall compaction and shear box compactor to fabricate cylindrical and beam specimens respectively. Marshall specimens were compacted to 7 ± 0.5 % air voids; whereas, shear box specimens were compacted to 4 ± 0.5 % air voids. Four types of mixtures namely VG30, VG30-WMA, VG30-L, and VG30-WMA-L were produced and tested in this study. Here, VG30 represents the HMA mixture without hydrated lime, VG30-WMA represents the WMA mixture without hydrated lime, VG30-L represents the HMA mixture with hydrated lime, and VG30-WMA-L represents the WMA mixture with hydrated lime.

Table 3.1: Properties of aggregate from Warangal quarry

Property	Test result	Specifications (MoRTH, 2013)
Bulk specific gravity	2.644	-
Combined flakiness and elongation index	27%	Max. 35%
Los Angeles abrasion value	22%	Max. 30%
Aggregate impact value	16%	Max. 24%
Water absorption	0.60%	Max. 2%
Retained coating of asphalt over aggregates	99%	Min. 95%

3.2 Aggregate

Locally available granite aggregate obtained from two sources are used for the study. Aggregate from Warangal quarry is used for preparing Marshall specimens and was tested for indirect tensile strength and the aggregate from the Chennai quarry is used to prepare shear box beams and were tested for fatigue. The basic tests on aggregates were investigated and

are tabulated in Table 3.1 and Table 3.2 for Warangal quarry and Chennai quarry respectively. Bituminous Concrete (BC) Grading II is adopted for the study, as it is used for wearing or profile corrective course as recommended by MoRTH (2013). Figure 3.1 shows the mid-gradation of bituminous concrete with 13.2 mm nominal maximum aggregate size selected for the study. The gradation of aggregates used for the current study is shown in Figure 3.1 where the gradation desired and the proportioned achieved matches with the mid-gradation of bituminous concrete grading II. Here, the proportion of the coarse aggregate, the fine aggregate, and the filler fractions are 38%, 55%, and 7%, respectively. The filler fraction includes 5% of aggregates passing 75 μm sieve and 2% of hydrated lime.

Table 3.2: Properties of aggregate from Chennai quarry

Property	Test result	Specifications (MoRTH, 2013)
Bulk specific gravity	2.833	-
Combined flakiness and elongation index	35%	Max. 35%
Aggregate impact value	19%	Max. 24%
Water absorption	0.40%	Max. 2%
Retained coating of asphalt over aggregates	99%	Min. 95%

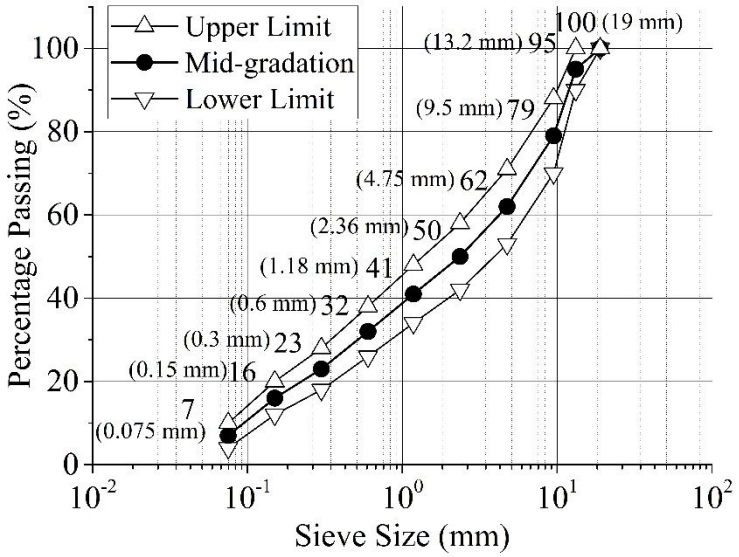

Fig. 3.1: Aggregate gradation (BC grade II) (MoRTH, 2013)

3.3 Asphalt

Unmodified VG30 asphalt following IS: 73 (2018) guidelines is selected for this study. One surfactant based warm mix additive was added to the VG30 binder at 160 °C at the proportion of 0.4 % by the weight of the binder. The proportion of warm mix additive was recommended by the manufacturer. Thorough mixing of Evotherm was achieved by mixing at 500 rpm for

15 minutes using a mechanical stirrer. The properties of the VG30 binder are shown in Table 3.3.

Table 3.3: Properties of VG30 binder

Binder Properties	Test result	Specifications (IS: 73, 2018)
Penetration, °C	47	Min. 45
Absolute viscosity (60 ºC), Poises	3335	2400-3600
Kinematic viscosity (135 ºC), cSt	534	Min. 350
Softening point, °C	52	Min. 47
Solubility in trichloroethylene, %	99	Min. 99
Flash point, °C	315	Min. 220
Test on residue after thin film oven test		
Viscosity ratio (60 °C)	2.93	Max. 4.0
Ductility (25 °C), cm	100+	Min. 40

3.4 Evotherm

Evotherm is a surfactant based warm mix additive. Evotherm is predominantly a chemical package that consists of cationic emulsification agents, chemicals to improve workability, and additives to enhance aggregate wetting and adhesion (Hurley and Prowell 2006). Evotherm was first introduced by MeadWestvaco in 2005 as a water-based emulsion technology as 'Evotherm ET'. Evotherm ET is a high residue emulsion containing about 70 % asphalt. Evotherm DAT, a dispersed additive technology was then introduced. Diluted with water, Evotherm DAT was injected directly into the asphalt line at the mixing plant. In 2008, Evotherm 3G, the third-generation water free technology was introduced. As the water was not used in this technology, the chemical additive was directly added to asphalt (NCHRP 691 2011). The surfactant based chemical present in Evotherm reduces the surface tension within asphalt as it enhances the wetting of aggregate at about 20-40 °C lower than conventional asphalt mixtures. The adhesion, workability, and compaction effort of the mixture is also improved at this lower working temperature. As recommended by the manufacturer, the Evotherm 3G dosages for unmodified binder range from 0.25 to 0.50 % and that of the modified binder are between 0.3 to 0.75 %. For this study, the Evotherm 3G is used and 0.4 % by the weight of VG30 binder was added to produce WMA mixtures.

3.5 Hydrated Lime

Hydrated lime or calcium hydroxide is an inorganic compound, obtained from slaking calcium oxide in water. For this study, hydrated lime is used as an anti-stripping additive and was added to both HMA and WMA. Lime when added to the asphalt mixture, interacts with both aggregate and asphalt physically and chemically to increase the bond between asphalt and aggregate surface. There exist four methods to add hydrated lime into the asphalt mixture (Little et al. 2006). In the first method, hydrated lime in powder form is directly added to the mixture in the mixing drum. In the second method, hydrated lime is added to dry aggregate and mixed in a pug mill. In the third method, hydrated lime is mixed with moist aggregate, and the aggregate-lime mixture is allowed to dry before mixing with asphalt and in the fourth method, slurry lime is mixed with dry aggregate. Physical properties of hydrated lime to be used in asphalt mixtures were satisfied as the maximum retained residue on 600-micron sieve and maximum retained residue on 75-micron sieve are 0.06 % (max. 3%) and 6.95 % (max. 20%), respectively as per AASHTO M303 (2014). The specific gravity of hydrated lime was found to be 2.349. For the preparation of asphalt mixture specimens, 2% hydrated lime by weight of aggregate was used by replacing equal weight of filler passing 75 μm sieve in the Bituminous Concrete mid-gradation. For this study, the second method is used to add hydrated lime. Hydrated lime was added to the batched dry mineral aggregate and was placed in a hot dry oven at mixing temperature for one hour.

3.6 Mixing and Compaction Temperature

Asphalt was mixed with aggregate and compacted at an elevated temperature such that the binder completely coats the aggregate and desired volumetric properties of the compacted mixture were attained. This makes the identification of mixing and compaction temperature an important parameter. To ensure proper wetting of aggregate and desired compaction of the asphalt mixture, the asphalt must attain specified viscosity. Two trials of viscosity data were collected using a rotational viscometer at 130, 140, 150, 160, and 170 °C to determine the mixing and compaction temperature as per ASTM D4402 (2015). The rotational speed of the spindle was set at 45, 55, 70, 75, and 95 RPM for 130, 140, 150, 160, and 170 °C respectively, to maintain the torque limit of the equipment within 10 to 90 %. The viscosity response of the VG30 binder at different temperature was assumed to be Newtonian and is shown in Figure 3.2. The average of stabilised viscosity at the 6^{th}, 7^{th}, and 8^{th} minute was taken (Table 3.4) and plotted against temperature as shown in Figure 3.3. The temperature

range at which the binder viscosity for mixing (170± 20 cSt) and compaction (280 ± 30 cSt) is attained were determined as per Asphalt Institute (2014).

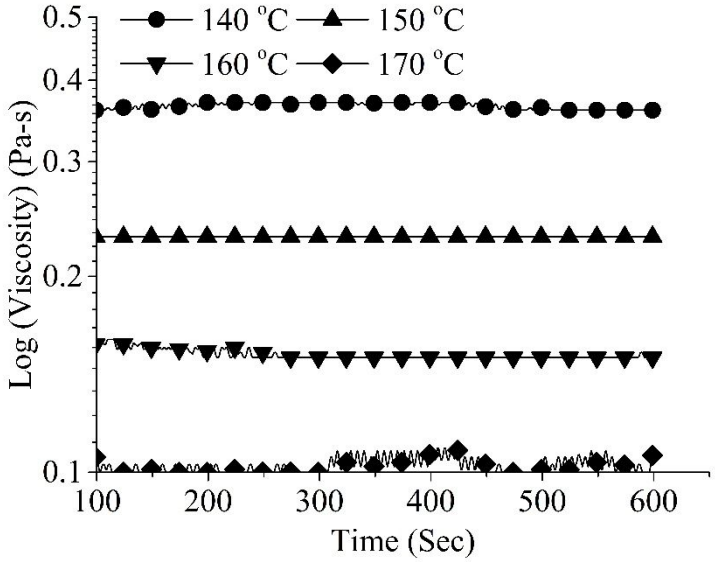

Fig. 3.2: Viscosity of VG30 asphalt at various temperatures

Table 3.4: Stabilised viscosity at different temperatures for VG30 asphalt

Time, min.	Viscosity, mPa-s			
	140 °C	150 °C	160 °C	170 °C
6th	376.4	238.6	156	108.4
7th	376.3	238.6	156	108.4
8th	370.9	238.6	156	107.4

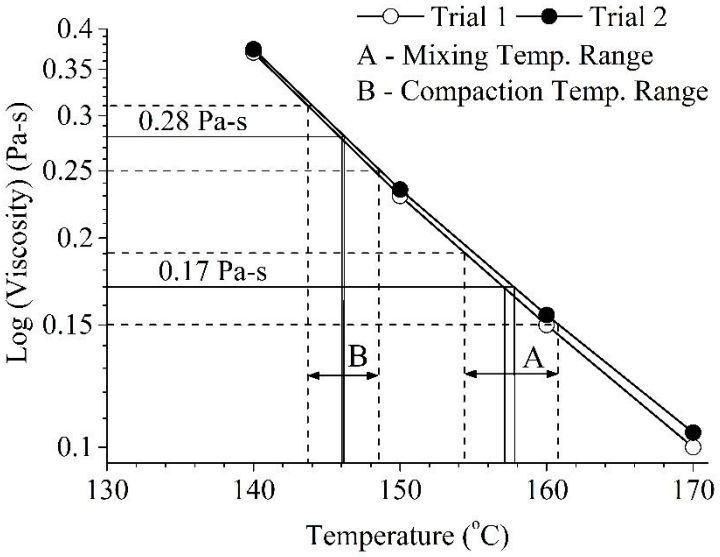

Fig. 3.3: Mixing and compaction temperature range for VG30 asphalt

After mixing, the asphalt mixtures were subjected to short-term conditioning for four hours to simulate the change in properties of the material in the plant for both HMA and WMA as per AASHTO R30 (2015). For WMA, mixing and compaction temperatures were decreased by 25 °C, as warm mix additive provides increased workability at a lower temperature (Hurley and Prowell 2006, Button et al. 2007). Table 3.5 shows the mixing and compaction temperature for HMA and WMA.

Table 3.5: Mixing and compaction temperatures for HMA and WMA

Binder	Temperature, °C			
	Aggregate	Mixing	Compaction	Short-term conditioning
VG30	175	160	150	135
VG30 with Evotherm	145	135	125	110

3.7 Marshall Mix Design

Marshall mix design method as per Asphalt Institute (2014) is used to determine optimal binder content for asphalt mixtures. Three sets of specimens were prepared at 5.2, 5.4, 5.6, 5.8, and 6 % binder content with Warangal quarry aggregate. The specific gravity of binder used in the study was 1.013. The asphalt mix was compacted using a Marshall compactor by applying 75 blows on each face to produce specimens of size 101 mm diameter and 63.5 mm height. All the specimens were tested for Marshall stability and Marshall flow value using Marshall testing equipment. Binder content was chosen at 4% air voids and is marked ‘A’ as shown in Figure 3.4a. Corresponding to the value of ‘A’, parameters Marshall stability (B) and Marshall flow (C) are determined as shown in Figure 3.4a and 3.4b respectively. Percentage voids in mineral aggregate and percentage voids filled with binder were computed accordingly. The optimum binder content (OBC) was determined such that all the parameters corresponding to binder content (A) at 4% air voids were satisfied in accordance with MoRTH (2013) and the consolidated results are presented in Table 3.6. The variation of bulk specific gravity as a function of binder content is shown in Figure 3.4b. The OBC thus computed is 5.7 % for Warangal quarry aggregate.

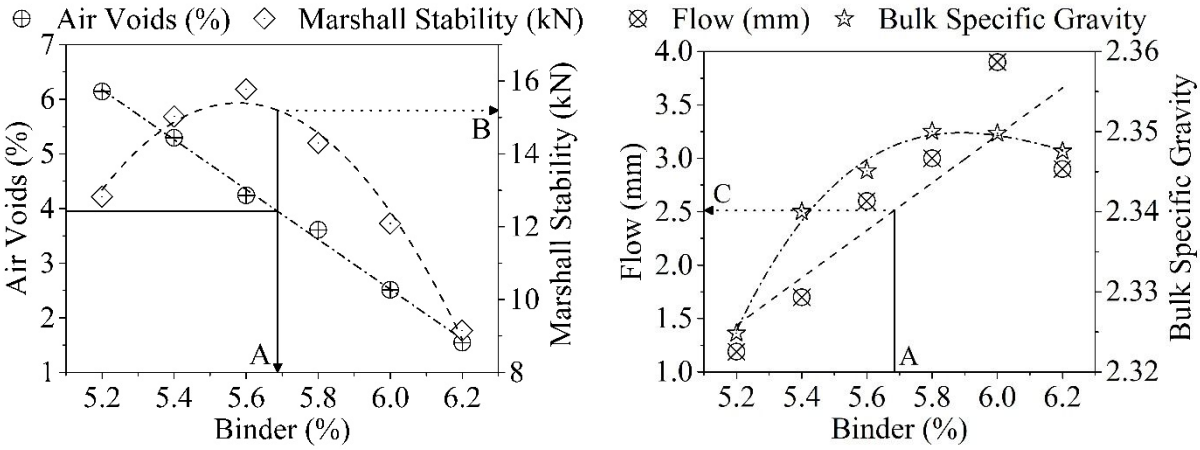

Fig. 3.4: Determining optimum binder content

Table 3.6: Properties of compacted asphalt mixtures

Mix design property	Test result	Specifications (MoRTH, 2013)
Air voids, %	4.041	3 to 5
Marshall stability, kN at 60 °C	15.1	Min. 9
Marshall flow, mm	3.2	2 - 4
Marshall quotient	4.7	2-5
Voids in mineral aggregate, %	16.21	Min. 13
Voids filled with asphalt, %	74.8	65 to 75
Optimum asphalt content, %	5.7	Min. 5.4

3.8 Theoretical Maximum Specific Gravity (G_{mm})

Theoretical maximum specific gravity (G_{mm}) was calculated in accordance with ASTM D6857 (2009). 2000 g of the loose mixture (Figure 3.5a) of BC grading II was prepared at mixing temperature. The mixture was placed at compaction temperature for 2 hours for volumetric conditioning as per AASHTO R30 (2015). The mixture was allowed to cool at room temperature while the particles were separated by hand (Figure 3.5b). G_{mm} was determined using the Corelok (Figure 3.5c). The measured G_{mm} values for Warangal aggregate and Chennai aggregate are shown in Tables 3.7 and 3.8 respectively. Tables 3.7 and 3.8 shows the maximum specific gravities obtained in various trials for Warangal quarry aggregates and Chennai quarry aggregates at 5.7% and 5.0% bitumen contents respectively.

a) Mixing for G_{mm}

b) Particle separation

c) Corelok

d) Vacuum sealed asphalt mixture

Fig. 3.5: G_{mm} measurement using Corelok

Table 3.7: G_{mm} for Warangal quarry aggregate

Sample	Binder	Sample weight, g	G_{mm}	Mean	Standard deviation
Trial 1	VG30	1395.44	2.448	2.448	0.0034 < 0.007 (ASTM D6857, 2018)
Trial 2	VG30	1389.31	2.451		
Trial 3	VG30	1378.54	2.449		
Trial 4	VG30	1397.91	2.443		

Table 3.8: G_{mm} for Chennai quarry aggregate

Sample	Binder	Sample Weight, g	G_{mm}	Mean	Standard deviation
Trial 1	VG30	1988.11	2.603	2.604	0.0037 < 0.007 (ASTM D6857, 2018)
Trial 2	VG30	1988.10	2.601		
Trial 3	VG30	1989.82	2.601		
Trial 4	VG30	1989.36	2.608		
Trial 5	VG30	1981.76	2.604		
Trial 6	VG30	1983.75	2.610		

3.9 Compaction of Asphalt Mixtures

3.9.1 Marshall Specimen

Aggregates (Warangal quarry) were sieved and batched to weigh 1200 g. Aggregate and binder were heated to mixing temperature and mixed uniformly. Following AASHTO R30 (2015), short term conditioning was carried out for four hours, and the mixture was heated to

compaction temperature. It should be noted here that neither ASTM nor AASHTO procedures recommend any curing for Marshall specimens, whereas Asphalt Institute suggests conditioning the Marshall specimen in accordance with AASHTO R30 (2015) before compaction (Asphalt Institute 2014). With the trial and error method, it was observed that 7 ± 0.5 % air voids could be achieved when 31 blows were applied on both faces of the Marshall specimen. The mixture was then placed inside the Marshall mould and compacted to 7 ± 0.5 % air voids. Cylindrical Marshall specimens of diameter 101 mm and height 63 mm were prepared and are shown in Figure 3.6. The compacted specimen along with the mould was allowed to cool for 12 hours before the specimen was extracted. All Marshall specimens were prepared to 7 ± 0.5 % air voids and were tested for indirect tension test (ITS). The list of the specimens prepared and tested is shown in Appendix A.

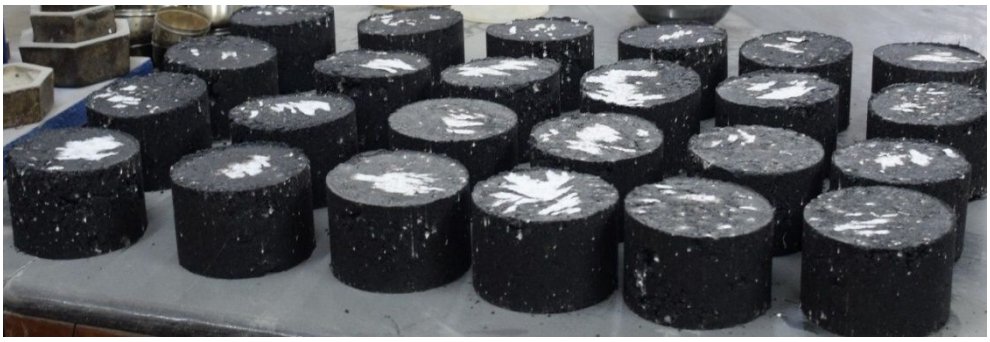

Fig. 3.6: Marshall specimen

3.9.2 Shear box Specimen

A shear box compactor is used to prepare beam specimens to be tested for fatigue. Binder content of 5 % was used with Chennai quarry aggregate to prepare shear box beams. As the specific gravity of aggregate from the Chennai quarry is 2.833, higher than 2.7; reduced binder content (5 %) was used as suggested by MoRTH (2013). Just enough binder was added to aggregate such that the compacted asphalt mixture has both viscous and elastic property and is impervious (Krishnan and Rao 2001). Asphalt mixtures were compacted using a shear box compactor following ASTM D7981 (2015). Sieving of aggregate was done using a mechanical sieve shaking machine, and aggregates of specific sizes were sorted (Figure 3.7a). The sieved material was then used for batching the required gradation to prepare the BC grade 2 mixture. Quantity of asphalt mixture required to prepare one shear box compacted beam is calculated using Equation (3.1). The batched aggregate was heated (Figure 3.7b) and mixed with asphalt at mixing temperature (Figure 3.7c) using a mechanical

mixer shown in Figure 3.7d. A compacted asphalt concrete beam of dimension 450 mm × 150 mm × 169 mm is shown in Figure 3.7e.

$$\text{Quantity of total mixture } = \frac{(100 - V_a) \times W \times L \times H \times G_{mm}}{1000}. \quad (3.1)$$

where, V_a is the target air voids (%), W is the width of the beam, L is the length of the beam, H is the height of the beam, and G_{mm} is the theoretical maximum specific gravity of the asphalt mixture. The height of the beam was set to 169 mm, such that four fatigue beams can be produced after slicing the shear box compacted beam. The width and length of the shear box beam are 150 mm and 450 mm respectively. For 4 % air voids and G_{mm} of 2.604, the total weight of the total mixture is 28.5 kg.

UTS16 software complying with ASTM D7981 (2015) is used to operate the shear box compactor (Figure 3.8). Total specimen weight, vertical stress, and G_{mm} were given as the input parameters along with termination air voids in UTS16 software. The compaction process automatically stops on reaching the termination air voids. The termination air voids were given higher than the desired air voids of the sliced beam so that the final air voids of the fatigue beam after slicing is in the range of 4 ± 0.5 %. With the trial and error method, the termination air voids of 5.6 % were selected. Vertical stress of 600 kPa was applied and the specimen was subjected to lateral stress to produce 4° sway in to and fro motion and the shear force measured in the load cell was recorded (ASTM D7981 2015). This allows the aggregate to reorient to achieve the desired compaction. The densification curve with respect to variation in shear force and air voids is shown in Figure 3.9. WMA specimens were prepared with a similar compaction effort to that required for HMA at reduced temperature. A total of 28.5 kg of the mixture were mixed in four batches of 7 kg each in a mechanical mixer. The mixture was short-term conditioned for four hours and then heated at compaction temperature for 30 minutes before compaction. The mixture was then immediately compacted to the target air voids. The mechanism on which the shear box compactor works is illustrated in Figure 3.10. The loose asphalt mixture was subjected to shear load at the top of the mould, along with the axial load that gradually compacts the mixture to desired density. A beam of dimension 450 mm × 150 mm × 169 mm was produced using a shear box compactor.

Locally available granite aggregates were used in this study. The granite aggregates obtained from Warangal quarry with bulk specific gravity of 2.644 were used for tensile strength ratio tests whereas the granite aggregates obtained from Chennai quarry with bulk specific gravity of 2.833 were used for fatigue tests. Optimum bitumen content of 5.7% was obtained for

Warangal aggregates through the Marshall mix design and this bitumen content was used to prepare specimens for tensile strength ratio tests. However, the large-sized prismatic beams used for fatigue tests were prepared using a shear box compactor where a lower bitumen content of 5% was used. The recommended bitumen content for Bituminous Concrete grading II is minimum 5.4% corresponding to aggregate specific gravity of 2.7. As the specific gravity of Chennai aggregate is greater than 2.7, the bitumen content shall be reduced proportionately. That is, for a 0.1 increase in aggregate specific gravity, the bitumen content shall be reduced by 0.2%. Thus, the minimum bitumen content for Chennai aggregate based on Marshall mix design shall be 5.1%. However, as the shear box compactor was used to compact the specimens, 5% bitumen content was selected to prepare large-sized prismatic beam specimens. A lower bitumen content of 5% was used consistently in the past to prepare large-sized prismatic beam specimens irrespective of the type or grade of the bitumen (Gupta and Narayan 2016, Roja and Krishnan 2016, Varma et al. 2019).

a) Sieving and storage of aggregate

b) Oven dry batched aggregate

c) Binder heater

d) Mechanical mixer

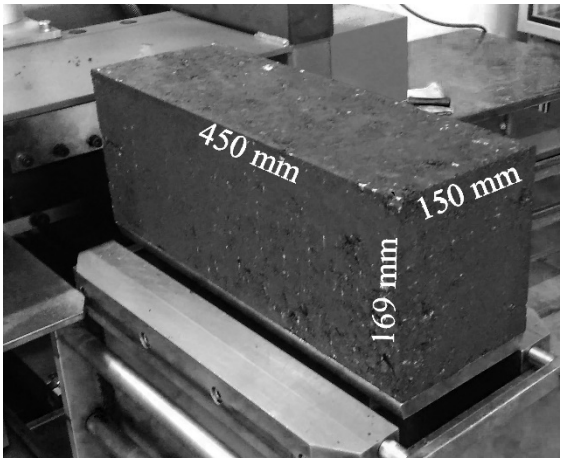

e) Compacted beam specimen

Fig. 3.7: Preparation of shear box beam

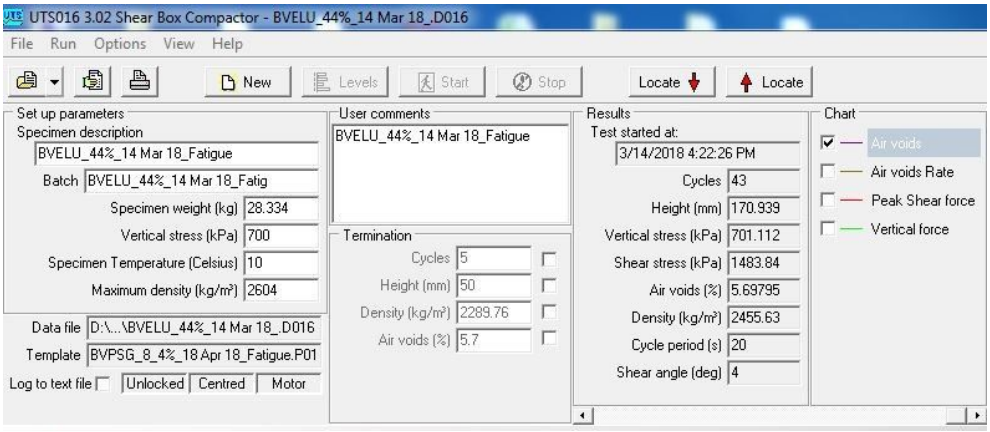

Fig. 3.8: UTS16 software

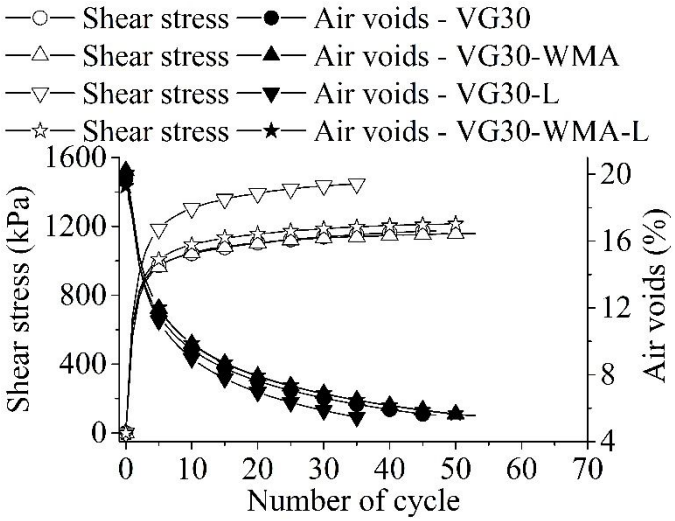

Fig. 3.9: Densification curve for VG30, VG30-WMA, VG30-L, and VG30-WMA-L mixtures

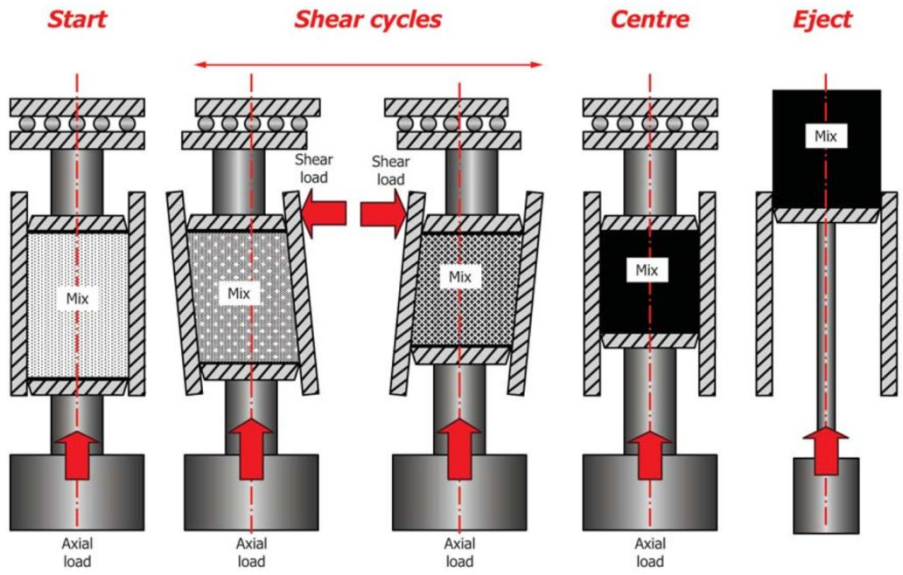

Fig. 3.10: Beam compaction process (ASTM D7981, 2015)

3.10 Production of Beam for Fatigue Test

The shear box beam was sliced as shown in Figure 3.11 using a wet-cutting diamond cutter blade setup (Krishnan and Veeraragavan 2016). The shear box beam was first sliced in two half and each half was sliced equally to obtain four beams of size 450 mm × 50 mm × 63 mm. This beam was then sliced on both sides to produce the fatigue beam of 380 mm length. Four fatigue beams of dimension 380 ± 6 mm × 50 ± 2 mm × 63 ± 2 mm were produced by slicing one large shear box beam in accordance with ASTM D7981 (2015). The shear box beam and sliced fatigue beam are shown in Figures 3.12a and 3.12b respectively. The details of specimen designation for all the mixture are listed in Table 3.9. Overall, 22 shear box beams were fabricated and 88 prismatic specimens were produced and the details of the beams tested are listed in Annexure A. Air voids of the sliced beams were then verified; the beams within 4 ± 0.5 % air voids range were used for fatigue testing. Air voids variation details of all the specimens are listed in Table 3.10. As Bituminous Concrete grading II is used for wearing or profile corrective courses, the recommended maximum air void content is 8% which corresponds to 92% of Gmm (IRC: 111 2009). Thus, a newly constructed bituminous layer is compacted to 6 to 8% air voids with an average 7% air voids. Therefore, Marshall specimens for moisture damage evaluation were prepared with 7% target air voids. The air voids in a bituminous layer at the end of design life would reach a limiting value of approximately 4% which is considered as the design air voids. Therefore, the beam specimens for fatigue testing were prepared with lower target air voids of 4% to achieve a higher fatigue life such that the damaging effect of moisture at higher strain levels could be captured.

Table 3.9: Specimen preparation details and specimen designation

Binder	Filler	Specimen Designation	
		Unconditioned	Moisture conditioned
VG30	Without lime	VG30	VG30-MC
	With lime	VG30-L	VG30-L-MC
VG30 + warm mix additive	Without lime	VG30-WMA	VG30-WMA-MC
	With lime	VG30-WMA-L	VG30-WMA-L-MC

Table 3.10: Total number of beams produced and air voids range

Asphalt Mixture	Number of specimens	Air voids range (%)
VG30	16	3.598 - 5.334
VG30-WMA	16	3.338 - 4.651
VG30-L	20	3.393 - 5.144
VG30-WMA-L	20	3.201 - 6.276

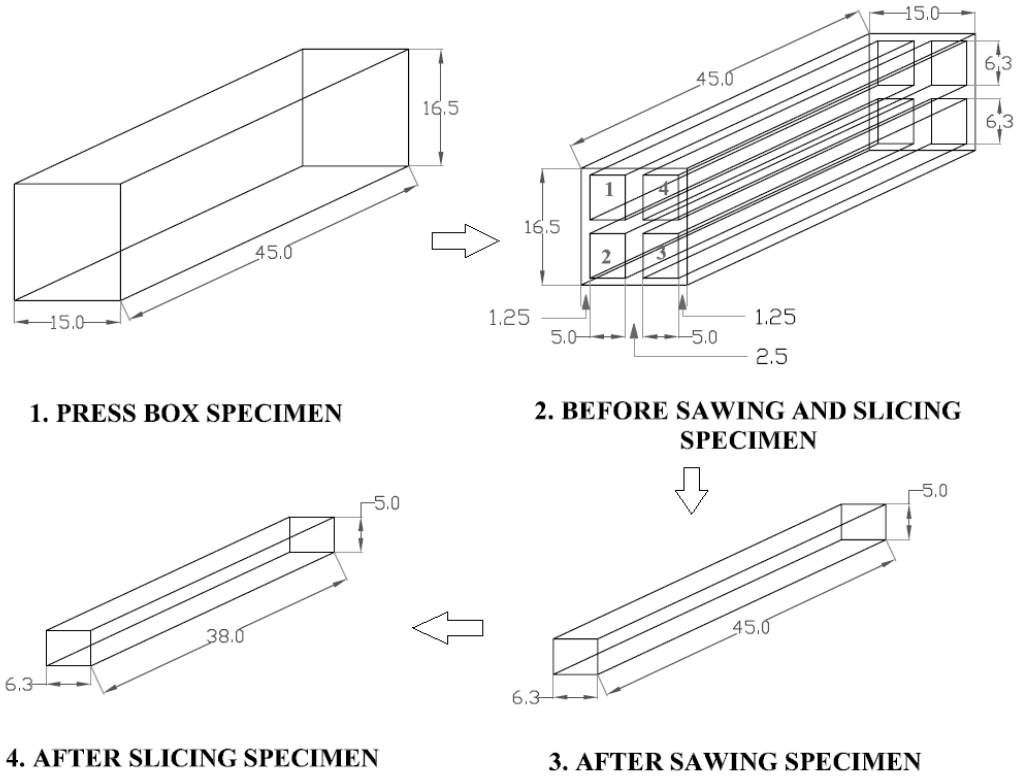

Fig. 3.11: Slicing of shear box beam (Krishnan and Veeraragavan 2016)

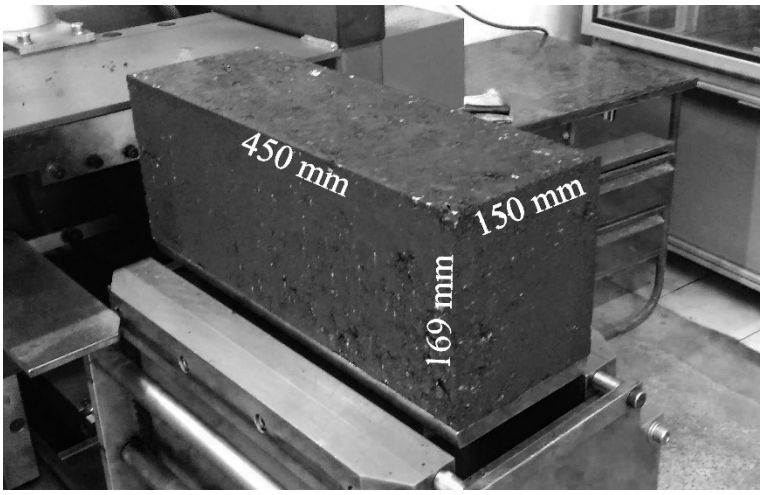

(a)

(b)

Fig. 3.12: (a) shear box beam (b) sliced beams

3.11 Summary

VG30 binder along with aggregate from two sources, the Warangal quarry, and the Chennai quarry was used in the study. Surfactant based warm mix additive Evotherm was used to produce warm mix asphalt. HMA and WMA specimens were produced through Marshall compaction and shear box compaction methods. HMA was produced at 150 °C whereas WMA was produced at 125 °C. Marshall specimens were prepared at 7 ± 0.5 % air voids to be tested for indirect tension strength, whereas shear box specimens were produced at 4 ± 0.5 % to be tested for fatigue. It was observed that the number of cycles for compaction of WMA at a reduced temperature was similar to that of HMA. Further, the conduct of experiments is discussed in the next chapter.

CHAPTER 4

EXPERIMENTAL INVESTIGATION

4.1 Introduction

To proceed with the proposed objective, the current chapter includes the methodology (Figure 4.1) to carry out the experimental investigation. Four types of asphalt mixtures including VG30, VG30-WMA, VG30-L, and VG30-WMA-L were prepared. Both the Marshall and beam specimens were tested in unconditioned and moisture conditioned form. The cylindrical Marshall specimens tested for ITS and TSR were used to evaluate the moisture resistance of various mixtures whereas, beam specimens were tested for fatigue and load-deformation data was recorded. PID tuning was carried out to obtain desired sinusoidal load-deformation waveform. This data was used to compute stress-strain data for the ongoing analysis.

Traditionally, AASHTO T283 (2014) test protocol is practised to simulate the moisture damage conditions in the laboratory. This protocol is prescribed for cylindrical specimen geometries. A moisture-conditioned specimen is subjected to indirect tension testing and the ratio of the failure load with a control specimen is used as a criterion to rank asphalt mixtures. In such procedures, the specimen is compacted to in-place air voids after construction (≈ 6-8 %), and hence the saturation of the specimen to the required level (70-80 %) is fairly straightforward and the whole process can be finished in 15 to 20 minutes. It is not clear whether such procedure could be adapted to quantify the moisture damage of beam specimen, where one is interested in characterizing the influence of moisture damage on the fatigue characteristics. Such specimens are compacted to 4 % air voids and hence subjecting the specimens to the required degree of saturation is not straightforward. It is also not clear how to saturate prismatic beam at 4 % air voids and what effect will the presence of additive will have on the degree of saturation.

The fatigue performance of asphalt mixtures is evaluated in the laboratory using a four-point beam bending test setup under controlled conditions. This test setup utilizes large-sized prismatic beam specimens. As the moisture damage accelerates the distresses in asphalt mixtures, quantification of such mechanisms requires moisture conditioning of the

specimens. Post moisture conditioning, these specimens can be further evaluated for fatigue response. As there is no standard test protocol available for moisture conditioning of these specimens, the initial focus of this study is on development of the moisture conditioning process for large-sized prismatic beam specimens.

From the ITS test, the influence of WMA and hydrated lime on TSR was evaluated and the observations are documented. The stress-strain data from the fatigue test was used to compute the evolution of flexural stiffness and total energy dissipation, which was used to verify the influence of WMA additive, hydrated lime, and moisture. Fatigue life using AASHTO, ASTM, energy ratio, and the ratio of dissipated energy change were computed. Further, the stress-strain data was used to separate damage dissipation and viscous dissipation from total dissipation using a pseudo strain concept, a constitutive assumption approach, and a linear viscoelastic rate type model.

4.2 Moisture Conditioning

4.2.1 AASHTO T283 Conditioning (AASHTO T283, 2014)

Two sets of specimens were prepared such that, air voids in both the sets are within the tolerance limits of 7 ± 0.5 % for the Marshall specimen. The first set of specimens were tested without conditioning. The second set of specimens were moisture conditioned following AASHTO T283 (2014). For saturation, a partial vacuum of 660 mm Hg was applied for 5 to 10 minutes with specimens submerged in water. An airtight desiccator was used for saturating the Marshall specimen. The degree of saturation was calculated by dividing the volume of the absorbed water by the volume of air voids as expressed in Equations (4.1) and (4.2).

$$S = \frac{100 \times (\mathrm{W_{sat}} - \mathrm{W_d})}{Vol_{air}}, \tag{4.1}$$

$$Vol_{air} = \frac{V_a \times V_{beam}}{100}. \tag{4.2}$$

where, S is the degree of saturation (%), W_{sat} is the saturated surface dry weight of beam after saturation (g), W_d is the weight of dry beam in the air (g), Vol_{air} is the volume of air voids (cm^3), V_a is the air voids (%), and V_{beam} is the volume of the beam (cm^3).

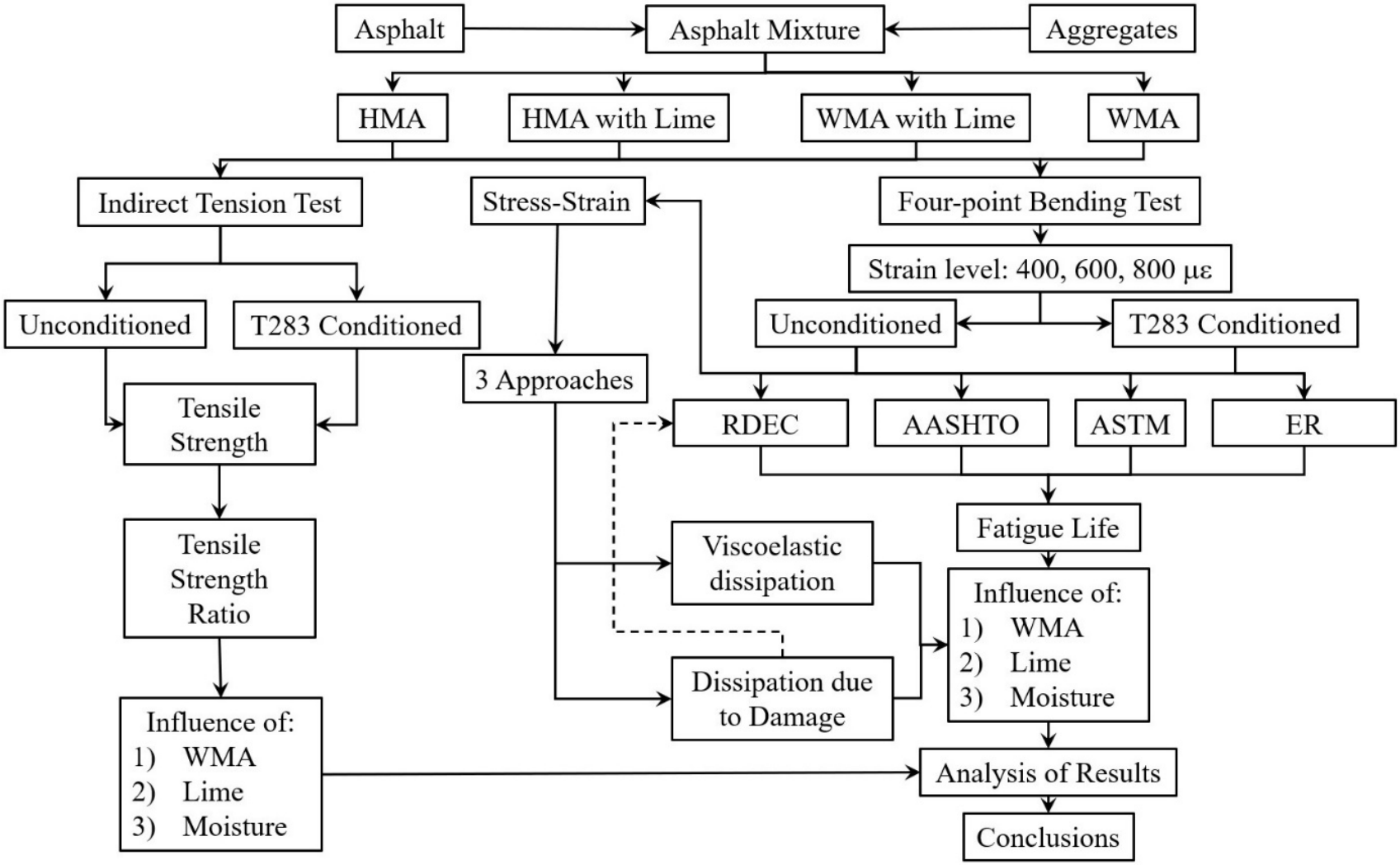

Fig. 4.1: Methodology flowchart

The specimens with the degree of saturation between 70-80 % were selected for testing. For the low degree of saturation (less than 70 %), the specimen was further subjected to saturation with a slightly higher partial vacuum at 700 mm Hg. For the degree of saturation more than 80 %, the specimen was considered to be damaged and were discarded. The specimens with saturation within 70 to 80 % were wrapped with plastic shrink wrap and sealed in a plastic bag containing 10 ± 0.5 ml of water. The specimens were then subjected to freezing at -18 ± 3 °C (Figure 4.2a) for 16 ± 1 hours and thawing at 60 ± 1 °C (Figure 4.2b) for the next 24 ± 1 hours. The time taken to reach 70-80 % saturation for Marshall specimen compacted to 7 ± 0.5% air voids ranges between 10 to 20 minutes.

a) Freezing b) Water bath

Fig. 4.2: Freezing and thawing process

4.2.2 Prismatic Beam Conditioning

The vacuum system consists of a vacuum pump, a non-return valve, a vacuum dial gauge, a vacuum controller, a moisture trap, and a glass vacuum chamber (Figure 4.3a). The high capacity vacuum pump used in this study is capable of applying vacuum up to 760 mm Hg. The non-return valve ensures that once the vacuum was created in the vacuum chamber, no air leakage occurs from the vacuum pump that in turn can affect the vacuum created in the chamber. It was also checked and ensured that there was no air leakage from any joints and the push-in pipe. A calibrated dial gauge was installed to accurately measure the applied vacuum. A trial and error approach was adopted to determine the intensity of partial vacuum for saturating a prismatic beam specimen. It was ascertained to apply a vacuum in the range of 700 to 740 mm of Hg. The vacuum controller, directly connected to a power supply of the vacuum pump was used to maintain the selected vacuum. A moisture trap was installed to filter any moisture from the air flowing from the vacuum chamber towards the vacuum pump during the process of saturation. A cylindrical glass vacuum chamber of 100 mm inner diameter and 550 mm height with a glass flange on top was used for moisture conditioning of

the specimen. The thickness of the wall of the glass cylinder is 5 mm. The top flange is connected to an outlet, through which vacuum is applied. The chamber is used to submerge the sliced fatigue beam in water during the saturation process.

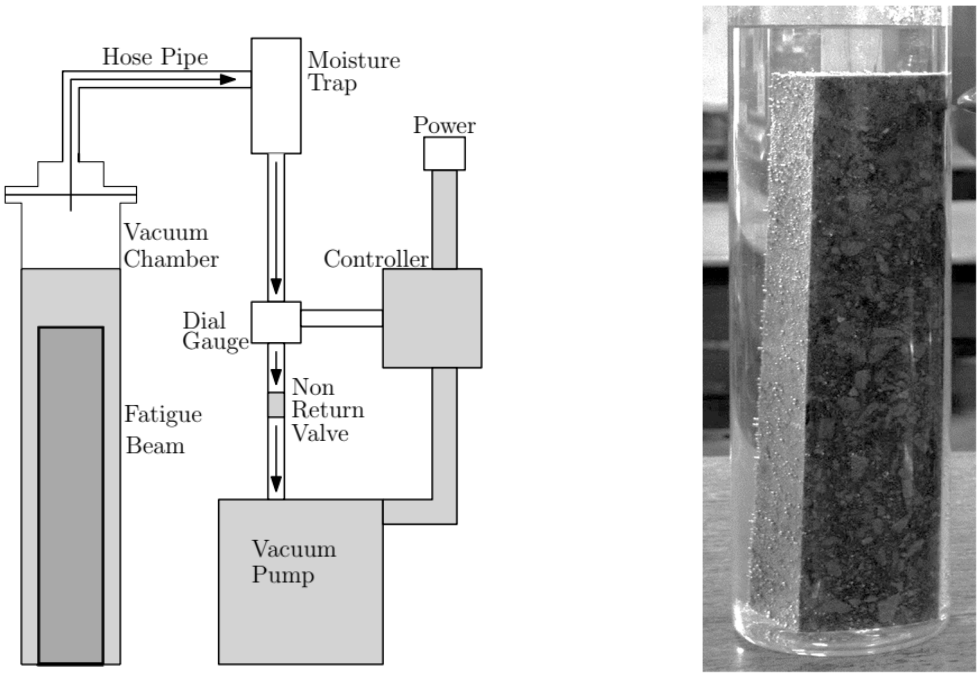

a) Vacuum saturation setup b) Specimen during saturation

Fig. 4.3: Vacuum saturation process of the beam

For moisture conditioning, the beams were saturated in water by application of partial vacuum and then subjected to freeze-thaw conditioning process in accordance with AASHTO T283 (2014) protocol. The setup for the vacuum application is shown in Figure 4.3a. For the saturation process, the beam was placed inside an airtight glass chamber of 100 mm inner diameter and 550 mm height with a glass flange on top and the beam was completely submerged in water. The vacuum during the saturation process was maintained between 740 to 700 mm Hg using a vacuum pump. Figure 4.3b shows a specimen during saturation. The existing AASHTO protocol (AASHTO T283 2014) is designed for a cylindrical specimen of 100 mm diameter and 63 mm height with a volume of $4.948\times10^{-4}m^3$ and a surface area of 0.0355 m^2 at 7 % air voids. This protocol suggests saturating the compacted asphalt mixture specimen to 70 to 80% and the time required for attaining this saturation level is found to be less than 5 to 10 min. In this study, the volume of the beam specimen used is 12.16×10^{-4} m^3 with a surface area of 0.09218 m^2. The initial air voids of the beam specimen are 4%. As no standard testing protocol exists for vacuum saturation of beam specimens, many preliminary trials of experiments were conducted to determine the time required to achieve the required degree of saturation. Since the volume of the specimen used in this study is high, the time

duration to achieve the required degree of saturation was found to be considerable. It was seen that specimens prepared with VG30 binder after saturating for 3 hours attained the degree of saturation between 70-80 %. The optimum time required to saturate the fatigue beam was found to be 3 hours. The air voids range, duration of saturation, and degree of saturation details for the test conducted are specified in Table 4.1.

Table 4.1: Details of data collected for the study

Asphalt mixture	Air voids range (%)	Duration (h)	No. of specimens	Degree of saturation (%)
VG30	4.1-4.5	3	3	68-82
VG30-WMA	3.8-4.5		8	75-82
VG30-L	3.9-4.3		4	68-74
VG30-WMA-L	3.5-4.6		8	67-81

The degree of saturation is calculated using the difference in weight in air of fatigue beam before and after saturation as shown in Equation (4.1) and the volume of air voids is computed using Equation (4.2). The beams were kept in a freezer maintained at -18 ± 3 °C for 16 hours and then placed in the water bath at 60 ± 0.5 °C for 24 hours. The moisture conditioned beams were then maintained at 20 °C for 2 hours before testing.

Analysis of Variance (ANOVA) was carried out to find the influence of various parameters on the degree of saturation. One-way ANOVA was performed at a 95% confidence interval. The influence of additive (Evotherm, hydrated lime, and Evotherm with lime) used was assessed. The fixed variable is the type of additive used in the study and the response variable is the degree of saturation. The null hypothesis for the study was stated as, that there is no statistical difference in the means between the variables. Also, the alternative hypothesis states that there is a statistical difference in the means between the variables. The null hypothesis was accepted if the tabulated p-value was greater than the p-critical (0.05) value, else the null hypothesis was rejected, and the alternative hypothesis was accepted.

One-way ANOVA analysis shows that there is no significant effect of the additives on the degree of saturation as shown in Table 4.2 for a given binder. One way ANOVA was carried out on 23 specimens. As the p-value (Table 4.2) is greater than 0.05 (p-critical), the null hypothesis was accepted which signifies that the means for all four variables are equal. Thus, it can be implied that the use of additives has a negligible effect on the variation of the degree

of saturation for a given binder. Within a given binder at analogous air voids and partial vacuum, the degree of saturation had no significant variation on the addition of Evotherm, lime, or Evotherm and lime together.

Table 4.2: Effect of additive on the degree of saturation (%)

Additive	VG-30				
	Mean	SD	f*	f	p
Control	76	7.9	3.1	2.1	0.12
Evotherm	78	4.0			
Lime	71	2.7			
Evotherm and lime	74	5.8			

Here, SD is the standard deviation, f* represents f critical, f represents the f calculated and p represents the p-value.

4.3 Indirect Tensile Strength (ITS) Test

Indirect tensile strength test was performed on cylindrical specimens by subjecting them to a constant displacement rate acting parallel to the vertical diametric plane using the uniaxial testing machine with a displacement rate of 50 mm per minute as per ASTM D6931 (2017). The specimens were soaked in a water bath at test temperature for 2 hours at 25 °C before testing for both unconditioned and moisture conditioned state. Three repetitions at each variable combination were carried out and the details are shown in Table 4.3. The ITS is calculated using Equation (4.3). The TSR is determined as the ratio of the ITS of conditioned specimens to the ITS of unconditioned specimens as given by Equation (4.4).

Table 4.3: ITS Test matrix

Conditioning	Test variables	Number of specimens			
	Temperature (°C)	VG30	VG30-WMA	VG30-L	VG30-WMA-L
Unconditioned	-	3	3	3	3
AASHTO T283 conditioned	-18 °C for 16h and 60 °C for 24h	3	3	3	3

$$\text{ITS} = \frac{2P}{\pi Dt}. \quad (4.3)$$

$$\text{TSR} = \frac{ITS_{wet}}{ITS_{dry}}. \quad (4.4)$$

where, P is the peak applied load (kN), D is the diameter of the specimen (mm), t is the thickness of the specimen (mm), ITS_{wet} is the indirect tensile strength of wet specimen, and ITS_{dry} is the indirect tensile strength of the unconditioned specimen.

The within-laboratory ITS value precision based on the standard deviation (SD) for cylindrical specimens of diameter 101.6 mm at 25 °C is 80 kPa as stated in ASTM D6931 (2017). The precision for the ITS test conducted for the study is shown in Table 4.4.

Table 4.4: Precision for ITS test for VG-30 (ASTM D6931, 2017)

Specimen	Unconditioned		AASHTO T283 conditioned		
	ITS, kPa	SD	ITS, kPa	Saturation range	SD
VG30	1549	47.08	1037	71.7 - 73.2	64.3
VG30-WMA	1156	59.12	694	72.2 - 78.5	35.26
VG30-L	796	3.99	781	63.7 - 68	32.8
VG30-WMA-L	1179	33.15	1102	73.1-78	54.26

4.4 Fatigue Test

4.4.1 Four Point Bending Jig

The load and deformation data of the asphalt mixture beam specimen was captured using a four-point bending jig (Figure 4.4) mounted inside an environmental control chamber. The apparatus consists of a pneumatic loading system, four-point bending jig, environmental chamber, IMACS integrated multi-axis control system, and data acquisition system (IPC Global 2016). The pneumatic control system ensures accurate control on load and sinusoidal waveshape with 10 Hz frequency and forces the specimen to return to its original position (AASHTO T 321-14). The four-point bending jig allows backlash free rotation and translation on all load and reaction points (Figure 4.5). The environmental chamber was maintained at the test temperature at 20 ± 0.5 ºC.

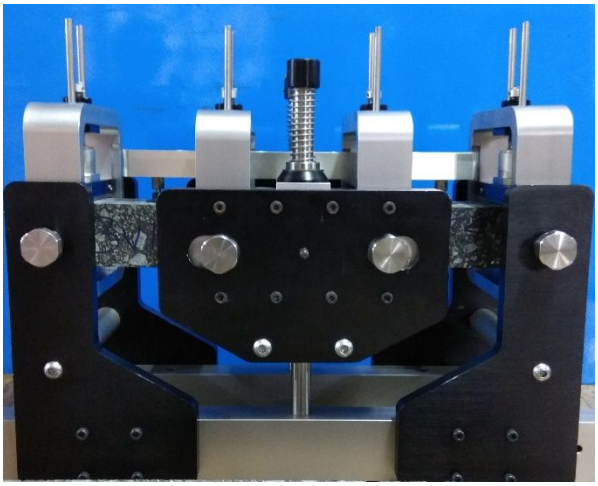

Fig. 4.4: Four-point bending jig

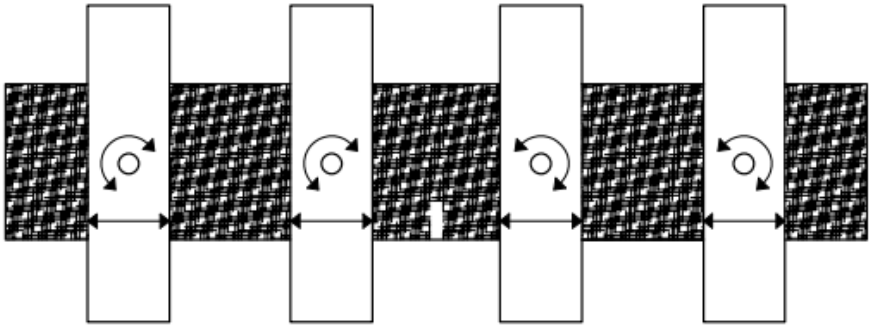

Fig. 4.5: Free rotation and translation of beam (AASHTO T 321-14)

4.4.2 UTS15 Software (IPC Global 2011)

For the beam fatigue test, 'UTS015' software (IPC Global 2011) was used to control and operate the fatigue test using four-point bending equipment as shown in Figure 4.6. A test template is created before every test to provide the test parameter for which the specimen is to be tested. Specimen identification details are given as input in the 'general' option, and specimen dimensions in the 'specimen' option. In the 'test parameter' option test details such as control mode, waveshape, test temperature, frequency, pulse width, peak to peak strain, Poisson ratio, initial stiffness cycle, and test termination criteria are entered.

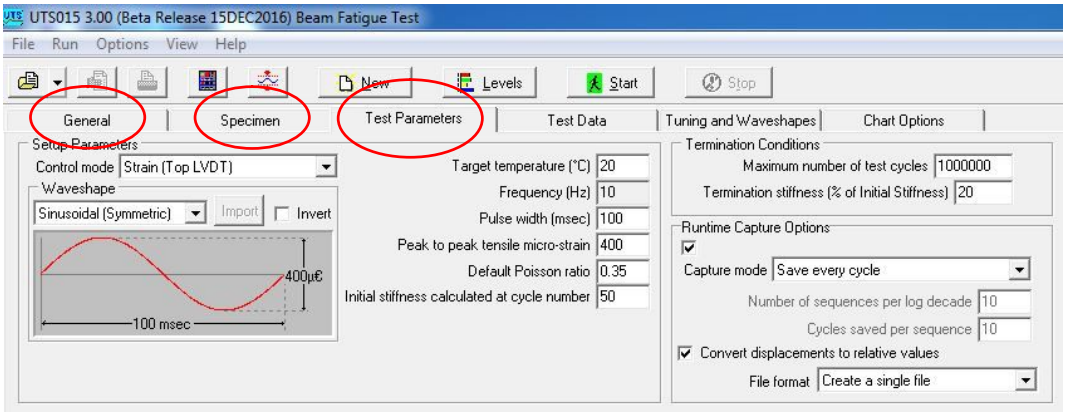

Fig. 4.6: UTS015 software manin menu

4.4.3 PID Tuning

The fatigue beam is subjected to sinusoidal bending between the inner clamps of the four-point bending setup. To ensure that the beam is experiencing a sinusoidal waveform, the actuator must be applying the right amount of load and deflection with time. PID tuning is carried out to minimize the root mean square error (RMSE) as the actuator applies load based on the value of proportional gain (P), integral gain (I), and derivative gain (D). PID tuning can be controlled from UTS015 software, under the "tuning and waveshapes" tab (Figure 4.7). Using a trial and error method different values of P, I, and D are assigned and the test is run for 1000 cycles. From these trials, the sinusoidal wave of form $a \times \sin(bx + c)$ was fit to the experimental sinusoidal waveform and PID value for which RMSE was minimum is selected for fatigue testing. Here, a, b and c are the sinusoidal wave parameters. It was observed that the value of P, I, and D for which the desired sinusoidal waveform is obtained are 500, 10 and 1200 respectively for all the mixtures (Figure 4.8). Tests were then carried out at specified PID values, and corresponding RMSE values were extracted to verify the sinusoidal waveform and these details are reported in Table 4.5.

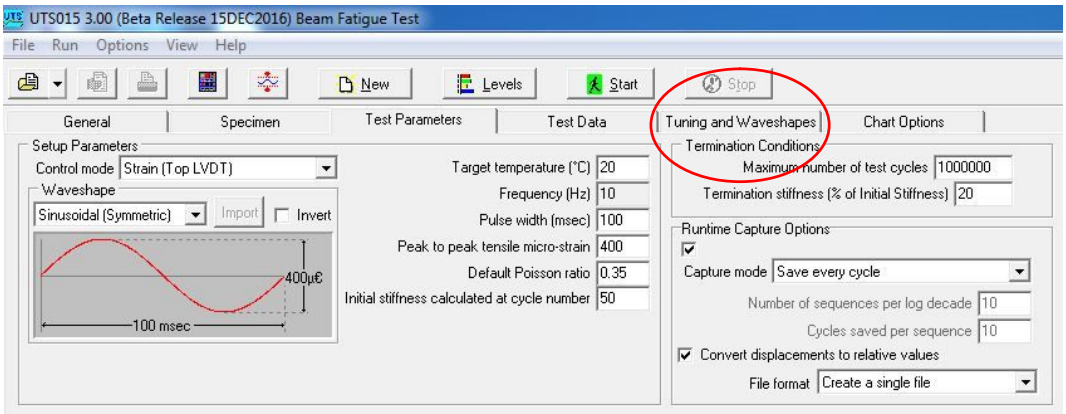

Fig. 4.7: Input parameters under 'test parameters' tab

Table 4.5: RMSE value for applied waveform

RMSE	50th cycle			1000th cycle		
	Strain			Strain		
	400 με	600 με	800 με	400 με	600 με	800 με
VG30	0.0036	0.0019	0.0033	0.0026	0.0021	0.0021
VG30-WMA	0.0011	0.0059	0.0050	0.0036	0.0057	0.0072
VG30-L	0.0010	0.0011	0.0012	0.0010	0.0040	0.0030
VG30-WMA -L	0.0010	0.0022	0.0035	0.0013	0.0047	0.0068
VG30-MC	0.0016	0.0016	0.0022	0.0013	0.0012	0.0035
VG30-WMA-MC	0.0017	0.0020	0.0204	0.0010	0.0013	0.0278
VG30-L-MC	0.0014	0.0028	0.0152	0.0012	0.0023	0.0160
VG30-WMA -L-MC	0.0015	0.0021	0.0030	0.0011	0.0021	0.0023

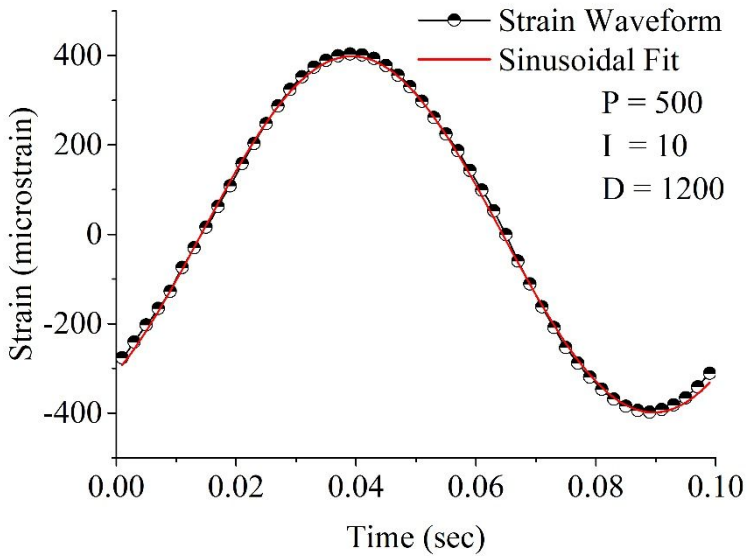

Fig. 4.8: Sinusoidal waveform at 800 microstrain

4.4.4 Four Point Bending

The unconditioned specimens and moisture conditioned specimens were tested using a four-point beam bending assembly mounted inside the temperature-controlled chamber. The repeated load in the sinusoidal pattern was applied, and the test was conducted in strain-controlled mode. The test was performed at three different strain levels including 400, 600, and 800 microstrain at 20 °C and 10 Hz frequency as shown in Table 4.6. A total of 80 beams were tested for fatigue, out of which data corresponding to 24 specimens was used for further analysis. The data acquisition system captured load and deformation with 99 data points in each cycle (0.1 s). The strain (Equation 4.5) and stress (Equation 4.6) were calculated from the respective load and deformation data as per AASHTO T321 (2014). The specimen stress and strain waveform data collected for the VG30 specimen tested at 600 microstrain is shown

in Figure 4.9. Complete waveform data were collected for every cycle and further used in all the analysis. The beam was subjected to continuous loading which terminated either on completing 1,000,000 cycles or on achieving a target reduction of 20% of the initial stiffness. The details of test termination cycles for all the specimens are listed in Table 4.7.

$$\varepsilon_t = \frac{12 \times \delta \times h}{(3 \times L^2 - 4 \times a^2)}. \quad (4.5)$$

$$\sigma_t = \frac{3 \times a \times P}{b \times h^2}. \quad (4.6)$$

where, ε_t is the maximum tensile strain, σ_t is the maximum tensile stress, δ is the maximum peak to peak deflection at the centre of the beam, P is the peak to peak load applied by actuator, h is the height of the beam, b is the width of the beam, L is the length of the beam between outer clamps and a is the space between inside clamp.

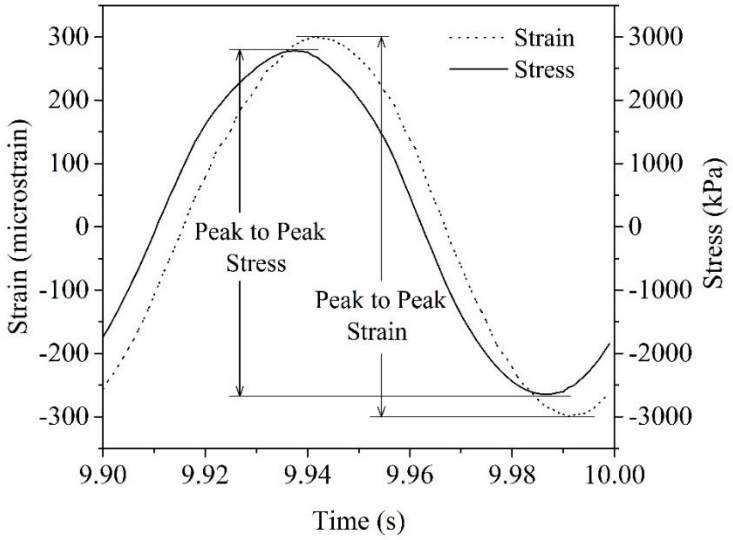

Fig. 4.9: Stress and strain waveform for VG30 specimen tested at 600 microstrain

Table 4.6: Fatigue test matrix

Asphalt mixture	Bituminous Concrete
Binder	VG30
Additive	Evotherm®, hydrated lime
Conditioning	Unconditioned, moisture conditioned
Frequency	10 Hz
Test temperature	20 °C
Peak to peak tensile micro-strain	400, 600, 800
Waveform	Sinusoidal
Test termination criterion	1,000,000 cycles (or) 20 % initial stiffness

Table 4.7: Fatigute test termination cycles

Specimen	Strain amplitude		
	400 με	600 με	800 με
VG30	55253	16990	6714
VG30-WMA	45970	17697	6427
VG30-L	104829	13698	3473
VG30-WMA-L	51089	14725	5155
VG30-MC	15389	5956	1392
VG30-WMA-MC	14779	10237	1967
VG30-L-MC	28529	6317	2268
VG30-WMA-L-MC	34206	9293	2451

The precision for four point beam bending test is not based on the actual test data collected, but on the computed fatigue life of the specimen. The standard deviation of the log of the number of cycles to failure for similar beams at the same strain level shall not exceed a value of 0.787 as stated in ASTM D7460 (2010). The precision details is shown in Table 4.8. Here the number of cycles to failure is computed following ASTM D7460 (2010).

Table 4.8: Fatigue test precision details

Specimen	Controlled micro-strain	Number of cycles to failure	Standard deviation for number of cycles to failure	Log of number of cycles to failure	Standard deviation of log of number of cycles to failure
VG30	400	35885	4941	4.555	0.066
	400	28898		4.461	
	600	12430	2632	4.094	0.109
	600	8708		3.940	
VG30-WMA	400	35431	9672	4.549	0.150
	400	21753		4.338	
	600	12946	6713	4.112	0.406
	600	3452		3.538	
VG30-L	400	74041	40948	4.869	0.468
	400	16132		4.208	
	600	9595	3067	3.982	0.185
	600	5257		3.721	
VG30-WMA-L	400	42108	25490	4.624	0.595
	400	6059		3.782	
	600	10488	5218	4.021	0.373
	600	3109		3.493	

At least two replicas of beam specimens were tested at each test condition. Altogether at least 48 specimens were tested and the data corresponding to 24 specimens was used for analysis.

4.5 Summary

In this chapter two moisture conditioning processes including AASHTO T283 conditioning for Marshall specimen, and prismatic beam conditioning process were discussed. A new process is developed in this study for moisture conditioning of the large-sized prismatic straight beam specimens. Since the beam specimens used in this study were compacted to 4% air voids, the time duration to achieve the required degree of saturation was found to be considerable. It was seen that specimens prepared with VG30 binder after saturating for 3 hours attained the degree of saturation between 70-80%. Guidelines related to the parameters to be considered during the moisture conditioning process were provided, and the relative effects of additives were quantified. Statistically, the effect of additives had no significant effect on the degree of saturation for a particular binder.

Indirect tension test and beam fatigue test were conducted to evaluate the moisture sensitivity of the asphalt mixtures. The within-laboratory precision for both the tests was obserevd to be within the limits of the given standards. Indirect tension test was conducted on Marshall specimens whereas fatigue test was conducted on beam specimens. The fatigue test was carried out at 20 °C and 10 Hz frequency at 400, 600, and 800 microstrain. PID tuning was done to assure that the waveform achieved was sinusoidal throughout the test. The next chapter discusses about the ITS test results conducted on asphalt mixtures.

CHAPTER 5

APPLICABILITY OF INDIRECT TENSILE STRENGTH TEST

5.1 Introduction

Most of the asphalt pavements fail prematurely due to poor drainage. Moisture accelerates the rate of distresses in asphalt pavements. Determination of moisture sensitivity of asphalt mixtures is one of the most critical aspects to be considered for evaluating the performance of asphalt pavements as the high moisture susceptible asphalt mixtures will deteriorate at a much rapid rate. Hence, simulation of field moisture damage conditions in the laboratory is required such that asphalt mixtures that are more resistant towards the moisture damage could be identified and used. Asphalt mixtures are subjected to the combined effects of vehicular traffic and climatic conditions over its service life. The loss in durability increases when this loading and unloading happens in the presence of water. Thus, it is very much essential to evaluate the moisture resistance of dense-graded asphalt mixtures which are widely used in the construction of wearing courses for National Highways in India. This chapter discusses the use of ITS test for evaluating moisture damage in asphalt mixtures, analysis of TSR data, and limitations of the ITS test.

5.2 Indirect Tensile Strength Test Results

The ITS for VG30, VG30-WMA, VG30-L, VG30-WMA-L specimens before and after AASHTO T283 conditioning is shown in Figure 5.1. The corresponding TSR is shown in Figure 5.2. It can be observed that ITS for VG30-WMA specimen is lower than VG30 specimen which shows that the VG30-WMA specimen is more susceptible to moisture compared to VG30 specimen. However, upon adding hydrated lime to VG30 mixture, the ITS reduced possibly due to the filler effect of hydrated lime acted upon by the high deformation rate (50 ± 5 mm/min) of the loading device. From Figure 5.2, it can be observed that both VG30 and VG30-WMA specimens show high moisture susceptibility as the TSR for both these mixtures are lower than the recommended value of 80%. However, the TSR increased due to the antistripping property of hydrated lime. An increase in TSR is observed for both the mixtures (VG30 and VG30-WMA) on the addition of hydrated lime.

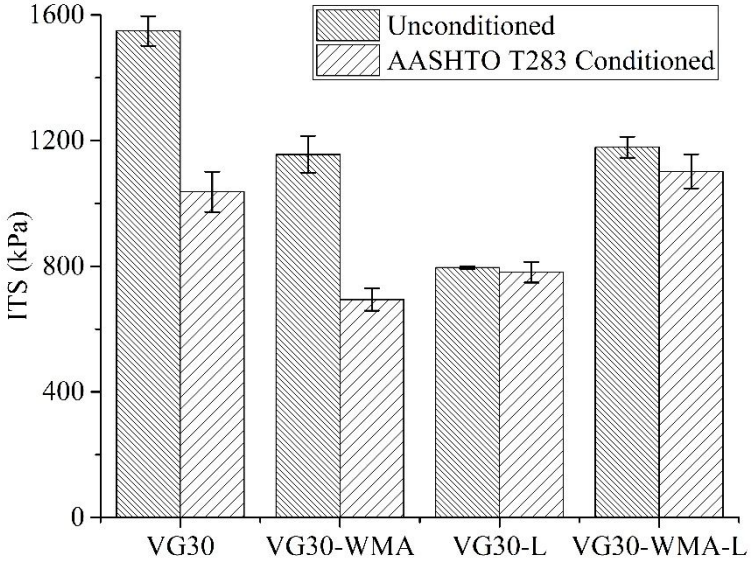

Fig. 5.1: Indirect tensile strength for unconditioned and AASHTO T283 conditioned specimens

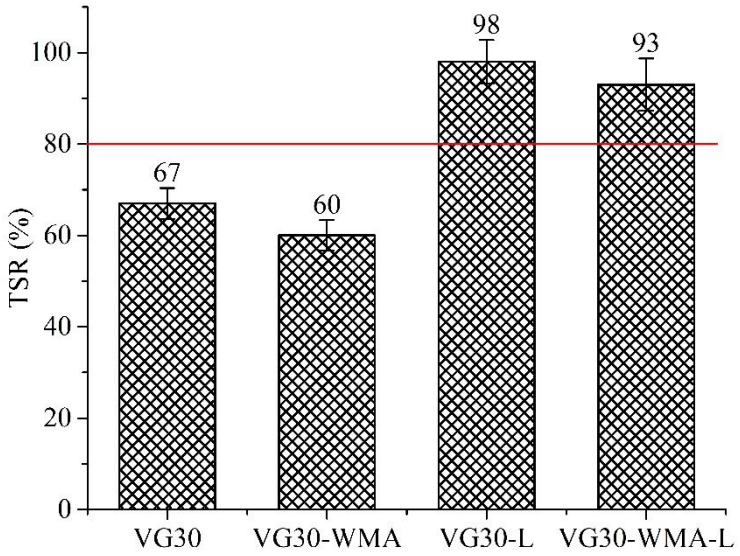

Fig. 5.2: Tensile strength ratio for HMA and WMA with and without hydrated lime

5.3 Issues Related to Indirect Tensile Strength Test

Even though AASHTO T283 has been used for several years to measure moisture susceptibility of asphalt mixtures, it cannot measure stripping precisely (Brown et al. 2001, Mallick et al. 2003). The conditioning procedure in AASHTO T283 is not dynamic in nature which does not closely represent the field environment and the tension strength parameter is not directly used in pavement design to predict moisture damage in the field (Vargas-

Nordcbeck et al. 2016). AASHTO T283 assesses the final effect of moisture damage by comparing the unconditioned and moisture conditioned mechanical property of asphalt mixtures but fails to provide the cause that can differentiate between good and poor performing asphalt mixtures. AASHTO T283 also does not quantify the moisture saturation of pavement in service (Bhasin et al. 2007). Further, the field performance of asphalt pavement and the AASHTO T283 test results are poorly correlated (Solaimanian et al. 1993, Kandhal 1994, Bahia and Ahmad 1999, West et al. 2004, Kanitpong and Bahia 2007, Vargas-Nordcbeck et al. 2016).

Though the indirect tensile strength test is simple to use, it has few disadvantages, such as permanent deformation under the loading strip, nonuniform strain distribution, unrealistic representation of the stress state, and local failure at the support as a result of high stress (Huang et al. 2005b). For various instances, though the tensile strength is statistically different (t-test at 5% level of significance) for unconditioned and conditioned specimens, TSR showed high variations. TSR is found to be higher than 80 % in some cases, while lower than 80 % in other cases. This variation shows that the static nature of the ITS test is not simulating the in-situ material behaviour (Bausano and Williams 2009).

Even though the specimen is compacted at similar air voids, a variation in TSR is observed and may not exhibit similar damage, and that the increase in moisture accessibility may not always increase the damage (Tarefder and Ahmad 2015a, Tarefder and Ahmad 2015b, Ahmad et al. 2018). Due to chemical changes during freeze-thaw cycles or pore pressure cycles at elevated temperatures, there might be inconsistencies in ITS measurement. The binder might get stiffened due to certain chemical changes but with low stripping, TSR shall exhibit higher value and vice versa (Ahmad et al. 2018). With the increase in permeability of asphalt mixtures, the retained tensile strength decreases (Tarefder and Ahmad, 2015a).

ANOVA analysis indicates that the effect of loading rate (0.5 mm/min and 50 mm/min) on the indirect tension test was not significant. The loading rate that takes a shorter time was recommended to carry out the ITS test (Yin et al. 2017). Following ASTM D6931 (2017) and AASHTO T283 (2014), the indirect tensile strength test specimen is loaded at a rate of 50 ± 5 mm/min unto failure. It was shown through statistical analysis that the level of saturation does not affect the tensile strength of moisture-conditioned specimen and a saturation level of 50-80 % was recommended to be used in the AASHTO T283 test (Epps et al. 2000). Khosla et al. (2000) observed that the variability of air voids and degree of saturation are the

dominant factors that may affect the variation of TSR. The current version of AASHTO T283 (2014) recommends saturating compacted asphalt at 7 ± 0.5 % air voids to 70-80 %.

5.4 Summary

Based on the ITS test carried out on VG30, VG30-WMA, VG30-L, and VG30-WMA-L specimens, it was observed that VG30 specimens and VG30-WMA specimens are highly moisture susceptible. WMA was found to be more moisture susceptible than HMA. The use of hydrated lime tends to increase the TSR for both VG30 and VG30-WMA mixtures. In India, the ITS test is the most preferred test to evaluate moisture resistance of asphalt mixtures as this test procedure is simple and quick, and the equipment used is less expensive. Moreover, it is also recommended by MoRTH (2013) where a single freeze-thaw cycle (freezing at -18 ± 3° C and thawing at 60 ± 1° C) is used to estimate long-term stripping susceptibility of asphalt mixtures. The primary limitation of the TSR is that it is a pass/fail test, as the peak load alone is used to determine the moisture susceptibility of mixtures. In the indirect tensile strength test, the load is applied in the diametrical direction where uniform tensile stress is developed along the vertical diametrical plane and the state of stress is biaxial. Further, the specimen in an indirect tensile strength test undergoes permanent deformation.

In the indirect tensile fatigue test a pulsating load is applied in the diametrical direction where uniform tensile stress is developed along the vertical diametrical plane and the state of stress is biaxial whereas in the four-point bend fatigue test, a pulsating or sinusoidal load is applied at third-points resulting in uniform bending moment within the beam mid span where specimen failure initiates in the region of relatively uniform stress and the state of stress is uniaxial (Tangella et al. 1990, Hartman and Gilchrist 2004). Four-point bend fatigue test has been considered for the current study which has the advantage of applying stress reversals which is practically impossible in the indirect fatigue test where the specimen also undergoes permanent deformation which is restricted in the four-point bend fatigue test (Tangella et al. 1990). This warrants the use of fatigue test to evaluate the moisture susceptibility of asphalt mixtures which realistically captures the incremental damage after each loading cycle. In the next chapter, fatigue test on the asphalt mixtures, its evolution of flexural stiffness and total energy dissipation, and influence of WMA additive, hydrated lime, and moisture damage on fatigue life are discussed.

CHAPTER 6

FATIGUE LIFE OF ASPHALT MIXTURES

6.1. Introduction

Quantification of the fatigue life of WMA is challenging due to various factors such as the extent of aging, moisture susceptibility, to mention a few. Hydrated lime as an anti-stripping material can enhance the fatigue life of moisture conditioned WMA. However, due to the filler effect of lime, the fatigue life can reduce. Four-point beam bending test on saturated asphalt mixtures simulates the repeated loading condition of pavements in the presence of moisture. In this investigation, specimens of HMA, and WMA with and without hydrated lime were subjected to fatigue testing using four-point bending at three strain levels (400, 600, and 800 microstrain) for unconditioned and moisture damaged conditions. The data collected was analyzed appealing to various post-processing methods. The addition of warm mix additive may enhance the fatigue life of asphalt mixtures. However, its moisture susceptible characteristics might result in increased fatigue damage compared to the HMA. Hydrated lime as an anti-stripping material may enhance the fatigue life of moisture conditioned WMA. However, the filler effect of hydrated lime may prevent the enhancement in fatigue life. This chapter tries to address all these issues.

6.2. Calculation of Flexural Stiffness and Energy Dissipation

The flexural stiffness was calculated following AASHTO T321 (2014). The maximum tensile stress and the maximum tensile strain are the input parameters required to compute the flexural stiffness as shown in Equation (6.1). The evolution of flexural stiffness calculated at all strain levels for VG30 specimen is shown in Figure 6.1. As expected, the flexural stiffness reduced due to repeated loading, and the rate of reduction is higher at 800 microstrain, followed by 600 and 400 microstrain. Further, following AASHTO T321 (2007), the number of cycles corresponding to 50 % of initial flexural stiffness is identified as the fatigue life of given asphalt mixture. The fatigue life corresponding to all the three strain levels are marked on the flexural stiffness evolution curve in Figure 6.1. In this study, the 50^{th} cycle is considered as an initial cycle.

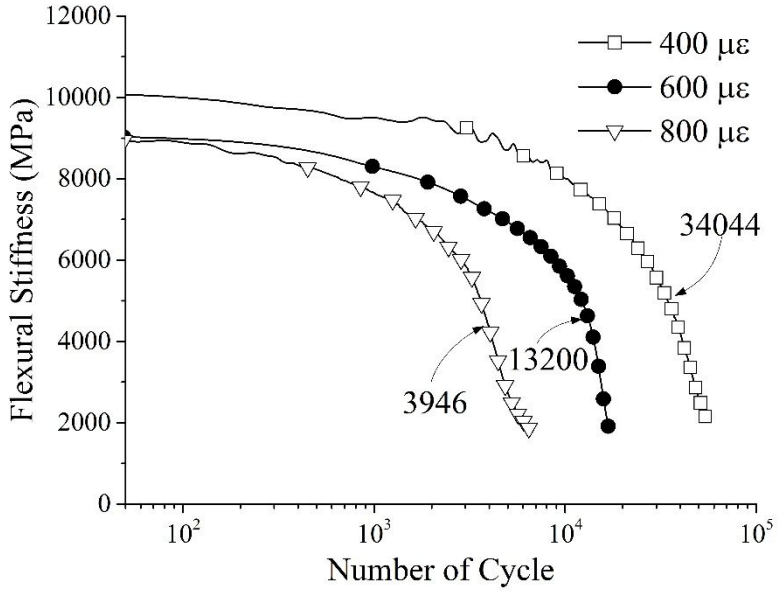

Fig. 6.1: Variation of flexural stiffness as a function of number of cycles for VG30 specimen

$$S_i = \frac{1000 \times \sigma_t}{\varepsilon_t}, \quad (6.1)$$

where, S_i is the flexural stiffness at ith cycle (MPa), σ_t is the maximum tensile stress (kPa), and ε_t is the maximum tensile strain (με).

The total energy dissipation in each cycle is calculated from the area enclosed by the stress-strain plot (Lissajous plot). The sample Lissajous plot for VG30 specimen at 800 microstrain is shown in Figure 6.2. For the calculation of the area of the Lissajous plot, each and every waveform data was extracted separately using MATLAB (MATLAB 2018) and the area was calculated for each cycle using trapezoidal numerical integration. The energy dissipation used here is the total dissipation that includes dissipation due to viscoelastic behaviour and dissipation due to damage (Varma et al. 2017). The energy dissipation calculated for VG30 specimen at all strain levels is shown in Figure 6.3. The energy dissipation is reduced due to repeated loading and the rate of reduction is higher at 800 microstrain followed by 600 and 400 microstrain. The evolution of flexural stiffness and total energy dissipation of all the specimens considered in this study are presented in Appendix B.

The initial flexural stiffness and energy dissipation of all the specimens tested are shown in Table 6.1. At the initial cycles of loading, the specimens can have different internal orientations and hence different flexural stiffness. Also, flexural stiffness at the initial few cycles of loading in a four-point beam bending test is expected to vary due to specimen heating and thixotropy (Benedetto et al. 2011). The variation in initial flexural stiffness and

energy dissipation of the specimen can be eliminated by normalizing the values. The flexural stiffness and energy dissipation are normalized with respect to the corresponding value at the 50th cycle listed in Table 6.1. Further, the influence of warm mix additive and hydrated lime on the evolution of flexural stiffness and energy dissipation of unconditioned and moisture conditioned specimens were analysed and results are reported in the subsequent sections.

Table 6.1: Flexural stiffness and energy dissipation corresponding to 50th cycle for all specimens

Specimen	Flexural stiffness (MPa)			Energy dissipation (kJ/m^3)		
	400 με	600 με	800 με	400 με	600 με	800 με
VG30	10073	9170	8860	0.373	0.818	1.396
VG30-WMA	7953	7640	8514	0.343	0.790	1.615
VG30-L	10285	9505	8573	0.364	0.867	1.448
VG30-WMA-L	9529	9081	8624	0.382	0.916	1.705
VG30-MC	9576	8695	8188	0.416	0.857	1.585
VG30-WMA-MC	8317	5743	5759	0.407	0.761	1.302
VG30-L-MC	11388	11625	11599	0.476	1.132	2.116
VG30-WMA-L-MC	10317	10648	9038	0.469	1.112	1.937

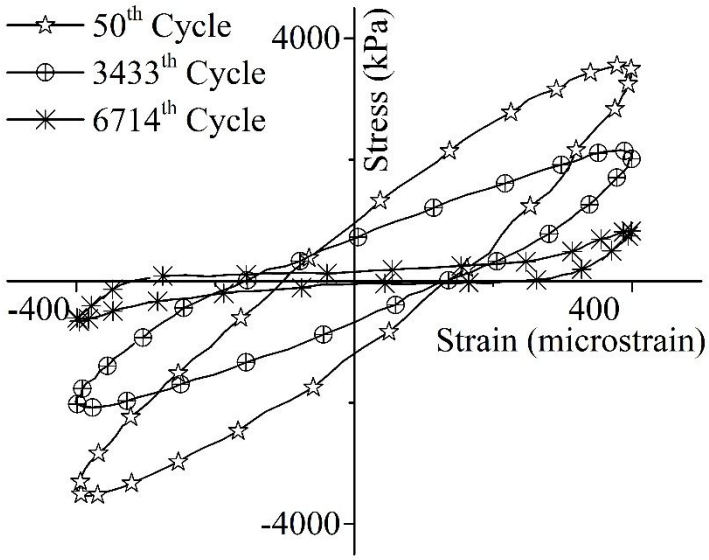

Fig. 6.2: Sample Lissajous plot for VG30 specimen at 800 microstrain

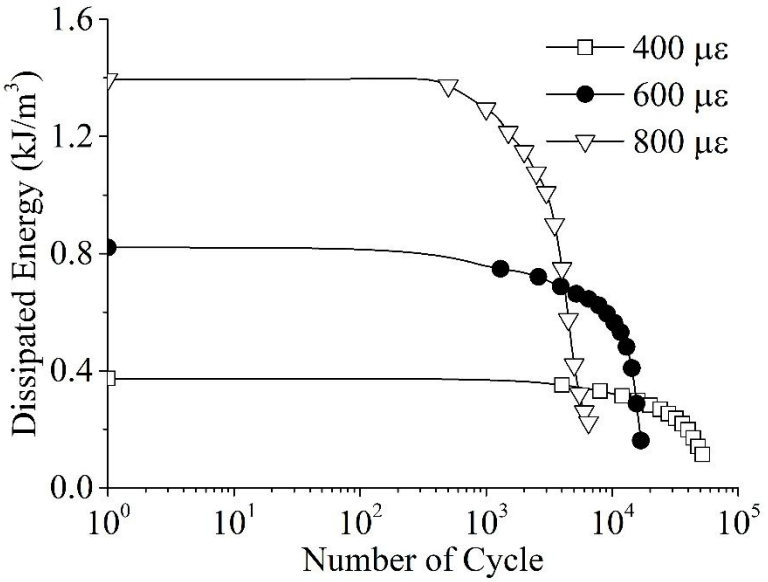

Fig. 6.3: Energy dissipation for VG30 specimen

6.3. Influence of Warm Mix Additive on the Evolution of Flexural Stiffness and Energy Dissipation

The influence of warm mix additive on the evolution of flexural stiffness is evaluated by comparing the normalized flexural stiffness of VG30 specimen with VG30-WMA specimen. Figure 6.4 shows the evolution of flexural stiffness due to repeated loading for VG30 and VG30-WMA specimens at 400 and 600 microstrain. The flexural stiffness curve exhibited two stage slope in which the first slope is gradual compared to the second slope. From Figure 6.4, at 400 microstrain, the reduction in flexural stiffness of VG30-WMA specimen at the initial stage is observed to be gradual compared to VG30 specimen. However, on continuous loading, flexural stiffness of VG30-WMA specimen is observed to reduce at a rapid rate compared to VG30 specimen. At 600 microstrain, the stiffness of VG30-WMA specimen reduced rapidly than the VG30 specimen. The variation in flexural stiffness at 800 microstrain is observed to be similar to that at 600 microstrain.

The trend in the evolution of energy dissipation of VG30 and VG30-WMA specimens is shown in Figure 6.5. The energy dissipation curve also exhibited two stage slope, similar to the evolution of flexural stiffness. However, on comparing the point of change in slope of energy dissipation and the number of cycles corresponding to 50 % of initial flexural stiffness that is marked on the energy dissipation curve, it is clear that the point of 50 % of initial stiffness occurred earlier than the point of change in the slope of energy dissipation (Figure 6.5).

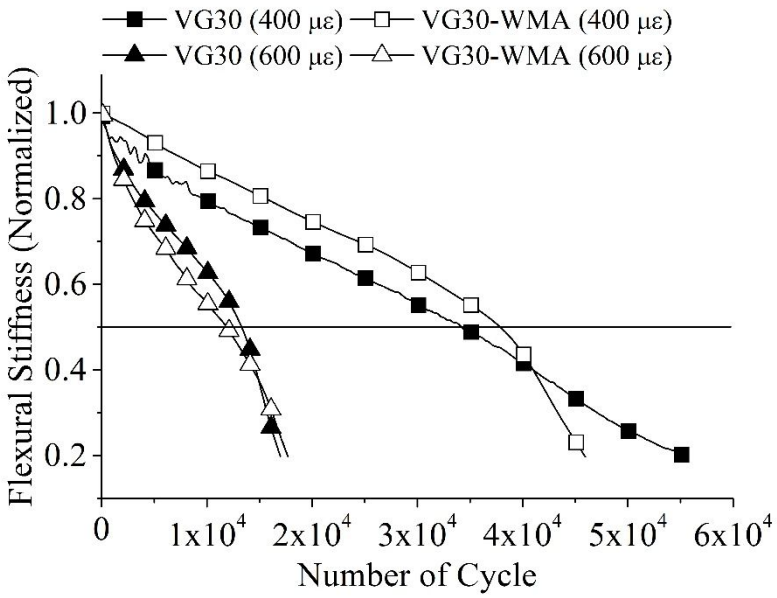

Fig. 6.4: Evolution of flexural stiffness of VG30 and VG30-WMA specimens

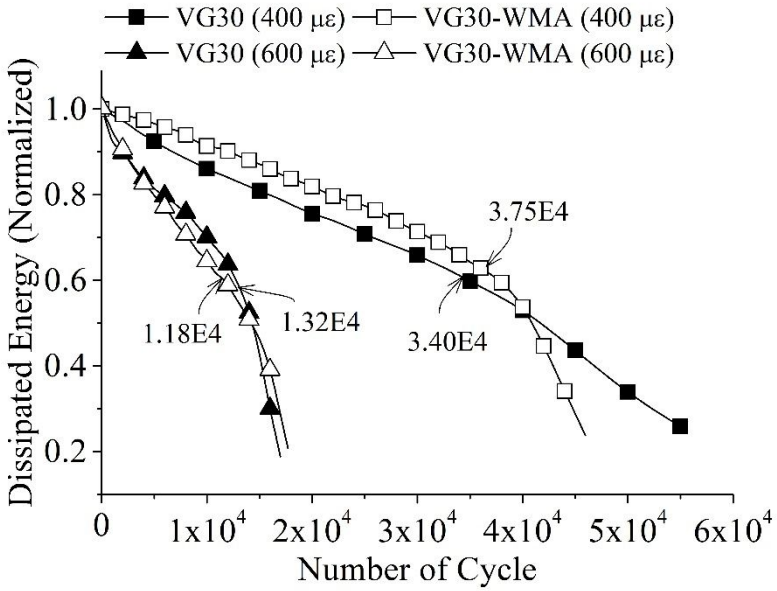

Fig. 6.5: Evolution of energy dissipation of VG30 and VG30-WMA specimens

6.4. Influence of Hydrated Lime on the Evolution of Flexural Stiffness and Energy Dissipation

The evolution of flexural stiffness of asphalt mixture specimens prepared with and without hydrated lime is compared in Figure 6.6. The energy dissipation curve of the WMA specimen with and without hydrated lime is shown in Figure 6.7. At 400 microstrain, the lime-treated specimen showed improved resistance to the reduction in the flexural stiffness and energy

dissipation compared to asphalt mixture specimen without lime. Similar observation with improved fatigue life of hydrated lime treated specimens was reported by Lesueur and Little (1999), Kim et al. (2003), and Little et al. (2006). However, the trend in the evolution of flexural stiffness and energy dissipation of hydrated lime treated specimens changed at higher strain levels (600 and 800 microstrain), where the lime-treated specimens exhibited an increased rate of change in flexural stiffness and energy dissipation. Further, the influence of hydrated lime on the moisture-damaged specimen is discussed in the following section.

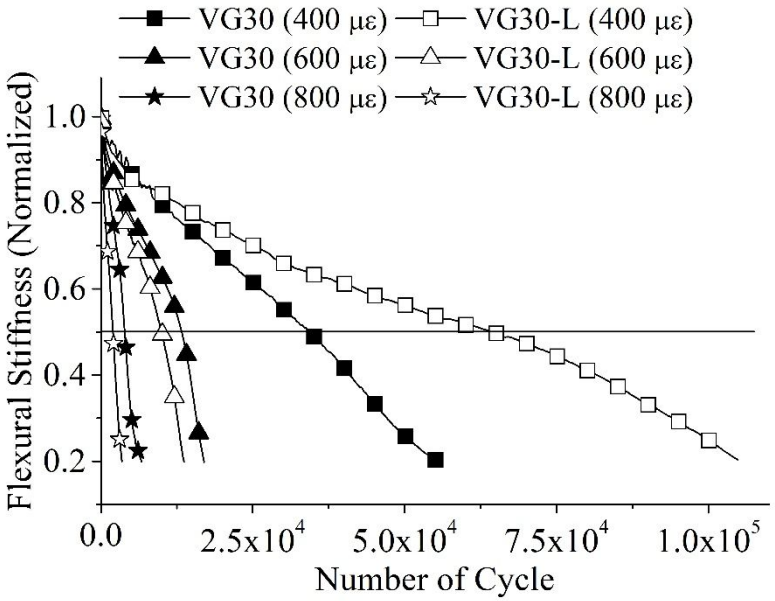

(a) VG30 and VG30-L specimens

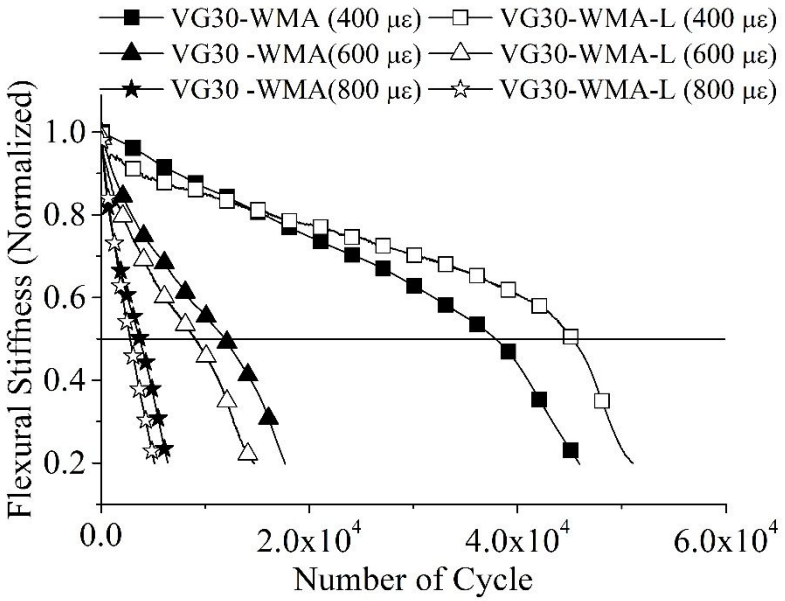

(b) VG30-WMA and VG30-WMA-L specimens

Fig. 6.6: Evolution of flexural stiffness of the specimen prepared with and without lime

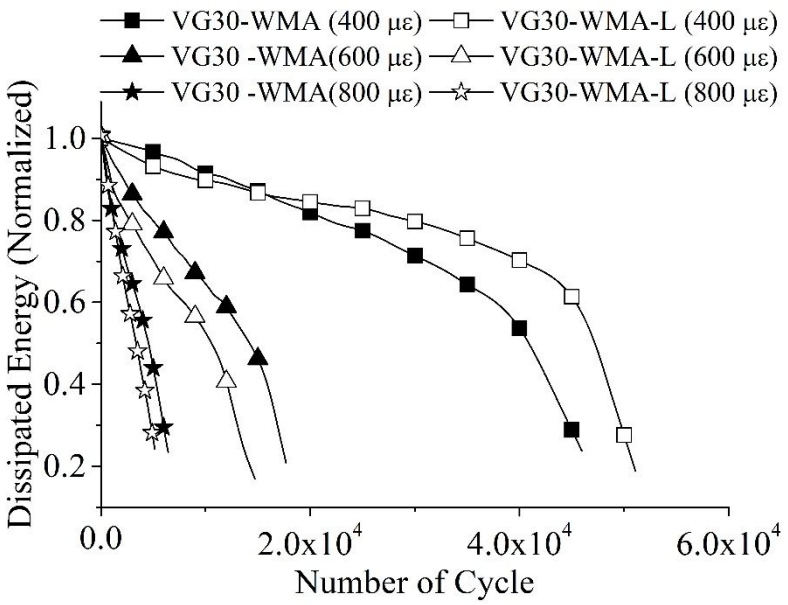

Fig. 6.7: Evolution of energy dissipation of WMA specimen with and without lime

6.5. Influence of Moisture Conditioning on the Evolution of Flexural Stiffness and Energy Dissipation

A sample data comparing the evolution of flexural stiffness of dry and moisture conditioned VG30 specimen at 600 microstrain and VG30-WMA specimen at 800 microstrain is shown in Figure 6.8a and 6.8b respectively. It is observed that all the moisture conditioned specimens exhibited an increased rate of reduction in flexural stiffness compared to unconditioned dry specimens. To study the influence of warm mix additive on the moisture sensitivity of asphalt mixtures, the flexural stiffness evolution of VG30-WMA-MC specimen at 400 microstrain is compared with VG30-MC specimen as shown in Figure 6.8c. The moisture conditioned WMA exhibited a rapid reduction in flexural stiffness compared to the HMA. It was inferred from Figure 6.4 and Figure 6.5 that the addition of WMA increased the fatigue resistance of the unconditioned specimen at 400 microstrain whereas Figure 6.8c indicates that the WMA is prone to be moisture susceptible compared to the HMA. Further, the influence of lime on moisture conditioning can also be inferred from Figure 6.8(a-c). For VG30-L specimen, at higher strain level (600 and 800 microstrain shown in Figure 6.6a), though the addition of hydrated lime did not show any beneficial effect on the dry specimen, from Figure 6.8a, it is clear that the reduction in flexural stiffness of VG30-L-MC specimen is gradual compared to the specimen without lime (VG30-MC specimen). At all strain levels, the addition of hydrated lime exhibited beneficial effect on moisture conditioned HMA and WMA specimens.

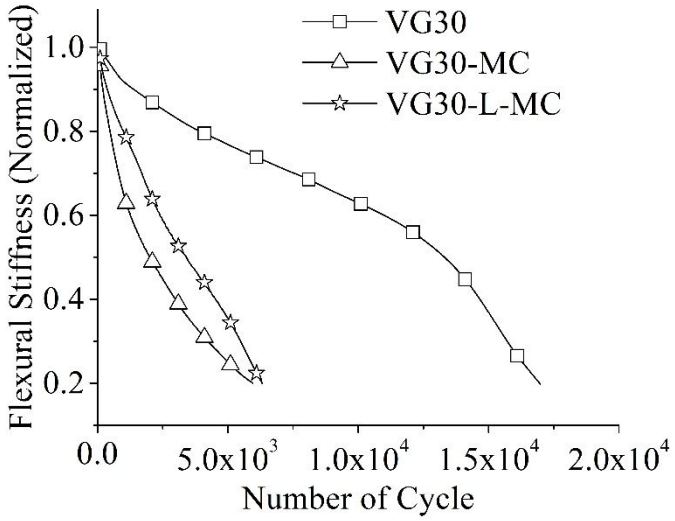

(a) HMA at 600 microstrain

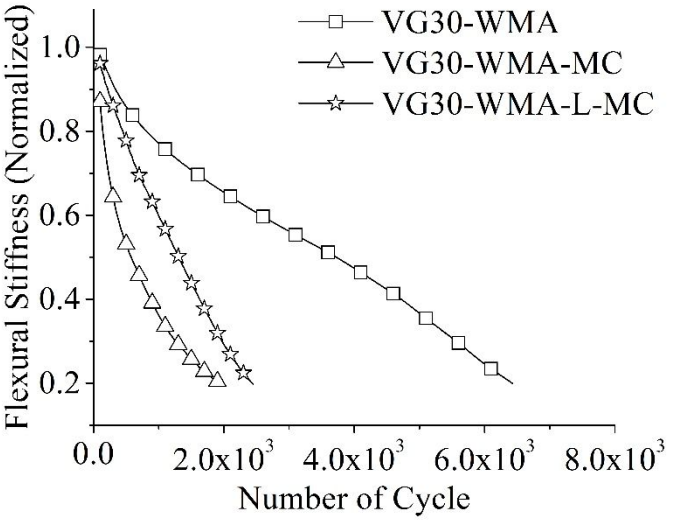

(b) WMA at 800 microstrain

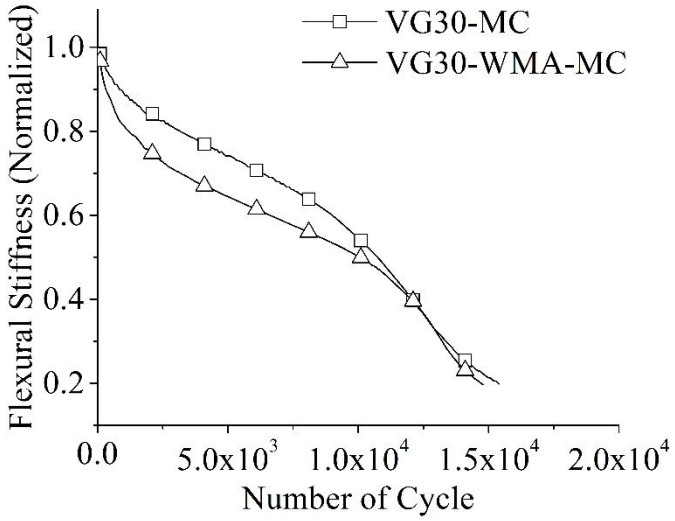

(c) VG30-MC and VG30-WMA-MC at 400 microstrain

Fig. 6.8: Evolution of flexural stiffness of moisture conditioned asphalt mixtures

6.6. Fatigue Life of Asphalt Mixtures

The fatigue life of the asphalt mixtures was estimated using four different post-processing techniques. Fatigue life of unconditioned and moisture conditioned asphalt mixtures was estimated firstly using the flexural stiffness modulus following AASHTO T321 (2007) protocol, secondly using the normalised modulus following ASTM D7640 (2010) protocol, thirdly using energy ratio concept following Rowe and Bouldin (2000), and lastly using the ratio of dissipated energy change (RDEC) concept proposed by Ghuzlan and Carpenter (2000).

6.6.1 Fatigue life using AASHTO

Following AASHTO T321 (2007), the number of cycles corresponding to 50 % of initial flexural stiffness is identified as the fatigue life of asphalt mixtures (Figure 6.1). The number of cycles corresponding to 50 % of initial flexural stiffness was identified for the specimens considered in this study and are presented in Table 6.2.

Table 6.2: Fatigue life using AASHTO T321 (2007)

Specimen	Strain amplitude		
	400 με	**600 με**	**800 με**
VG30	34044	13200	3946
VG30-WMA	37483	11771	3653
VG30-L	63427	10038	1975
VG30-WMA-L	45301	8995	2807
VG30-MC	10738	1985	686
VG30-WMA-MC	10199	4100	580
VG30-L-MC	17205	3410	877
VG30-WMA-L-MC	14190	5310	1315

6.6.2 Fatigue life using Energy Ratio

The fatigue life of asphalt mixtures can also be calculated from the energy dissipation in the material. Following Rowe and Bouldin (2000), ASTM D7460 (2010) estimates the fatigue life based on energy ratio, where the energy ratio (W_n) is defined by Equation (6.2).

$$W_n = \frac{n \times w_0}{w_n}. \tag{6.2}$$

Here, n represents the number of cycles, w_0 is energy dissipated at the initial cycle, and w_n is energy dissipated at the n^{th} cycle. The energy dissipation at the initial cycle and the n^{th} cycle is given by $w_0 = \pi\varepsilon_o^2 S_o \sin\delta_0$ and $w_n = \pi\varepsilon_o^2 S_n \sin\delta_n$, where, ε_o represent the strain

amplitude, S_o and S_n represents the flexural stiffness at initial and at n^{th} cycle, and δ_0 and δ_n represents the phase angle at initial and at n^{th} cycle. On assuming the variation in the phase angle between the initial and n^{th} cycle to be negligible, Equation (6.2) reduces to Equation (6.3).

$$W_n = \frac{n \times S_0}{S_n}. \tag{6.3}$$

For the estimation of fatigue life based on energy ratio, ASTM D7460 (2010) uses a modified form of Equation (6.3) in which the normalized modulus (NM) is defined based on the product of the number of cycle and flexural stiffness as shown in Equation (6.4).

$$NM = \frac{S_i \times n_i}{S_0 \times n_0}, \tag{6.4}$$

where, S_i is the flexural stiffness at i^{th} cycle, S_o is the initial flexural beam stiffness and n_o is the cycle at which initial flexural beam stiffness is considered. For further analysis, energy ratio was directly determined from the energy dissipation using Equation (6.2), and the fatigue life was estimated from the change in the slope of the energy ratio.

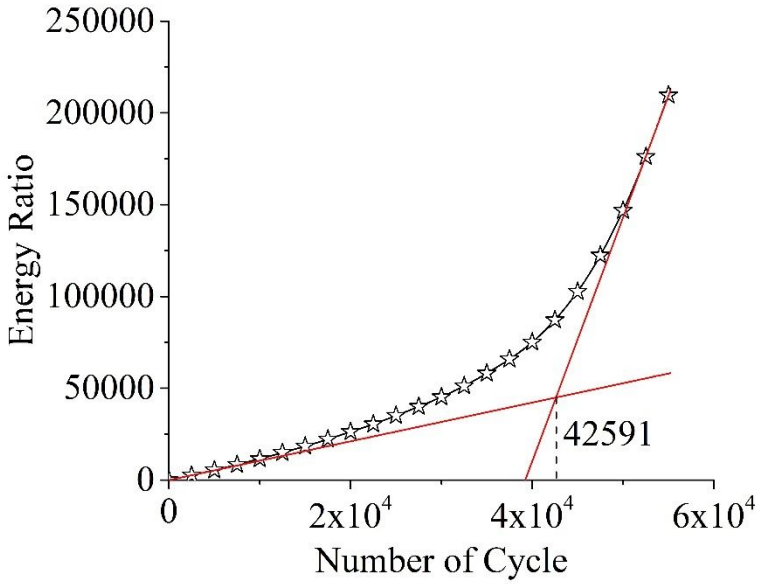

Fig. 6.9: Energy ratio for VG30 specimen at 400 microstrain

The variation in energy ratio with the number of cycles for VG30 specimen when tested at 400 microstrain is shown in Figure 6.9. The energy ratio curve exhibits two stage slope showing the rapid rate of energy dissipation in the second stage. The fatigue life is assessed as the point where the energy dissipation changes drastically, and it is determined using two tangents, as shown in Figure 6.9 (Pronk and Hopman 1990). The fatigue life estimated from

the energy ratio for all the specimens at different strain levels is shown in Table 6.3. Energy ratio plots for remaining all specimens are documented in Appendix B.

Table 6.3: Fatigue life using Rowe and Bouldin (2000)

Specimen	Strain amplitude		
	400 με	**600 με**	**800 με**
VG30	42591	14845	4356
VG30-WMA	40444	15403	5112
VG30-L	84894	11980	2631
VG30-WMA-L	46598	12120	4006
VG30-MC	11974	4059	973
VG30-WMA-MC	12252	7989	1217
VG30-L-MC	19956	5168	1427
VG30-WMA-L-MC	22699	7147	1866

6.6.3 Fatigue life using ASTM

ASTM D7460 (2010) defines the fatigue life based on normalised modulus (NM) calculated using Equation (6.4).

where, S_i is flexural beam stiffness at n_i^{th} cycle, S_0 is initial flexural beam stiffness and n_0 is the 50th cycle at which initial flexural beam stiffness is considered.

ASTM D7460 (2010) estimates fatigue life as the number of cycle corresponding to the peak of normalised modulus (NM) curve plotted versus number of cycles and are tabulated in Table 6.4. The evolution of normalized modulus for VG30-WMA specimen at 800 microstrain is shown in Figure 6.10a. The fatigue damage of asphalt mixtures initiates as the microcracks that are coalesced to form macrocracks. At the initial stage of the normalized modulus curve, there is a linear increase, and Rowe and Bouldin (2000) represented this phase as a microcrack formation phase. On continuous loading, as the damage progresses, the normalized modulus reduces, and ASTM D7460 (2010) estimates fatigue life as the number of cycles corresponding to the peak of the normalized modulus curve. In some of the normalized modulus plots, especially for moisture conditioned specimen, as shown in Figure 6.10b and 6.11c, the normalized modulus initially showed a linear increase, and there was no notable change after few thousands of cycles of loading. Varma et al. (2016) reported a similar type of normalized modulus curve for the modified asphalt mixtures. In the case of WMA subjected to moisture conditioning with or without hydrated lime, different micromechanical processes play a critical role, and hence the normalized modulus loses its significance. In such cases, the fatigue life estimation of asphalt mixtures using this approach

is not clear. The same issues exist for the recent AASHTO method of fatigue life estimation (AASHTO T321, 2014) in which, the fatigue life is considered as the point at which the product of flexural stiffness and number of cycles is maximum. Normalised modulus plots for remaining all specimens are documented in Appendix B.

Table 6.4: Fatigue life using ASTM D7460 (2010)

Specimen	Strain amplitude		
	400 με	**600 με**	**800 με**
VG30	35885	12430	3433
VG30-WMA	35431	12946	4361
VG30-L	74041	9595	2073
VG30-WMA-L	42108	10488	3329
VG30-MC	9817	4439	789
VG30-WMA-MC	10644	7651	-
VG30-L-MC	17457	4455	-
VG30-WMA-L-MC	20910	6395	1448

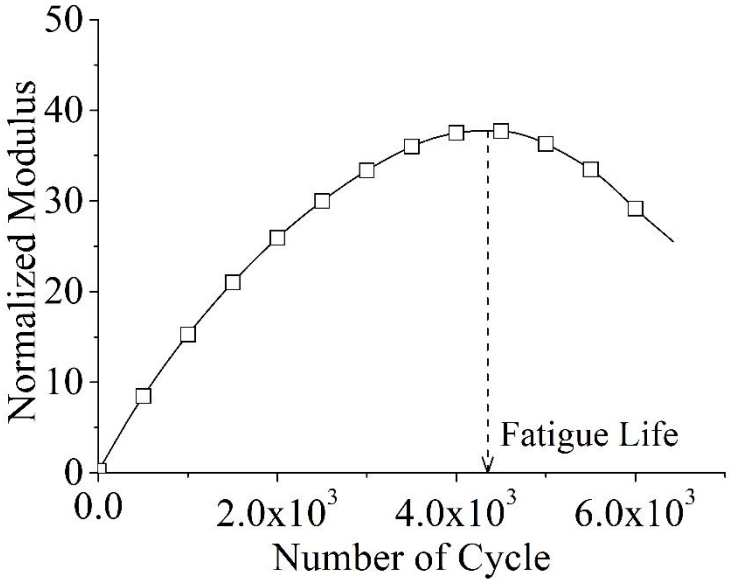

(a) VG30-WMA specimen at 800 microstrain

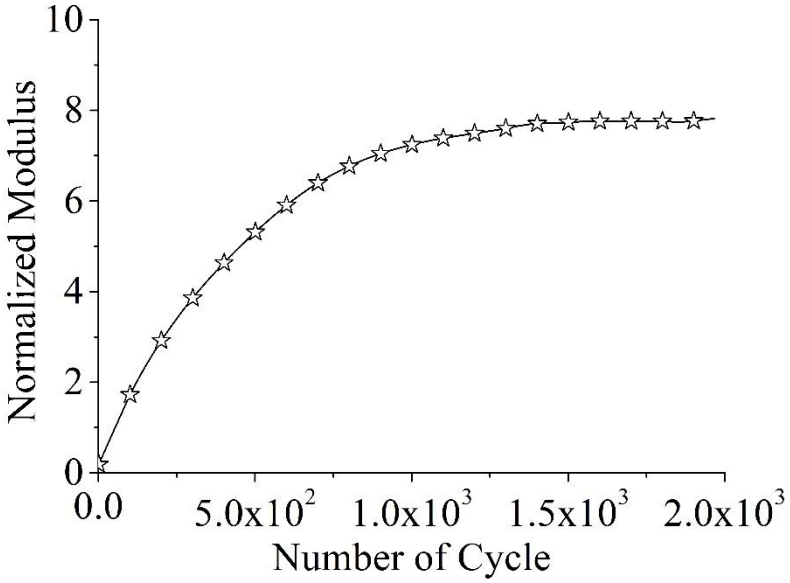

(b) VG30-WMA-MC specimen at 800 microstrain

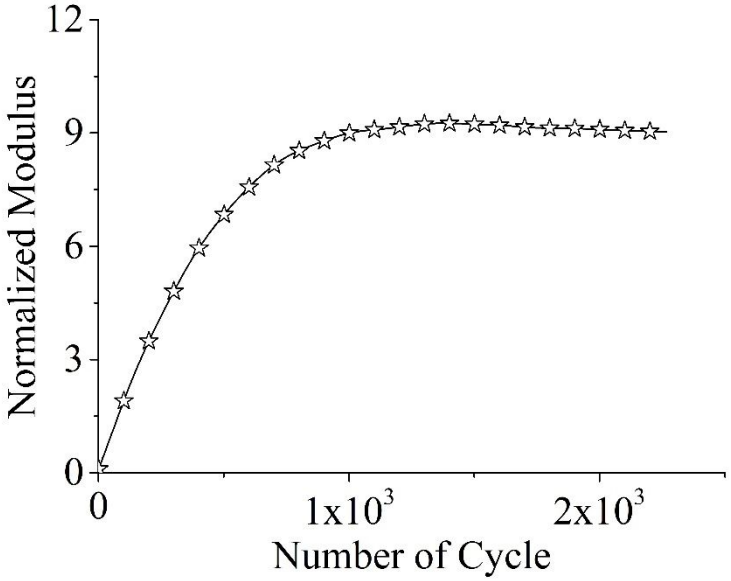

(c) VG30-L-MC specimen at 800 microstrain

Fig. 6.10: Different trends in normalized modulus

6.6.4 Fatigue life using RDEC

The ratio of dissipated energy change (RDEC), proposed by Ghuzlan and Carpenter (2000) is defined in Equation (6.5).

$$\boldsymbol{RDEC} = \frac{\Delta \boldsymbol{DE}}{\boldsymbol{DE}} \qquad (\mathbf{6.5})$$

where, $\Delta \boldsymbol{DE}$ is the change in dissipated energy between cycles $\boldsymbol{n}$ and $\boldsymbol{n+1}$, and $\boldsymbol{DE}$ is the total dissipated energy for load cycle $\boldsymbol{n}$.

The RDEC curve computed using Equation (6.5) when plotted against the number of cycles show a "bathtub" shaped curve with three phases as shown in Figure 6.11 and Figure 6.12. As the material reaches failure, the RDEC curve tends to increase rapidly which creates phase III (Ghuzlan and Carpenter 2000, Carpenter et al. 2003). The RDEC curve gives the true representation of damage between two consecutive cycles and indicates the percentage of dissipated energy that causes damage for a given cycle. Phase II in the RDEC plot indicates the period during which a constant percentage of total dissipation is causing damage in the asphalt mixtures and is represented as the plateau value (Figure 6.11). Phase III in the RDEC curve shows the rapid increase in damage proportion between two consecutive cycles and is considered as the ultimate failure of the asphalt mixtures (Carpenter et al. 2003).

Table 6.5: Fatigue life using Ghuzlan and Carpenter (2000)

Specimen	Strain amplitude		
	400 με	**600 με**	**800 με**
VG30	44188	-	4106
VG30-WMA	39190	-	-
VG30-L	86011	11954	2514
VG30-WMA-L	45977	9837	4184
VG30-MC	13122	3450	771
VG30-WMA-MC	12893	8727	-
VG30-L-MC	-	4909	-
VG30-WMA-L-MC	12884	-	-

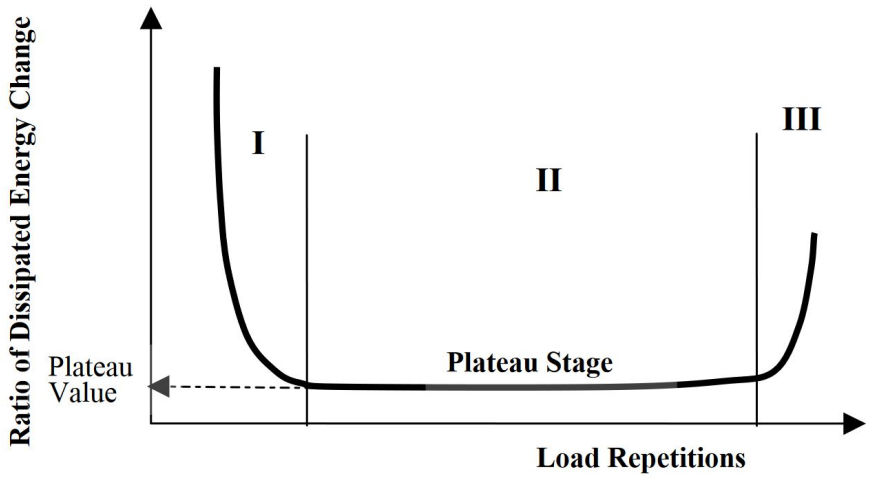

Fig. 6.11: Typical RDEC plot with three behaviour zones (Carpenter et al. 2003)

It has to be noted here that the total energy dissipated is the sum of viscous dissipation and damage dissipation. The assumption made here is that the viscous dissipation remains

constant throughout the fatigue test and only the damage dissipation increases with the number of cycles. This assumption made here may not hold correct for asphalt mixtures as the viscous dissipation and the damage dissipation may vary with the number of cycles, and the difference of energy dissipation between cycles n and $n+1$ may include both the change in damage dissipation and the change in viscous dissipation. It is therefore more likely that the RDEC plots may not always give a decisive phase III curve to estimate fatigue life as shown in Figure 6.13. Fatigue life estimated using RDEC is shown in Table 6.5. RDEC plots for remaining all specimens are documented in Appendix B.

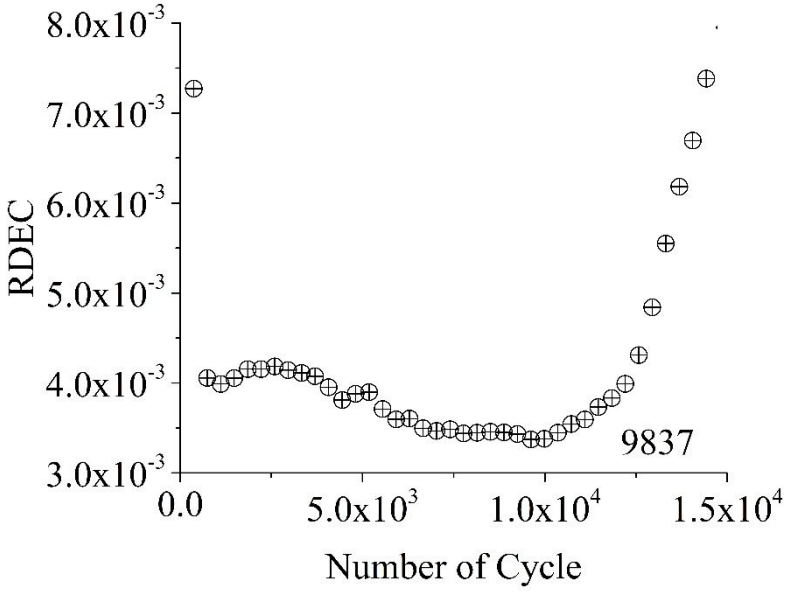

Fig. 6.12: Fatigue life estimation using RDEC for VG30-WMA-L specimen at 600 με

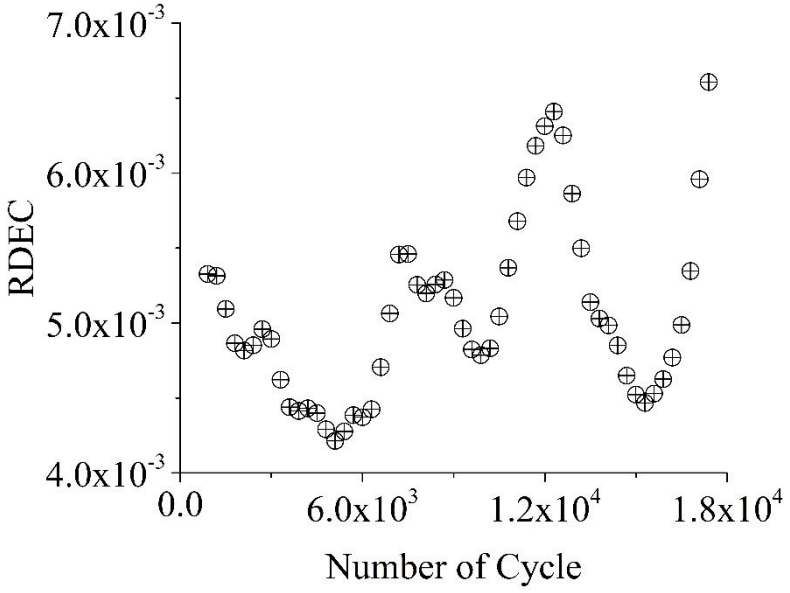

(a) VG30-WMA specimen at 600 με

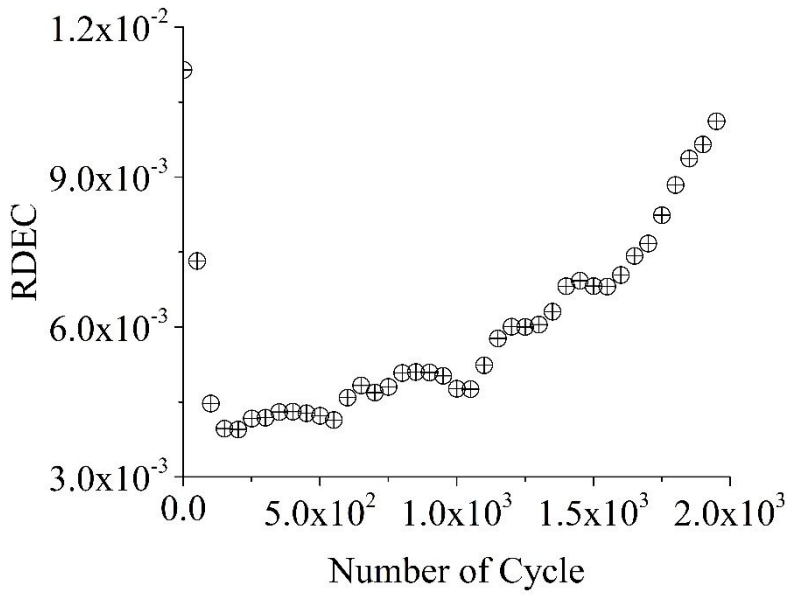

(b) VG30-WMA-MC specimen at 800 με

Fig. 6.13: Various trends in RDEC

6.7. Fatigue Life Comparison

On comparing the fatigue life obtained from the AASHTO method and energy ratio method, for all the specimens, the fatigue life based on energy ratio was observed to be higher than the AASHTO method of fatigue life estimation. Further, the influence of warm mix additive and hydrated lime on the fatigue life of dry and moisture conditioned specimens were analyzed. Fatigue life using the ASTM method and the RDEC method was not considered in the comparison as the fatigue life determination for few specimens using these methods is not clear.

From the fatigue life calculated from the flexural stiffness and energy dissipation (Figure 6.14 and Figure 6.15), the addition of warm mix additive increased the fatigue life of asphalt mixtures at 400 microstrain and reduced the fatigue life of asphalt mixtures at 600 and 800 microstrain. The addition of hydrated lime also increased the fatigue life of HMA and WMA at 400 microstrain and reduced the fatigue life at higher strain level. The fatigue life of HMA and WMA reduced due to moisture conditioning. Lime treated moisture conditioned specimens also exhibited reduced fatigue life compared to the unconditioned control specimens. However, the addition of hydrated lime reduced the extent of damage.

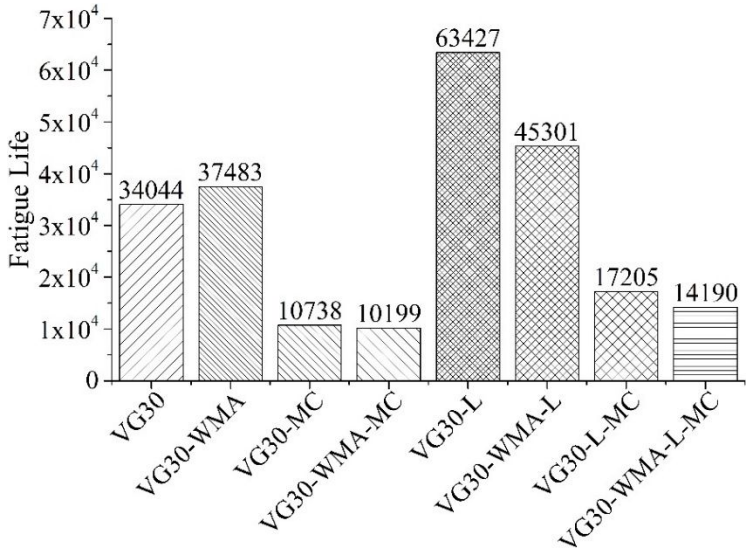

(a) 400 microstrain

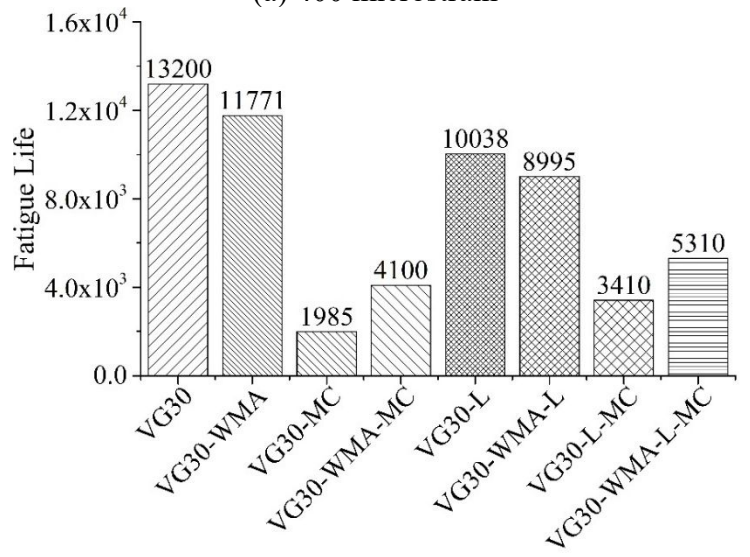

(b) 600 microstrain

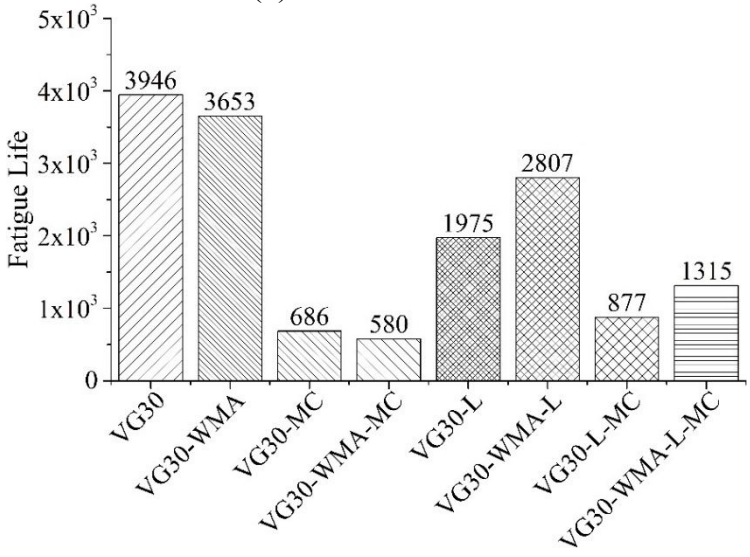

(c) 800 microstrain

Fig. 6.14: Fatigue life (AASHTO) comparison

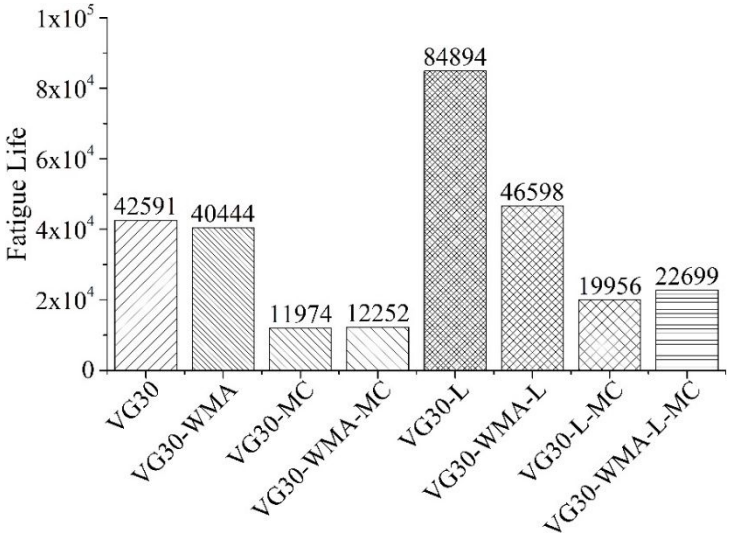

(a) 400 microstrain

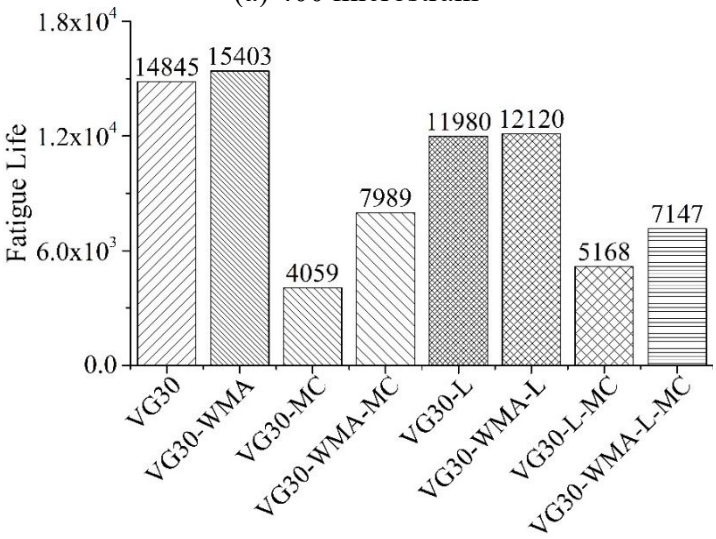

(b) 600 microstrain

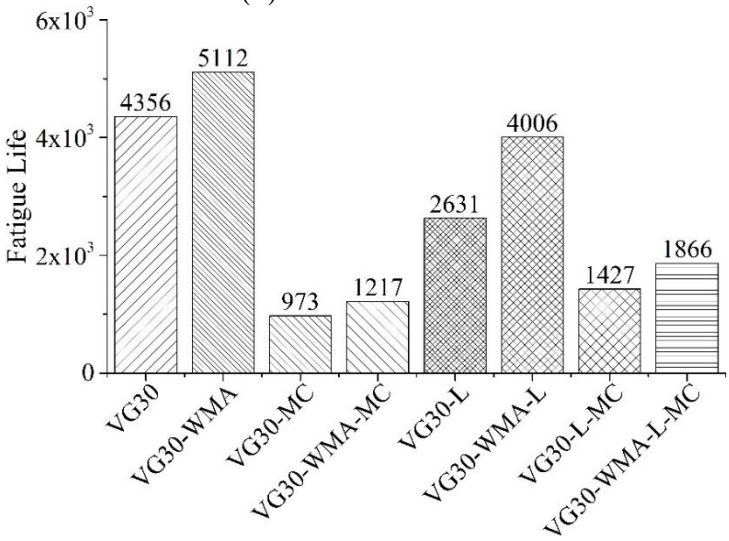

(c) 800 microstrain

Fig. 6.15: Fatigue life (energy ratio) comparison

6.8. Summary

This chapter discussed the computation of flexural stiffness and energy dissipation, the influence of WMA additive, hydrated lime, and moisture damage on the evolution of flexural stiffness and total energy dissipation with respect to the applied strain. The fatigue life was computed using four methods and was discussed in detail. Fatigue life using the AASHTO method and energy ratio method was used to compare fatigue life. The variation in fatigue life due to the effect of WMA additive, hydrated lime, and moisture damage was also discussed.

The total dissipation is the sum of viscous dissipation and damage dissipation. An attempt to separate damage dissipation from total dissipation is discussed in the next chapter using three different approaches. The effect of WMA additive, hydrated lime, and moisture damage on damage dissipation proportion are elaborated.

CHAPTER 7

VISCOELASTIC DISSIPATION AND DISSIPATION DUE TO DAMAGE IN ASPHALT MIXTURES

7.1 Introduction

In the previous chapter, the fatigue performance of asphalt mixtures with the use of WMA additive and hydrated lime in presence of moisture was discussed. In summary, warm mix asphalt additive enhances the fatigue life of asphalt mixture due to reduced aging whereas the residual moisture present in the aggregate due to lower mixing and compaction temperature can increase the moisture susceptibility of the asphalt mixtures resulting in lower fatigue life. The antistripping nature of hydrated lime improves the moisture resistance of asphalt mixtures and at the same time reduces chemical aging of the binder resulting in higher fatigue life. However, the temperature-dependent filler effect of the hydrated lime increases the stiffness of the asphalt mixtures and results in lower fatigue life.

This chapter discusses such effects on the relative energy dissipated due to viscoelasticity and damage. Further, the presence of surfactant-based WMA additives and hydrated lime can significantly affect the energy dissipated due to viscoelasticity and damage. The energy dissipated due to damage can be quantified by knowing the total energy dissipation and the viscoelastic dissipation. Several approaches are available to separate the total energy dissipation into viscoelastic dissipation and dissipation due to damage (Kim and Little 1989, Varma et al. 2017, Varma et al. 2019). This study considered three such approaches to separate the viscoelastic dissipation and dissipation due to damage from the total energy dissipation. Cumulative damage dissipation using all the three approaches was initially computed. Subsequently, these three approaches are used to quantify the relative effects of moisture, warm mix additive, and hydrated lime on cumulative damage dissipation at three different strain levels. Considering the complexity of the problem at hand, the following questions are sought to be answered using these three approaches.

1. Since WMA is expected to have increased fatigue resistance due to reduced aging, can one expect that the dissipation due to damage will start later compared to dissipation due to viscous effects?

2. Is it possible to quantify the relative energy dissipation of a moisture conditioned specimen (both HMA and WMA) with the unconditioned specimen?
3. Since the addition of hydrated lime can increase the stiffness of the material, will the energy dissipation due to damage likely to increase for unconditioned HMA and WMA? In the case of moisture conditioned specimens, will the lime treated specimen exhibit lower energy dissipation due to damage?

7.2 Approaches to Separate Damage Dissipation from Total Energy Dissipation

In the strain-controlled testing, the material is subjected to the strain history of the form given in Equation (7.1). The response stress for any given cycle *n* can be written in the form of Equation (7.2).

$$\epsilon(t) = \epsilon_0 \sin \omega t, \tag{7.1}$$

$$\sigma_n(t) = E_n \epsilon_0 \sin(\omega t + \delta_n), \tag{7.2}$$

where, ϵ_0 is the strain amplitude, ω is the frequency, E_n is the dynamic modulus and δ_n is the phase lag at n^{th} cycle. The current state of the material changes with each loading cycle and hence E_n and δ_n changes with number of load cycles. For the strain and stress of the form given in Equation (7.1) and (7.2), the energy dissipation (W_T) for any load cycle can be computed using Equation (7.3).

$$W_{T_n} = \oint \sigma_n(t)\dot{\epsilon}(t)\mathrm{dt} = \pi E_n \epsilon_0^2 \sin \delta_n, \tag{7.3}$$

where, $\dot{\epsilon}(t)$ is the strain rate. Here, the first order derivative of $\epsilon(t)$ is used for obtaining $\dot{\epsilon}(t)$. The total energy dissipation (W_{T_n}) of the material at any point of time is the sum of dissipation due to the viscoelastic behaviour (W_{ve_n}) and dissipation due to damage (W_{d_n}).

$$W_{T_n} = \mathrm{W}_{ve_n} + \mathrm{W}_{d_n}. \tag{7.4}$$

Total dissipation for each load cycle was obtained by calculating the area within the Lissajous plot by trapezoidal numerical integration using MATLAB (MATLAB 2018). Figure 7.1 shows the total energy dissipation of the VG30-WMA-MC specimen at 400, 600, and 800 με. Further, three approaches were used to separate the total energy dissipation into dissipation due to viscoelasticity (W_{ve_n}) and dissipation due to damage (W_{d_n}). The first approach is based on the pseudo-strain concept (Kim and Little 1989), the second approach is based on

the constitutive assumption that the viscoelastic phase angle does not change with damage (Varma et al. 2019), and in the third approach a linear viscoelastic model is used and the material parameters are assumed to be constant during damage progression (Varma et al. 2017). Further, for all the computations MATLAB (MATLAB 2018) was used.

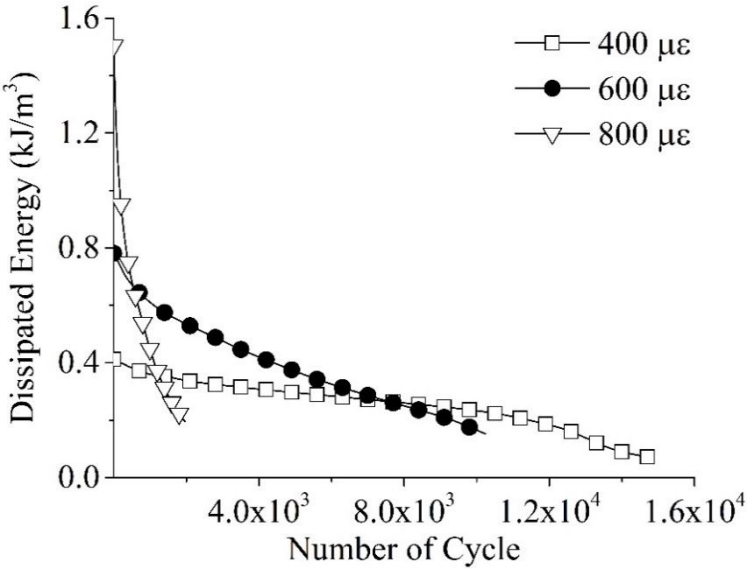

Fig. 7.1: Total energy dissipation of VG30-WMA-MC specimen

7.2.1 Approach 1 (Kim and Little 1989)

Kim and Little (1989) used the pseudo-strain concept to characterize the viscoelastic property of asphalt mixtures by distinguishing W_{d_n} and W_{ve_n} from the total dissipation. To estimate W_{d_n}, the pseudo-strain concept is used that defines a 'strain-like' quantity ($\epsilon_R(t)$) as shown in Equation (7.5):

$$\epsilon_R(t) := \frac{\sigma_{ve}(t)}{E_R}, \tag{7.5}$$

where, $\sigma_{ve}(t)$ is the viscoelastic stress at time 't' and E_R is the reference modulus and is assumed to be equal to $|E^*_{ve}|$. Here, pseudo strain is given by $\epsilon_R(t) = \epsilon_0 \sin(\omega t + \delta_{ve})$., where, $|E^*_{ve}|$ and δ_{ve} is considered as the dynamic modulus and phase angle of the material at undamaged state. The dissipation calculated using pseudo-strain is termed as dissipated pseudo-strain energy (DPSE). Kim and Little (1989) considered DPSE as the fatigue damage in the material. Further, the damage dissipation and viscoelastic dissipation for any cycle can be calculated using Equations (7.6) and (7.7) respectively.

$$W_{d_n} = \pi\, E_n\, \varepsilon_0^2 \sin(\delta_n - \delta_{ve}), \tag{7.6}$$

$$W_{ve_n} = \pi\, E_n\, \varepsilon_0^2 \sin(\delta_{ve}). \tag{7.7}$$

Following the methodology proposed by Varma et al. (2019), the DPSE (which is considered as damage dissipation) and viscoelastic dissipation were calculated for each cycle of loading for all the strain levels and materials tested. The cumulative value of viscoelastic dissipation and damage dissipation computed using pseudo-strain for VG30-WMA-L specimen and VG30-WMA specimen at 600 and 800 με is shown in Figure 7.2. In all the cases, it was observed that damage dissipation is less than 10 % of total dissipation. Also, the cumulative damage dissipation reached the steady value indicating that the damage dissipation near the specimen failure stage is not significant. In addition, Varma et al. (2019) showed that for a viscoelastic material under damaged condition, the sum of damage and viscous dissipation obtained based on the pseudo-strain approach will always be greater than total dissipation. The cumulative value of viscoelastic dissipation and damage dissipation computed using pseudo-strain for all the specimens is documented in Appendix C.1.

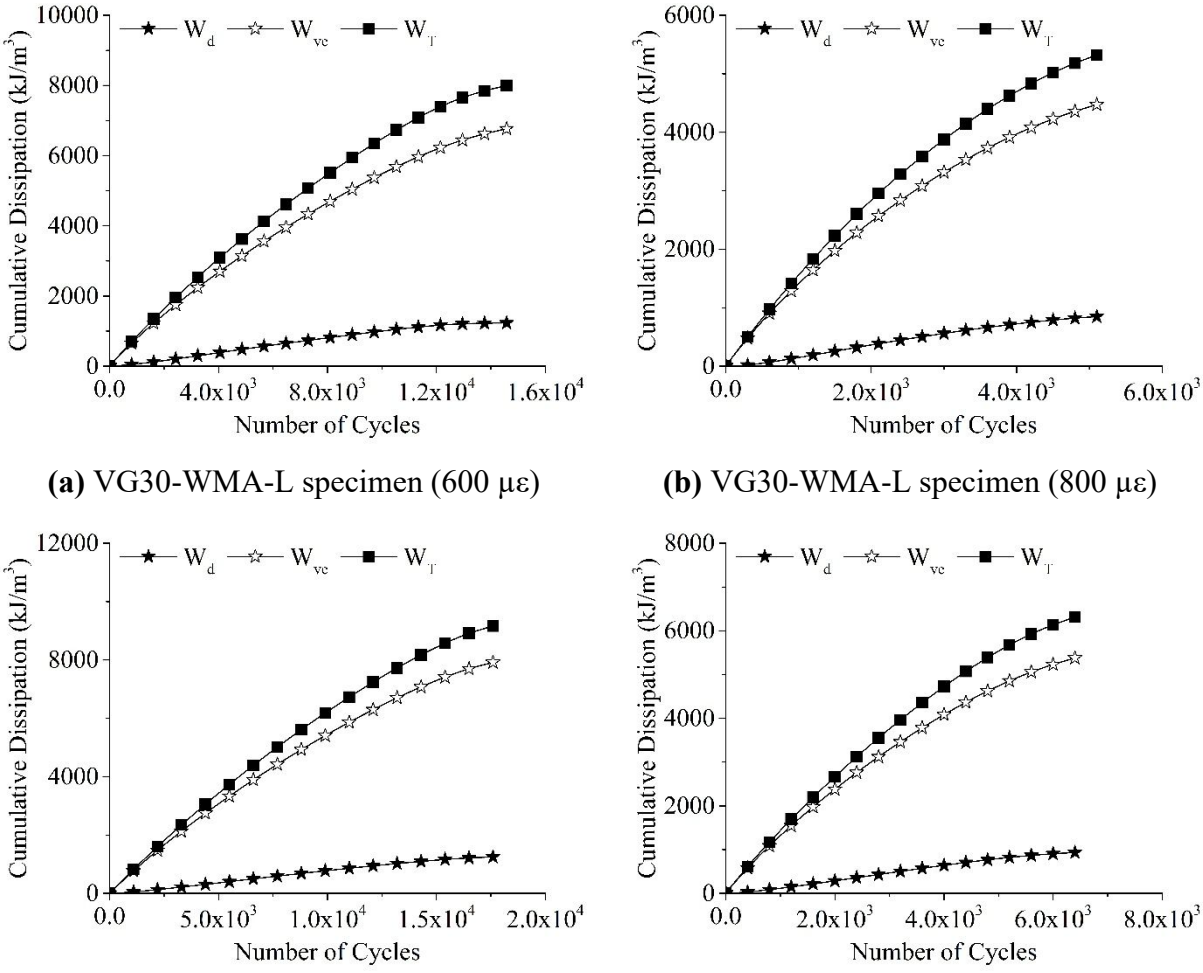

(a) VG30-WMA-L specimen (600 με)

(b) VG30-WMA-L specimen (800 με)

(c) VG30-WMA specimen (600 με)

(d) VG30-WMA specimen (800 με)

Fig. 7.2: Cumulative viscoelastic and damage dissipation based on pseudo-strain approach

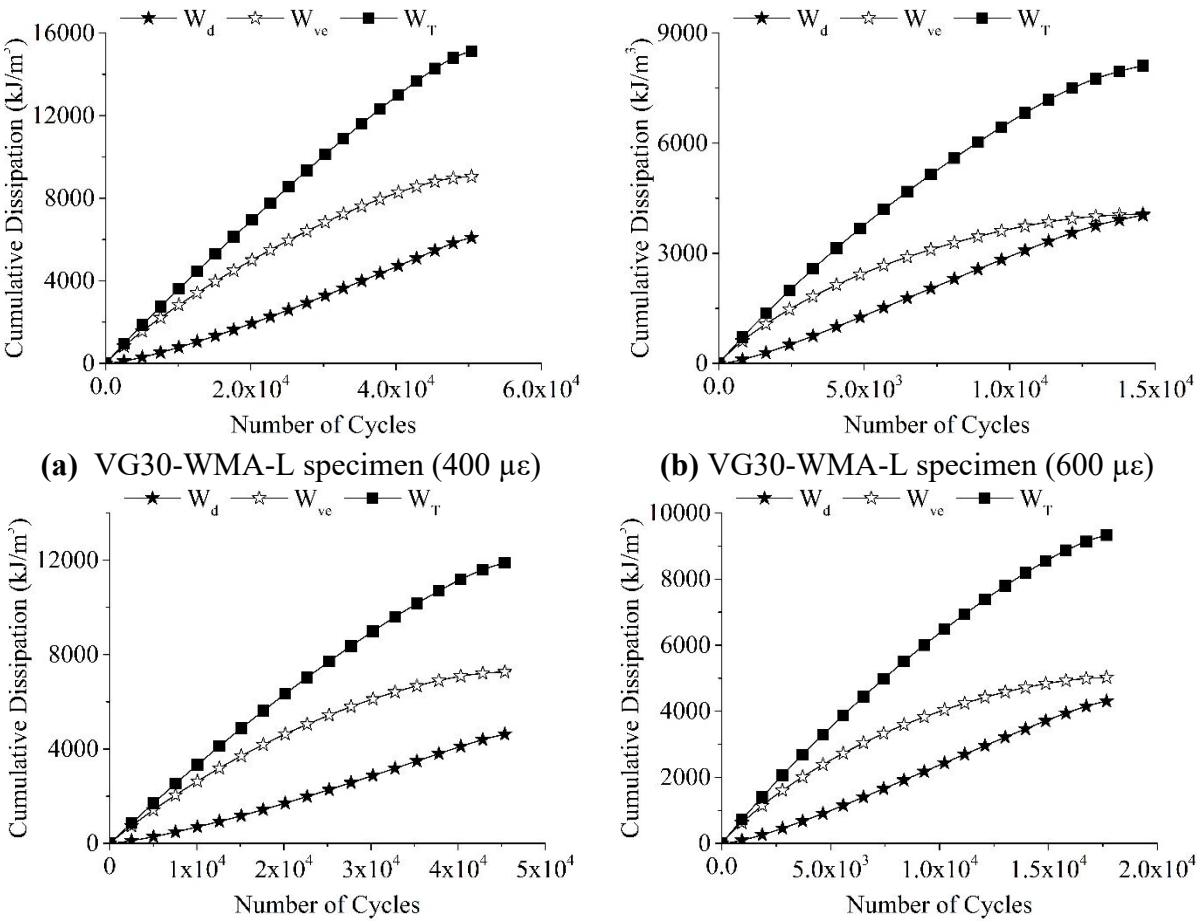

(a) VG30-WMA-L specimen (400 με) **(b)** VG30-WMA-L specimen (600 με)

(c) VG30-WMA specimen (400 με) **(d)** VG30-WMA specimen (600 με)

Fig. 7.3: Cumulative viscoelastic and damage dissipation using approach 2

7.2.2 Approach 2 (Varma et al. 2019)

In this approach, viscous dissipation of asphalt mixtures is calculated using a constitutive assumption that states, damage state of the material does not alter the viscous behaviour of the material. For any given stress history, the dissipation due to viscoelastic behaviour was assumed to be constant. With this assumption, the viscoelastic dissipation was calculated using Equation (7.8).

$$W_{ve_n} = \pi \frac{E_n^2}{E_{ve}^*} \varepsilon_0^2 \sin(\delta_{ve}). \tag{7.8}$$

Further, knowing the total dissipation, the damage dissipation was calculated using Equations (7.8) and (7.4). Figure 7.3 shows the cumulative viscoelastic and damage dissipation of VG30-WMA specimen and VG30-WMA-L specimen. In the strain controlled test, the stress history changes with each cycle of loading. The viscoelastic dissipation for the corresponding stress history of each cycle is shown as a function of number of load cycles in Figure 7.3. For all cases shown in Figure 7.3, it can be observed that the cumulative viscoelastic dissipation reached a steady value with the progress in damage. This indicates that viscoelastic dissipation becomes insignificant as the damage accumulates in the material. The cumulative viscoelastic dissipation and damage dissipation computed using approach 2 for all the specimens is documented in Appendix C.2.

7.2.3 Approach 3 (Varma et al. 2017)

In this approach of separating viscoelastic dissipation from total dissipation, Varma et al. (2017) used one dimensional linear viscoelastic rate type model to determine the viscoelastic dissipation. Varma et al. (2017) used Burgers model as described in Equation (7.9) for this purpose.

$$\sigma + \left(\frac{\eta_1}{R_1} + \frac{\eta_1}{R_2} + \frac{\eta_2}{R_2}\right)\dot{\sigma} + \frac{\eta_1\eta_2}{R_1R_2}\ddot{\sigma} = \eta_1\dot{\varepsilon} + \frac{\eta_1\eta_2}{R_2}\ddot{\varepsilon}, \tag{7.9}$$

where, $\dot{\sigma}$ and $\ddot{\sigma}$ represents first order and second order time derivative of stress and $\dot{\varepsilon}$ and $\ddot{\varepsilon}$ represents first order and second order time derivative of strain. The model functions η_1, η_2, R_1, and R_2 were determined for the undamaged condition of the specimen, and these functions were assumed to be the same for all cycles of loading till damage of the specimen. Here, 50th cycle was used which represents the undamaged specimen. The model functions η_1, η_2, R_1, and R_2 determined for 300th cycle stress and strain data for 400 and 600 με, and for 50th cycle for 800 με are listed in Table 7.1.

The viscoelastic dissipation for any given stress history is calculated using the integral expression given in the Equation (7.10).

$$W_{ve_n} = \int_0^t \sigma_n(t)\dot{\varepsilon_n}(t)dt. \tag{7.10}$$

For each cycle of stress history that was obtained experimentally, $\dot{\varepsilon_n}(t)$ were determined using the Burgers model functions given in the Table 7.1 and the expression given in the Equation (7.9). Further, the computation of viscoelastic dissipation was terminated at a point where the damage in the material dominated. This point of termination was identified using the shape of the Lissajous plot. The Lissajous plot of the undamaged specimen is a perfect ellipse. As the damage progress, the distortion in the shape of the Lissajous plot was observed and also the orientation of the Lissajous plot changes with the progress in damage. To determine the point of distortion of the Lissajous plot, 50th stress-strain cycle was considered as the reference cycle, and a second order polynomial conic ellipse as expressed in Equation (7.11) (Fitzgibbon et al. 1999) were used and the deviation in the Lissajous plot of n^{th} cycle from ellipse were measured in terms of R^2 value.

$$F(a,\ x) = ax^2 + bxy + cy^2 + dx + ey + f = 0, \tag{7.11}$$

where, a, b, c, d, e, and f are the model parameters. The evolution of R^2 was computed using Al-Khateeb and Shenoy (2011) approach to evaluate the variation in the shape of the Lissajous plot with reference to the initial cycle. The variation of R^2 for VG30 specimen at 400 microstrain is shown in Figure 7.4. Here, for VG30 specimen tested at 400 microstrain, the viscoelastic dissipation calculation was terminated at 32016 cycles and beyond this point, the total dissipation is considered completely as the damage dissipation. The point α as indicated in Figure 7.4 was identified for all the specimens tested and is consolidated in Table 7.2. Total dissipation and viscoelastic dissipation for VG30 specimen and VG30-MC specimen are shown in Figure 7.5. The total dissipation and viscoelastic dissipation computed using approach 3 for all the specimens is documented in appendix C.3.

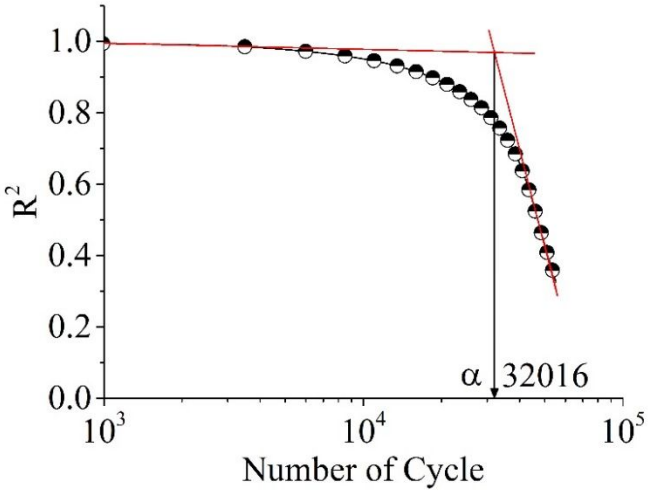

Fig. 7.4: Variation of R^2 for VG30 specimen at 400 microstrain

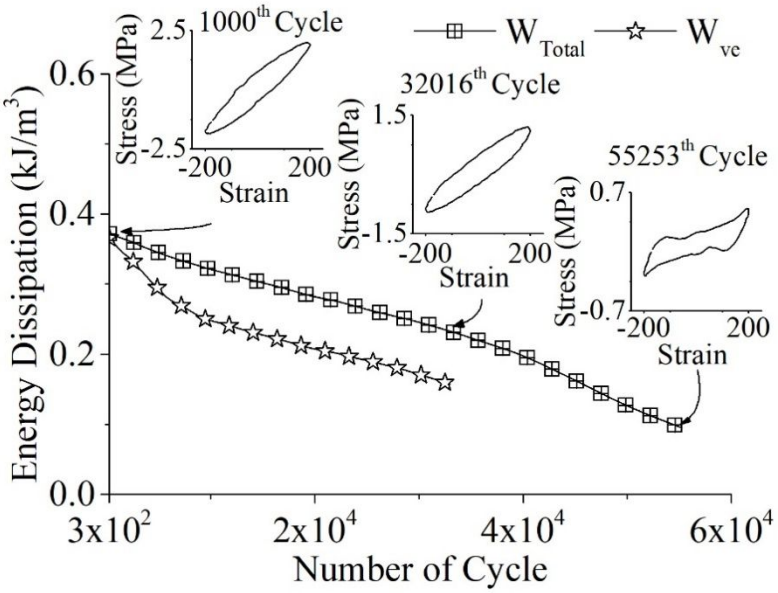

(a) VG30 specimen at 400 microstrain

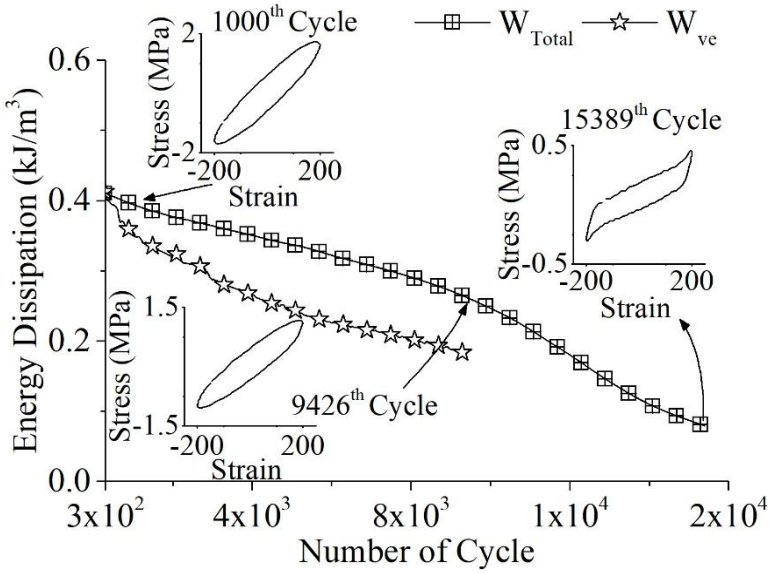

(b) VG30-MC specimen at 400 microstrain

Fig. 7.5: Evolution of W_T and W_{ve} calculated using approach 3

Figure 7.6 compares the cumulative damage dissipation obtained from different approaches for the selected specimens at 600 microstrain. Total dissipation being same for all the cases, the proportion of damage dissipation obtained using pseudo-strain approach (approach 1) was found to be lower than other approaches. Also, as highlighted before, the cumulative damage dissipation reached a steady value as the damage in the specimen is amplified (near the end of testing condition). Varma et al. (2019) also theoretically showed that the sum of viscous dissipation and damage dissipation calculated based on the pseudo-strain approach is equal to total dissipation only at undamaged condition of the specimen or when the specimen exhibits elastic behaviour. In this study, all the experiments were conducted at the temperature of 20 °C where the elastic behaviour dominates. Hence, the damage dissipation calculated using approach 1 for undamaged condition (at initial cycles of loading) at 20 °C can closely predict the actual damage in the material. It is also to be highlighted that the damage dissipation calculated based on pseudo-strain using Equation (7.6) largely depends on the viscoelastic phase angle (δ_{ve}). Kim et al. (2003) and Bhasin et al. (2009) termed this phase angle as true viscoelastic phase angle and Kim et al. (2003) used low strain amplitude test to measure this true viscoelastic phase angle. The damage dissipation calculated using approach 3 at the undamaged condition of the specimens (at initial cycles of loading) closely matches with approach 1. However, on continuous loading, as the damage accumulates, the dissipation calculated based on approach 3 increased thus predicting the expected trend. The dissipation

calculated based on approach 2 for the undamaged condition of the specimen is higher for all the three approaches. Hence, the application of approach 2 methodology for the specimen that is tested especially at lower strain levels (where the damage accumulates gradually) needs to be validated. The dissipation calculated based on approach 2 for the damaged specimen (near the end of the test) closely matched with approach 3. Further, the sensitivity of the damage dissipation obtained based on these approaches to strain level, WMA additive, hydrated lime, moisture condition was analyzed. For this purpose, a few hypotheses were made based on the expected behaviour of material at different strain amplitudes due to WMA additive, hydrated lime with and without moisture conditioning and the sensitivity of these approaches to capture the damage dissipation of material were verified.

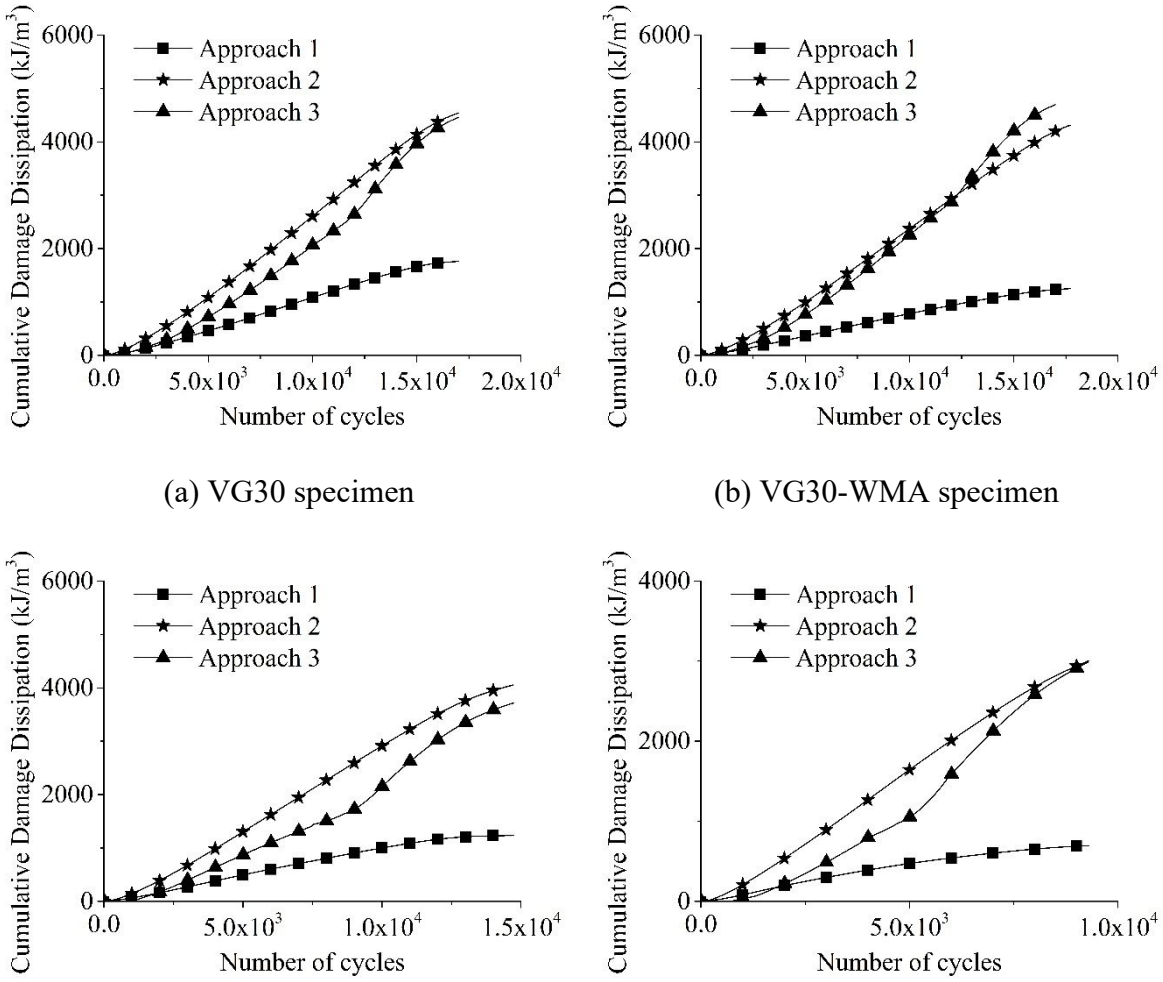

(a) VG30 specimen

(b) VG30-WMA specimen

(c) VG30-WMA-L specimen

(d) VG30-WMA-L-MC specimen

Fig. 7.6: Comparison of cumulative damage dissipation of different approaches at 600 microstrain

Table 7.1: Burgers model parameters

Specimen	400 με				600 με				800 με			
	η_1	η_2	R_1	R_2	η_1	η_2	R_1	R_2	η_1	η_2	R_1	R_2
	Pa-s		N/m^2		Pa-s		N/m^2		Pa-s		N/m^2	
VG30	0.28	12.0	361427	193.1	0.25	12.0	370104	206.1	0.24	12.3	391910	214.7
VG30-WMA	0.21	12.1	262244	183.3	0.18	12.2	255315	186.1	0.19	12.2	269288	186.3
VG30-L	0.11	10.2	2814176	843.3	0.27	12.0	377128	201.3	0.21	12.1	262785	184.1
VG30-WMA-L	0.27	12.0	361588	196.3	0.23	12.3	376240	208.6	0.20	12.1	275959	182.9
VG30-MC	0.25	12.1	373358	201.2	0.20	12.1	257509	184.3	0.16	13.7	147397	154.6
VG30-WMA-MC	0.19	12.1	257287	181.1	0.12	13.4	131564	153.7	0.10	16.5	88567	149.0
VG30-L-MC	0.10	10.2	3274792	928.2	0.21	10.7	976104	321.5	0.24	12.1	371010	198.6
VG30-WMA-L-MC	0.26	12.1	359760	189.1	0.25	12.1	359189	187.6	0.18	12.2	261007	175.9

Table 7.2: Termination cycles for the computation of viscoelastic dissipation using Varma et al. (2017)

Strain	VG30	VG30-WMA	VG30-L	VG30-WMA-L	VG30-MC	VG30-WMA-MC	VG30-L-MC	VG30-WMA-L-MC
400 με	32016	35240	67999	43701	9426	9955	13697	9354
600 με	11995	12072	9436	9137	1549	4629	3560	5238
800 με	3161	3502	1655	2603	564	413	565	1097

7.3 Hypotheses

The hypothesis made based on the expected behaviour of material at different strain amplitudes due to WMA additive, hydrated lime with and without moisture conditioning are listed below:

1. WMA is expected to have increased fatigue resistance due to reduced aging compared to HMA. It is therefore expected that the dissipation due to damage shall start at the later stage compared to dissipation due to viscous effects.
2. In a moisture damaged specimen, it is expected that out of the total dissipation, the dissipation due to damage can start dominating from the initial cycle itself. It is thus hypothesized that the moisture conditioned specimen (both HMA and WMA) dissipates more energy due to damage than the unconditioned specimen.
3. Moisture conditioned WMA is expected to have higher damage dissipation than moisture conditioned HMA due to higher moisture susceptibility.
4. With the addition of hydrated lime, stiffness is likely to increase due to filler effect and supposedly the damage dissipation shall be higher at higher strain for unconditioned HMA and unconditioned WMA. At lower strain, as the rate of loading is slow, the damage dissipation shall be lower for hydrated lime treated specimens for both unconditioned HMA and unconditioned WMA.
5. Due to the anti-stripping property of hydrated lime, the hydrated lime treated moisture conditioned specimens shall have lower damage dissipation compared to unconditioned HMA and WMA.

These hypotheses are also schematically represented in Figure 7.7. Further, the sensitivity of damage dissipation is verified for the above mentioned five hypotheses.

7.4 Hypothesis Testing

7.4.1 Hypothesis 1

Figure 7.6b shows the damage dissipation for VG30-WMA specimen at 600 microstrain. It is expected that the damage dissipation of WMA to be slower at initial cycles of loading and on comparing three approaches, the dissipation based on pseudo-strain approach (approach 1) is closely predicting the expected trend during initial cycles of loading.

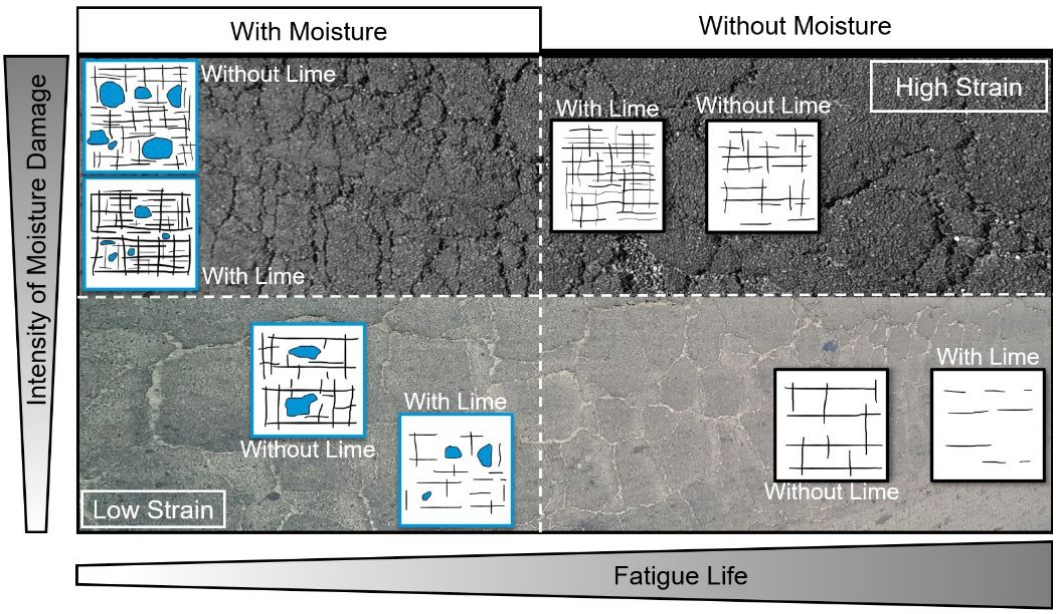

Fig. 7.7: Schematics of the influence of strain, lime filler and moisture on the fatigue life of asphalt mixtures

7.4.2 Hypothesis 2

Table 7.3 to 7.5 shows the proportion of damage dissipation of HMA and WMA specimens on dry and moisture conditioned state. Table 7.6 to 7.8 shows the proportion of damage dissipation in HMA and WMA specimens with and without hydrated lime filler. The sensitivity of various approaches used in the damage calculation to satisfy hypothesis 2 is verified using Table 7.3, 7.4 and 7.5. Table 7.3 shows that the proportion of damage dissipation in 1000^{th}, 500^{th}, and 100^{th} cycle for 400, 600, and 800 με respectively calculated based on approach 1 in the moisture conditioned HMA specimen are comparatively less than their respective dry specimens. This indicates that the damage dissipation calculated based on approach 1 could not capture the effect of moisture damage in the specimen. The proportion of damage dissipation based on approach 2 (Table 7.4) and approach 3 (Table 7.5) in the moisture conditioned specimen in most of the cases corresponding to 400 and 600 microstrain are found to be more than their corresponding dry specimens and it is as expected. All the damage dissipation calculations for 800 microstrain were computed from the 50^{th} cycle. At higher strain levels of 800 microstrain, the damage might have started well before 50 cycles of loading. Hence, 800 microstrain data are not used in checking the sensitivity of all the three approaches in damage dissipation calculation.

7.4.3 Hypothesis 3

On comparing the proportion of damage dissipation of VG30-MC specimen and VG30-WMA-MC specimen in Table 7.3, 7.4 and 7.5, the damage dissipation of VG30-WMA-MC specimen at 400 microstrain are found to be higher compared to moisture conditioned HMA specimen.

7.4.4 Hypothesis 4

Table 7.6 to 7.8 is used to check the sensitivity of damage dissipation of approaches 1, 2, and 3 in the 40000th, 10000th, and 2500th cycle for 400, 600, and 800 microstrain respectively. The damage dissipation of VG30-L specimen at lower strain levels was expected to be lower than VG30 specimen. At higher strain levels, the filler effect due to lime is expected to dominate and hence higher proportion of damage is expected for lime treated specimens. From Table 7.6, it can be observed that approach 1 is not sensitive to capture the filler effect at different strain levels. Approach 3 (Table 7.8) can clearly capture the strain sensitivity of hydrated lime filler effect on the damage dissipation.

Table 7.3: Proportion of viscous and damage dissipation on dry and moisture conditioned HMA and WMA specimens based on approach 1

Specimen	400 με	600 με	800 με
	1000th Cycle	500th Cycle	100th Cycle
VG30	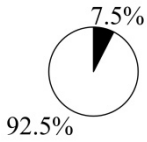		
VG30-MC	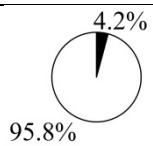	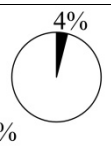	
VG30-WMA	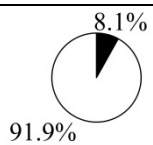		
VG30-WMA-MC	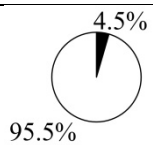		

Table 7.4: Proportion of viscous and damage dissipation on dry and moisture conditioned HMA and WMA specimens based on approach 2

Specimen	400 με	600 με	800 με
	1000th Cycle	500th Cycle	100th Cycle
VG30	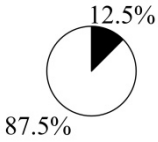		
VG30-MC	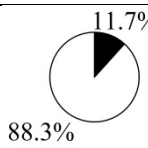		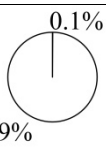
VG30-WMA	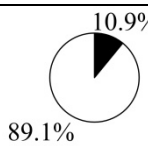		
VG30-WMA-MC	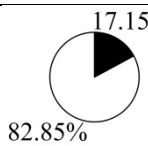		

Table 7.5: Proportion of viscous and damage dissipation on dry and moisture conditioned HMA and WMA specimens based on approach 3

Specimen	400 με	600 με	800 με
	1000th Cycle	500th Cycle	100th Cycle
VG30	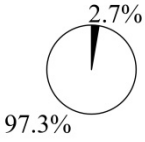		
VG30-MC	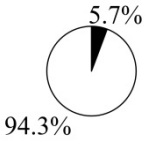		
VG30-WMA	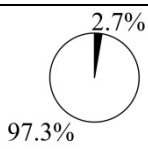		
VG30-WMA-MC	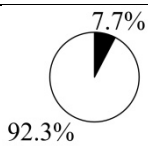		

Table 7.6: Proportion of viscous and damage dissipation on HMA and WMA specimens with and without hydrated lime based on approach 1

Specimen	400 με	600 με	800 με
	40000th Cycle	10000th Cycle	2500th Cycle
VG30	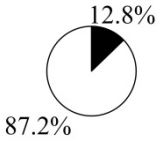		
VG30-L	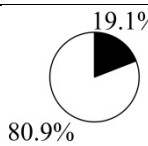		
VG30-WMA	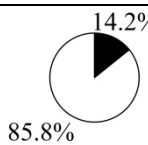		
VG30-WMA-L	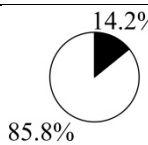		

Table 7.7: Proportion of viscous and damage dissipation on HMA and WMA specimens with and without hydrated lime based on approach 2

Specimen	400 με	600 με	800 με
	40000th Cycle	10000th Cycle	2500th Cycle
VG30	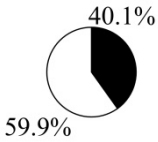		
VG30-L	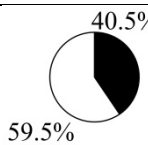		
VG30-WMA	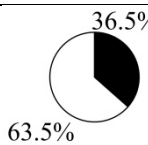	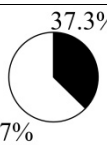	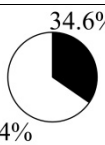
VG30-WMA-L	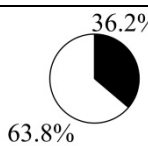		

Table 7.8: Proportion of viscous and damage dissipation on HMA and WMA specimens with and without hydrated lime based on approach 3

Specimen	400 με	600 με	800 με
	40000th Cycle	10000th Cycle	2500th Cycle
VG30	32.7% / 67.3%	31.6% / 68.4%	29.9% / 70.1%
VG30-L	11.4% / 88.6%	35.9% / 64.1%	47.4% / 52.6%
VG30-WMA	34.1% / 65.9%	30.6% / 69.4%	32.7% / 67.3%
VG30-WMA-L	13% / 87%	34.5% / 65.5%	33.6% / 66.4%

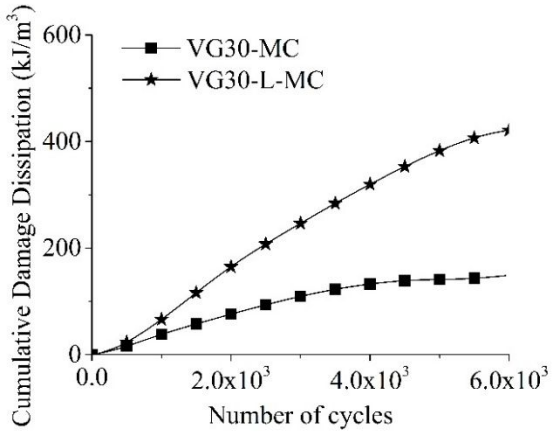

(a) Approach 1

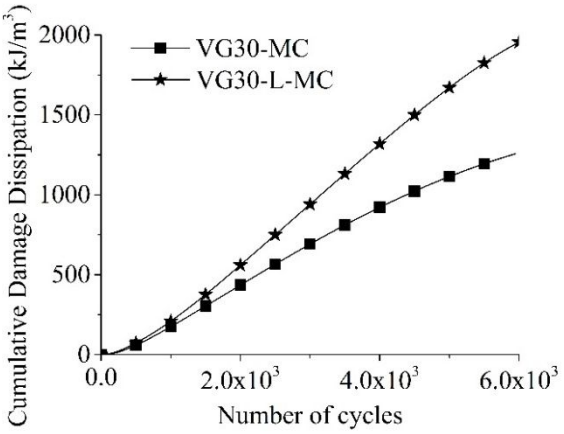

(b) Approach 2

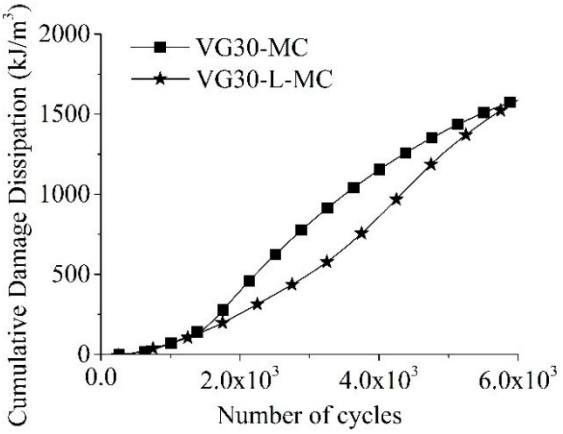

(c) Approach 3

Fig. 7.8: Damage dissipation of moisture conditioned VG30 specimens

7.4.5 Hypothesis 5

Figure 7.8 is used to check the sensitivity of damage dissipation based on various approaches for moisture conditioned lime specimens. VG30-L-MC specimen is expected to exhibit lower damage than VG30-MC specimen. Figure 7.8a and 7.8b shows the reversal trend and Figure 7.8c captures the expected trend. The same behaviour is also observed in WMA specimen.

7.5 Summary

In this chapter, three approaches are used to separate damage dissipation from total dissipation. The three approaches are pseudo-strain concept (Kim and Little 1989), approach based on the constitutive assumption (Varma et al. 2019), and the approach based on a linear viscoelastic model (Varma et al. 2017). The computation of damage dissipation using the three approaches are elaborated in this chapter. The influence of WMA additive, hydrated lime, and moisture damage on the damage dissipation based on three approaches were discussed. Five hypotheses were made and the validation of the hypotheses was done using proportion of damage dissipation based on the influence of WMA additive, hydrated lime, and moisture damage. Through analysis, it is observed that approach 3 could capture the change in the proportion of damage dissipation of asphalt mixtures due to the warm mix additive, lime additive and moisture conditioning of the specimen.

The next chapter presents the summary of the entire research work, conclusions drawn from the study, and pointers for future work.

CHAPTER 8

SUMMARY AND CONCLUSIONS

8.1 Summary

The study consists of four stages. In the first stage, the process to saturate and moisture condition large-sized fatigue beam was developed. In the second stage, ITS tests were conducted on cylindrical specimens and the results revealed that hydrated lime improved moisture susceptibility of both HMA and WMA specimens. In the third stage, fatigue tests were conducted on beam specimens and the evolution of flexural stiffness and evolution of energy dissipation were used to quantify the influence of warm mix additive, hydrated lime, and moisture conditioning. The fatigue life of asphalt mixtures were calculated using AASHTO, energy ratio, ASTM and RDEC methods. In the fourth stage, the total energy dissipated in each cycle were separated into viscoelastic dissipation and dissipation due to damage using three approaches. The damage dissipation was then used to verify the sensitivity of the three approaches and the influence of warm mix additive, hydrated lime, and moisture conditioning on damage dissipation were discussed. The conclusions drawn from the study are presented in the next section.

8.2 Conclusions

From the experimental investigations including the ITS test and four-point beam bending test on HMA and WMA with and without hydrated lime on dry and moisture conditioned specimens, the following conclusions are drawn.

1. The efficacy of indirect tensile strength ratio test in evaluating the moisture sensitivity of asphalt mixture is quantified through indirect tensile strength and tensile strength ratio and the following conclusions are drawn:
    a) In order to evaluate the effect of hydrated lime and warm mix additive on indirect tensile strength of asphalt mixtures in both dry and wet condition, indirect tensile strength tests were initially conducted. On comparing the indirect tensile strength test results on cylindrical specimens subjected to constant displacement rate of 50 mm per minute, it is observed that even though the addition of lime reduced the tensile strength of dry HMA specimen, the tensile strength remained constant for WMA

specimen. For moisture conditioned specimen, even though there is reduction in tensile strength for HMA specimen with the addition of lime, there is an increase in tensile strength for WMA specimen. Thus, mixed trends are observed in tensile strength test results as the cylindrical specimens were subjected to higher strains. This shows that indirect tensile strength as a parameter is not effective in capturing the relative effects of lime and warm mix additive.

b) In order to evaluate the effect of hydrated lime and warm mix additive on moisture resistance of asphalt mixtures, the tensile strength ratio was calculated from the dry and wet indirect tensile strengths. It is observed that tensile strength ratio for VG30-WMA specimen is lower than VG30 specimen showing that the VG30-WMA specimen is more susceptible to moisture than VG30 specimen. Further, the tensile strength ratio for both VG30 and VG30-WMA specimens are lower than the recommended value of 80% which shows that both these mixtures are highly moisture susceptible. However, upon adding hydrated lime to both these mixtures, the tensile strength ratio for VG30-L and VG30-WMA-L specimens increased beyond 80% due to the antistripping characteristics of hydrated lime. Overall, the moisture resistance of VG30-L specimen is superior followed by VG30-WMA-L, VG30, and VG30-WMA specimens. This shows that the tensile strength ratio as a parameter is effective in quantifying the improvement in moisture resistance of asphalt mixtures due to addition of hydrated lime. Even though the indirect tensile strength test acts as a rapid test to capture the relative effects of hydrated lime and warm mix additive on the moisture resistance of asphalt mixtures, it fails to capture the relative effects of hydrated lime and warm mix additive separately in dry and wet conditions as the test specimens are subjected to massive strains.

c) The primary limitation of the TSR is that it is a pass/fail test, as the peak load alone is used to determine the moisture susceptibility of asphalt mixtures. In the indirect tensile strength test, the load is applied in the diametrical direction where uniform tensile stress is developed along the vertical diametrical plane and the state of stress is biaxial. Further, the specimen in an indirect tensile strength test undergoes permanent deformation. This warrants the use of fatigue test to evaluate the moisture susceptibility of asphalt mixtures which realistically captures the incremental damage after each loading cycle. Further, four-point bend fatigue test has been considered for the current study as it has the advantage of applying stress reversals which is practically impossible in the indirect fatigue test where the specimen also undergoes

permanent deformation which is restricted in the four-point bend fatigue test. Moreover, a sinusoidal load is applied at third-points in the four-point bend fatigue test resulting in uniform bending moment within the beam mid span where specimen failure initiates in the region of relatively uniform stress and the state of stress is uniaxial.

2. The rate of reduction in flexural stiffness and energy dissipation is observed to be higher at 800 microstrain followed by 600 and 400 microstrain. Similarly, the fatigue life is higher at 400 microstrain followed by 600 and 800 microstrain. At 400 microstrain, the lime-treated dry specimen showed improved resistance to reduction in flexural stiffness and energy dissipation whereas at higher strains (600 and 800 microstrain), the lime-treated dry specimen showed reduced resistance to reduction in flexural stiffness and energy dissipation. However, the addition of hydrated lime exhibited beneficial effects on moisture conditioned specimens at all strain levels. This shows that the beneficial effect of hydrated lime could be seen for moisture conditioned specimens and not for dry specimens at higher strain levels. In the similar lines, on comparing the indirect tensile strength test results on cylindrical specimens subjected to constant displacement rate of 50 mm per minute, it is observed that even though the addition of lime reduced the tensile strength of dry HMA specimen, the tensile strength remained constant for WMA specimen. For moisture conditioned specimens, even though there is reduction in tensile strength for HMA specimen with the addition of lime, there is an increase in tensile strength for WMA specimen. Thus, mixed trends are observed in tensile strength test results on cylindrical specimens which were subjected to higher strains.

   Fatigue tests on beam specimens through four-point bending were conducted to evaluate the influence of warm mix additive, hydrated lime, and moisture conditioning on the evolution of flexural stiffness and energy dissipation. As no standard test protocols are available for the simulation of moisture damage in the beam specimens, a suitable methodology was initially designed in this study to simulate the moisture damage in the beam specimens and the following conclusions are drawn:

   a. The influence of warm mix additive on the evolution of flexural stiffness is studied by comparing the normalized flexural stiffness of VG30 specimen with VG30-WMA specimen. The flexural stiffness curve exhibited two-stage slope in which the first slope is gradual compared to the second slope. At 400 microstrain, the reduction in flexural stiffness of VG30-WMA specimen at the initial stage was observed to be gradual compared to VG30 specimen. However, on continuous

loading, flexural stiffness of VG30-WMA specimen was observed to reduce at a rapid rate compared to VG30 specimen. At 600 microstrain, the stiffness of VG30-WMA specimen reduced rapidly than VG30 specimen. The variation in flexural stiffness at 800 microstrain is similar to 600 microstrain.

b. The influence of hydrated lime on the evolution of flexural stiffness is studied by comparing the normalized flexural stiffness of VG30 with VG30-L and VG30-WMA with VG30-WMA-L. At 400 microstrain, the lime-treated specimen showed improved resistance to reduction in the flexural stiffness and energy dissipation compared to asphalt mixture specimen without lime. However, the trend in the evolution of flexural stiffness and energy dissipation of lime treated specimens changed at higher strain levels (600 and 800 microstrain) where the lime-treated specimens exhibited an increased rate of change in flexural stiffness and energy dissipation.

c. All the moisture conditioned specimens exhibited an increased rate of reduction in flexural stiffness compared to unconditioned dry specimens. On comparing the flexural stiffness evolution of VG30-WMA-MC at 400 microstrain with VG30-MC, it is observed that the moisture conditioned WMA mixture exhibited a rapid reduction in flexural stiffness compared to the HMA mixture. Thus, the WMA mixture is prone to moisture susceptibility compared to the HMA mixture. Even though the addition of lime did not show any beneficial effect on the dry specimen, the reduction in flexural stiffness of VG30-L-MC specimen is gradual compared to the specimen without lime (VG30-MC). At all strain levels, the beneficial effect of hydrated lime is observed on moisture conditioned VG30 and VG30-WMA specimens.

d. The flexural stiffness as a function of a number of cycles for both WMA and HMA specimens with and without hydrated lime under dry and moisture damaged state exhibited two stage slopes. The number of cycles corresponding to 50% of initial flexural stiffness coincided with the point of change of slope. Energy dissipation for all the test specimens also exhibited two slopes, and the point of change of slope occurred later than the point of 50% of initial flexural stiffness.

3. In order to quantify the influence of moisture and hydrated lime on the fatigue life of hot mix asphalt and warm mix asphalt, the fatigue life of the asphalt mixtures is estimated using four different post-processing techniques and the following conclusions are drawn:

a. Fatigue life estimated from the flexural stiffness was found to be consistently lower than the fatigue life estimated using the energy ratio method. For the ASTM method of estimation of fatigue life of asphalt mixtures, especially for the moisture damaged specimens, the sharp peak in the normalized modulus curve could not be defined. For the RDEC method, the "bathtub" curve did not show decisive phase III. Thus, fatigue life using the ASTM method and the RDEC method is not considered in the comparison as the fatigue life for few specimens could not be determined using these two methods.
b. The addition of warm mix additive slightly increased the fatigue life at 400 microstrain and decreased the fatigue life at 600 and 800 microstrain.
c. The addition of hydrated lime improved the fatigue life of both WMA and HMA mixture at 400 microstrain. At higher strain level, the addition of hydrated lime reduced the fatigue life of both mixtures. On moisture conditioning, the fatigue life of the asphalt mixtures decreased and the percentage reduction is observed to be in the range of 60 to 70% compared to the dry specimen.
d. A reduction in fatigue life due to moisture damage also occurred in specimens with hydrated lime. However, the addition of hydrated lime reduced the magnitude of moisture damage.

4. In order to evaluate the effect of moisture on viscoelastic dissipation and dissipation due to damage on addition of hydrated lime in hot mix asphalt and warm mix asphalt, it is necessary to separate dissipation due to damage from the total dissipation for which three different existing approaches are used. As the proportion of viscous and damage dissipation depends on the type of materials and moisture damage state of the specimen, the sensitivity of these three approaches to determine the damage dissipation based on the expected fatigue damage criteria in the material were verified and the following conclusions are drawn:
    a. The damage dissipation determined based on pseudo-strain approach (approach 1) is minimal compared to other two approaches.
    b. The damage dissipation obtained from approach 1 and approach 3 is coinciding for the undamaged condition of the specimen.
    c. The damage dissipation obtained from approach 2 and approach 3 is coinciding for the damaged state of the specimen.

d. The damage dissipation based on approach 1 and approach 2 did not capture the change in fatigue damage trend of asphalt mixtures due to the warm mix additive, lime additive, and moisture conditioning of the specimen.
e. The damage dissipation based on approach 3 could capture the change in fatigue damage trend of asphalt mixtures due to the warm mix additive, lime additive, and moisture conditioning of the specimen. However, this approach has to be restricted to the strain amplitude level where the response of the material is linear.

8.3 Scope for Further Study

Following points can be considered to extend the current research study:

1. The entire set of specimens considered in this study were prepared using one single gradation of aggregates including bituminous concrete grading II and one grade of unmodified asphalt. Such dense-graded asphalt mixtures are used for high density traffic corridors in India. However, the performance of the asphalt mixtures is expected to be different for other gradations including gap-graded and open-graded mixtures. Further, modified binders are expected to have varied performance characteristics. Use of modified binders considering various gradations of aggregate can be explored.
2. Two types of additives, lime a conventional antistripping additive, and Evotherm a commercial warm mix additive was used in the present investigation. The moisture sensitivity of asphalt mixtures including the interactions between the additives and the binder very much depends on the type of additives. Usage of several other types and combinations of additives in asphalt mixtures can have a significant effect on the performance of the asphalt mixtures especially when coupled with binder aging.
3. The vacuum saturation described in this study subjected the specimens to a prolonged duration of vacuum saturation. During such a process, the air voids structure of the material can change, and additional investigations are required to ensure that the integrity of the internal structure of the specimens is preserved.
4. The possibility of an optimum dosage of hydrated lime leading to improved fatigue life exists and it is expected that such dosage will also depend on the temperature of testing. Additional experimental investigation and analysis of data are needed to link the influence of hydrated lime on the mechanical response during fatigue and fracture.
5. The performance of asphalt mixtures in this study was evaluated using indirect tension test and four-point beam bending fatigue test. Other performance tests on asphalt mixtures including dynamic modulus, permanent deformation, and semi-circular fracture

toughness tests can be carried out to understand moisture susceptibility of the asphalt mixtures at varied temperatures, states of stress, and rate of loading.

APPENDIX A

Table A.1: Specimen fabricated and air voids details used in ITS test

Serial No.	Mixture	Specimen ID	Air Voids	Test Details	Data Included in Report (Y/N)
1	VG-30	VG30	6.6	25 °C, ITS	Y
2	VG-30	VG30	6.9	25 °C, ITS	Y
3	VG-30	VG30	6.1	25 °C, ITS	Y
4	VG-30	VG30-MC	7.2	25 °C, ITS, T283	Y
5	VG-30	VG30-MC	6.7	25 °C, ITS, T283	Y
6	VG-30	VG30-MC	7.1	25 °C, ITS, T283	Y
7	VG-30	VG30-WMA	6.7	25 °C, ITS	Y
8	VG-30	VG30-WMA	6.8	25 °C, ITS	Y
9	VG-30	VG30-WMA	6.6	25 °C, ITS	Y
10	VG-30	VG30-WMA-MC	6.8	25 °C, ITS, T283	Y
11	VG-30	VG30-WMA-MC	6.4	25 °C, ITS, T283	Y
12	VG-30	VG30-WMA-MC	6.2	25 °C, ITS, T283	Y
13	VG-30	VG30-L	6.8	25 °C, ITS	Y
14	VG-30	VG30-L	6.6	25 °C, ITS	Y
15	VG-30	VG30-L	6.9	25 °C, ITS	Y
16	VG-30	VG30-L-MC	7.2	25 °C, ITS, T283	Y
17	VG-30	VG30-L-MC	6.1	25 °C, ITS, T283	Y
18	VG-30	VG30-L-MC	6.8	25 °C, ITS, T283	Y
19	VG-30	VG30-WMA-L	7.1	25 °C, ITS	Y
20	VG-30	VG30-WMA-L	6.9	25 °C, ITS	Y
21	VG-30	VG30-WMA-L	6.1	25 °C, ITS	Y
22	VG-30	VG30-WMA-L-MC	6.5	25 °C, ITS, T283	Y
23	VG-30	VG30-WMA-L-MC	6.2	25 °C, ITS, T283	Y
24	VG-30	VG30-WMA-L-MC	6.4	25 °C, ITS, T283	Y

Table A.2: Specimen fabricated and air voids details used in fatigue test

Serial No.	Mixture	Specimen ID	Air Voids	Test Details	Considered for Testing/ Data Included in Report (Y/N)
1	VG-30	BVPU-03-TL	4.715	10 Hz, 20 °C, 800 με	Y/Y
2	VG-30	BVPU-03-TR	4.025		
3	VG-30	BVPU-03-BL	5.334	-	-
4	VG-30	BVPU-03-BR	4.492	10 Hz, 20 °C, 400 με	Y/Y
5	VG-30	BVPU-05-TL	4.623	10 Hz, 20 °C, 600 με	Y/Y
6	VG-30	BVPU-05-TR	4.319		
7	VG-30	BVPU-05-BL	5.011	-	-
8	VG-30	BVPU-05-BR	4.325		
9	VG-30	BVEPU-06-TL	4.651	10 Hz, 20 °C, 400 με	Y/Y
10	VG-30	BVEPU-06-TR	4.417	10 Hz, 20 °C, 600 με	Y/Y
11	VG-30	BVEPU-06-BL	4.398	10 Hz, 20 °C, 800 με	Y/Y
12	VG-30	BVEPU-06-BR	4.072		
13	VG-30	BVELU-07-TL	4.229	10 Hz, 20 °C, 400 με	Y/Y
14	VG-30	BVELU-07-TR	4.073	10 Hz, 20 °C, 600 με	Y/Y
15	VG-30	BVELU-07-BL	4.108		
16	VG-30	BVELU-07-BR	4.008	10 Hz, 20 °C, 800 με	Y/Y
17	VG-30	BVELU-10-TL	Communication Error	-	-
18	VG-30	BVELU-10-TR		-	-
19	VG-30	BVELU-10-BL		-	-
20	VG-30	BVELU-10-BR		-	-
21	VG-30	BVLPU-11-TL	3.957	10 Hz, 20 °C, 600 με	Y/Y
22	VG-30	BVLPU-11-TR	4.197	10 Hz, 20 °C, 400 με	Y/Y
23	VG-30	BVLPU-11-BL	3.911		

Serial No.	Mixture	Specimen ID	Air Voids	Test Details	Considered for Testing/ Data Included in Report (Y/N)
24	VG-30	BVLPU-11-BR	4.561	10 Hz, 20 °C, 800 με	Y/Y
25	VG-30	BVLPU-12-TL	4.054		
26	VG-30	BVLPU-12-TR	3.428		
27	VG-30	BVLPU-12-BL	3.994		
28	VG-30	BVLPU-12-BR	4.070		
29	VG-30	BVPU-13	Air voids Not Achieved	-	-
30	VG-30	BVPU-13		-	-
31	VG-30	BVPU-13		-	-
32	VG-30	BVPU-13		-	-
33	VG-30	BVPU-14	Air voids Not Achieved	-	-
34	VG-30	BVPU-14		-	-
35	VG-30	BVPU-14		-	-
36	VG-30	BVPU-14		-	-
37	VG-30	BVLPU-15-TL	3.687	10 Hz, 20 °C, 400 με	Y/N
38	VG-30	BVLPU-15-TR	4.092	10 Hz, 20 °C, 400 με, MC	Y/Y
39	VG-30	BVLPU-15-BL	3.393	-	-
40	VG-30	BVLPU-15-BR	3.632	10 Hz, 20 °C, 600 με	Y/N
41	VG-30	BVPU-16-TL	3.911	10 Hz, 20 °C, 600 με	Y/N
42	VG-30	BVPU-16-TR	4.567	10 Hz, 20 °C, 600 με, MC	Y/Y
43	VG-30	BVPU-16-BL	3.791	10 Hz, 20 °C, 400 με	Y/N
44	VG-30	BVPU-16-BR	4.541	10 Hz, 20 °C, 400 με, MC	Y/Y
45	VG-30	BVEPU-17-TL	3.858	10 Hz, 20 °C, 400 με, MC	Y/N
46	VG-30	BVEPU-17-TR	3.338	10 Hz, 20 °C, 400 με	Y/N
47	VG-30	BVEPU-17-BL	3.617	10 Hz, 20 °C, 600 με	Y/N
48	VG-30	BVEPU-17-BR	4.532	10 Hz, 20 °C, 600 με, MC	Y/N
49	VG-30	BVELU-18-TL	4.028	10 Hz, 20 °C, 400 με, MC	Y/N

Serial No.	Mixture	Specimen ID	Air Voids	Test Details	Considered for Testing/ Data Included in Report (Y/N)
50	VG-30	BVELU-18-TR	4.527	10 Hz, 20 °C, 400 με	Y/N
51	VG-30	BVELU-18-BL	3.713	10 Hz, 20 °C, 600 με	Y/N
52	VG-30	BVELU-18-BR	4.087	10 Hz, 20 °C, 600 με, MC	Y/N
53	VG-30	BVLPU-19-TL	4.146		
54	VG-30	BVLPU-19-TR	5.144	-	-
55	VG-30	BVLPU-19-BL	3.958	10 Hz, 20 °C, 600 με, MC	Y/Y
56	VG-30	BVLPU-19-BR	4.268	10 Hz, 20 °C, 800 με, MC	Y/N
57	VG-30	BVPU-20-TL	Air voids Not Achieved	-	-
58	VG-30	BVPU-20-TR		-	-
59	VG-30	BVPU-20-BL		-	-
60	VG-30	BVPU-20-BR		-	-
61	VG-30	BVPU-21-TL	3.598		
62	VG-30	BVPU-21-TR	4.144	10 Hz, 20 °C, 800 με, MC	Y/Y
63	VG-30	BVPU-21-BL	4.897		
64	VG-30	BVPU-21-BR	4.544		
65	VG-30	BVEPU-22-TL	4.286	10 Hz, 20 °C, 800 με, MC	Y/N
66	VG-30	BVEPU-22-TR	3.586		
67	VG-30	BVEPU-22-BL	4.300	10 Hz, 20 °C, 600 με, MC	Y/Y
68	VG-30	BVEPU-22-BR	3.986	10 Hz, 20 °C, 400 με, MC	Y/N
69	VG-30	BVELU-23-TL	4.950	-	-
70	VG-30	BVELU-23-TR	4.629	10 Hz, 20 °C, 600 με, MC	Y/N
71	VG-30	BVELU-23-BL	3.532	10 Hz, 20 °C, 800 με, MC	Y/Y
72	VG-30	BVELU-23-BR	3.201	10 Hz, 20 °C, 400 με, MC	Y/N
73	VG-30	BVLPU-30-TL	4.592		
74	VG-30	BVLPU-30-TR	4.584		
75	VG-30	BVLPU-30-BL	4.340	10 Hz, 20 °C, 800 με, MC	Y/Y

Serial No.	Mixture	Specimen ID	Air Voids	Test Details	Considered for Testing/ Data Included in Report (Y/N)
76	VG-30	BVLPU-30-BR	3.744		
77	VG-30	BVEPU-31-TL	4.443	10 Hz, 20 °C, 800 με, MC	Y/Y
78	VG-30	BVEPU-31-TR	4.286	10 Hz, 20 °C, 400 με, MC	Y/Y
79	VG-30	BVEPU-31-BL	4.288	10 Hz, 20 °C, 400 με, MC	Y/N
80	VG-30	BVEPU-31-BR	3.933		
81	VG-30	BVELU-32-TL	4.485	10 Hz, 20 °C, 600 με, MC	Y/Y
82	VG-30	BVELU-32-TR	4.980	10 Hz, 20 °C, 400 με, MC	Y/Y
83	VG-30	BVELU-32-BL	6.276	-	-
84	VG-30	BVELU-32-BR.	5.486	-	-
85	VG-30	BVELU-44-TL	4.647		
86	VG-30	BVELU-44-TR	4.429		
87	VG-30	BVELU-44-BL	3.736		
88	VG-30	BVELU-44-BR	4.104	10 Hz, 20 °C, 400 με, MC	Y/N

APPENDIX B

B.1. Flextural Stiffness Plots

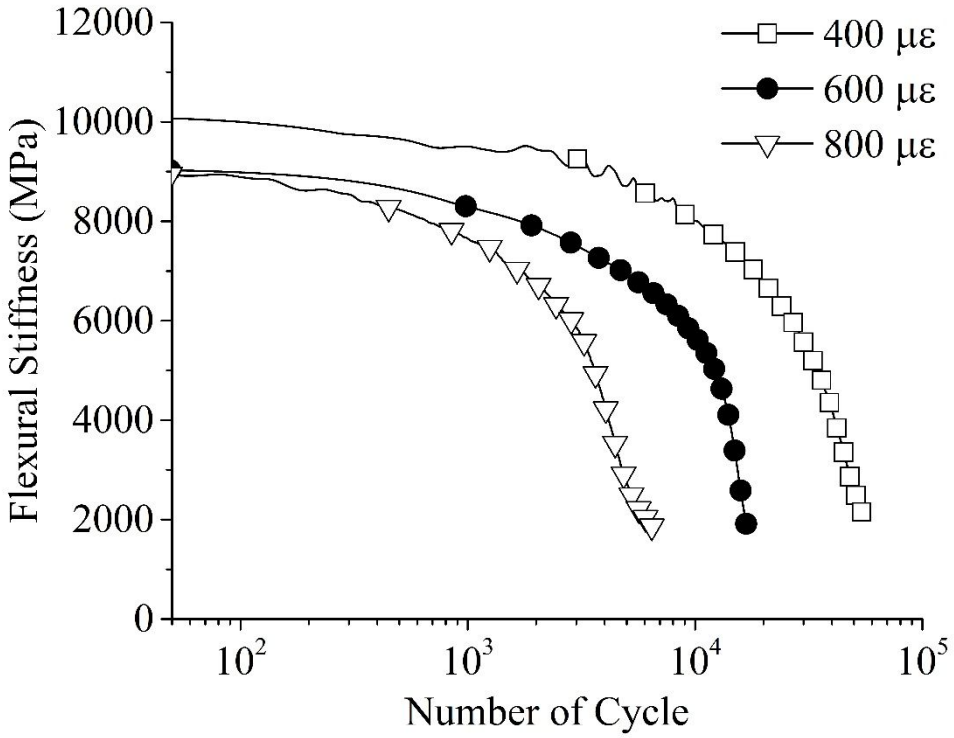

Fig. B.1: Flexural stiffness for VG30

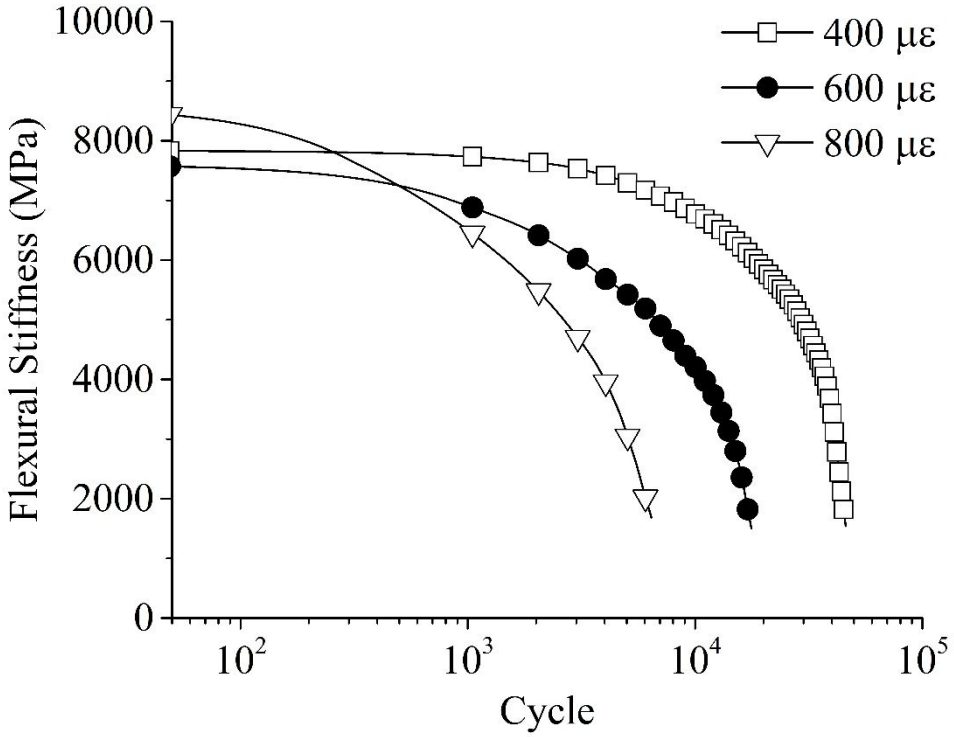

Fig. B.2: Flexural stiffness for VG30-WMA

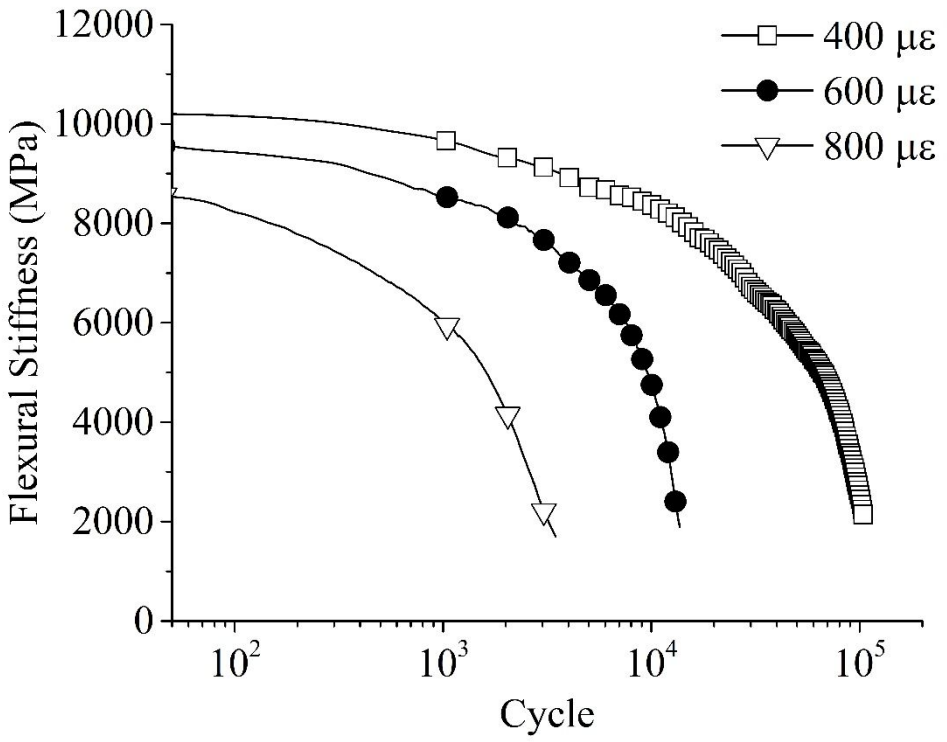

Fig. B.3: Flexural stiffness for VG30-L

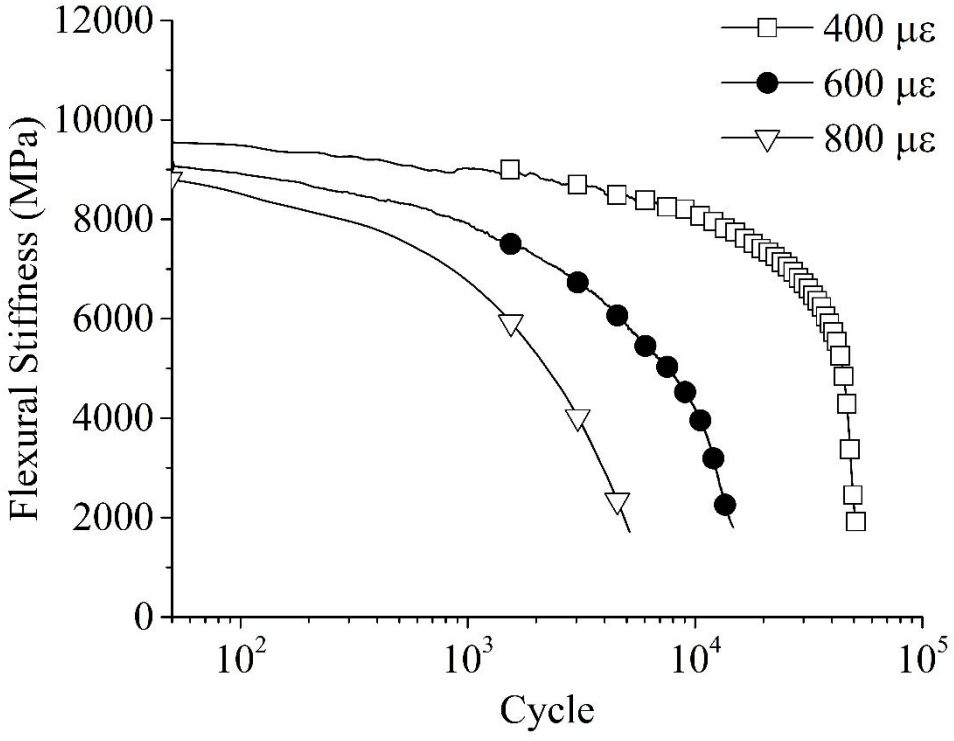

Fig. B.4: Flexural stiffness for VG30-WMA-L

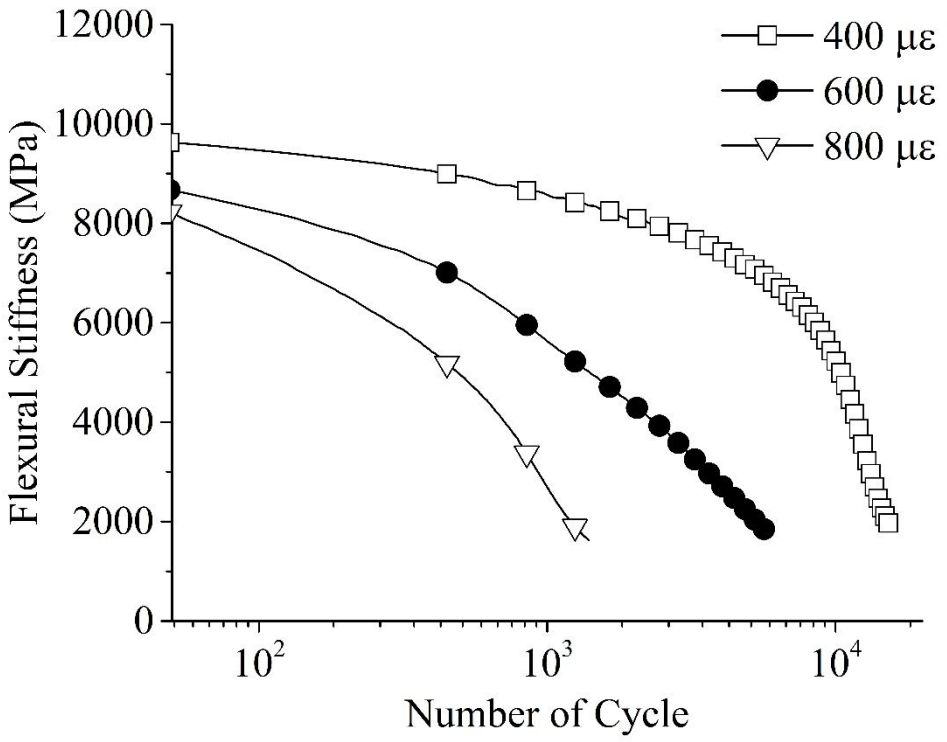

Fig. B.5: Flexural stiffness for VG30-MC

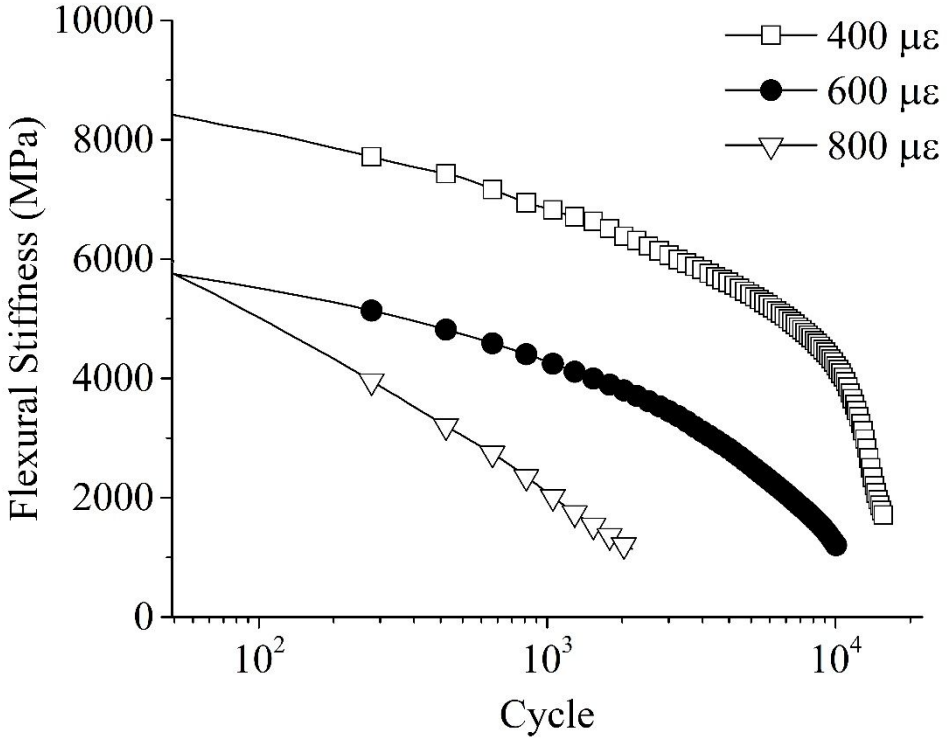

Fig. B.6: Flexural stiffness for VG30-WMA-MC

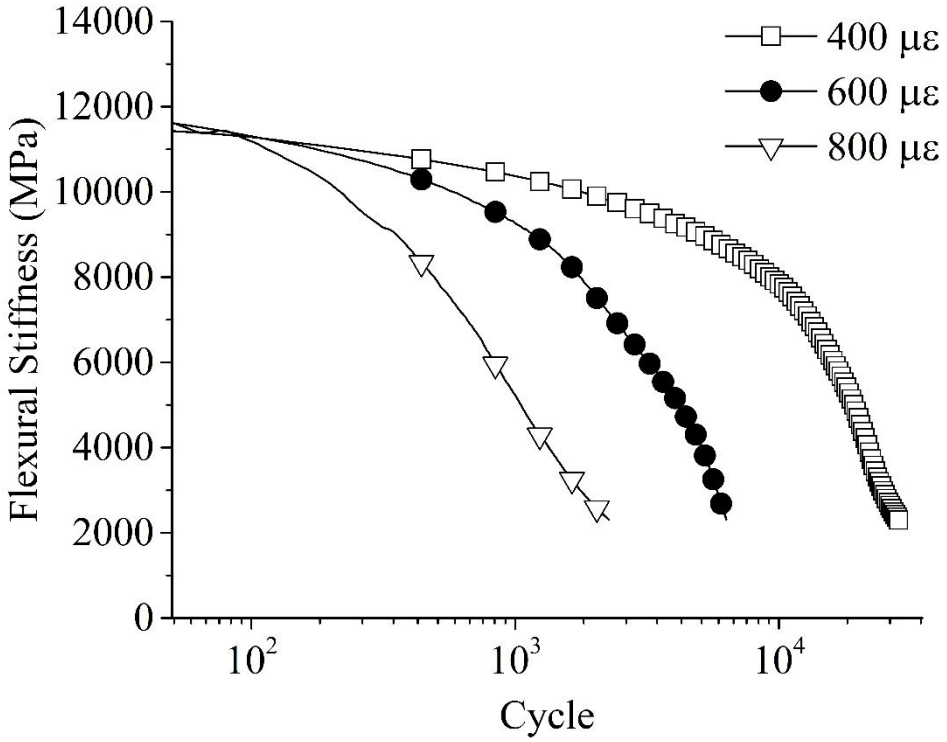

Fig. B.7: Flexural stiffness for VG30-L-MC

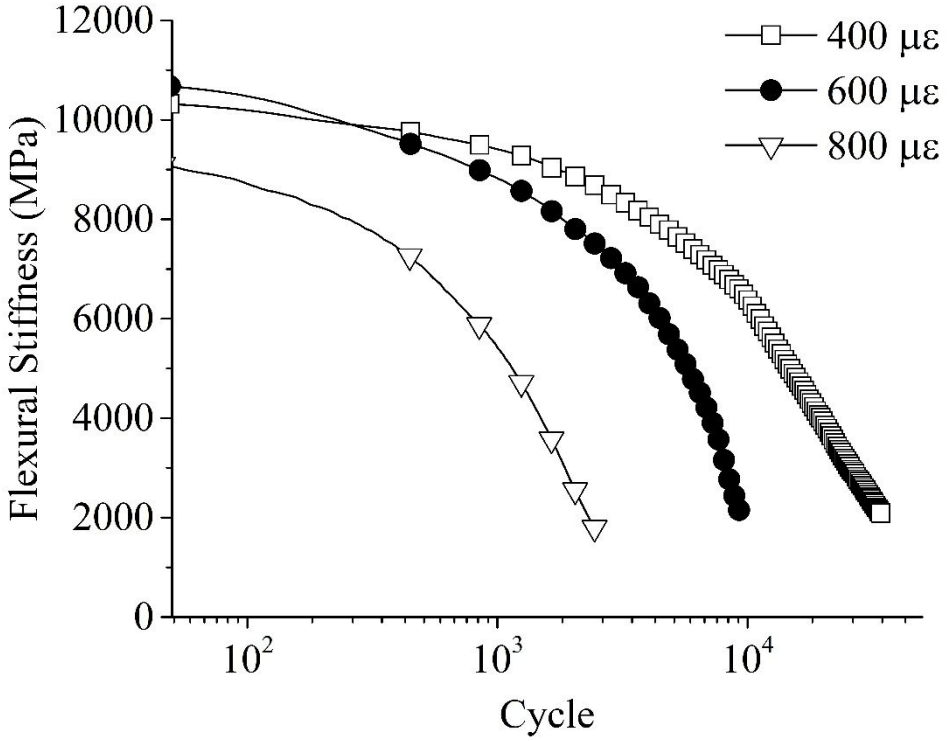

Fig. B.8: Flexural stiffness for VG30-WMA-L-MC

B.2. Total Energy Dissipation Plots

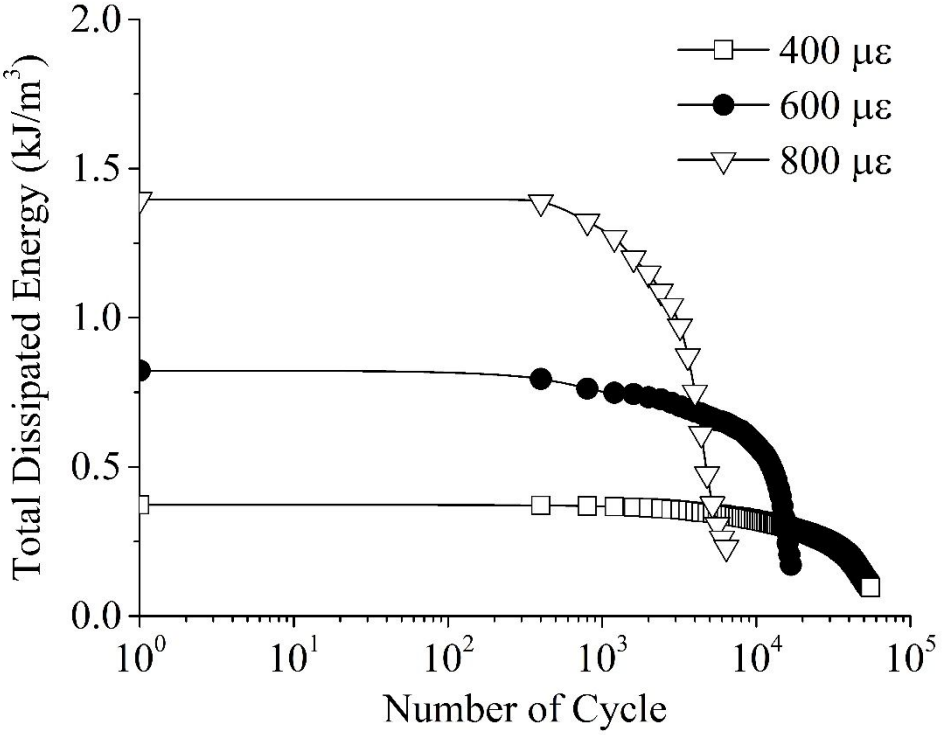

Fig. B.9: Total energy dissipation for VG30

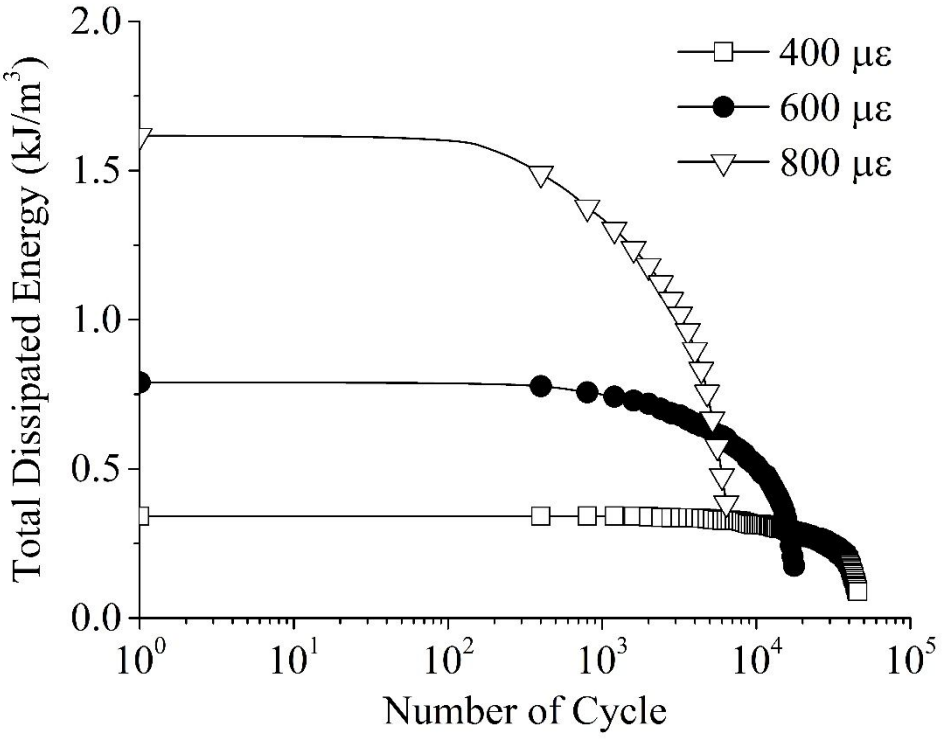

Fig. B.10: Total energy dissipation for VG30-WMA

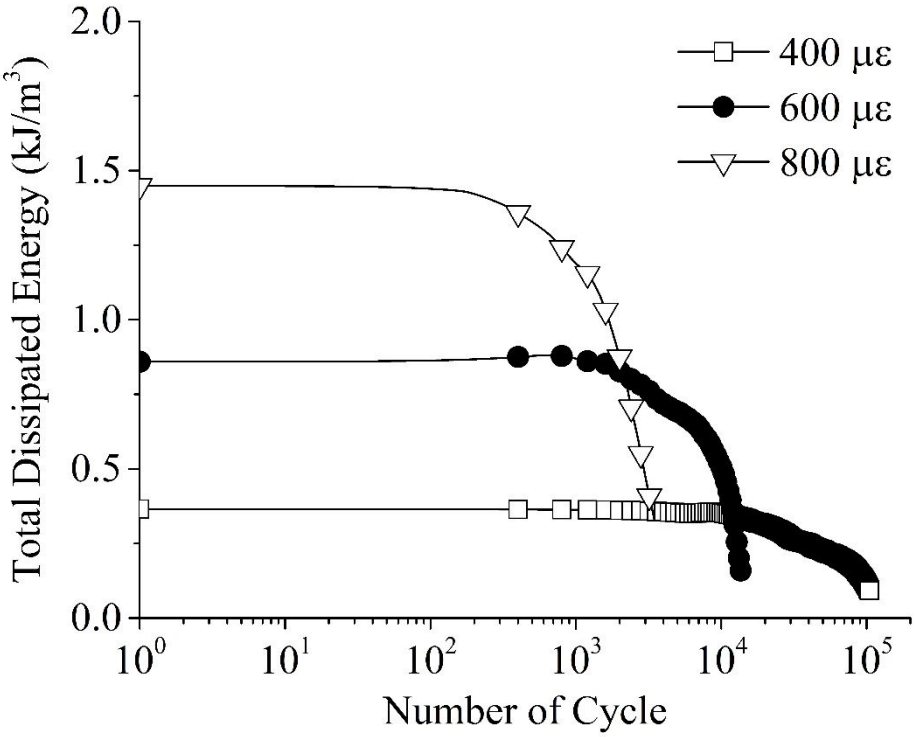

Fig. B.11: Total energy dissipation for VG30-L

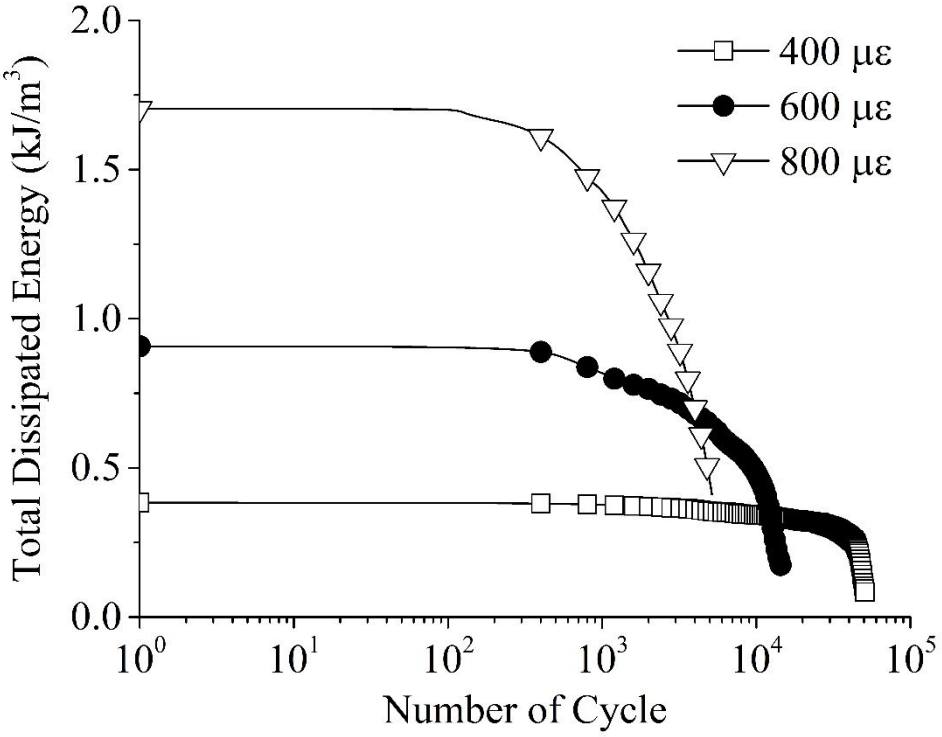

Fig. B.12: Total energy dissipation for VG30-WMA-L

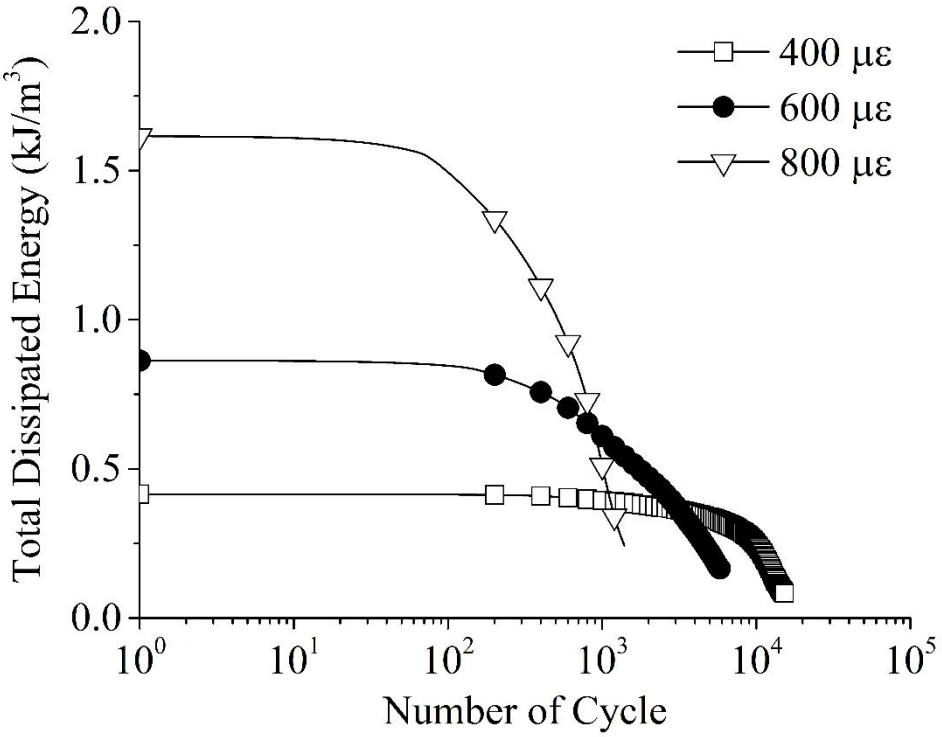

Fig. B.13: Total energy dissipation for VG30-MC

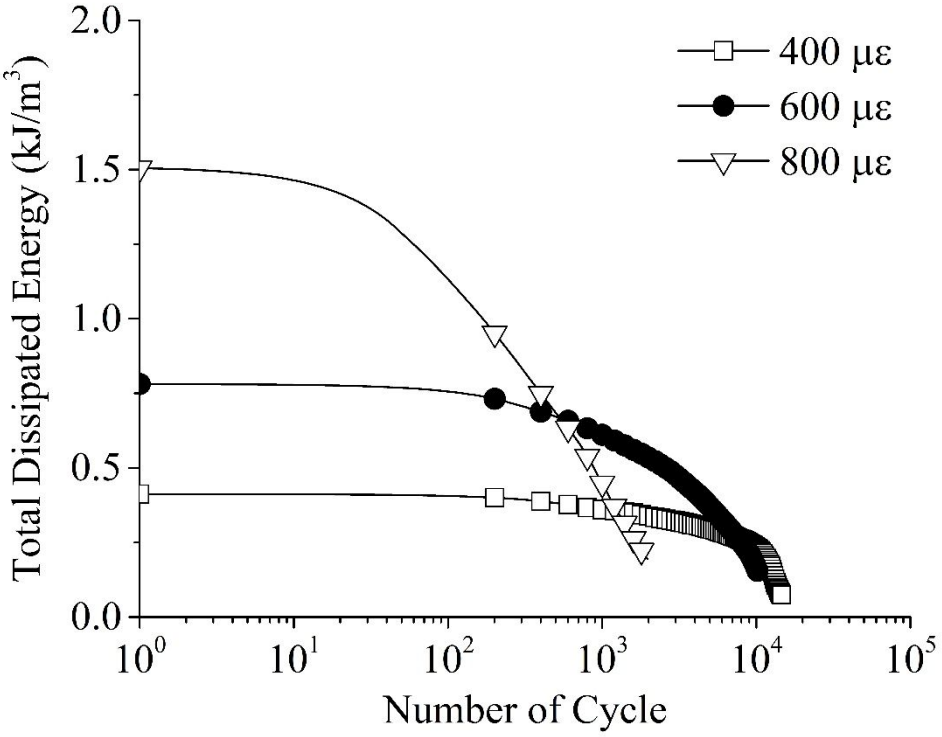

Fig. B.14: Total energy dissipation for VG30-WMA-MC

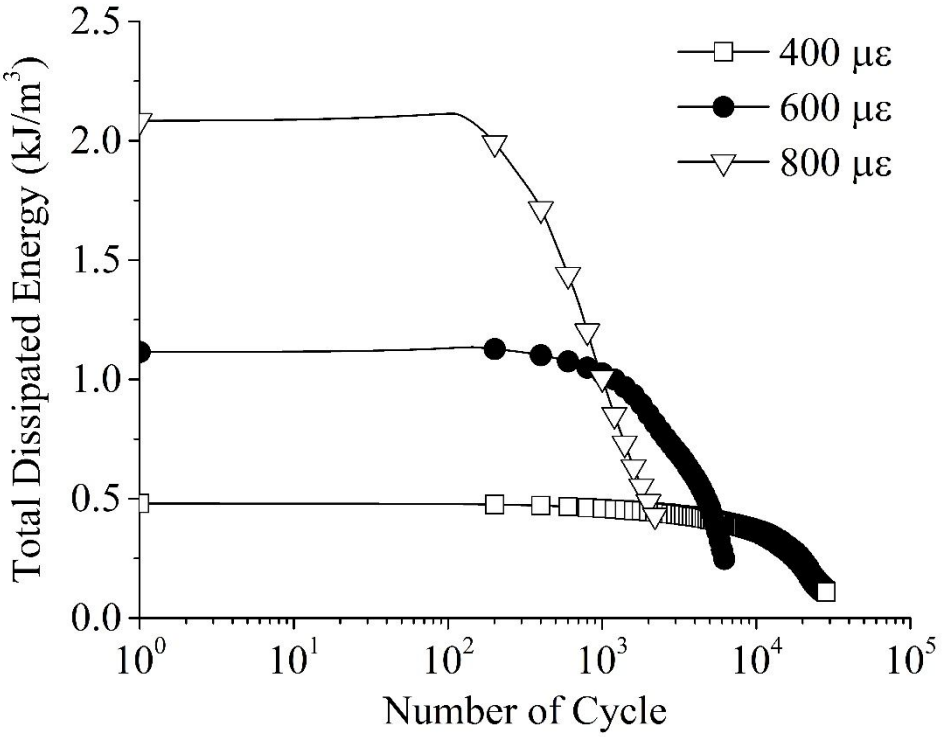

Fig. B.15: Total energy dissipation for VG30-L-MC

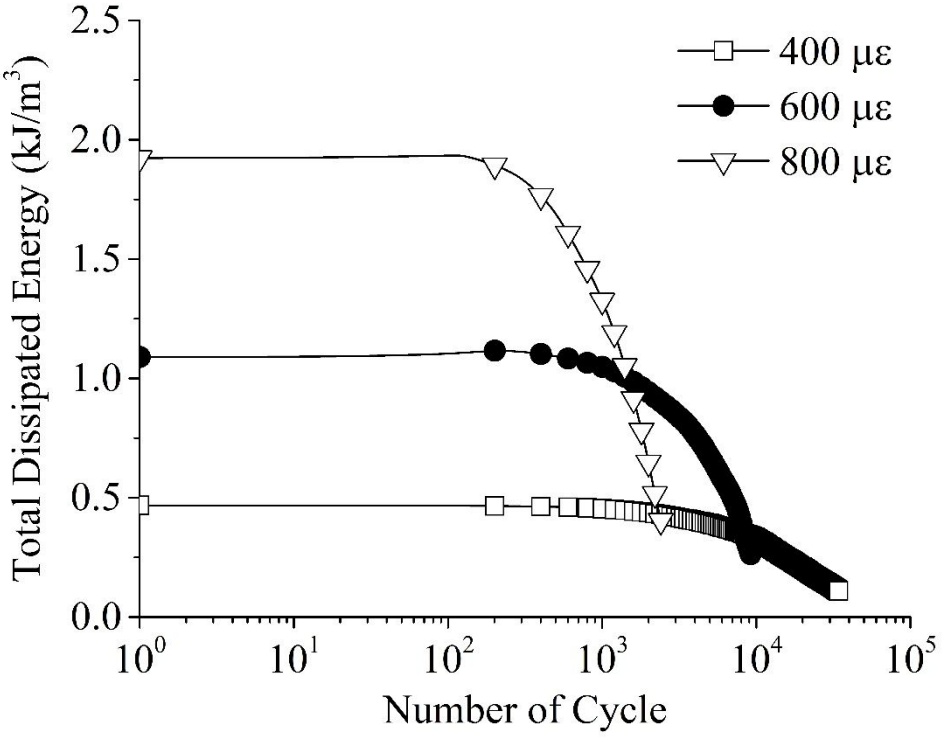

Fig. B.16: Total energy dissipation for VG30-WMA-L-MC

B.3. Normalised Modulus Plots

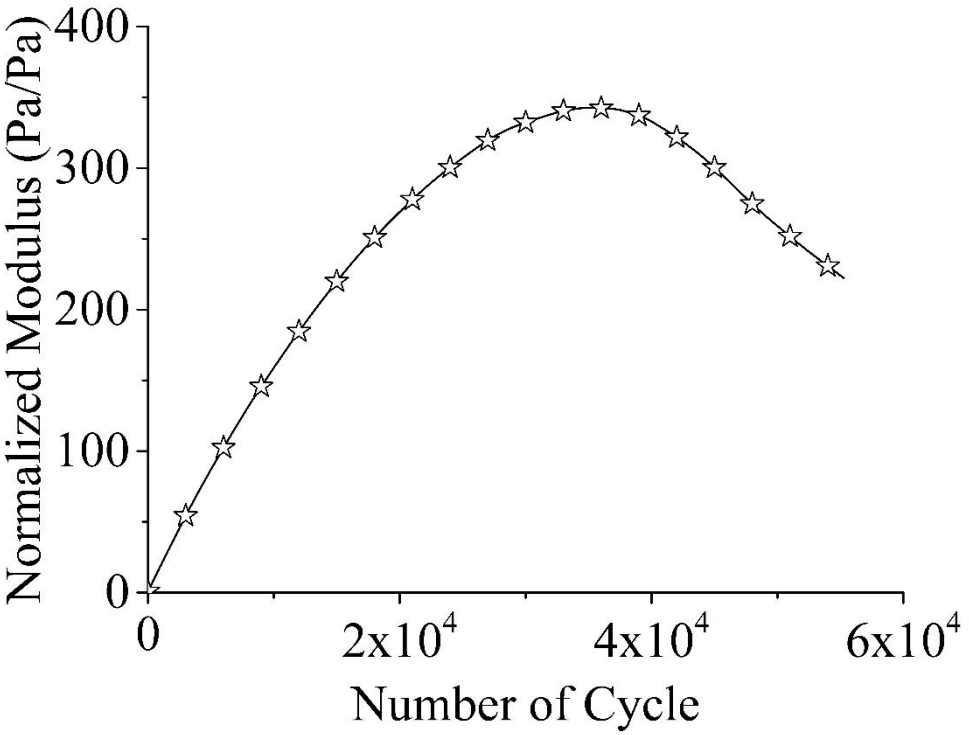

Fig. B.17: Normalised Modulus for VG30 at 400 microstrain

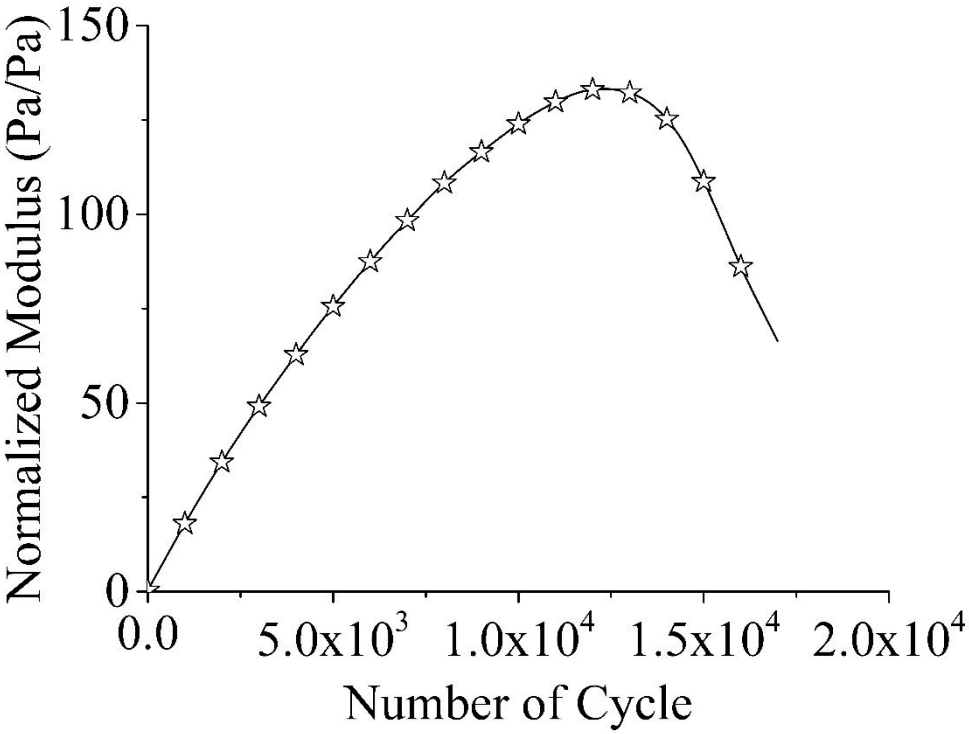

Fig. B.18: Normalised Modulus for VG30 at 600 microstrain

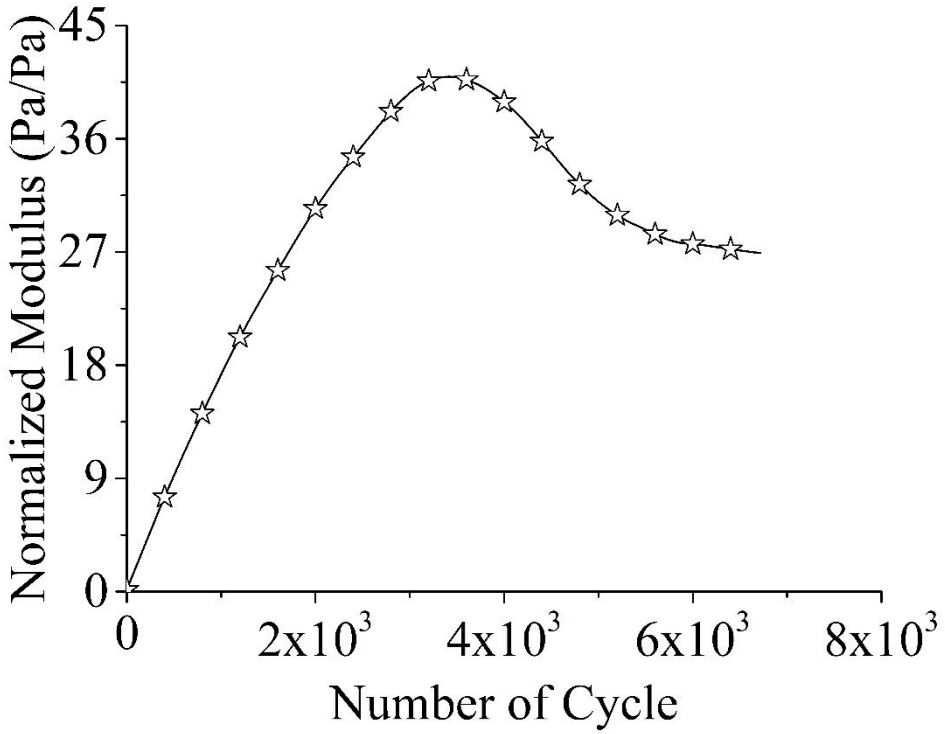

Fig. B.19: Normalised Modulus for VG30 at 800 microstrain

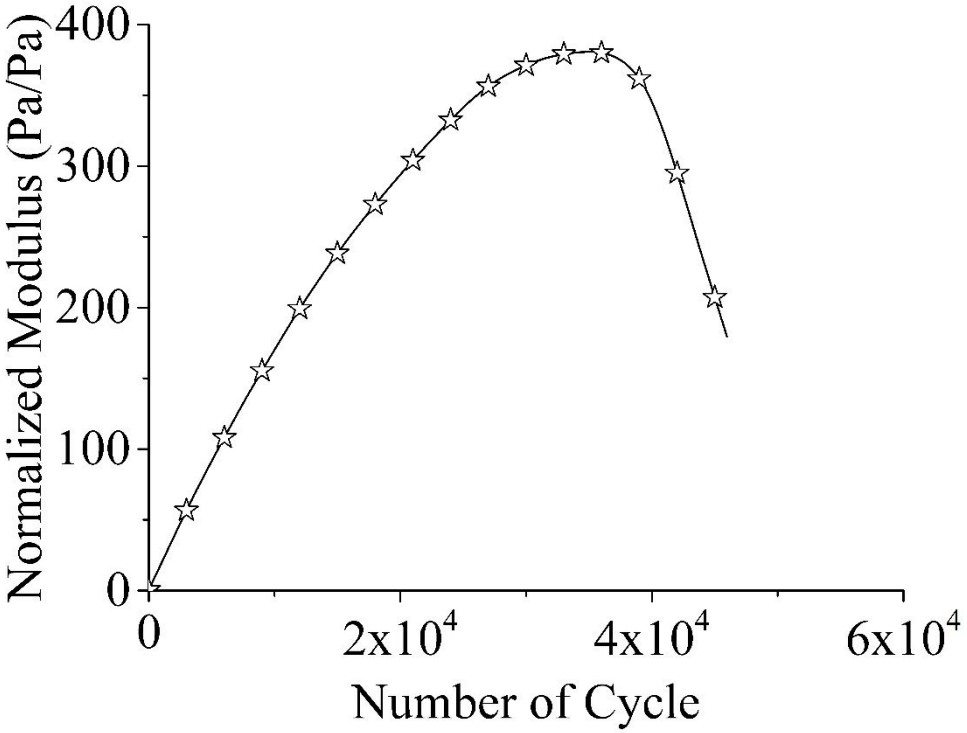

Fig. B.20: Normalised Modulus for VG30-WMA at 400 microstrain

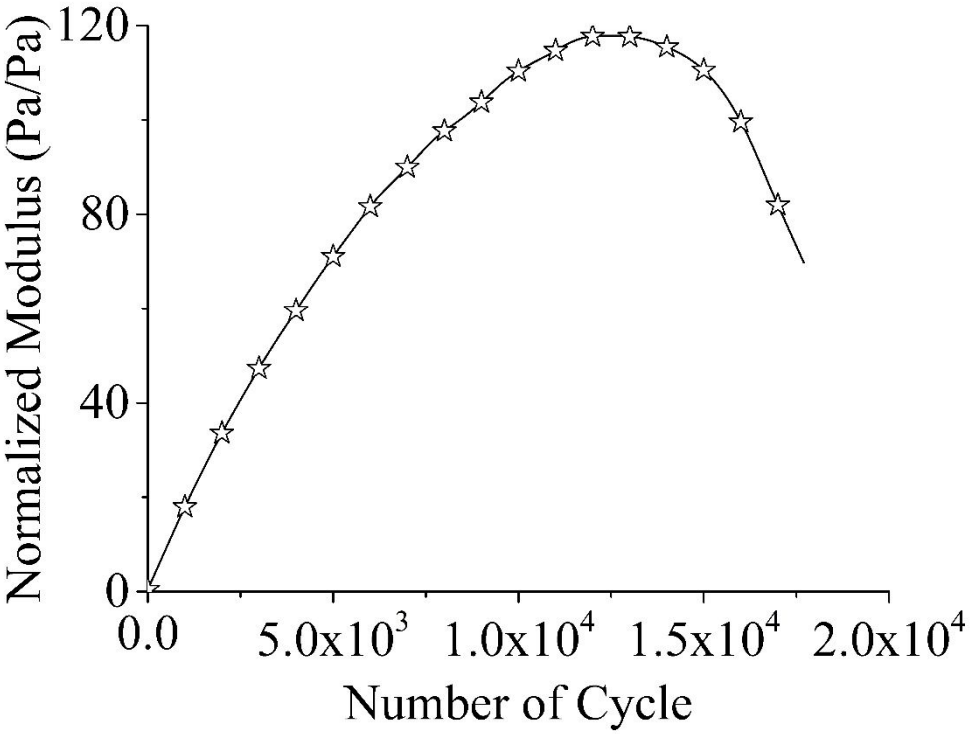

Fig. B.21: Normalised Modulus for VG30-WMA at 600 microstrain

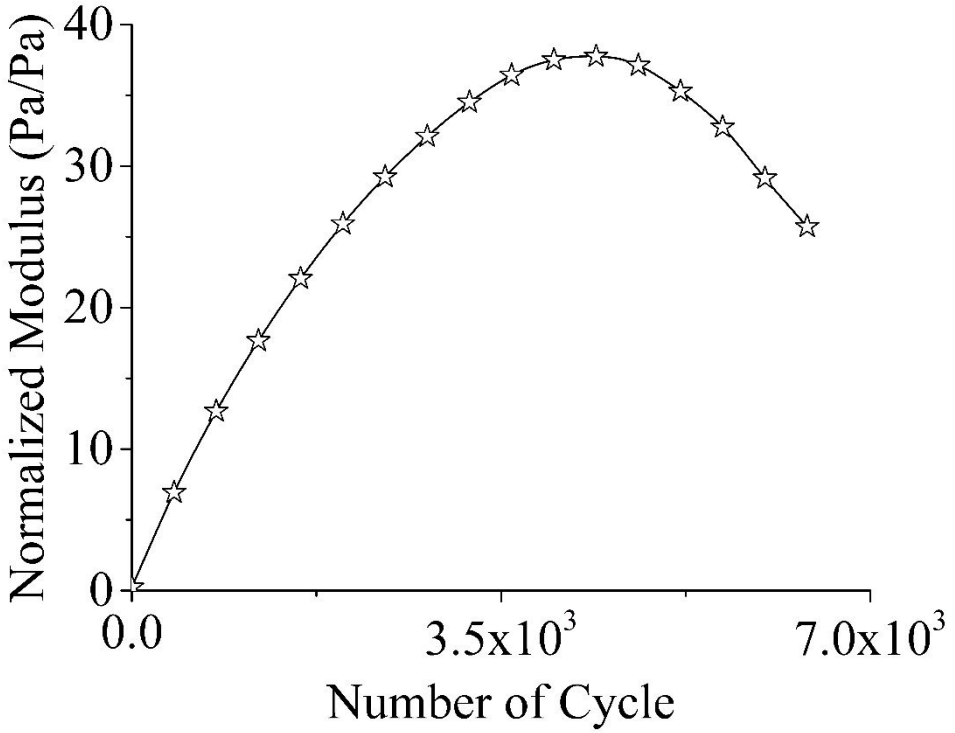

Fig. B.22: Normalised Modulus for VG30-WMA at 800 microstrain

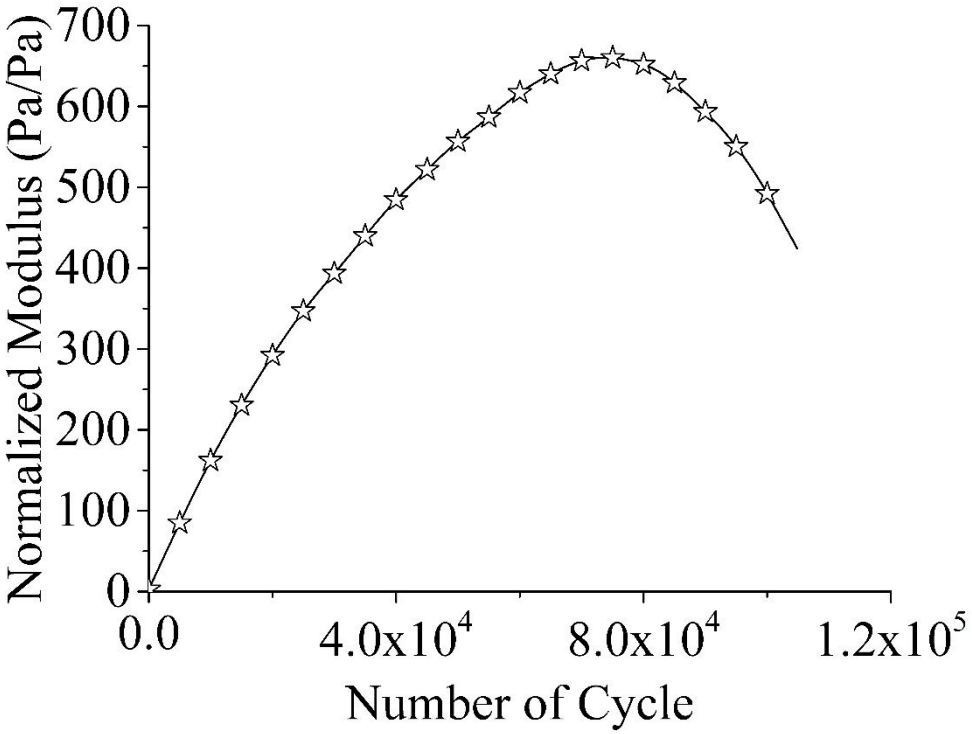

Fig. B.23: Normalised Modulus for VG30-L at 400 microstrain

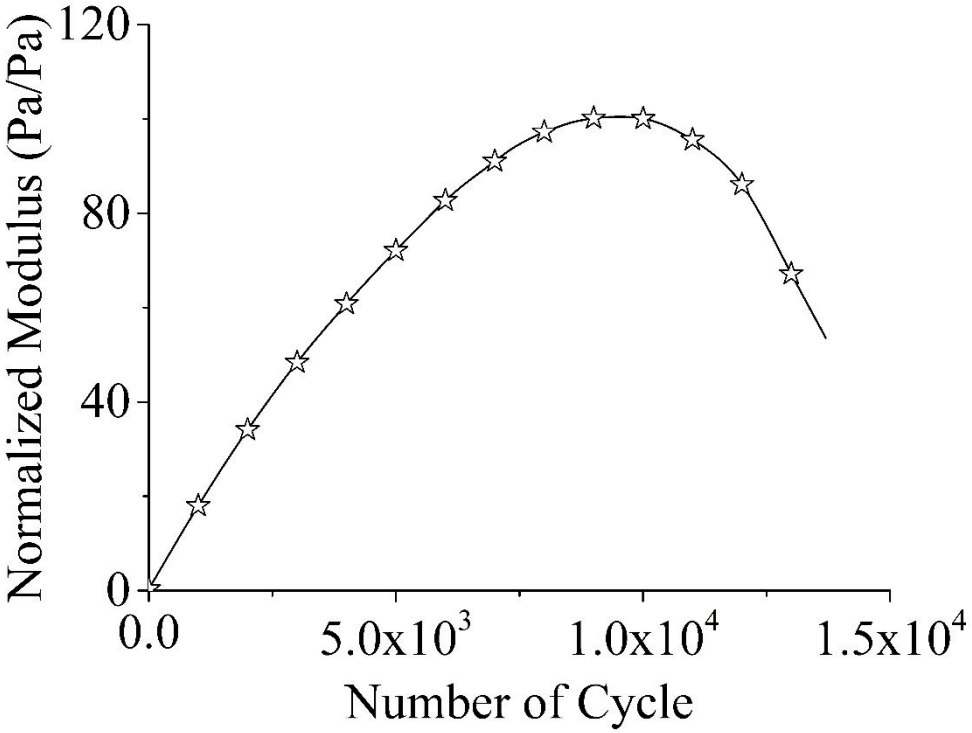

Fig. B.24: Normalised Modulus for VG30-L at 600 microstrain

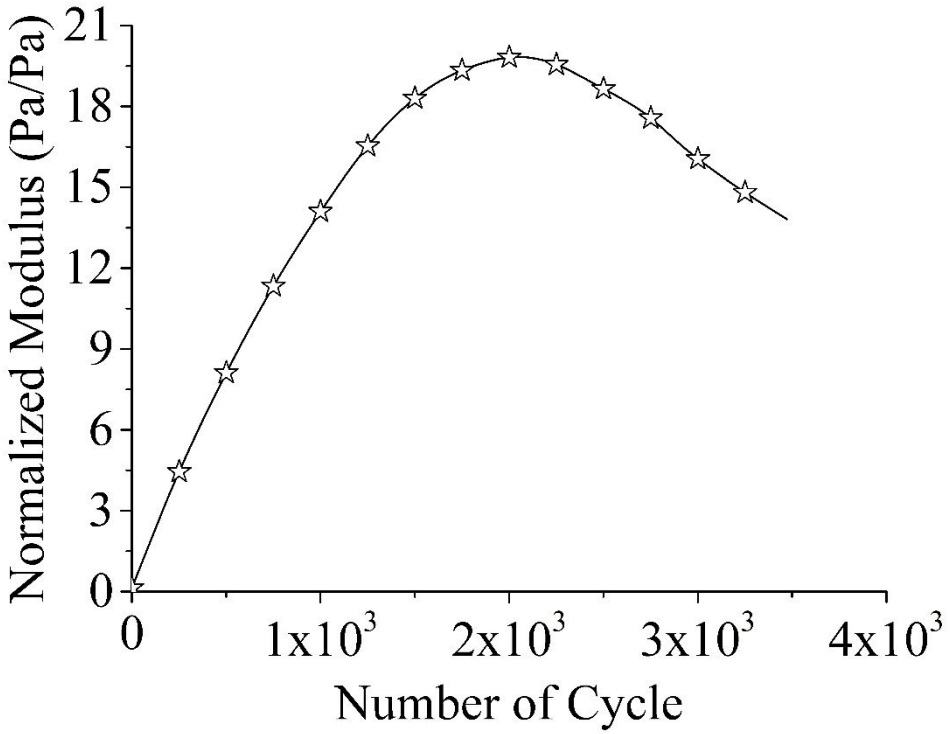

Fig. B.25: Normalised Modulus for VG30-L at 800 microstrain

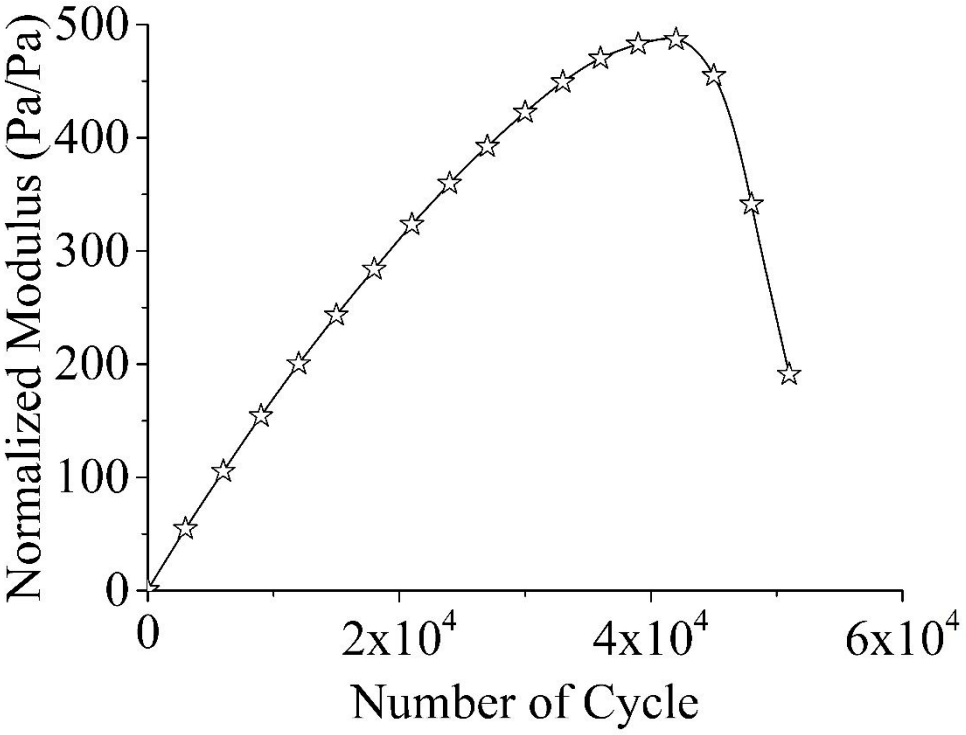

Fig. B.26: Normalised Modulus for VG30-WMA-L at 400 microstrain

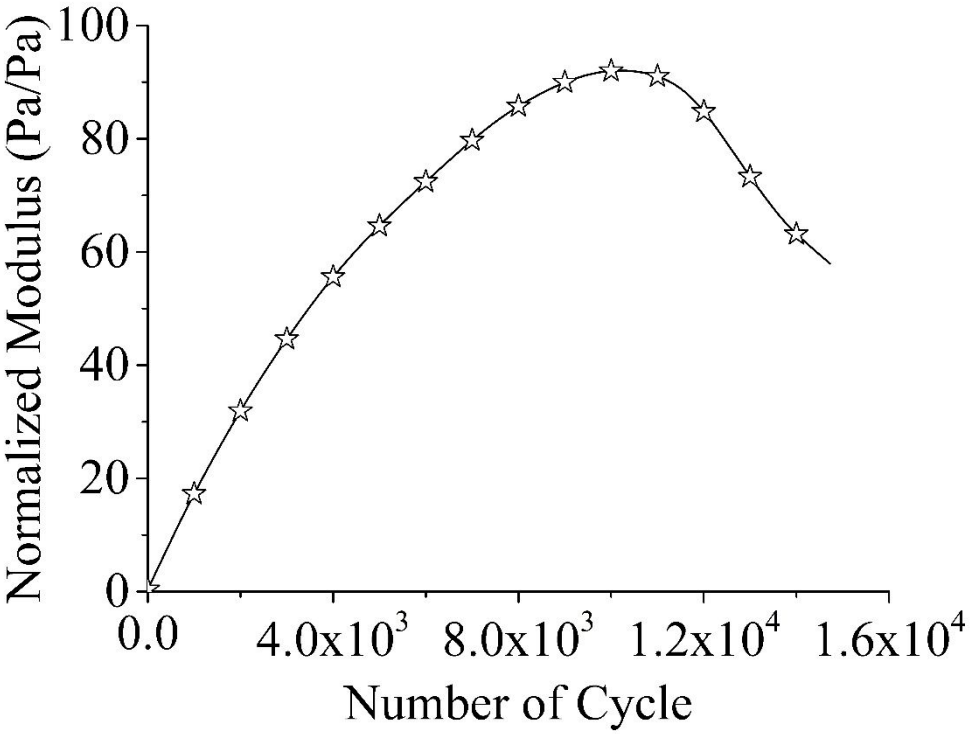

Fig. B.27: Normalised Modulus for VG30-WMA-L at 600 microstrain

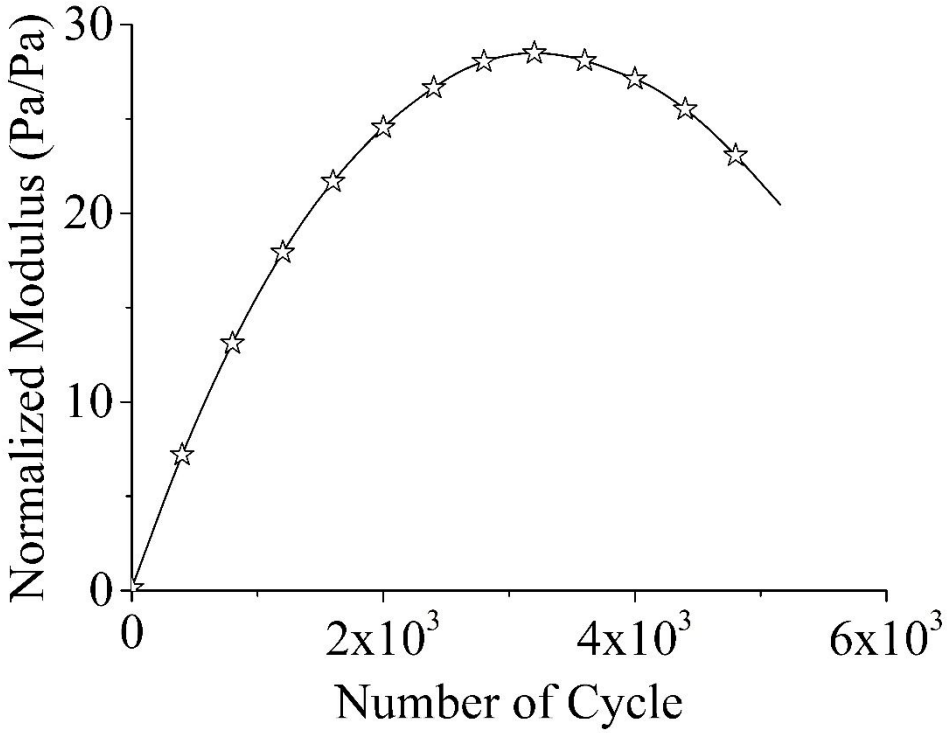

Fig. B.28: Normalised Modulus for VG30-WMA-L at 800 microstrain

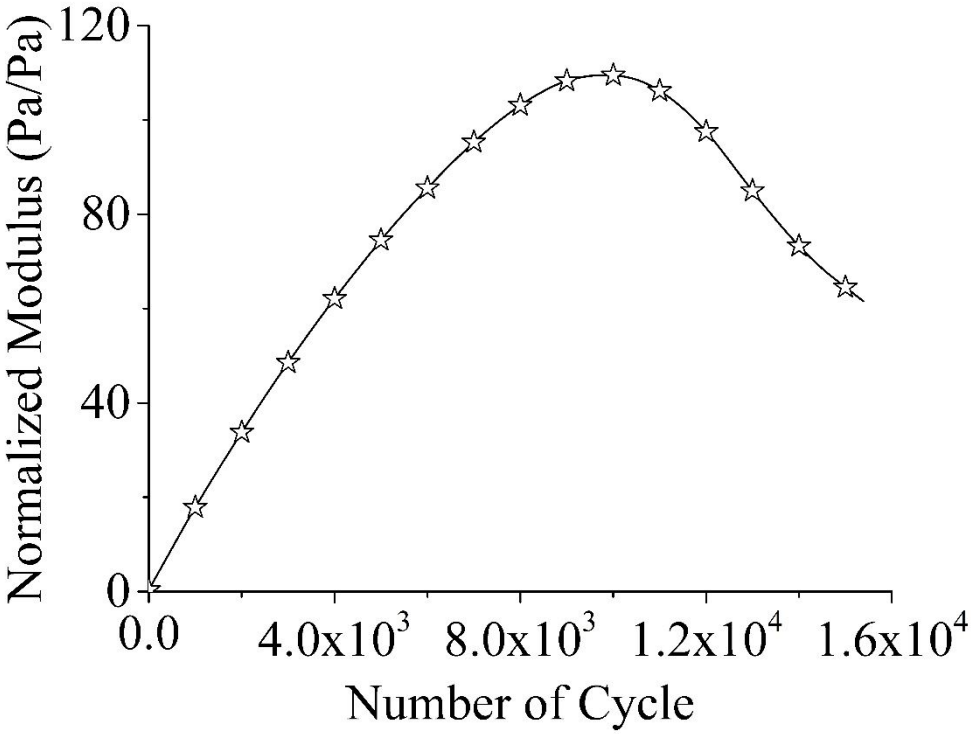

Fig. B.29: Normalised Modulus for VG30-MC at 400 microstrain

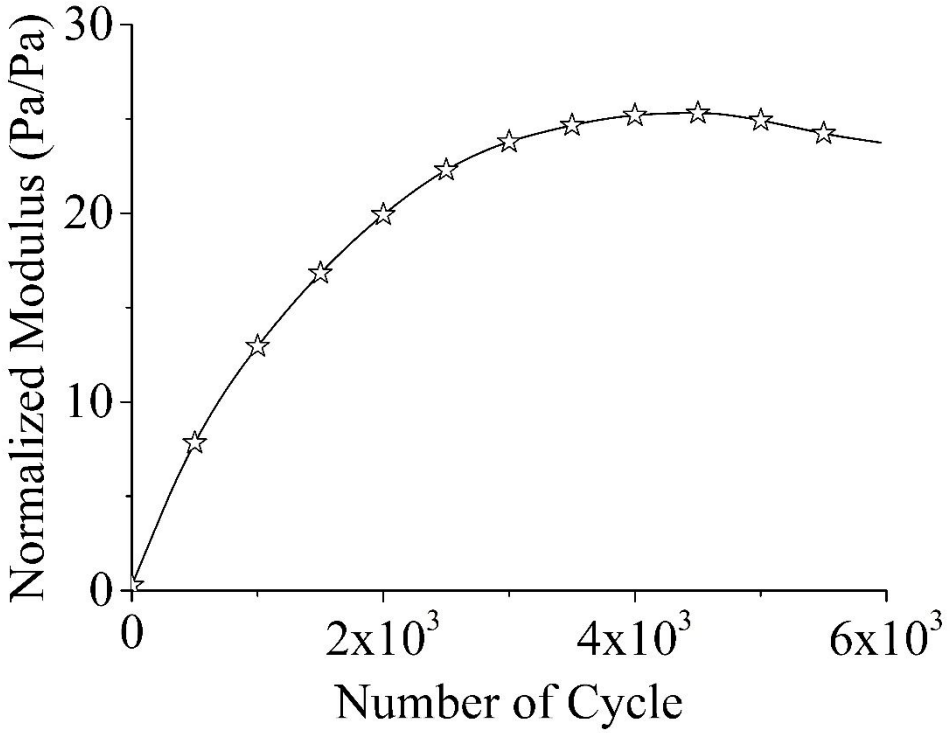

Fig. B.30: Normalised Modulus for VG30-MC at 600 microstrain

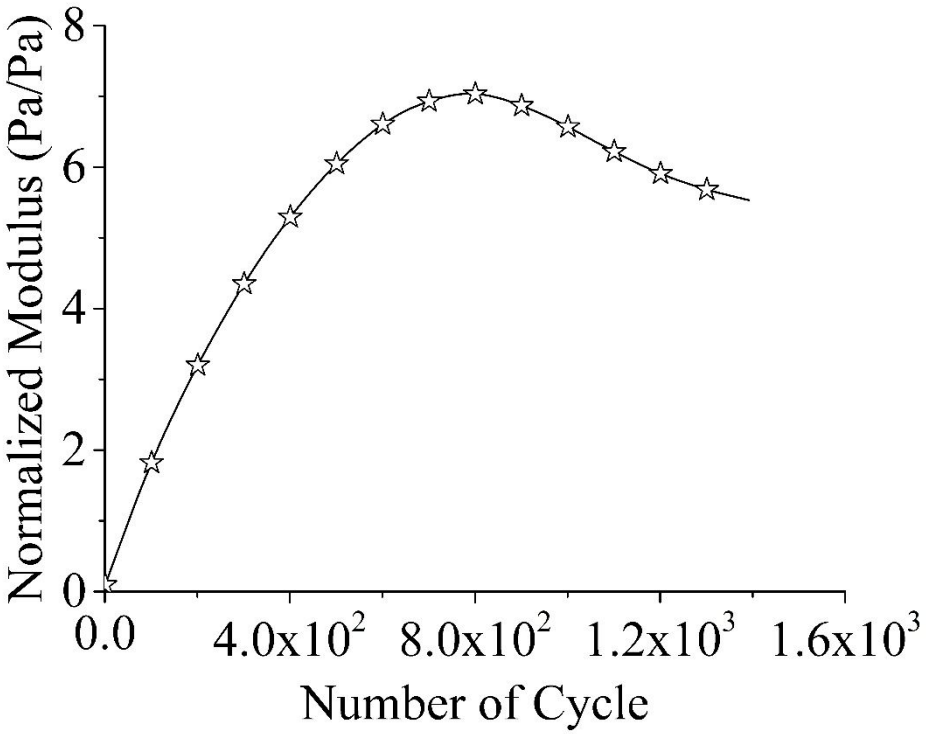

Fig. B.31: Normalised Modulus for VG30-MC at 800 microstrain

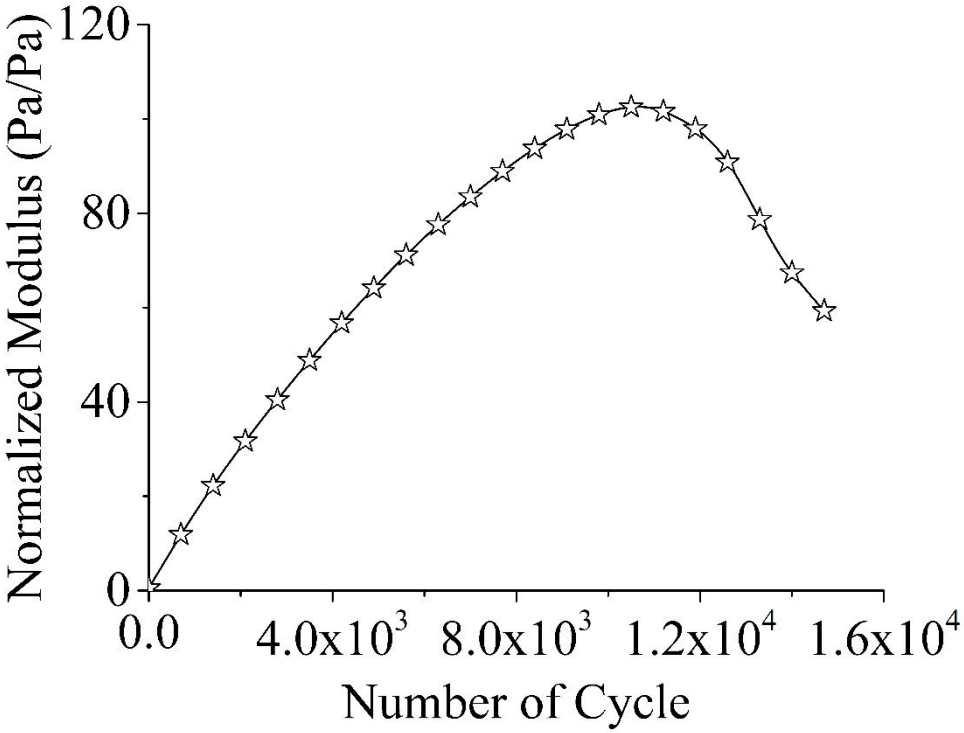

Fig. B.32: Normalised Modulus for VG30-WMA-MC at 400 microstrain

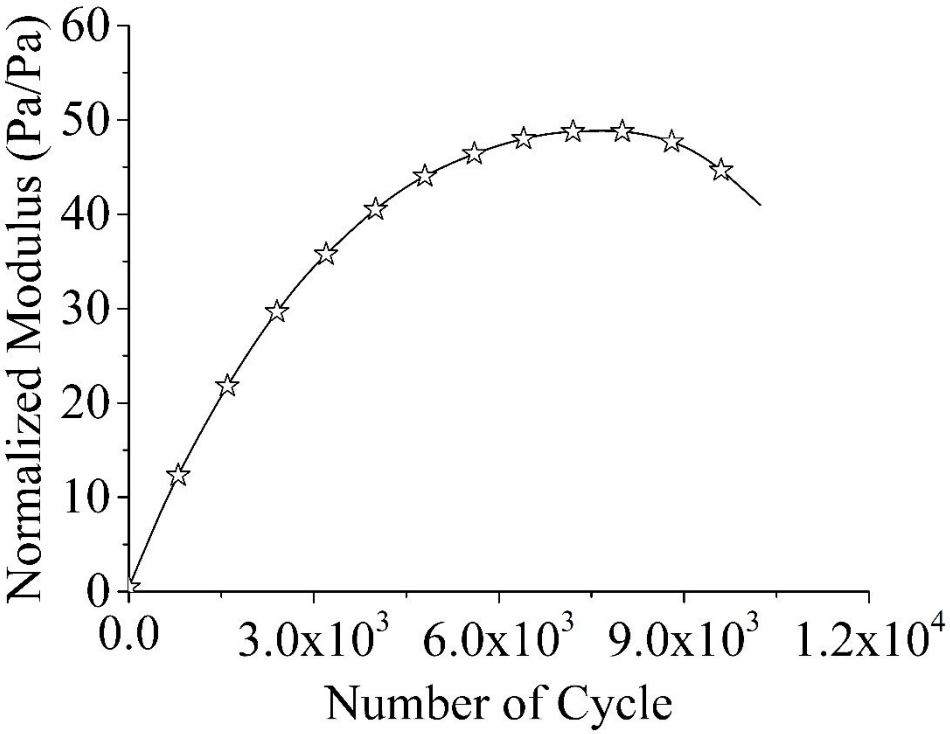

Fig. B.33: Normalised Modulus for VG30-WMA-MC at 600 microstrain

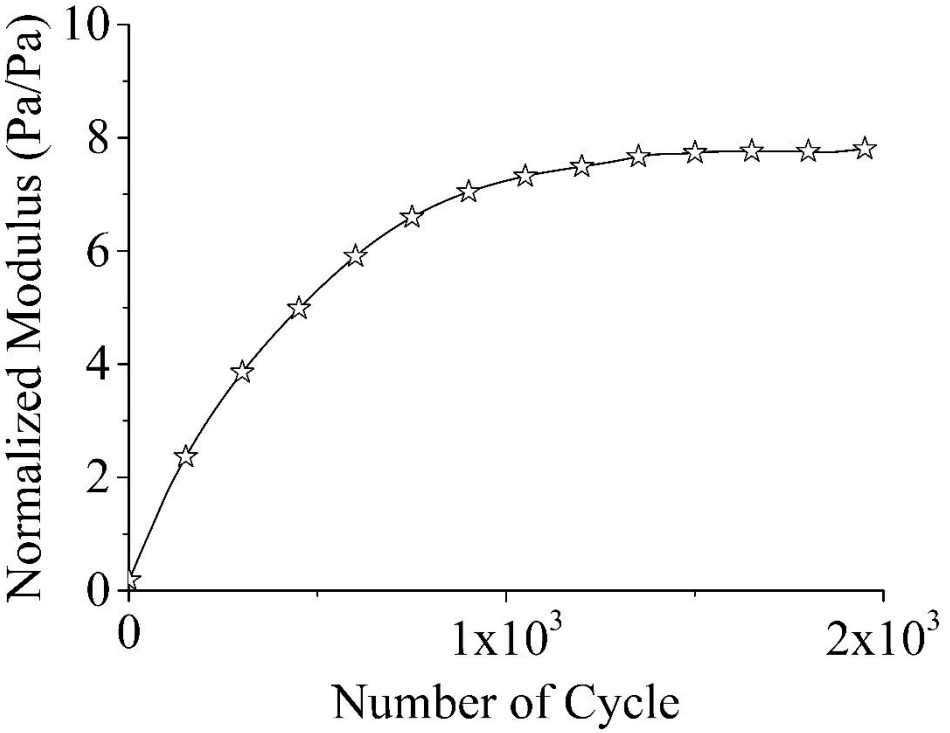

Fig. B.34: Normalised Modulus for VG30-WMA-MC at 800 microstrain

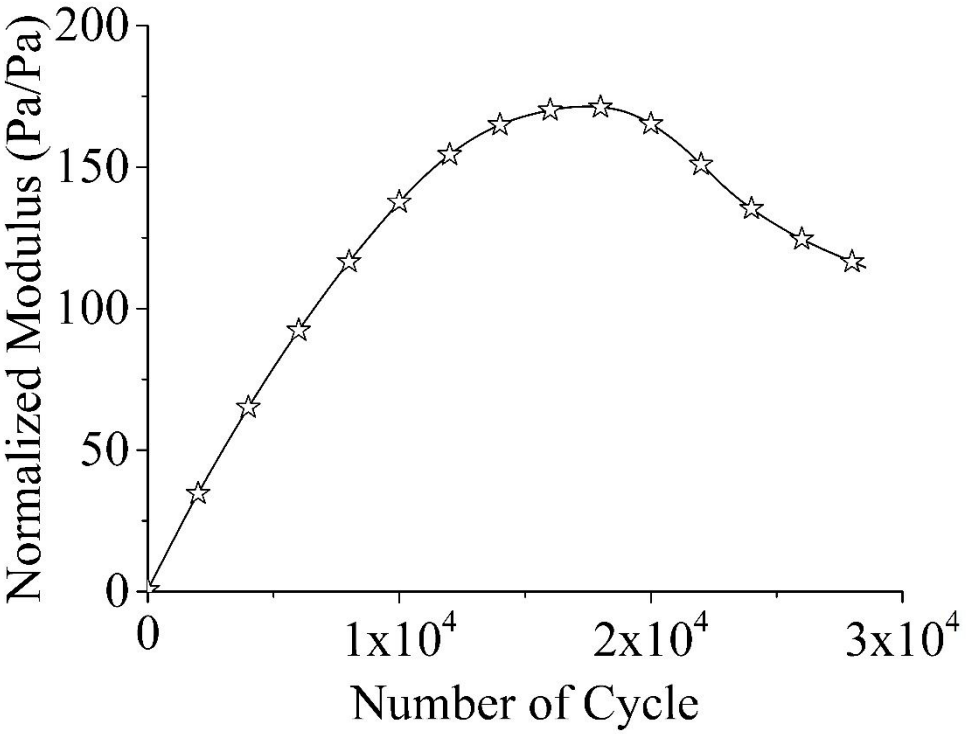

Fig. B.35: Normalised Modulus for VG30-L-MC at 400 microstrain

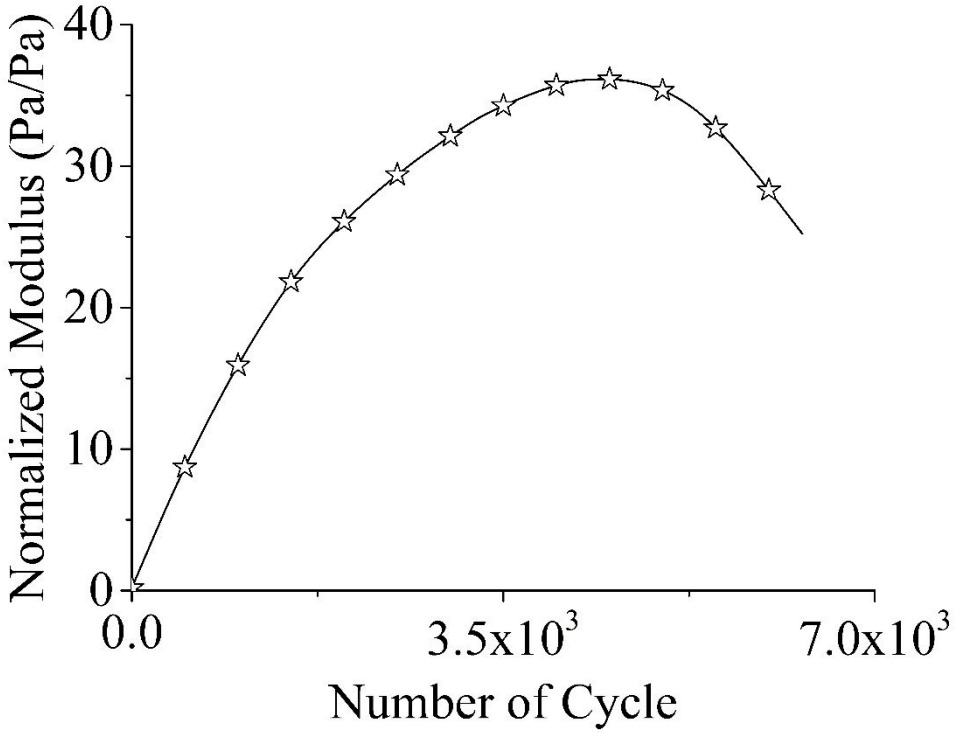

Fig. B.36: Normalised Modulus for VG30-L-MC at 600 microstrain

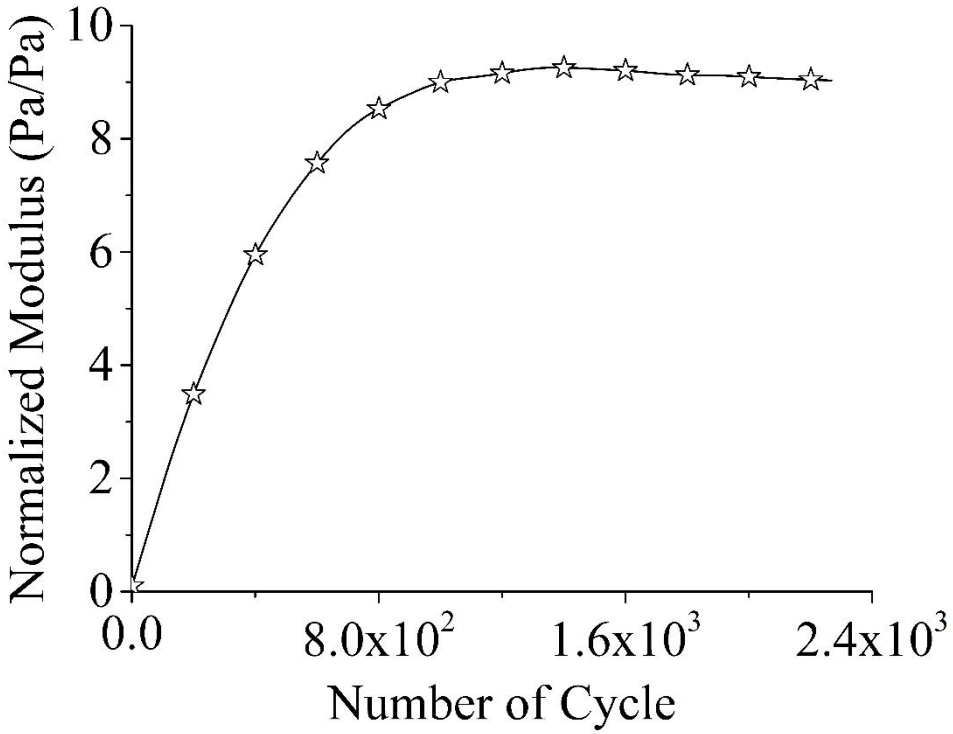

Fig. B.37: Normalised Modulus for VG30-L-MC at 800 microstrain

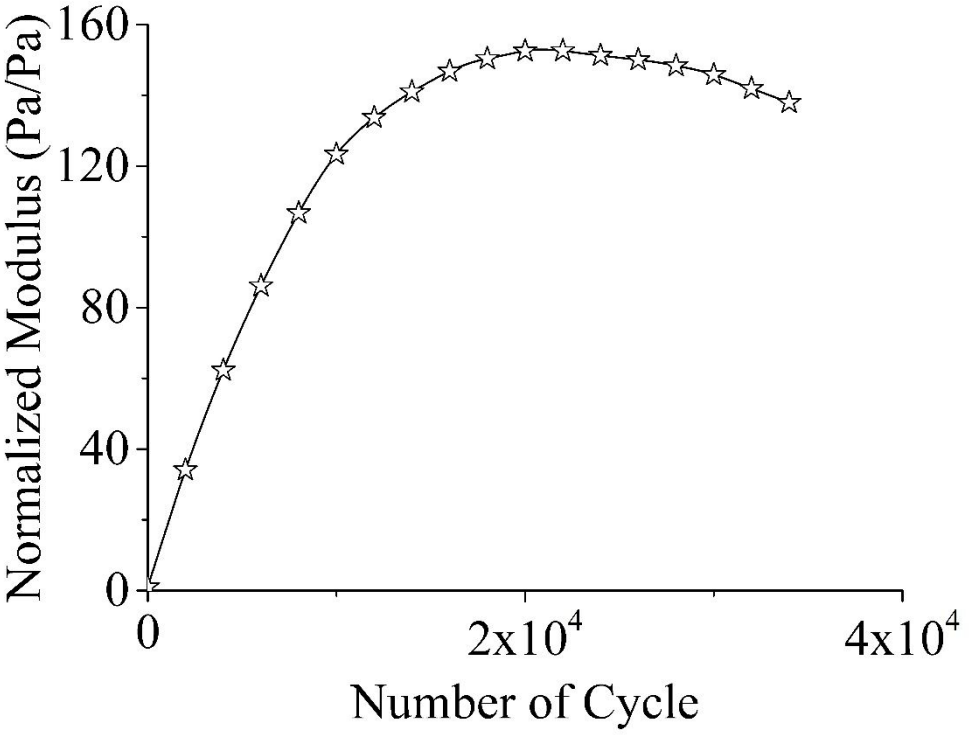

Fig. B.38: Normalised Modulus for VG30-WMA-L-MC at 400 microstrain

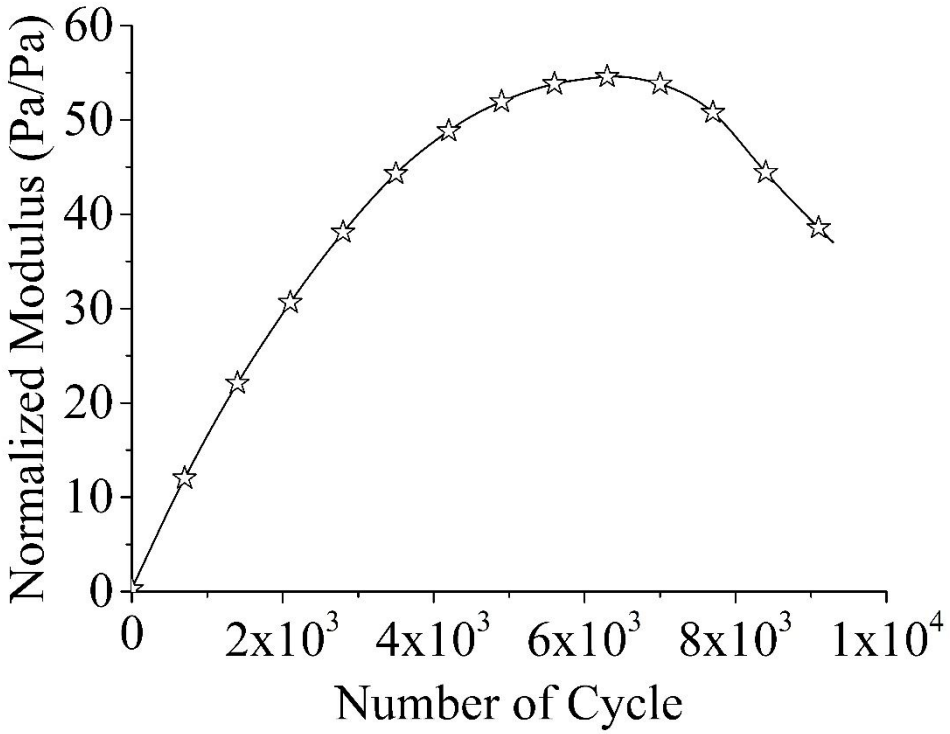

Fig. B.39: Normalised Modulus for VG30-WMA-L-MC at 600 microstrain

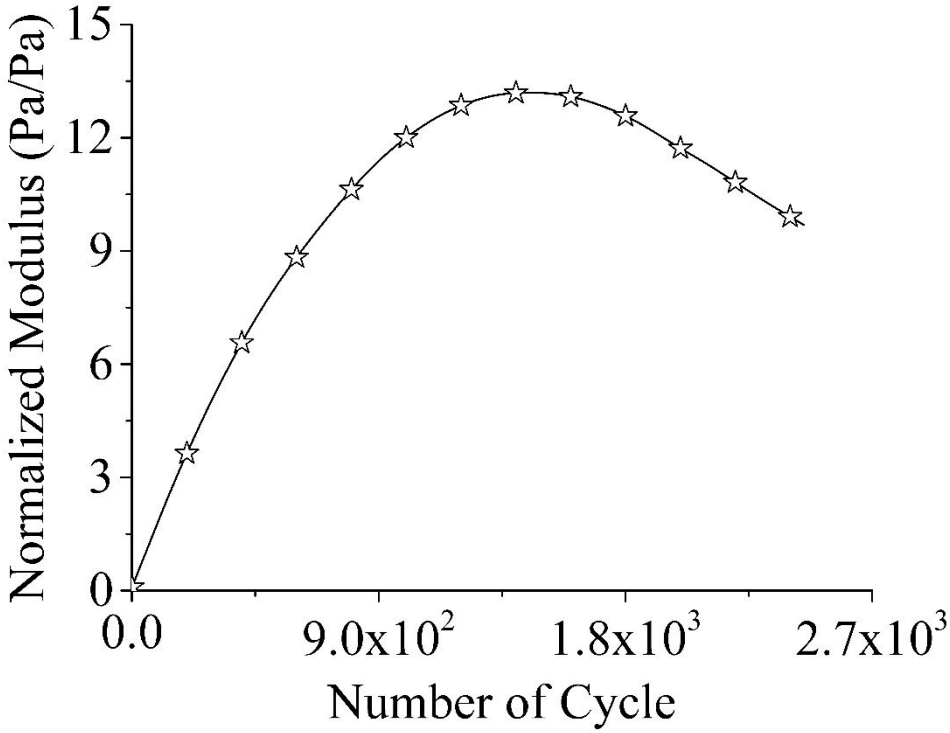

Fig. B.40: Normalised Modulus for VG30-WMA-L-MC at 800 microstrain

B.4. Energy Ratio Plots

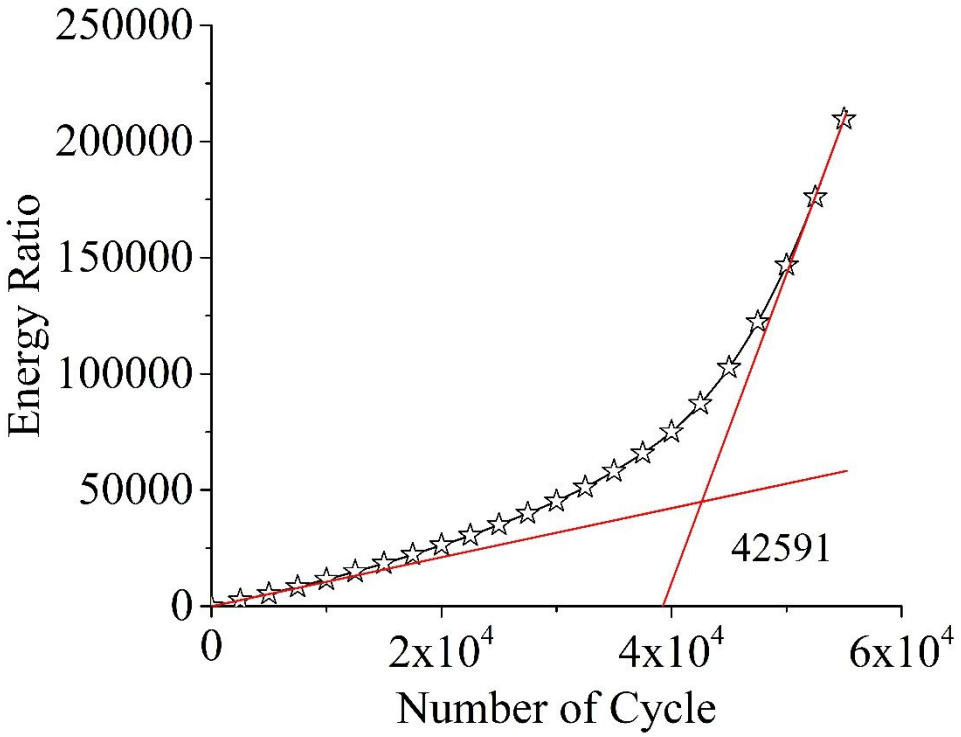

Fig. B.41: Energy Ratio for VG30 at 400 microstrain

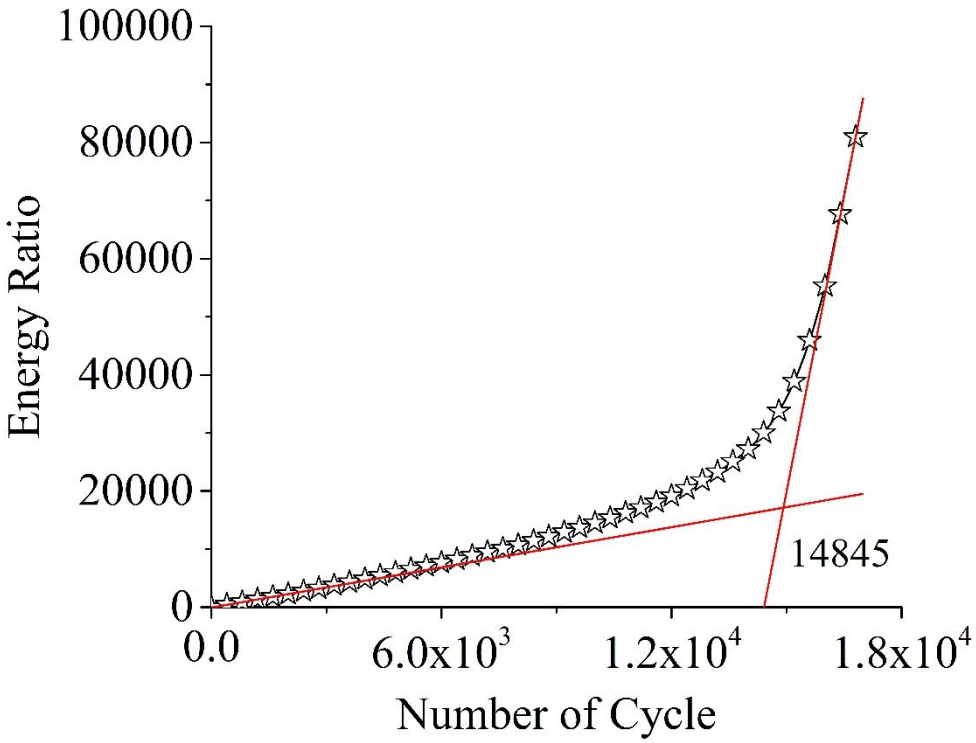

Fig. B.42: Energy Ratio for VG30 at 600 microstrain

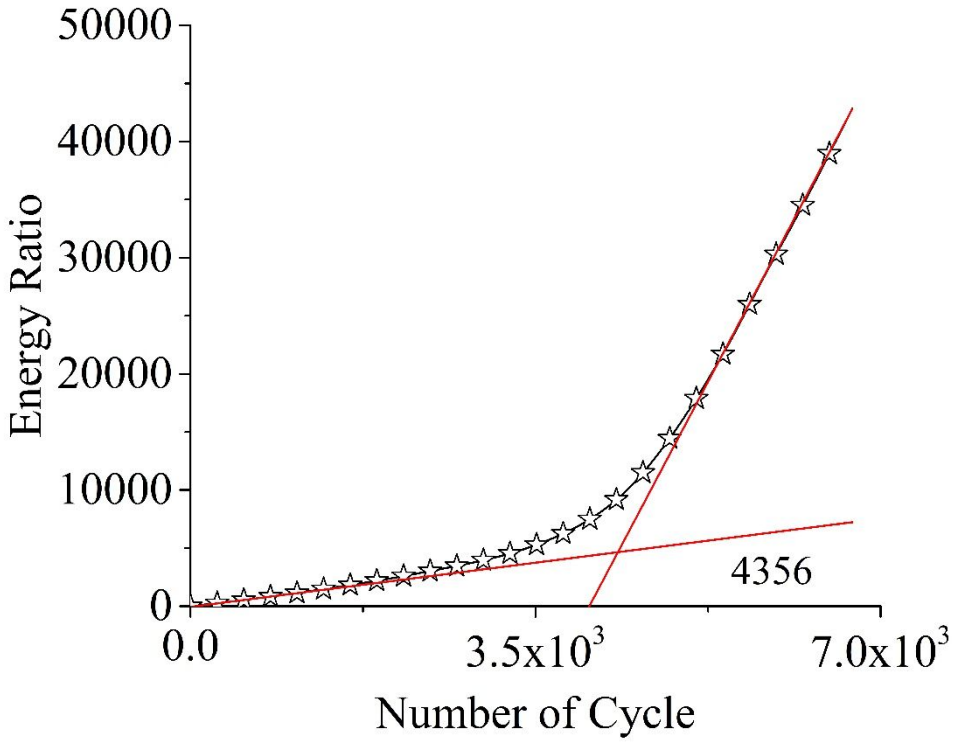

Fig. B.43: Energy Ratio for VG30 at 800 microstrain

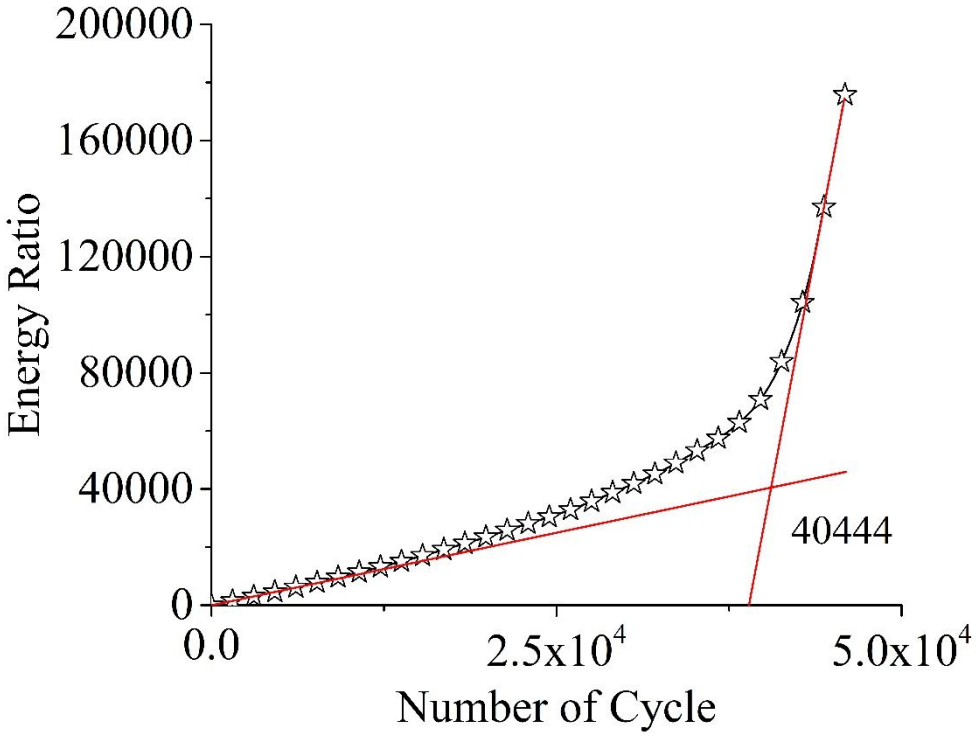

Fig. B.44: Energy Ratio for VG30-WMA at 400 microstrain

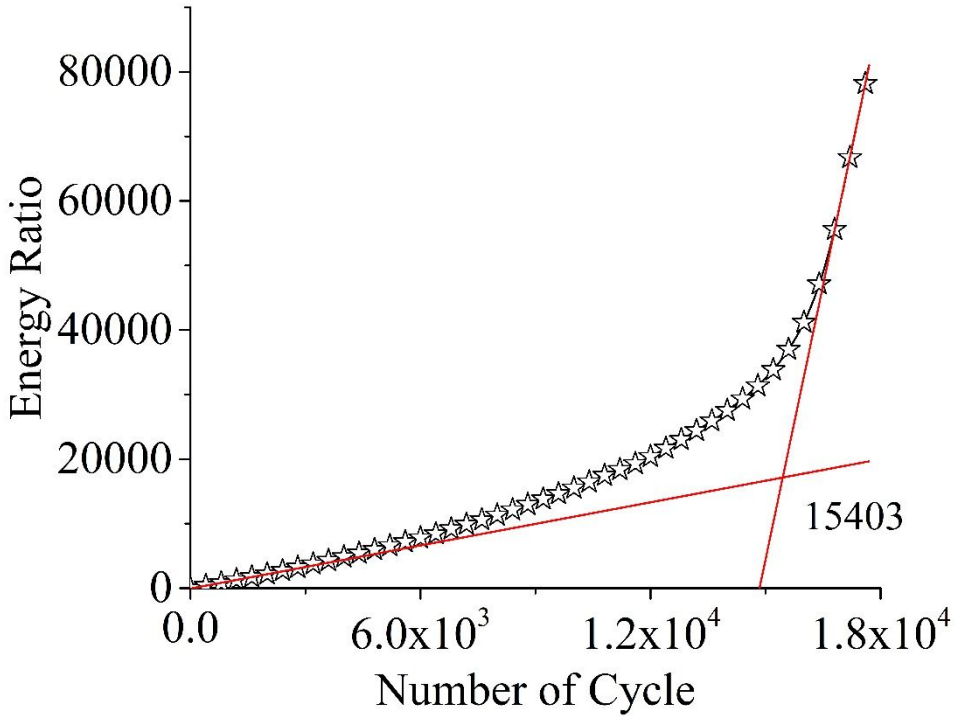

Fig. B.45: Energy Ratio for VG30-WMA at 600 microstrain

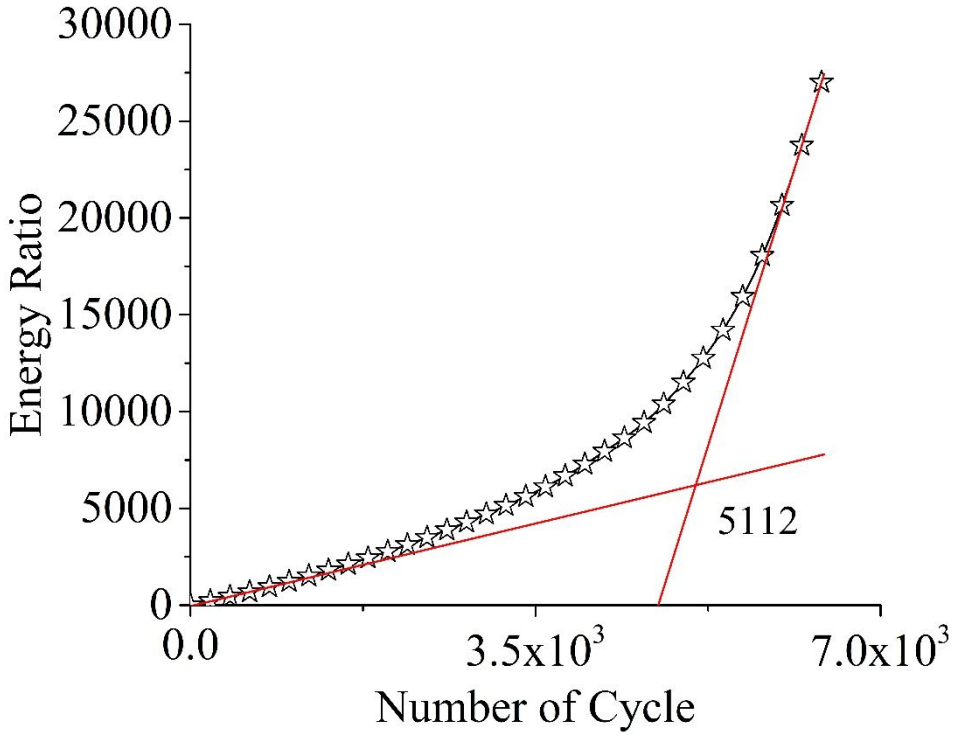

Fig. B.46: Energy Ratio for VG30-WMA at 800 microstrain

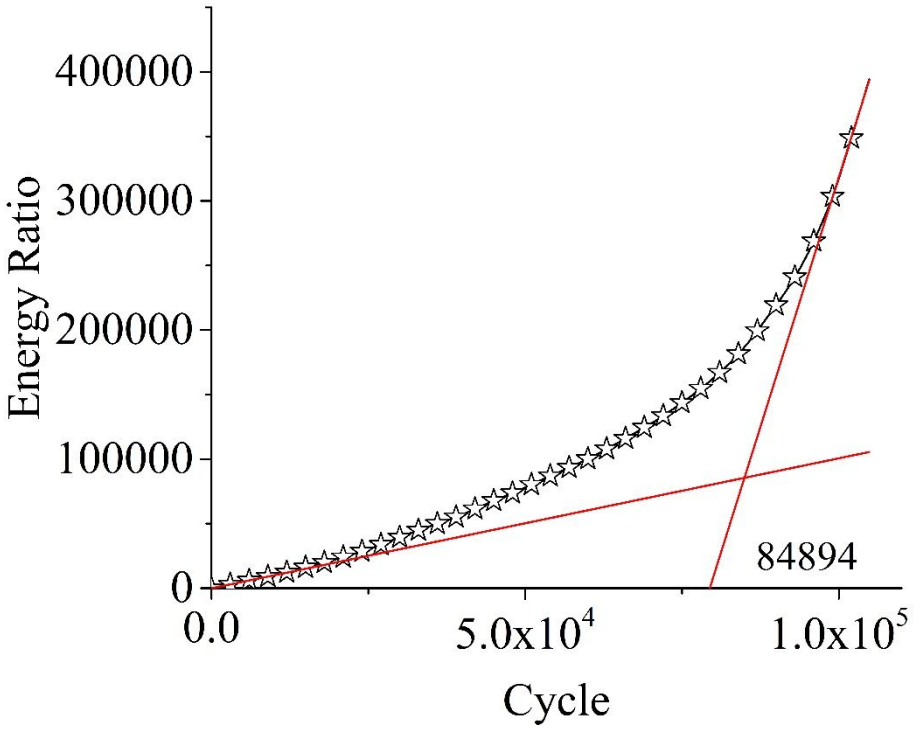

Fig. B.47: Energy Ratio for VG30-L at 400 microstrain

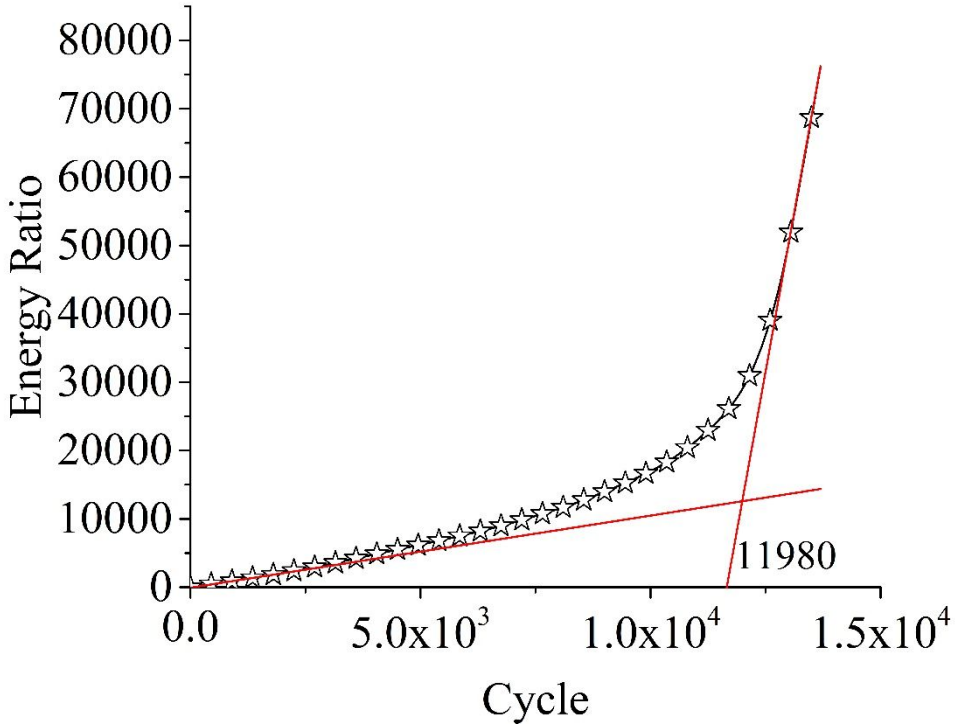

Fig. B.48: Energy Ratio for VG30-L at 600 microstrain

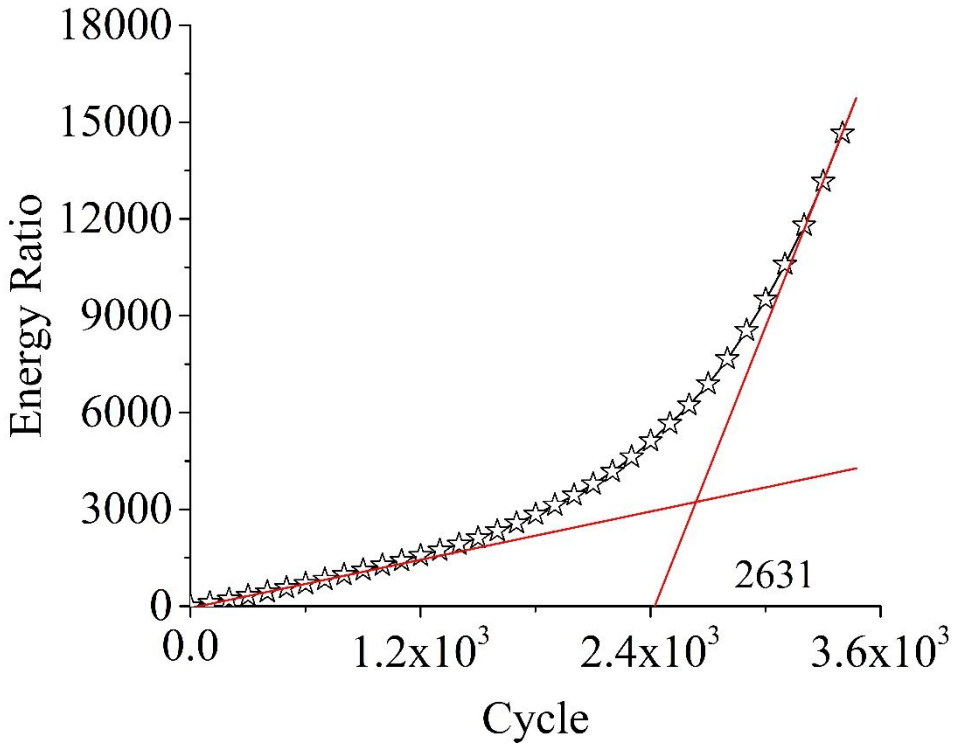

Fig. B.49: Energy Ratio for VG30-L at 800 microstrain

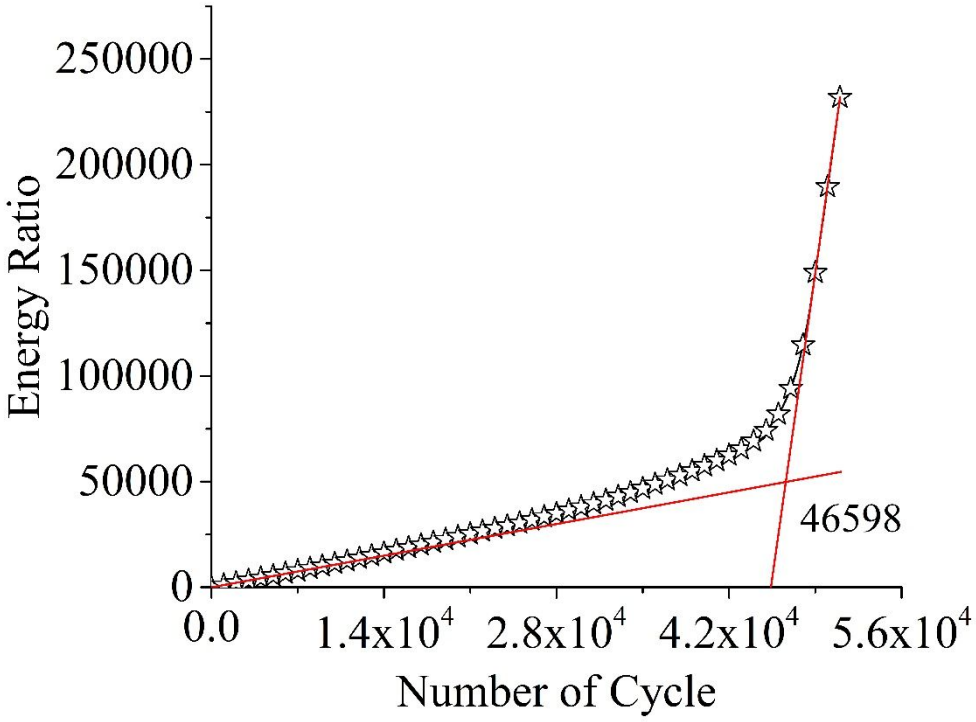

Fig. B.50: Energy Ratio for VG30-WMA-L at 400 microstrain

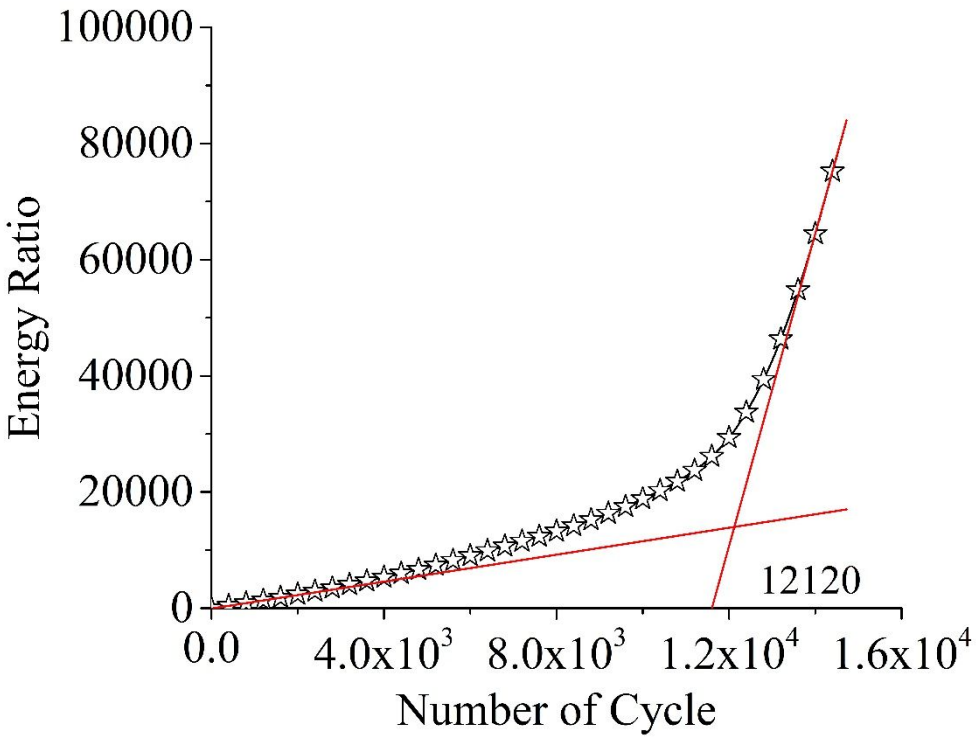

Fig. B.51: Energy Ratio for VG30-WMA-L at 600 microstrain

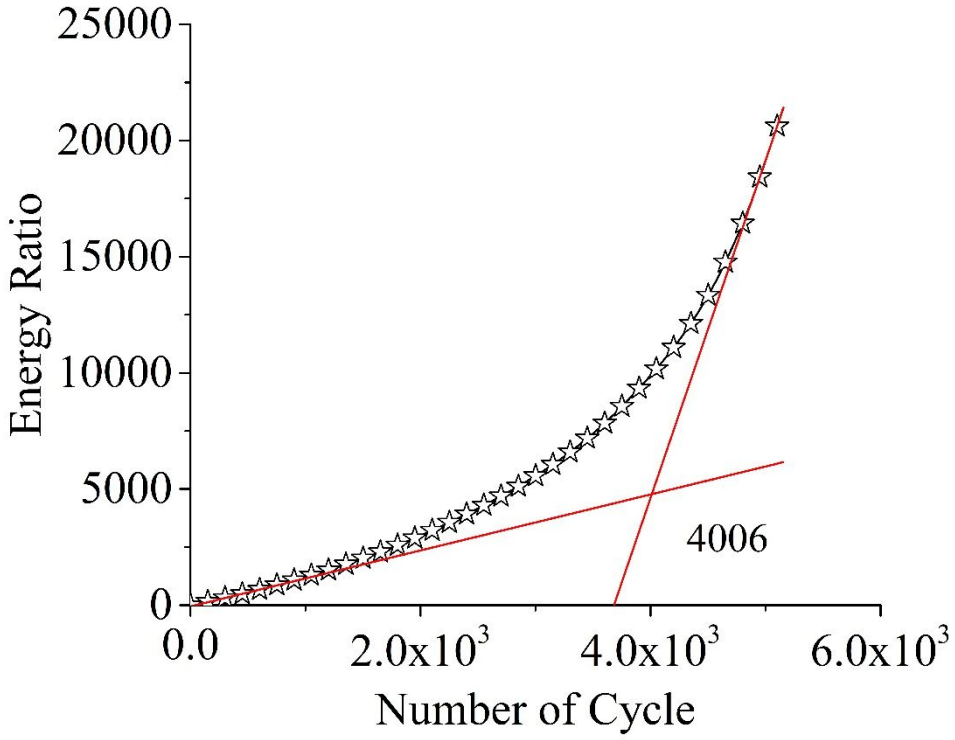

Fig. B.52: Energy Ratio for VG30-WMA-L at 800 microstrain

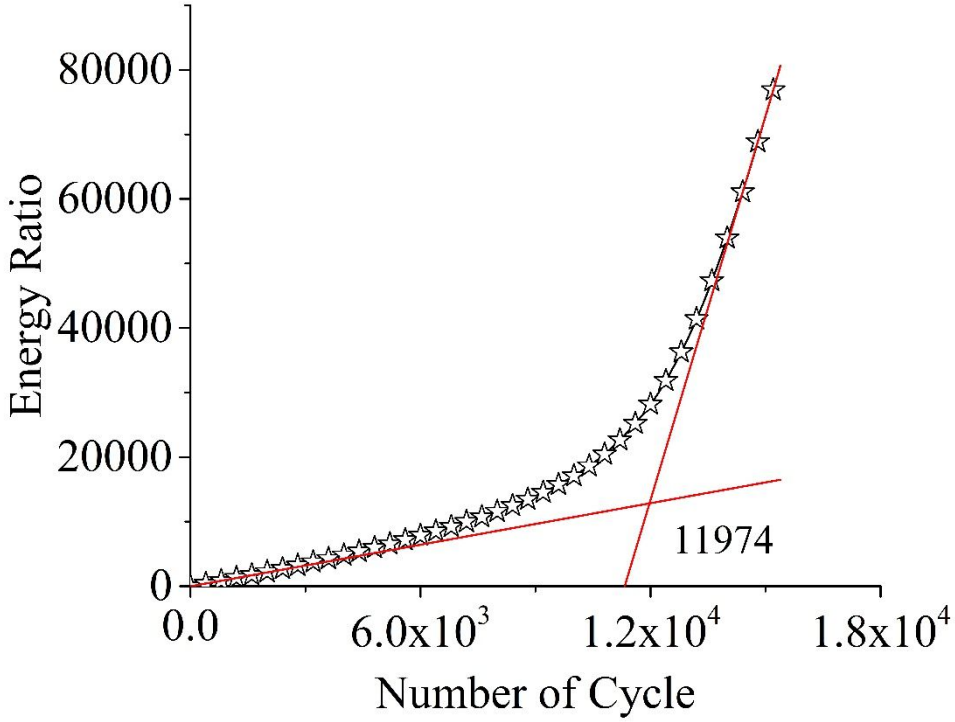

Fig. B.53: Energy Ratio for VG30-MC at 400 microstrain

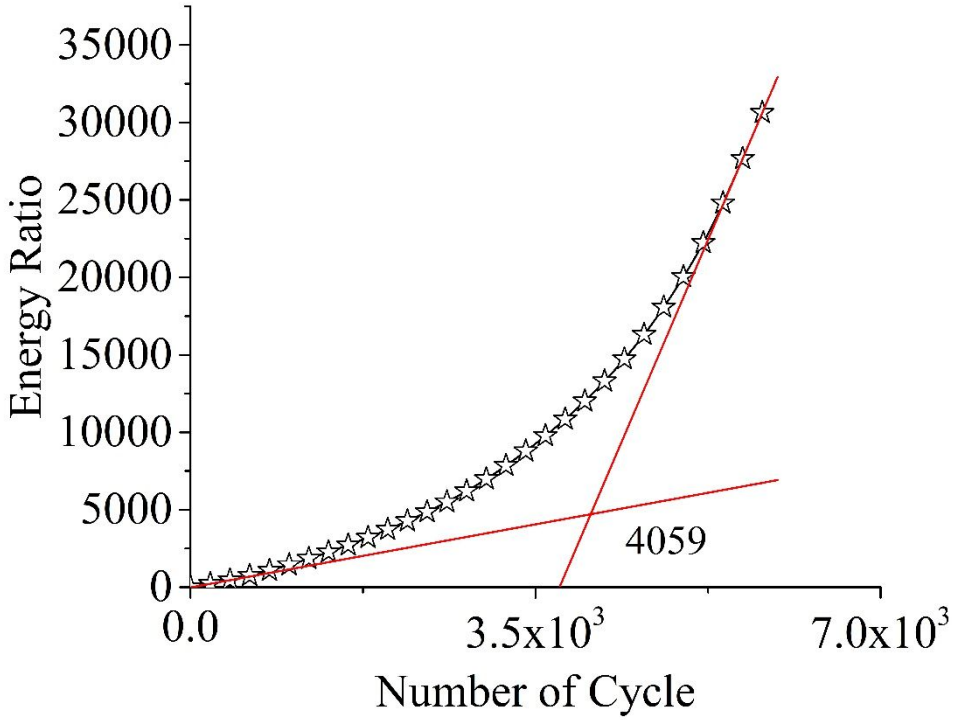

Fig. B.54: Energy Ratio for VG30-MC at 600 microstrain

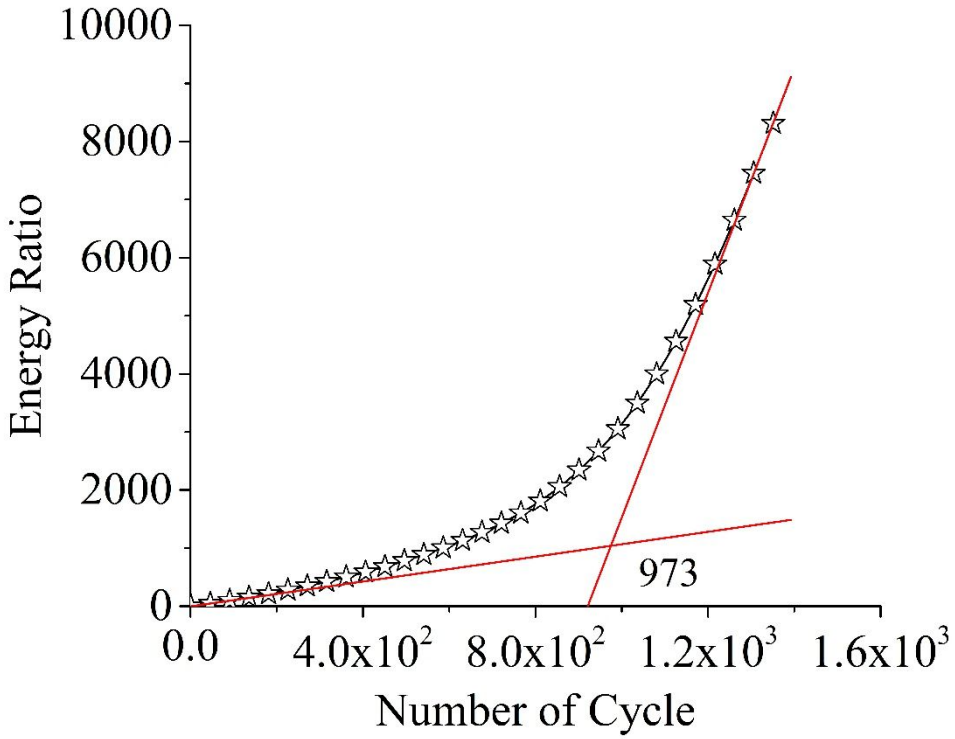

Fig. B.55: Energy Ratio for VG30-MC at 800 microstrain

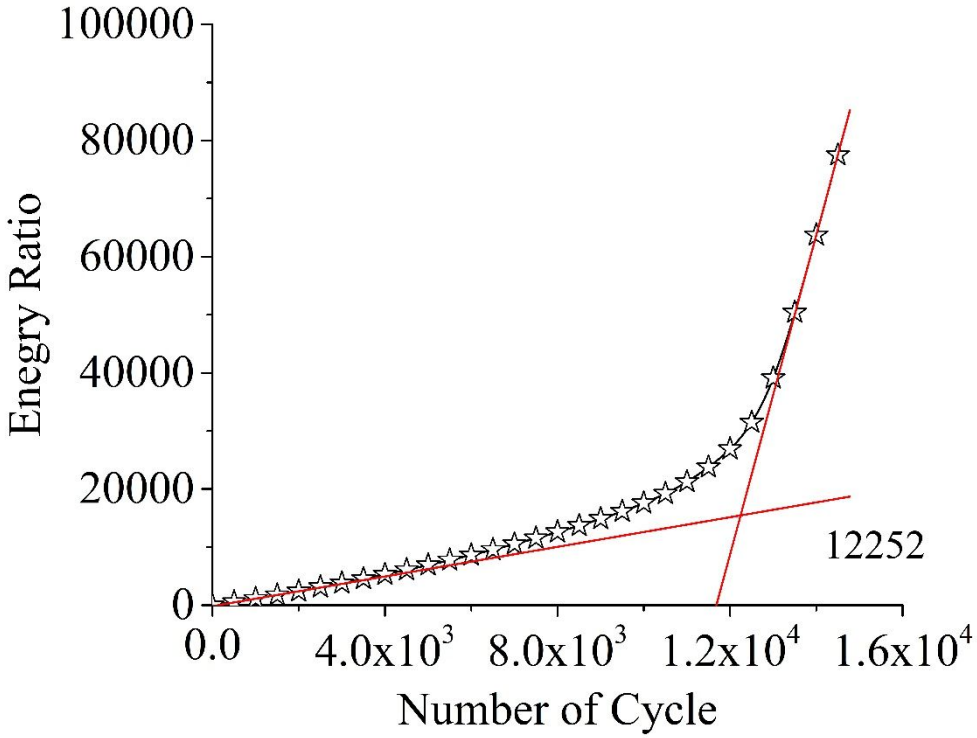

Fig. B.56: Energy Ratio for VG30-WMA-MC at 400 microstrain

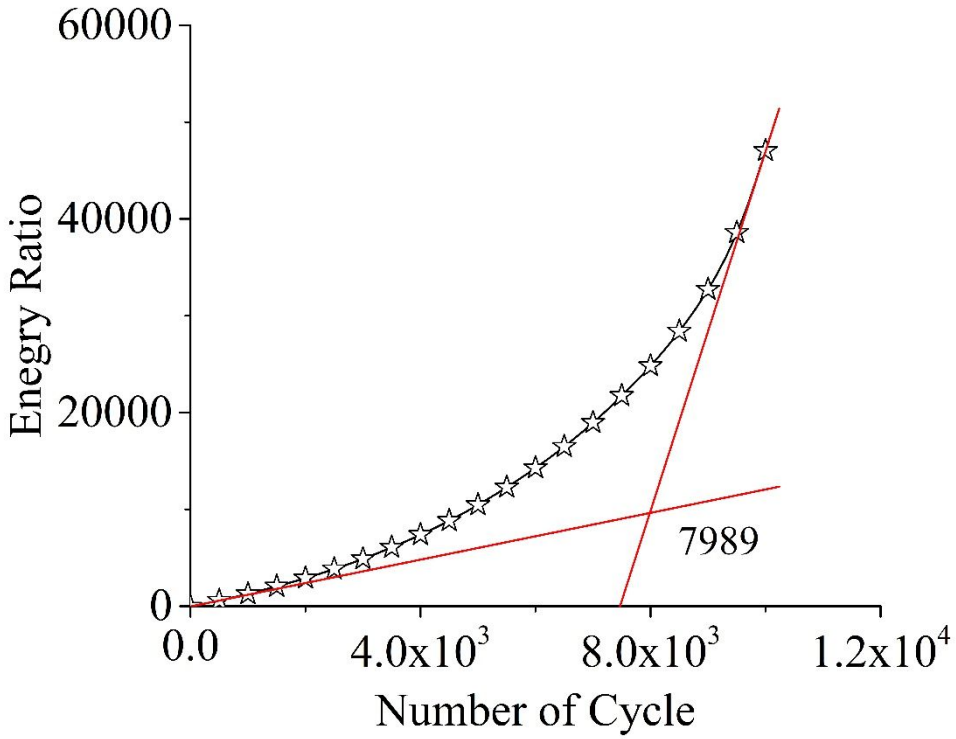

Fig. B.57: Energy Ratio for VG30-WMA-MC at 600 microstrain

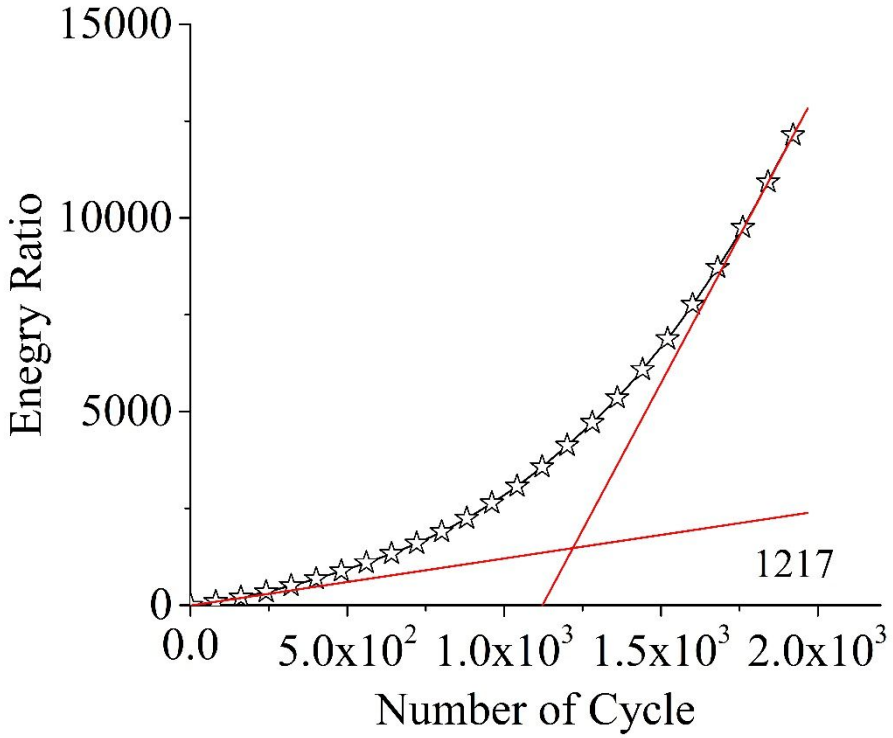

Fig. B.58: Energy Ratio for VG30-WMA-MC at 800 microstrain

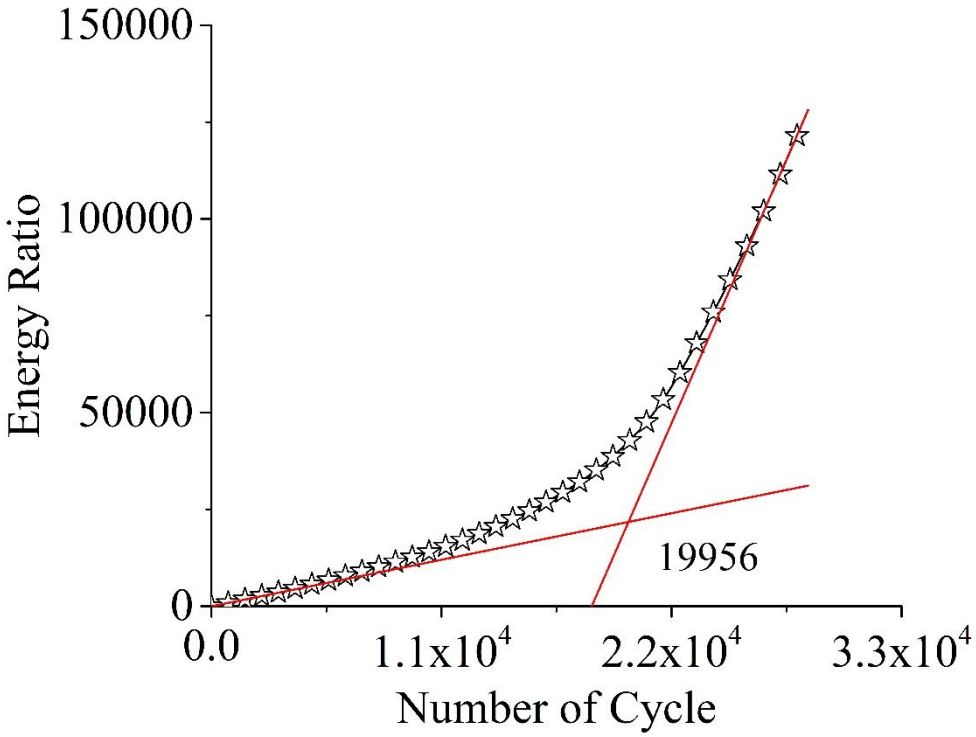

Fig. B.59: Energy Ratio for VG30-L-MC at 400 microstrain

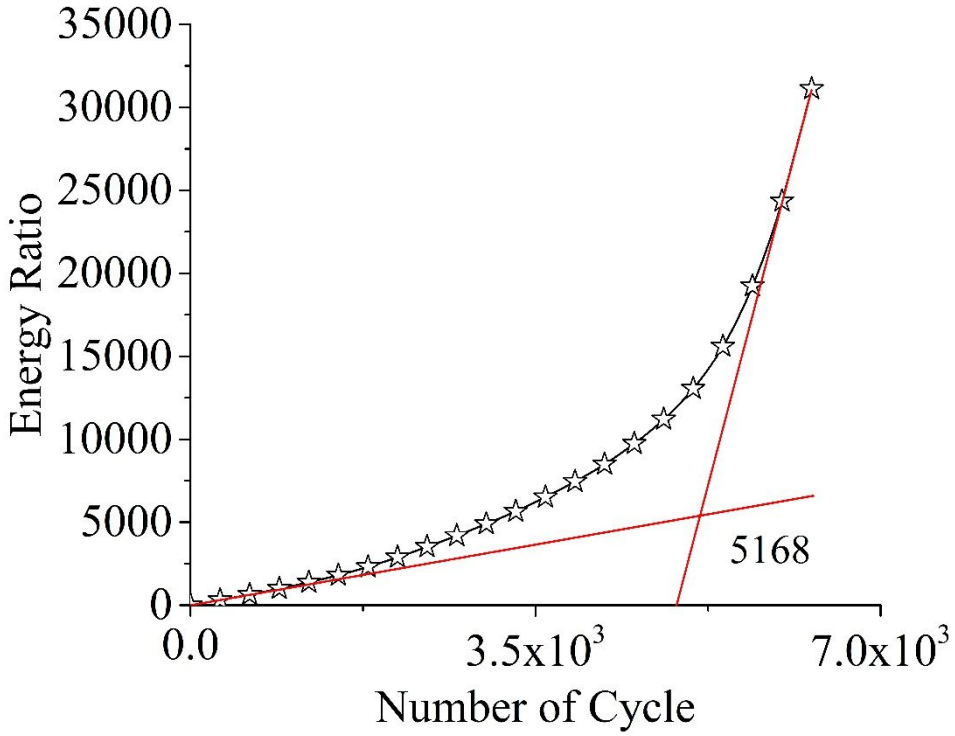

Fig. B.60: Energy Ratio for VG30-L-MC at 600 microstrain

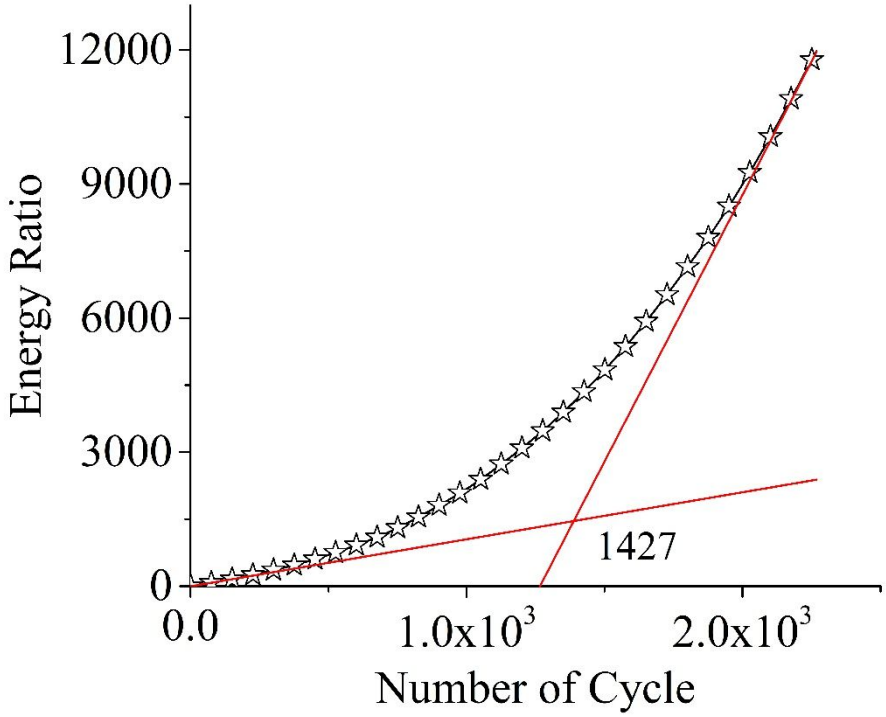

Fig. B.61: Energy Ratio for VG30-L-MC at 800 microstrain

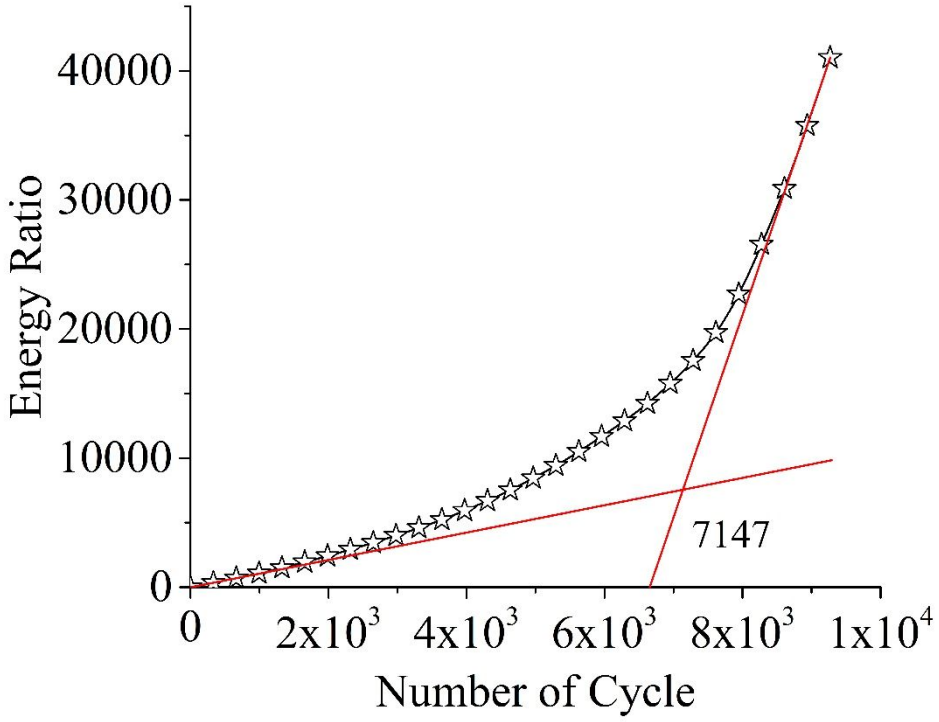

Fig. B.62: Energy Ratio for VG30-WMA-L-MC at 400 microstrain

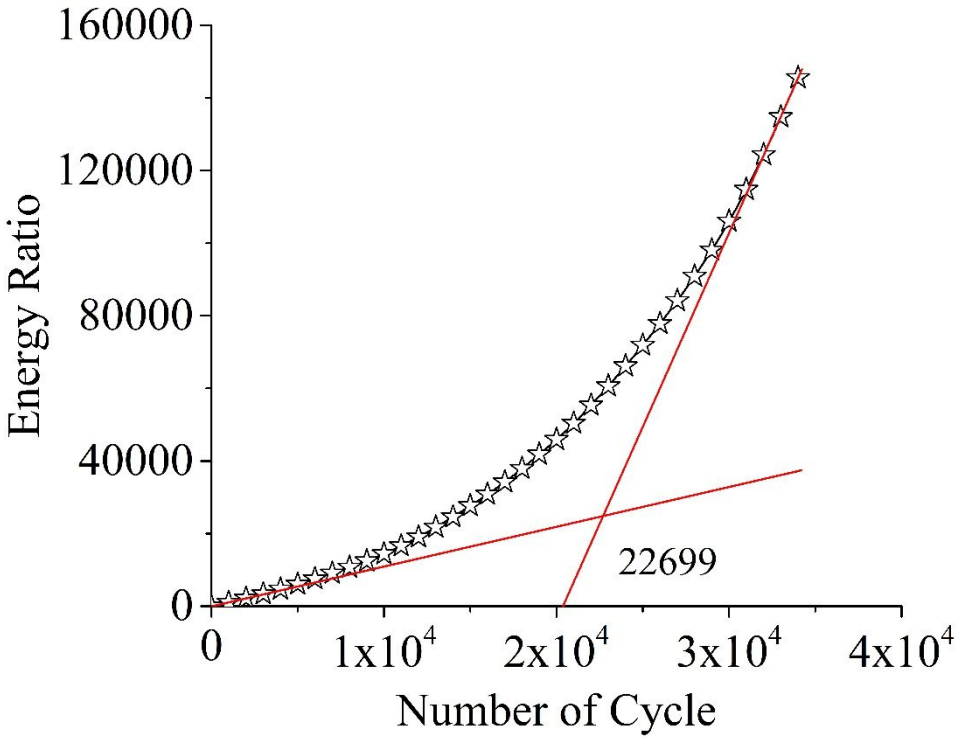

Fig. B.63: Energy Ratio for VG30-WMA-L-MC at 600 microstrain

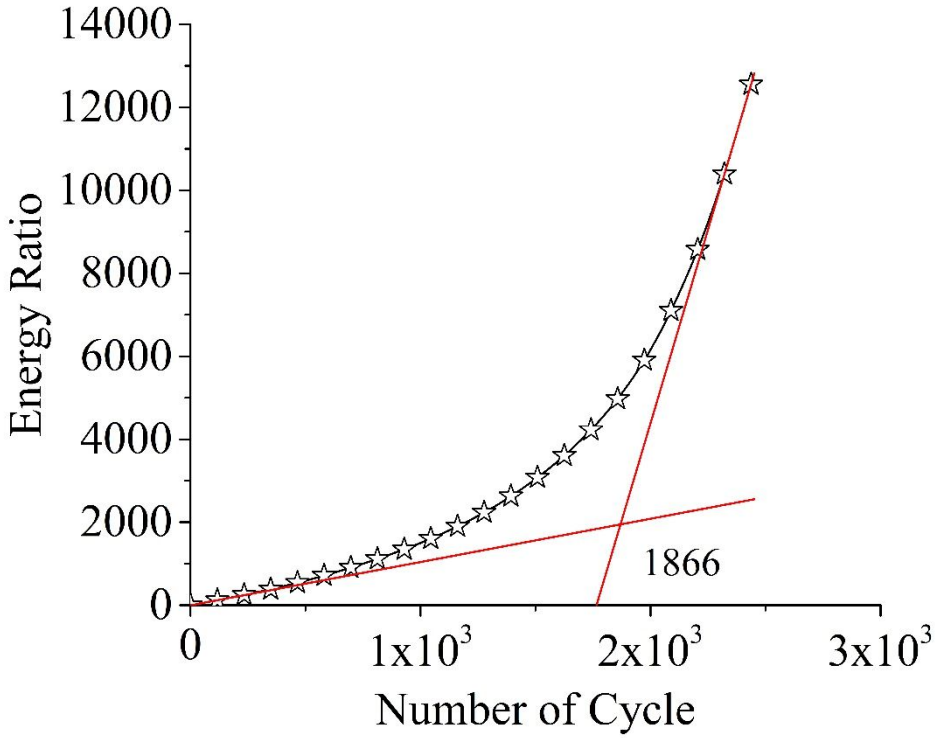

Fig. B.64: Energy Ratio for VG30-WMA-L-MC at 800 microstrain

B.5. RDEC Plots

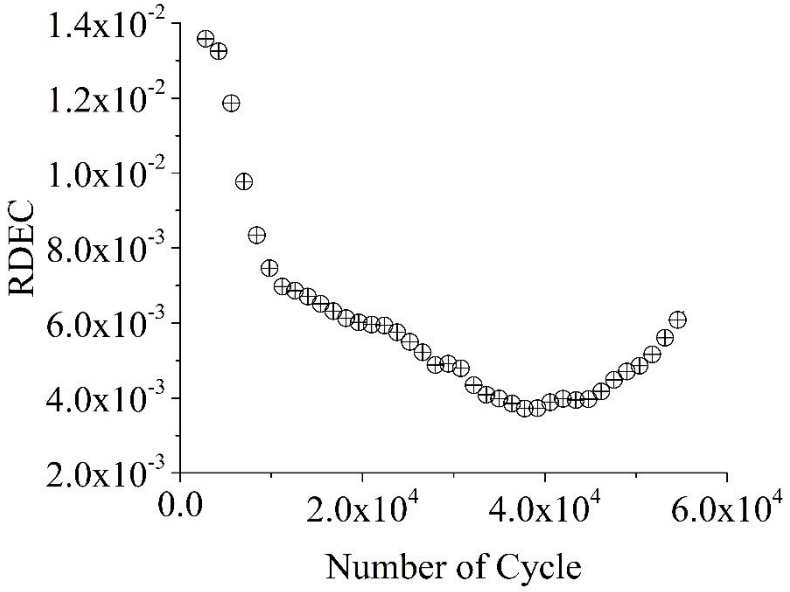

Fig. B.65: RDEC using Ghuzlan and Carpenter (2000) for VG30 at 400 microstrain

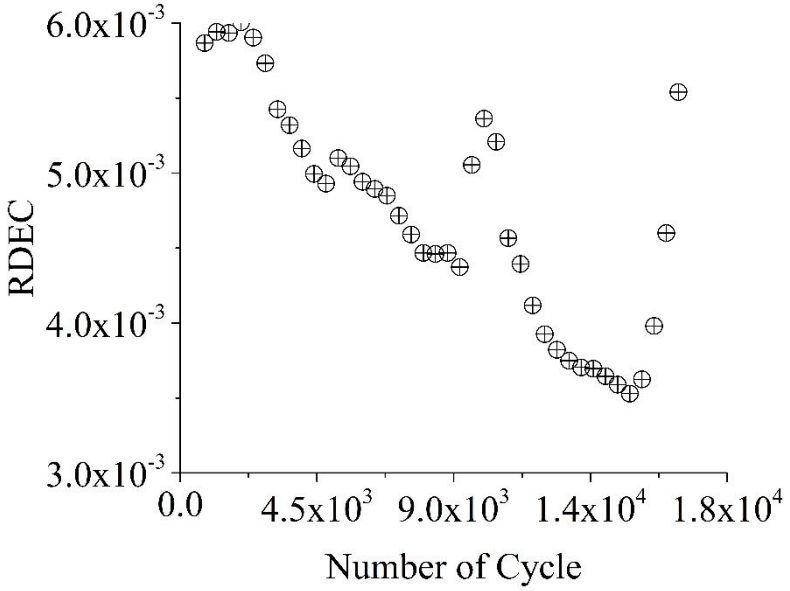

Fig. B.66: RDEC using Ghuzlan and Carpenter (2000) for VG30 at 600 microstrain

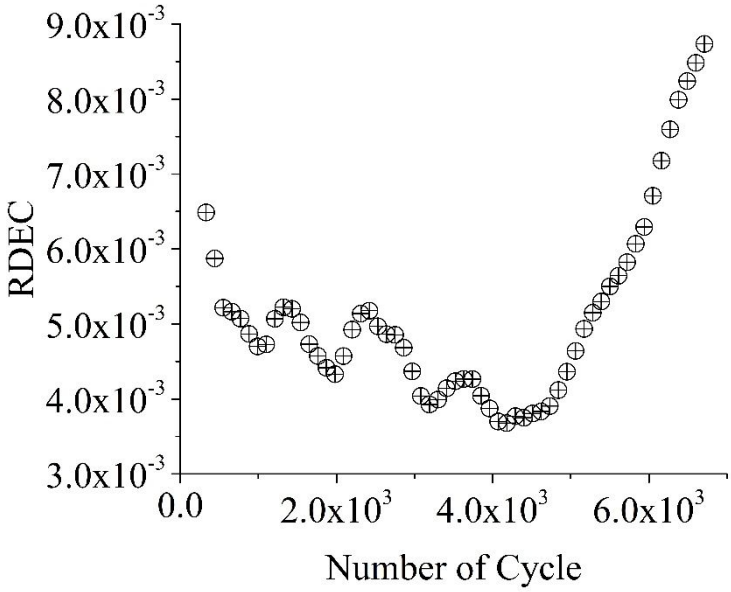

Fig. B.67: RDEC using Ghuzlan and Carpenter (2000) for VG30 at 800 microstrain

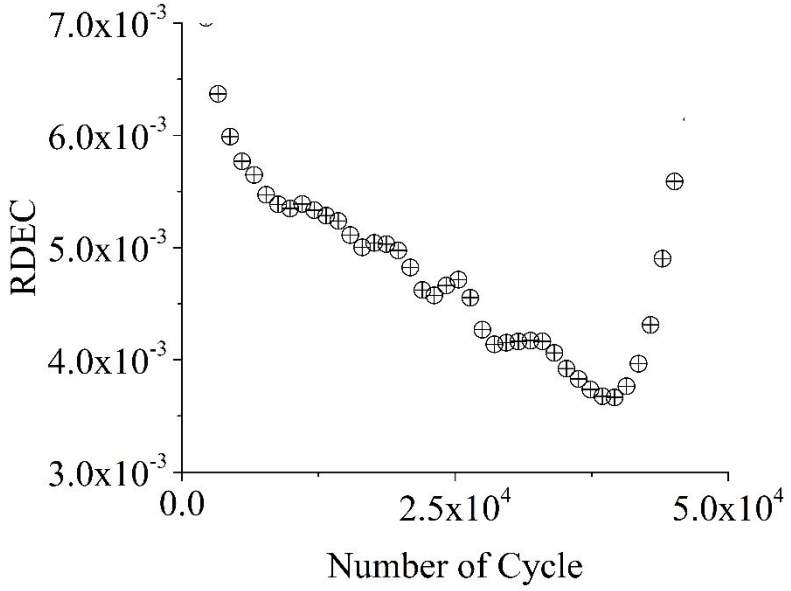

Fig. B.68: RDEC using Ghuzlan and Carpenter (2000) for VG30-WMA at 400 microstrain

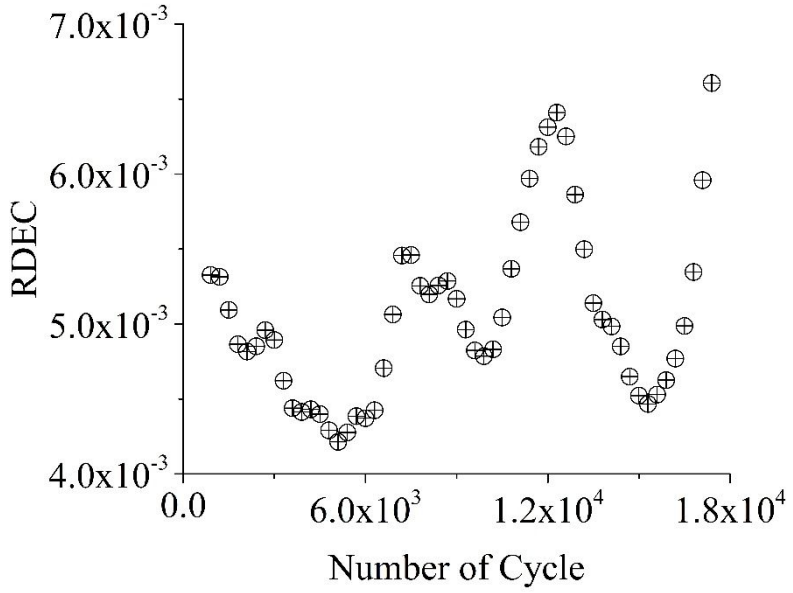

Fig. B.69: RDEC using Ghuzlan and Carpenter (2000) for VG30-WMA at 600 microstrain

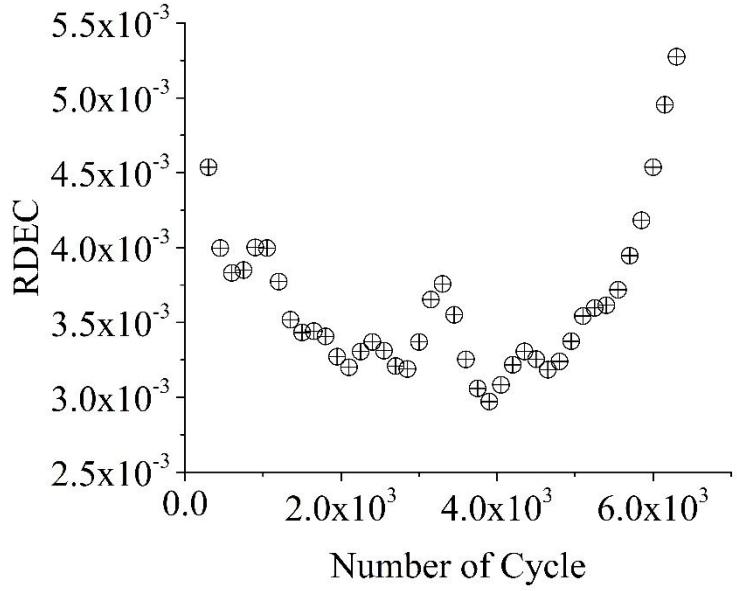

Fig. B.70: RDEC using Ghuzlan and Carpenter (2000) for VG30-WMA at 800 microstrain

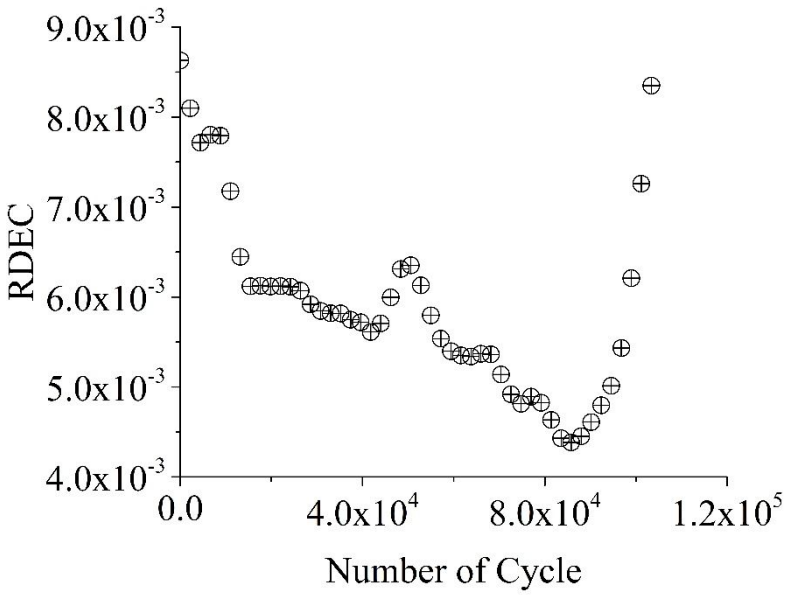

Fig. B.71: RDEC using Ghuzlan and Carpenter (2000) for VG30-L at 400 microstrain

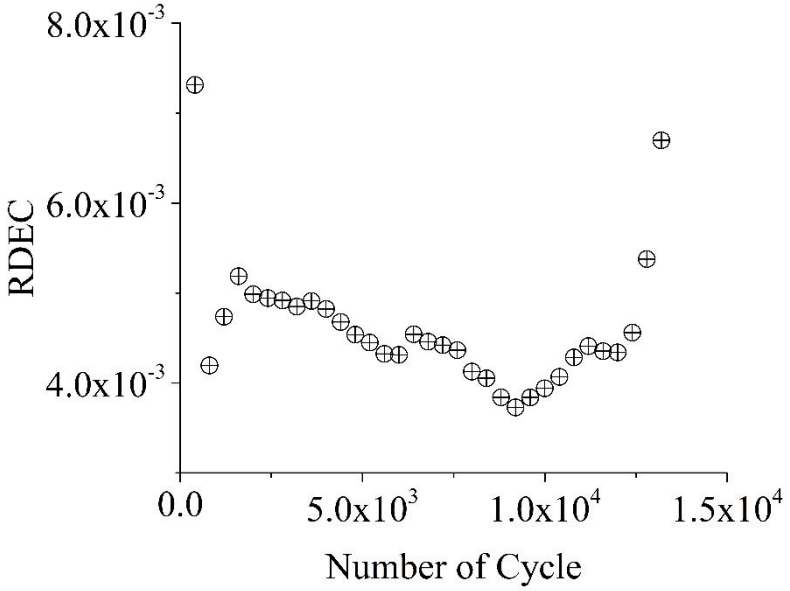

Fig. B.72: RDEC using Ghuzlan and Carpenter (2000) for VG30-L at 600 microstrain

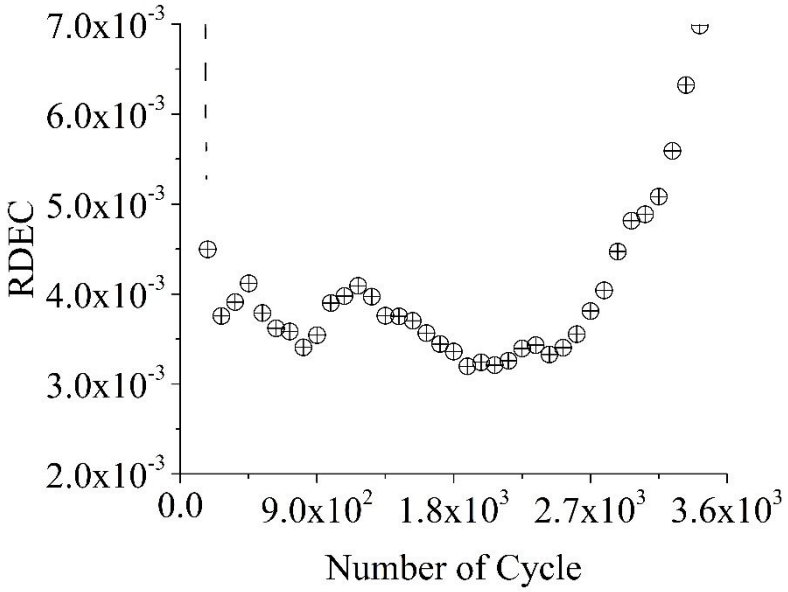

Fig. B.73: RDEC using Ghuzlan and Carpenter (2000) for VG30-L at 800 microstrain

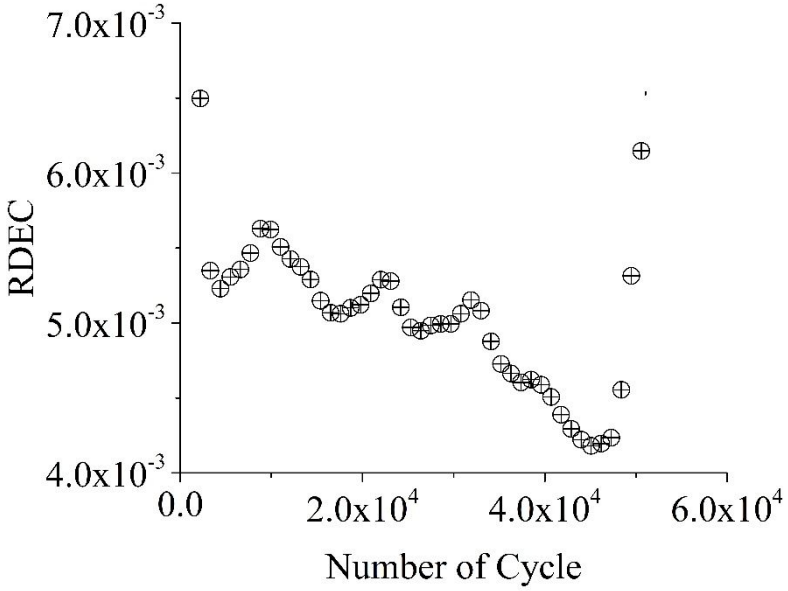

Fig. B.74: RDEC using Ghuzlan and Carpenter (2000) for VG30-WMA-L at 400 microstrain

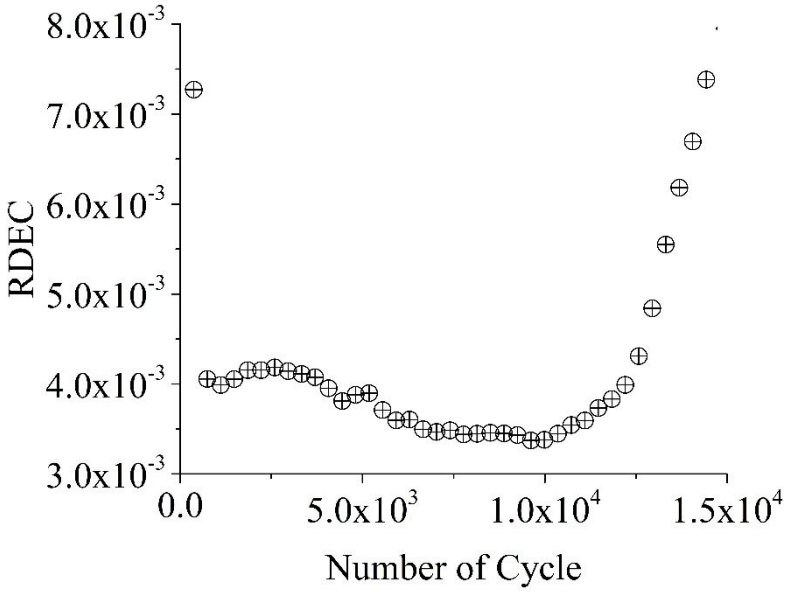

Fig. B.75: RDEC using Ghuzlan and Carpenter (2000) for VG30-WMA-L at 600 microstrain

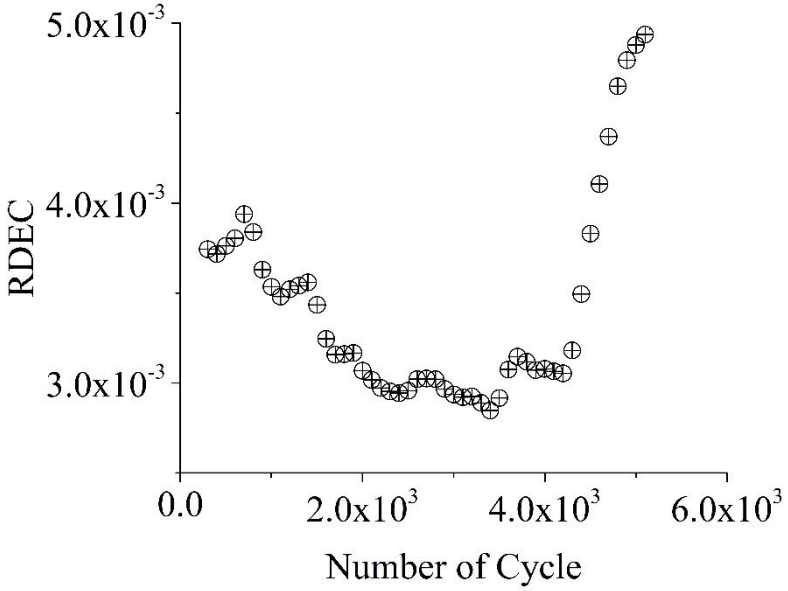

Fig. B.76: RDEC using Ghuzlan and Carpenter (2000) for VG30-WMA-L at 800 microstrain

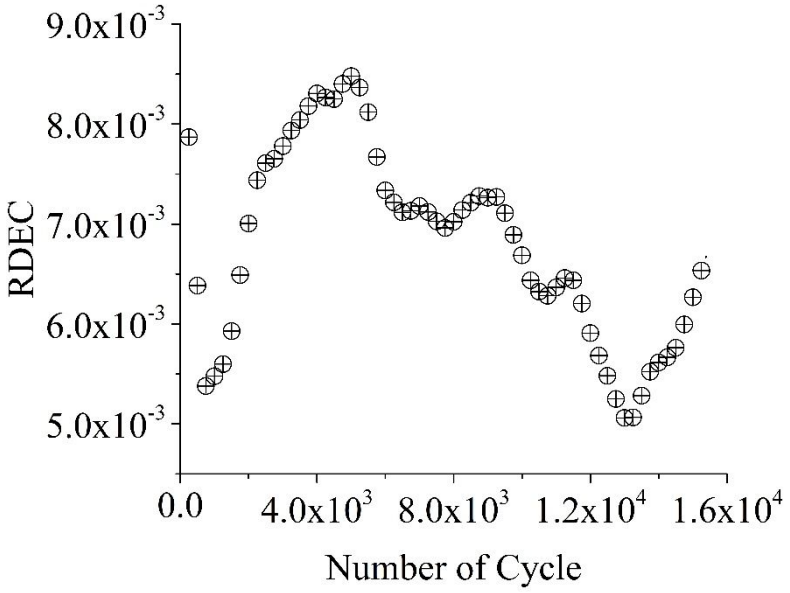

Fig. B.77: RDEC using Ghuzlan and Carpenter (2000) for VG30-MC at 400 microstrain

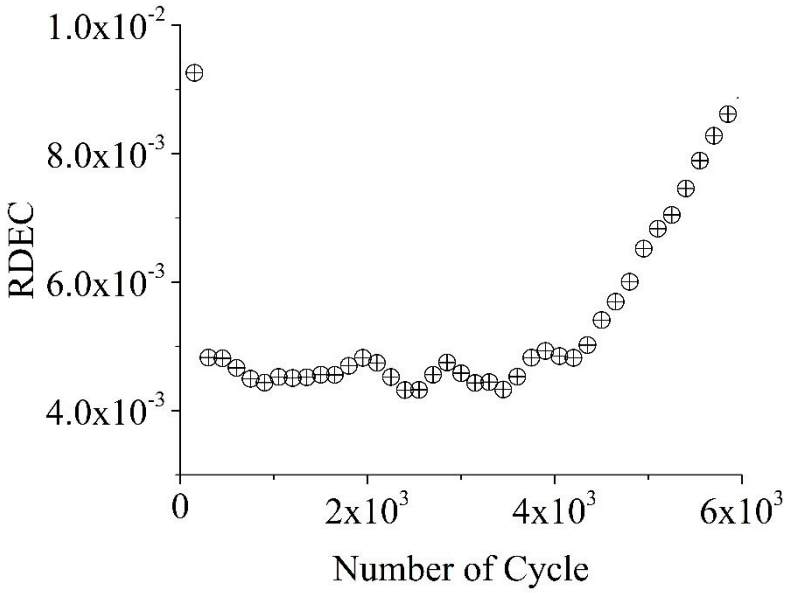

Fig. B.78: RDEC using Ghuzlan and Carpenter (2000) for VG30-MC at 600 microstrain

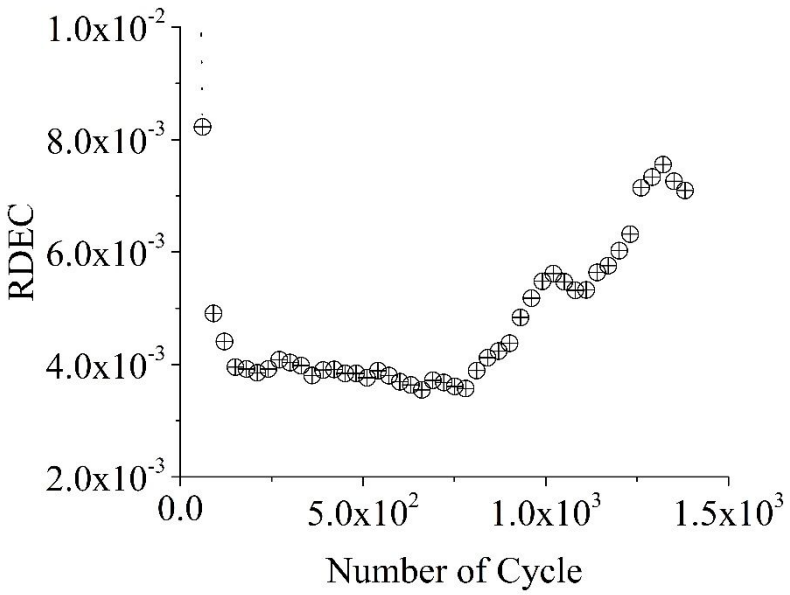

Fig. B.79: RDEC using Ghuzlan and Carpenter (2000) for VG30-MC at 800 microstrain

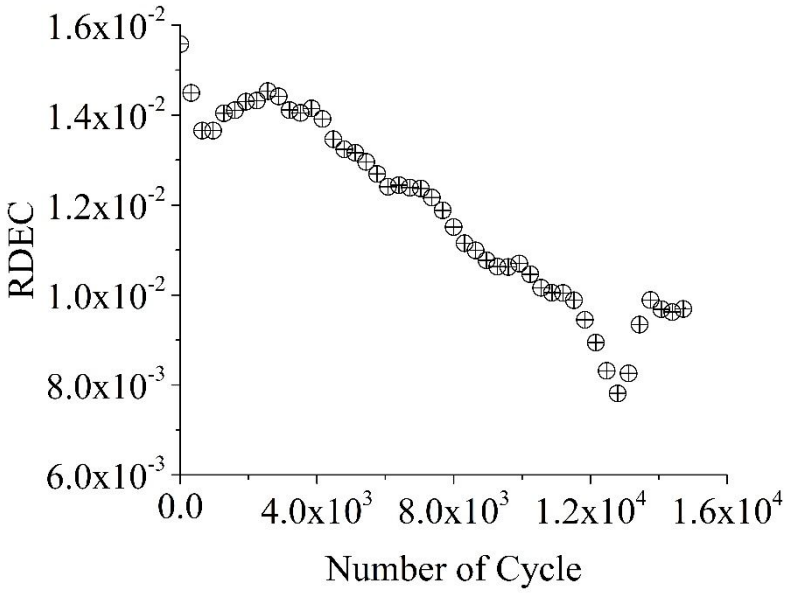

Fig. B.81: RDEC using Ghuzlan and Carpenter (2000) for VG30-WMA-MC at 400 microstrain

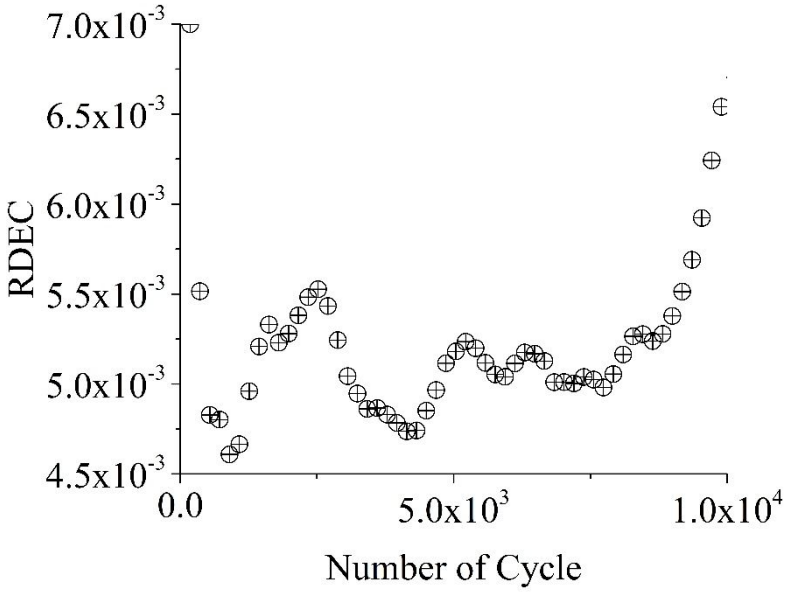

Fig. B.81: RDEC using Ghuzlan and Carpenter (2000) for VG30-WMA-MC at 600 microstrain

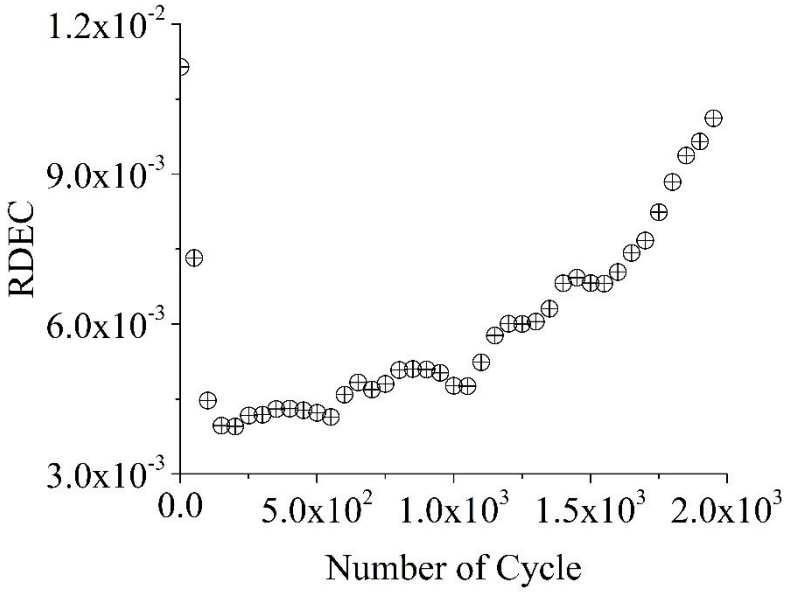

Fig. B.82: RDEC using Ghuzlan and Carpenter (2000) for VG30-WMA-MC at 800 microstrain

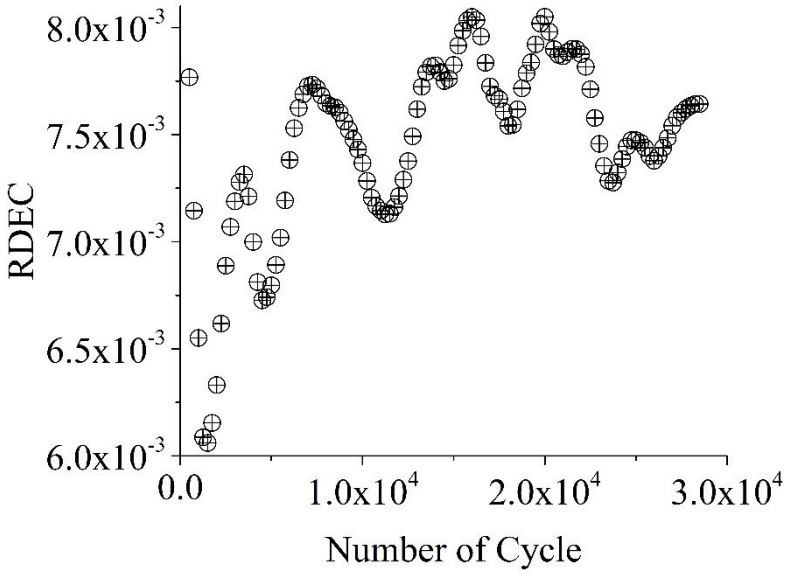

Fig. B.83: RDEC using Ghuzlan and Carpenter (2000) for VG30-L-MC at 400 microstrain

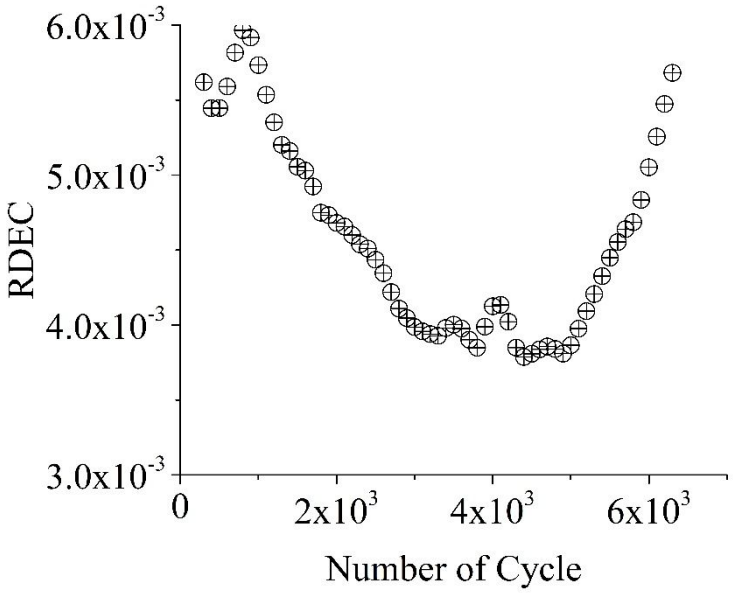

Fig. B.84: RDEC using Ghuzlan and Carpenter (2000) for VG30-L-MC at 600 microstrain

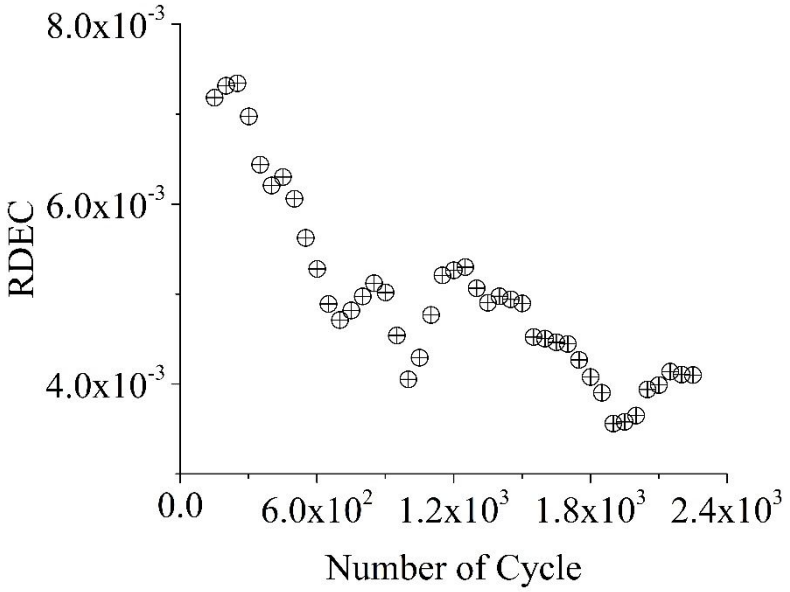

Fig. B.85: RDEC using Ghuzlan and Carpenter (2000) for VG30-L-MC at 800 microstrain

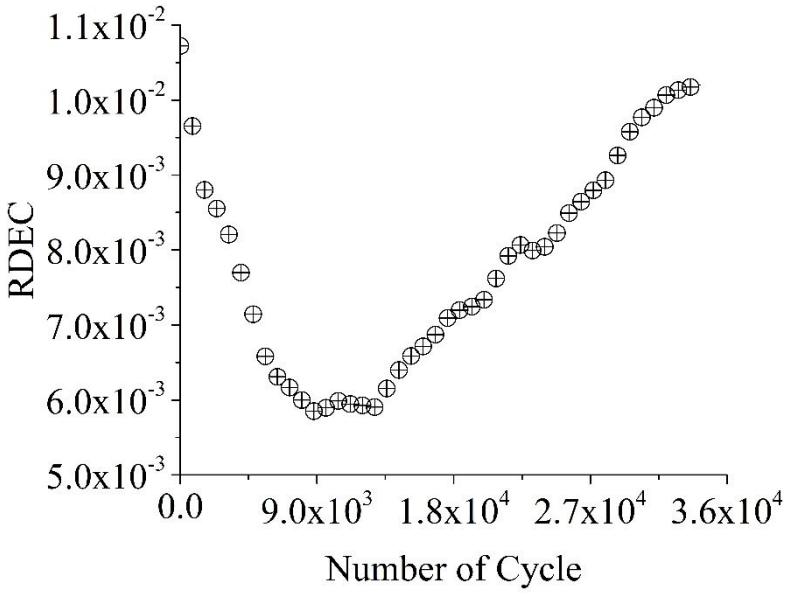

Fig. B.86: RDEC using Ghuzlan and Carpenter (2000) for VG30-WMA-L-MC at 400 microstrain

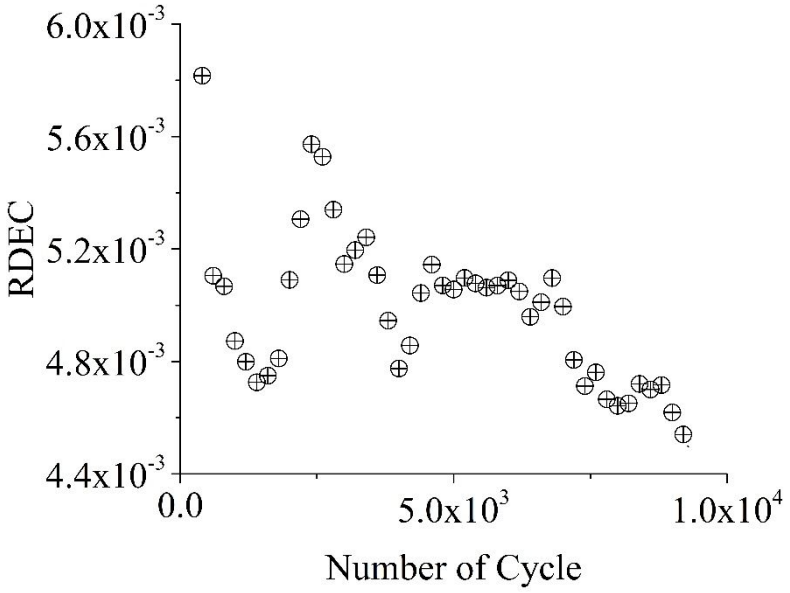

Fig. B.87: RDEC using Ghuzlan and Carpenter (2000) for VG30-WMA-L-MC at 600 microstrain

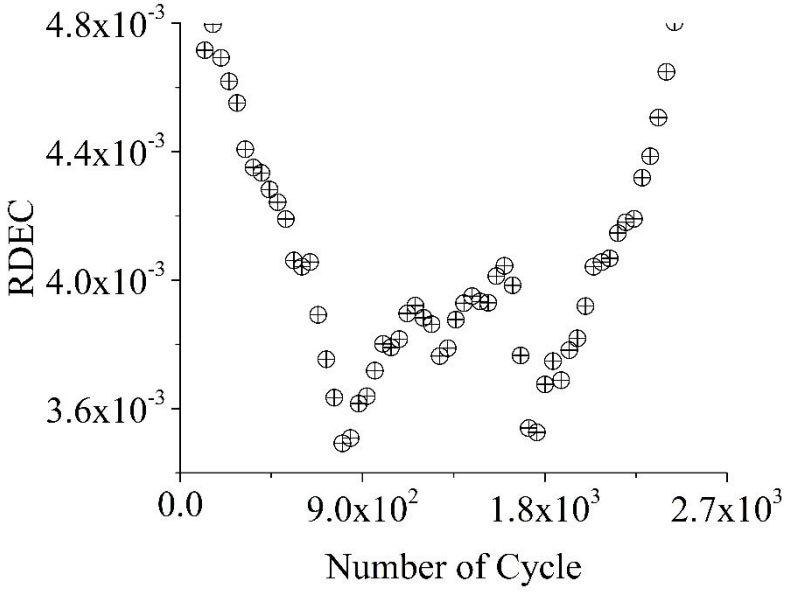

Fig. B.88: RDEC using Ghuzlan and Carpenter (2000) for VG30-WMA-L-MC at 800 microstrain

APPENDIX C

C.1. Cummulative Dissipation – Approach 1

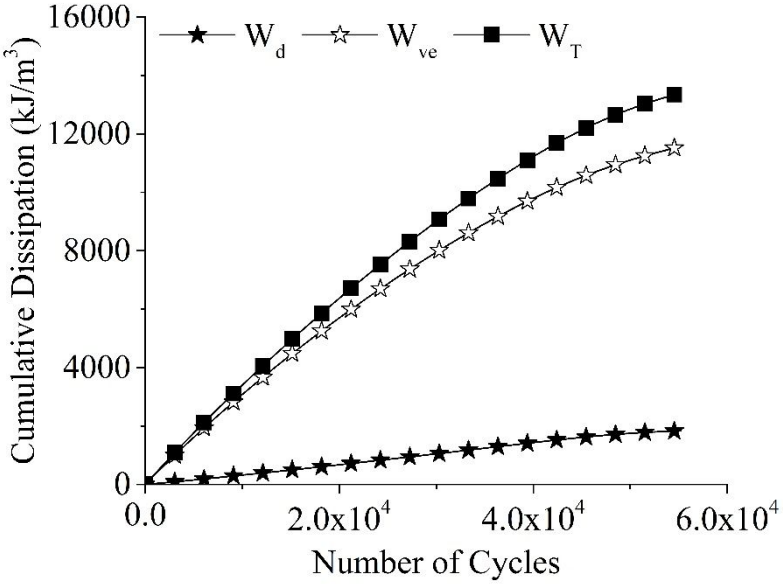

Fig. C.1: Cumulative viscoelastic, and damage dissipation based on pseudo-strain approach for VG30 at 400 microstrain

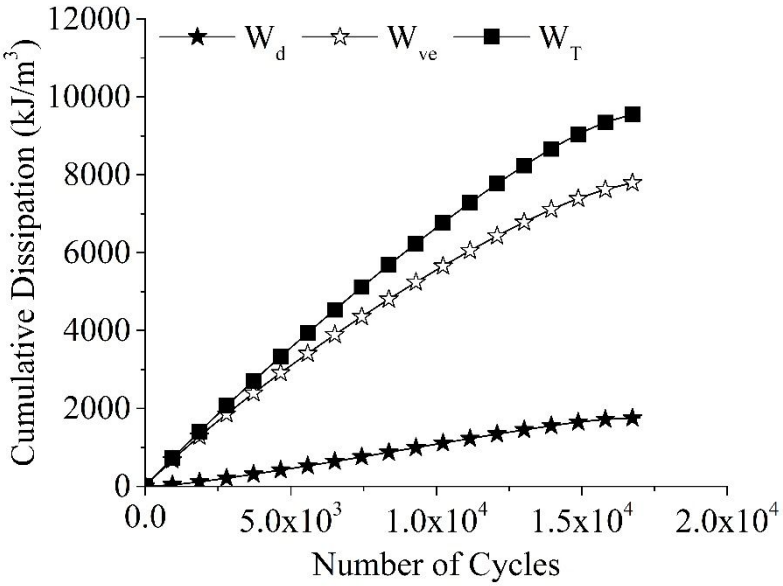

Fig. C.2: Cumulative viscoelastic, and damage dissipation based on pseudo-strain approach for VG30 at 600 microstrain

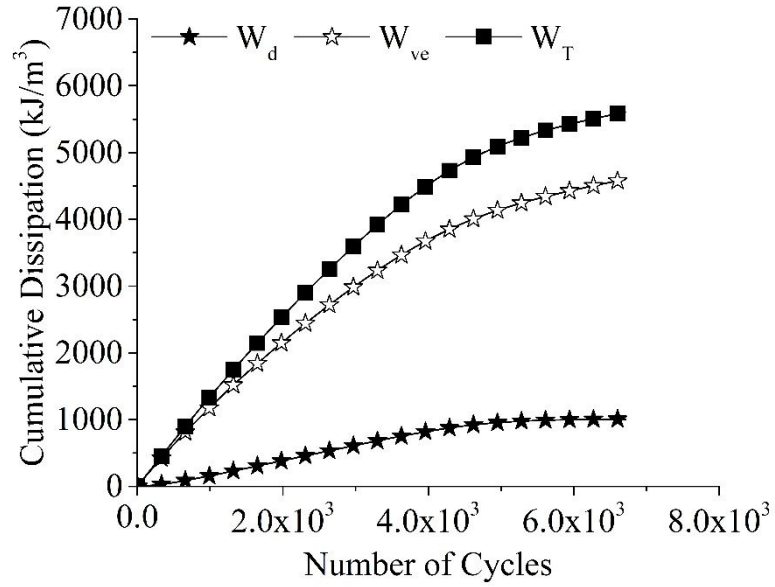

Fig. C.3: Cumulative viscoelastic, and damage dissipation based on pseudo-strain approach for VG30 at 800 microstrain

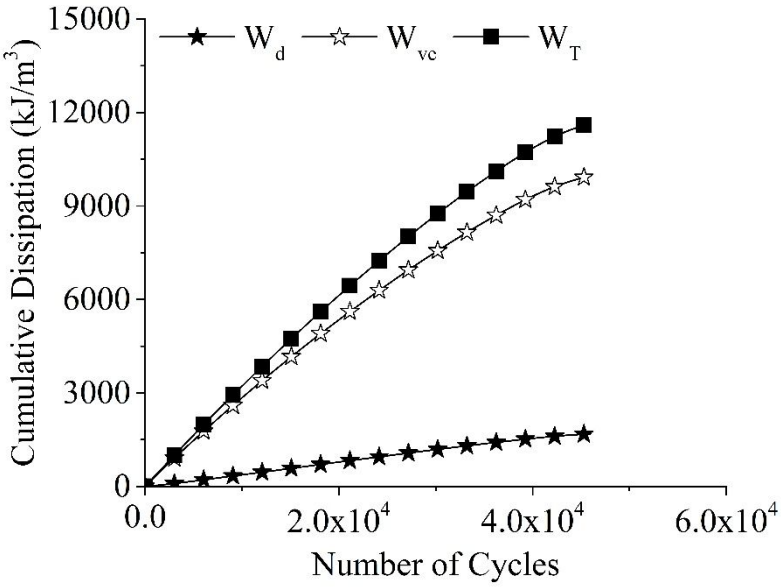

Fig. C.4: Cumulative viscoelastic, and damage dissipation based on pseudo-strain approach for VG30-WMA at 400 microstrain

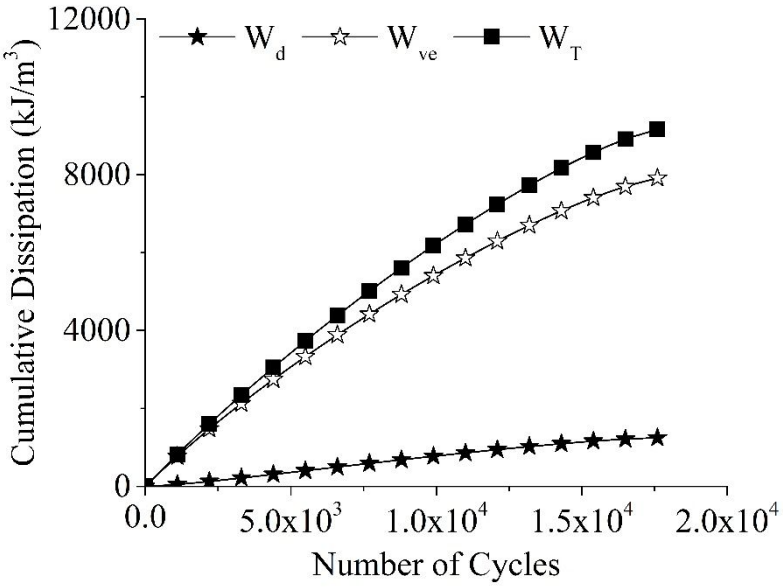

Fig. C.5: Cumulative viscoelastic, and damage dissipation based on pseudo-strain approach for VG30-WMA at 600 microstrain

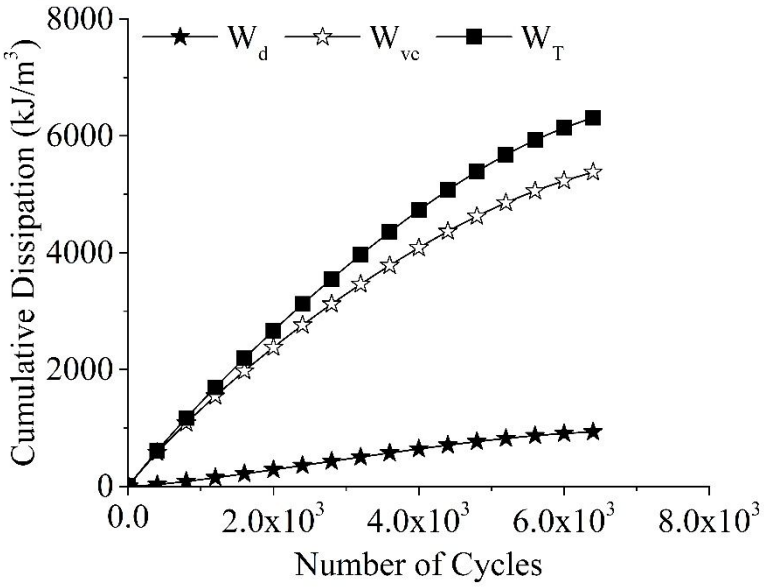

Fig. C.6: Cumulative viscoelastic, and damage dissipation based on pseudo-strain approach for VG30-WMA at 800 microstrain

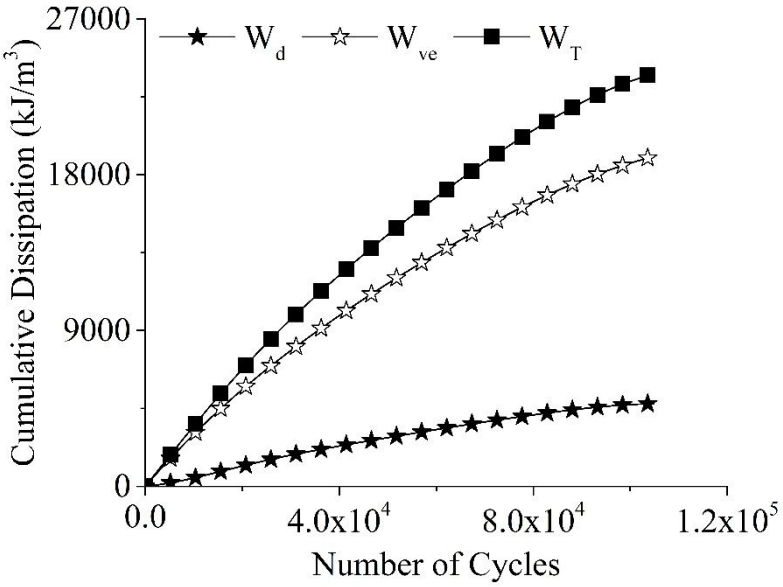

Fig. C.7: Cumulative viscoelastic, and damage dissipation based on pseudo-strain approach for VG30-L at 400 microstrain

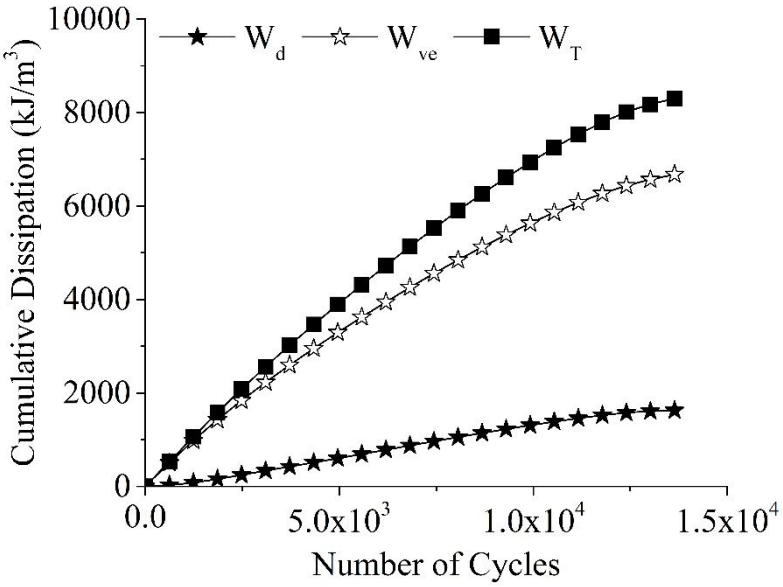

Fig. C.8: Cumulative viscoelastic, and damage dissipation based on pseudo-strain approach for VG30-L at 600 microstrain

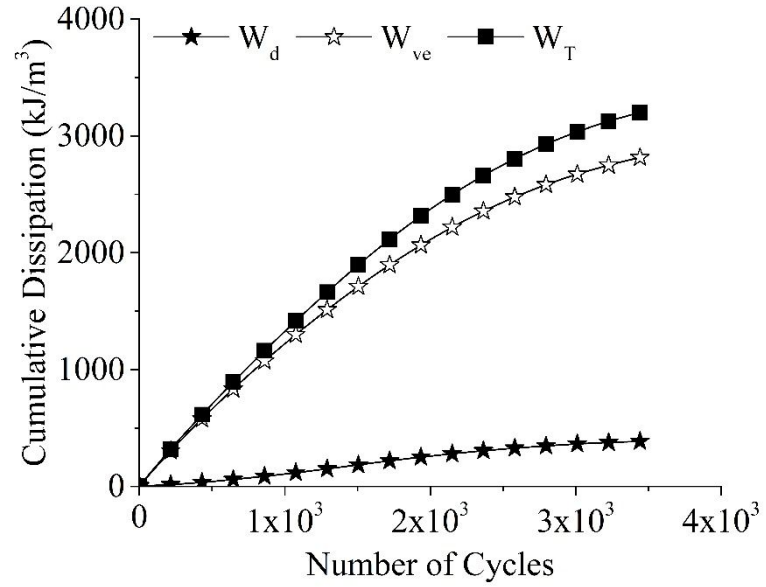

Fig. C.9: Cumulative viscoelastic, and damage dissipation based on pseudo-strain approach for VG30-L at 800 microstrain

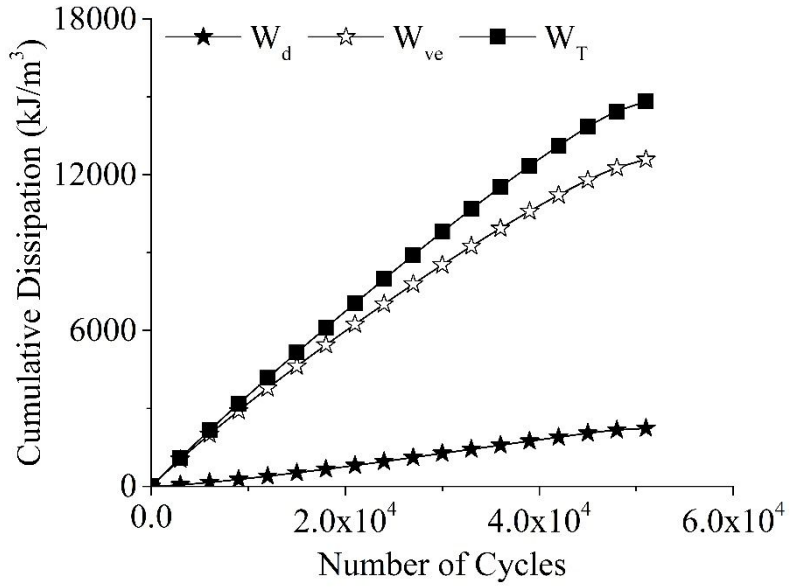

Fig. C.10: Cumulative viscoelastic, and damage dissipation based on pseudo-strain approach for VG30-WMA-L at 400 microstrain

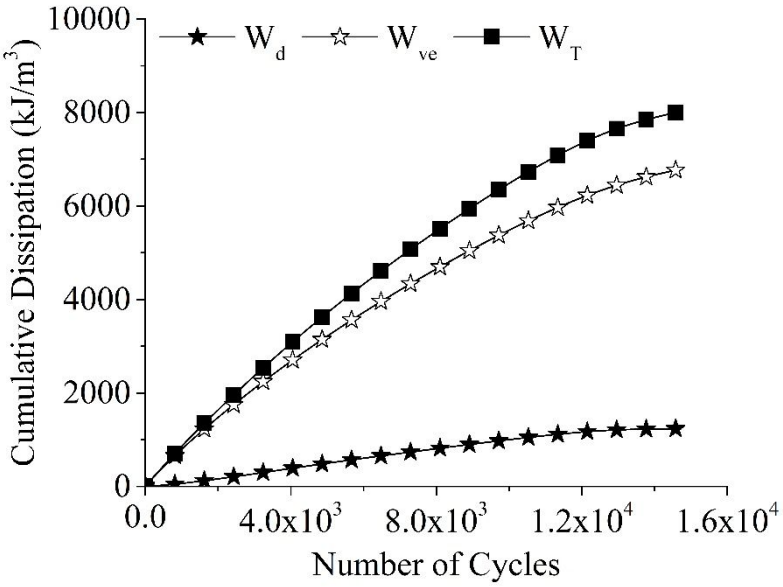

Fig. C.11: Cumulative viscoelastic, and damage dissipation based on pseudo-strain approach for VG30-WMA-L at 600 microstrain

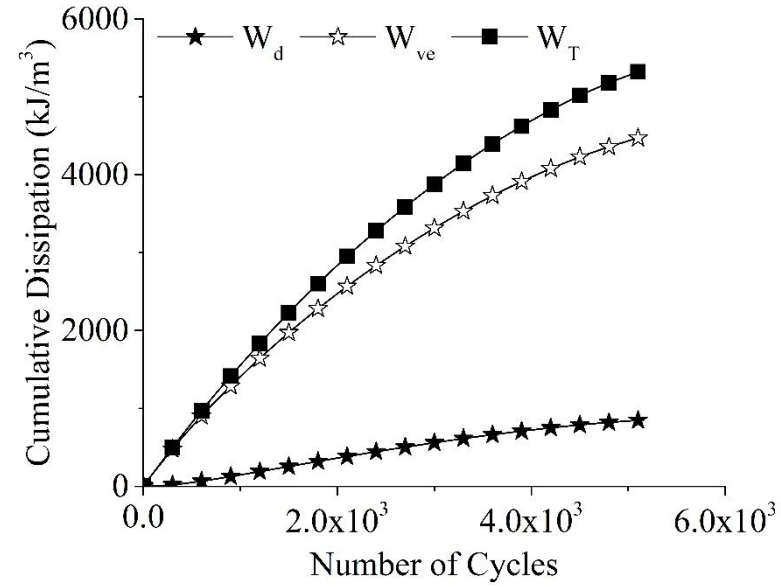

Fig. C.12: Cumulative viscoelastic, and damage dissipation based on pseudo-strain approach for VG30-WMA-L at 800 microstrain

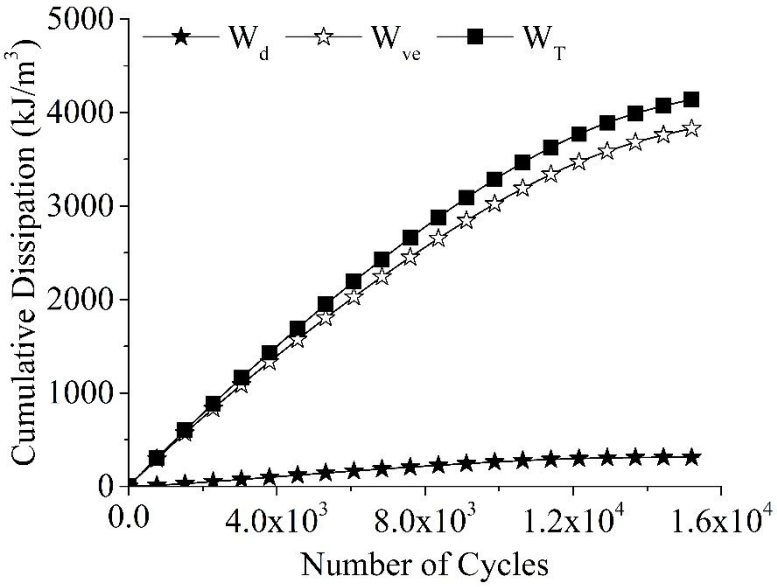

Fig. C.13: Cumulative viscoelastic, and damage dissipation based on pseudo-strain approach for VG30-MC at 400 microstrain

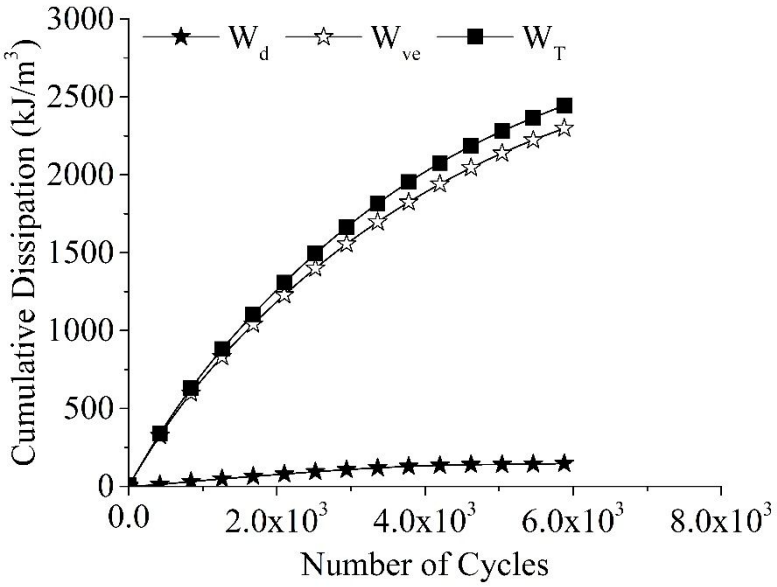

Fig. C.14: Cumulative viscoelastic, and damage dissipation based on pseudo-strain approach for VG30-MC at 600 microstrain

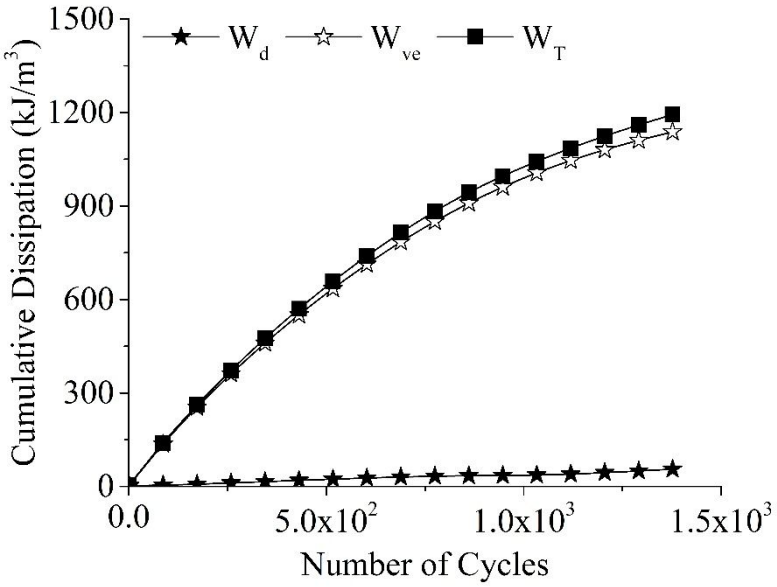

Fig. C.15: Cumulative viscoelastic, and damage dissipation based on pseudo-strain approach for VG30-MC at 800 microstrain

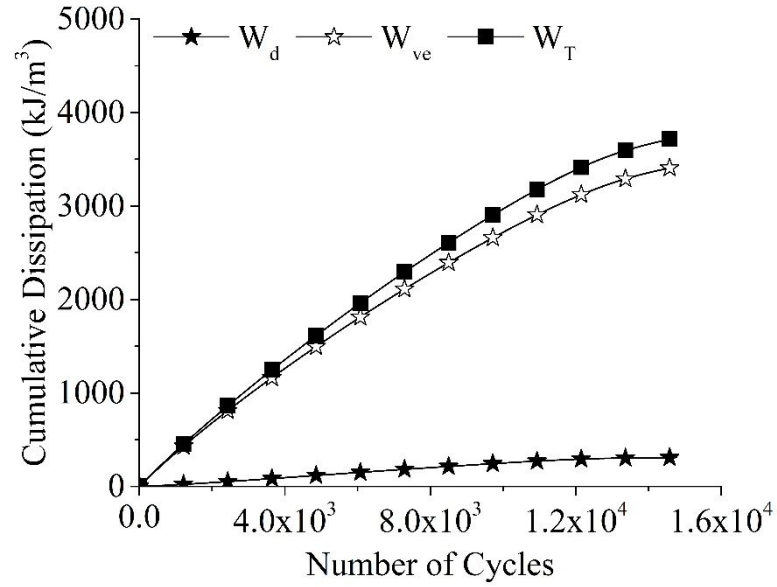

Fig. C.16: Cumulative viscoelastic, and damage dissipation based on pseudo-strain approach for VG30-WMA-MC at 400 microstrain

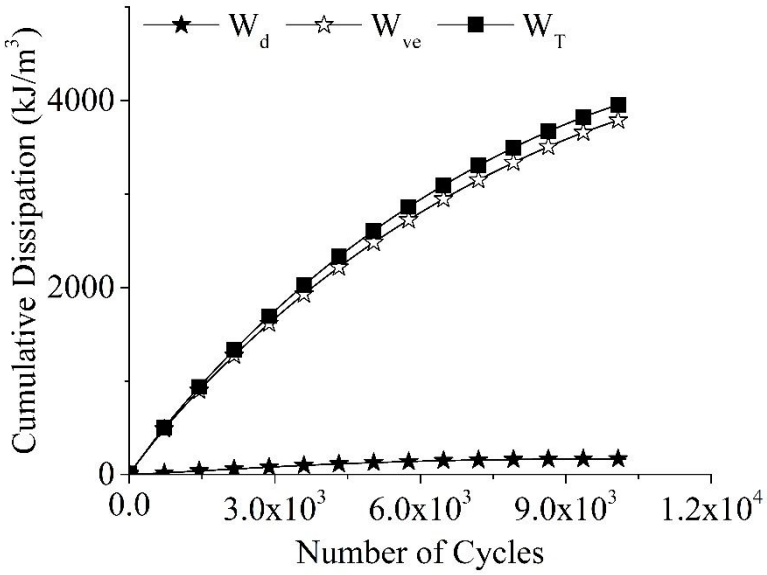

Fig. C.17: Cumulative viscoelastic, and damage dissipation based on pseudo-strain approach for VG30-WMA-MC at 600 microstrain

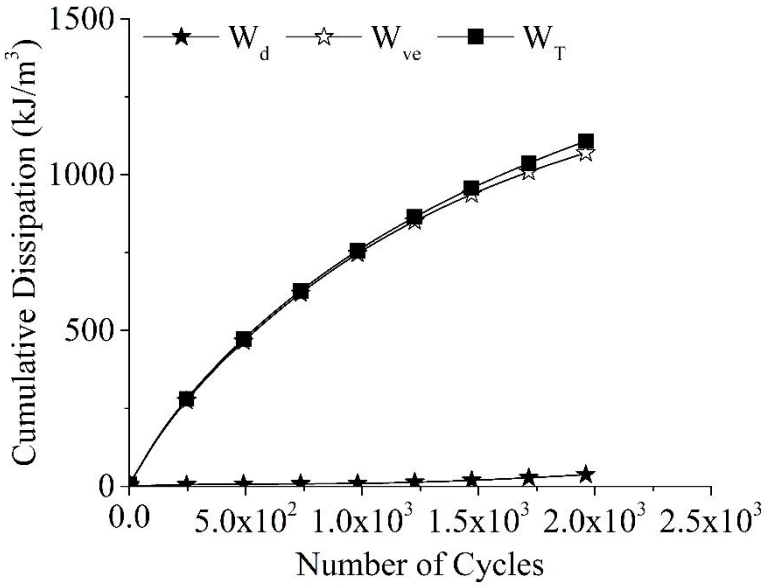

Fig. C.18: Cumulative viscoelastic, and damage dissipation based on pseudo-strain approach for VG30-WMA-MC at 800 microstrain

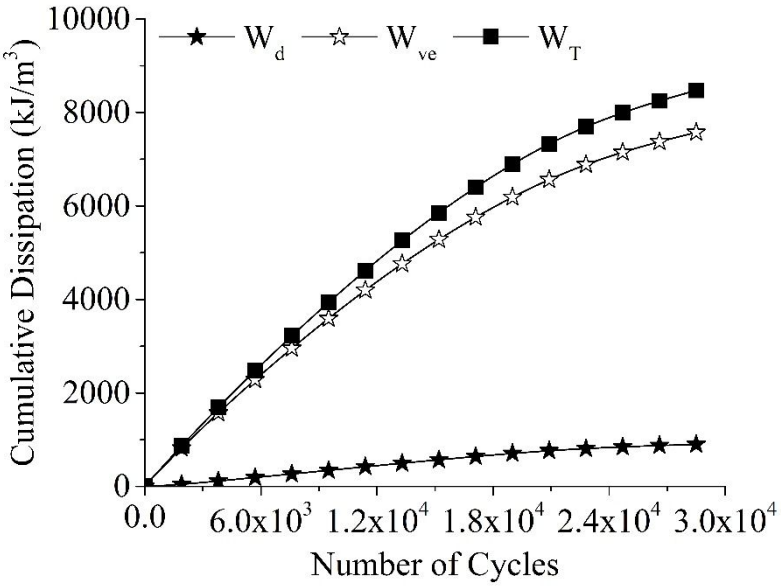

Fig. C.19: Cumulative viscoelastic, and damage dissipation based on pseudo-strain approach for VG30-L-MC at 400 microstrain

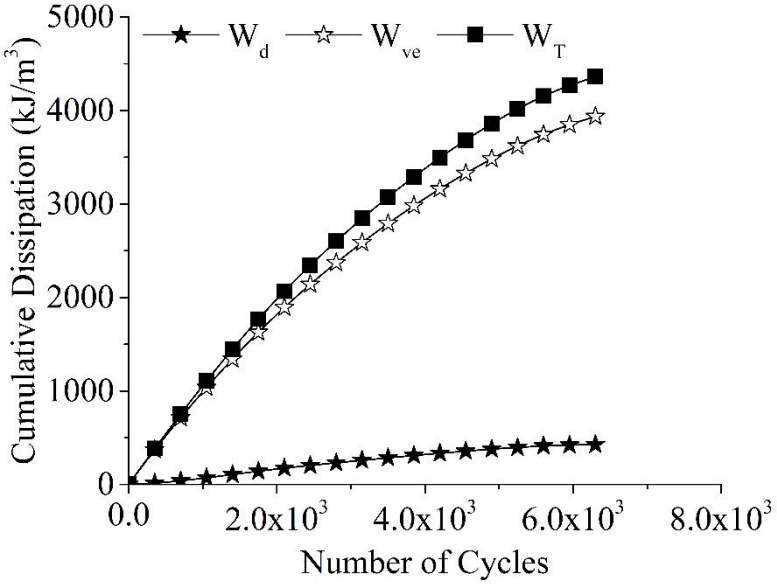

Fig. C.20: Cumulative viscoelastic, and damage dissipation based on pseudo-strain approach for VG30-L-MC at 600 microstrain

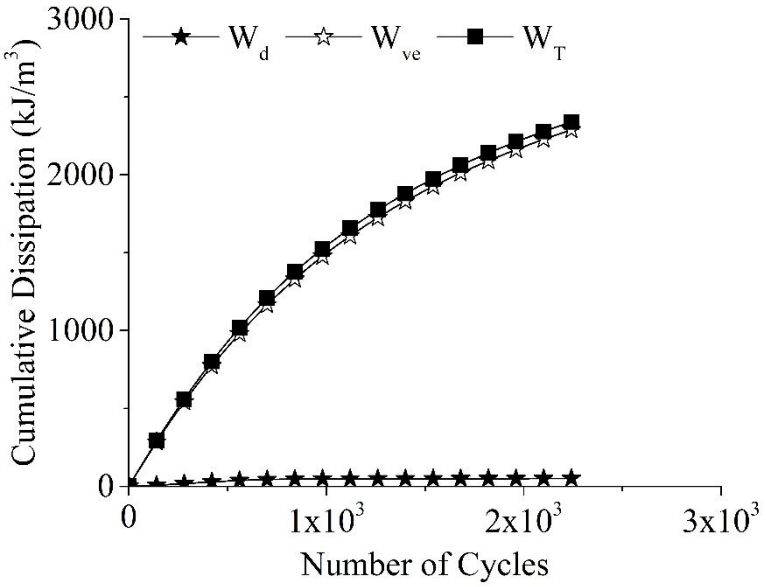

Fig. C.21: Cumulative viscoelastic, and damage dissipation based on pseudo-strain approach for VG30-L-MC at 800 microstrain

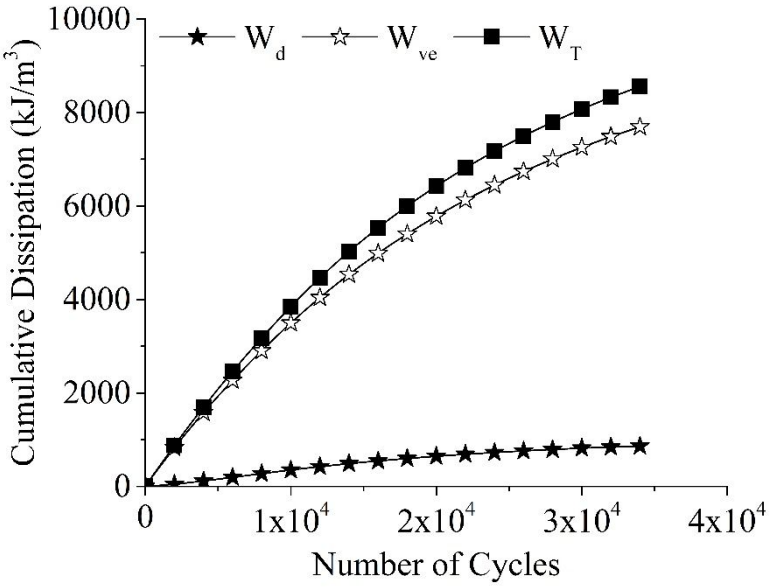

Fig. C.22: Cumulative viscoelastic, and damage dissipation based on pseudo-strain approach for VG30-WMA-L-MC at 400 microstrain

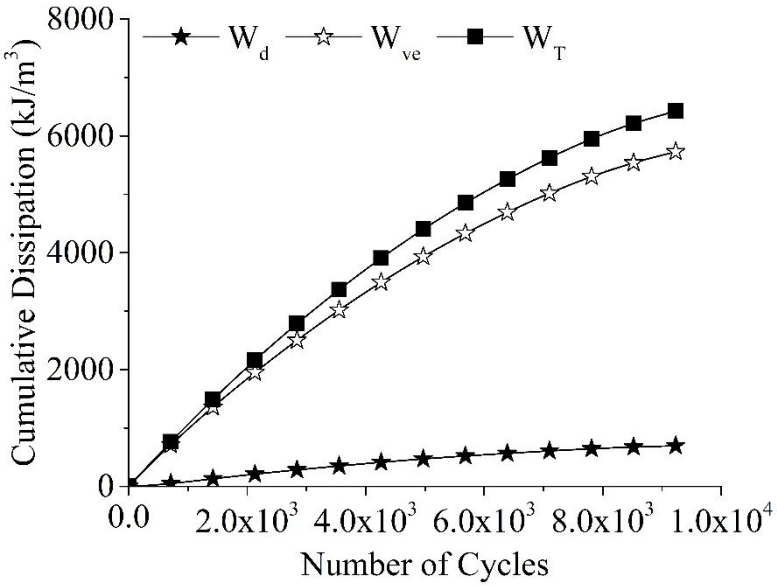

Fig. C.23: Cumulative viscoelastic, and damage dissipation based on pseudo-strain approach for VG30-WMA-L-MC at 600 microstrain

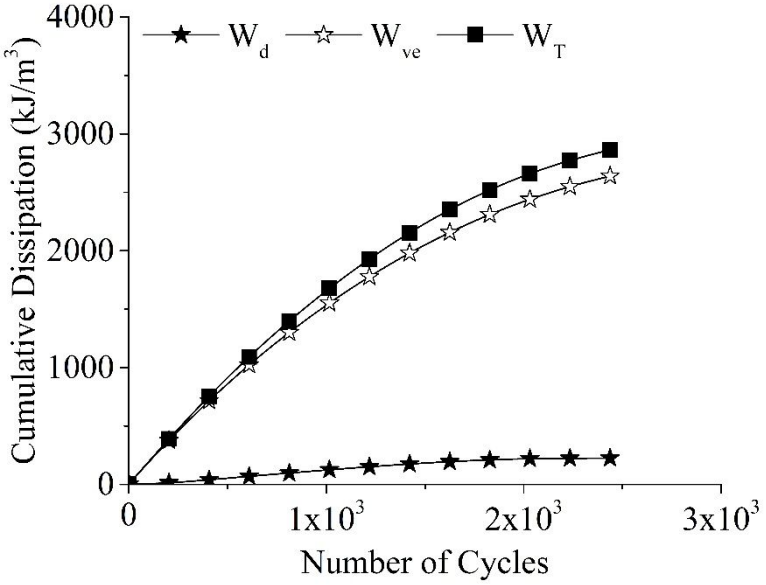

Fig. C.24: Cumulative viscoelastic, and damage dissipation based on pseudo-strain approach for VG30-WMA-L-MC at 800 microstrain

C.2. Cummulative Dissipation – Approach 2

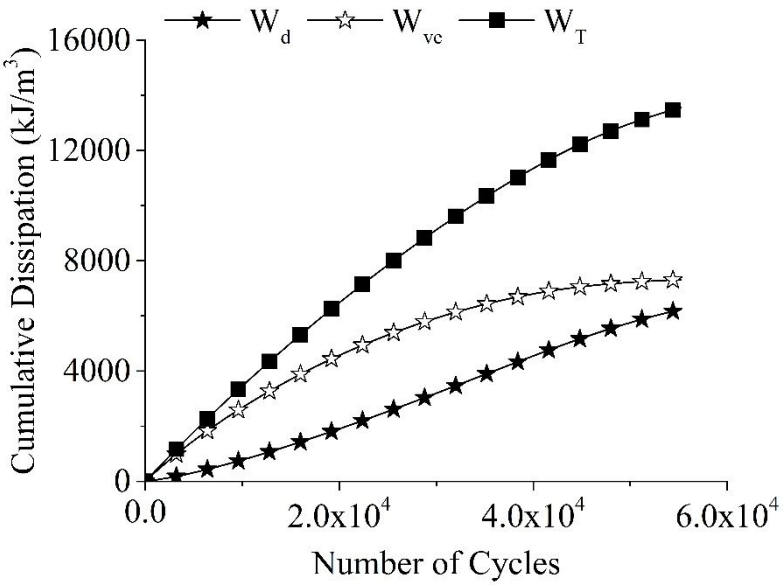

Fig. C.25: Cumulative viscoelastic, and damage dissipation using the methodology proposed by Varma et al. 2019 for VG30 at 400 microstrain

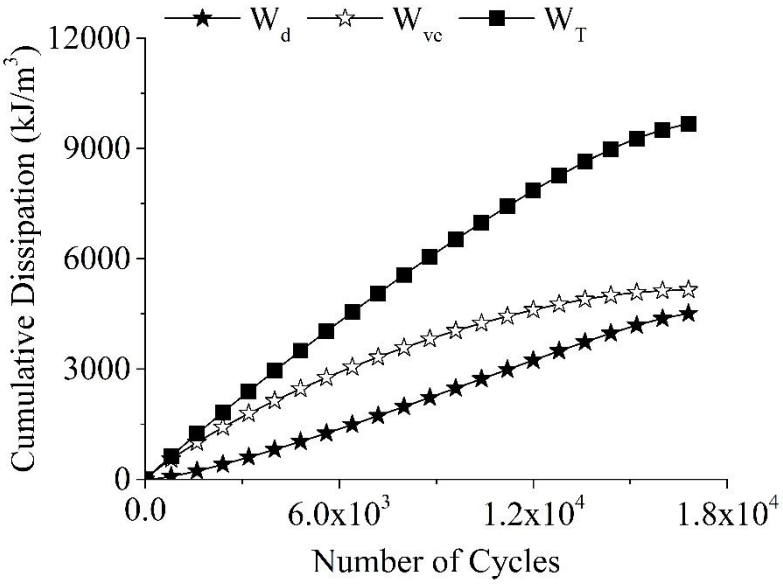

Fig. C.26: Cumulative viscoelastic, and damage dissipation using the methodology proposed by Varma et al. 2019 for VG30 at 600 microstrain

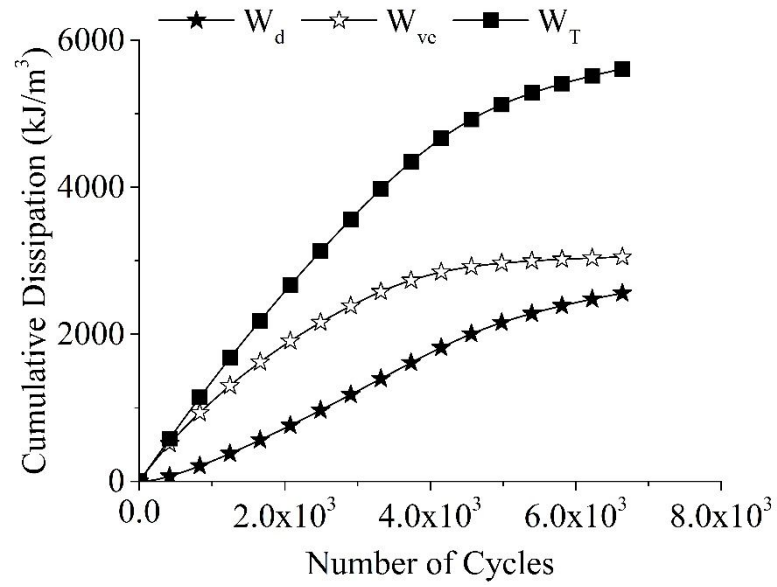

Fig. C.27: Cumulative viscoelastic, and damage dissipation using the methodology proposed by Varma et al. 2019 for VG30 at 800 microstrain

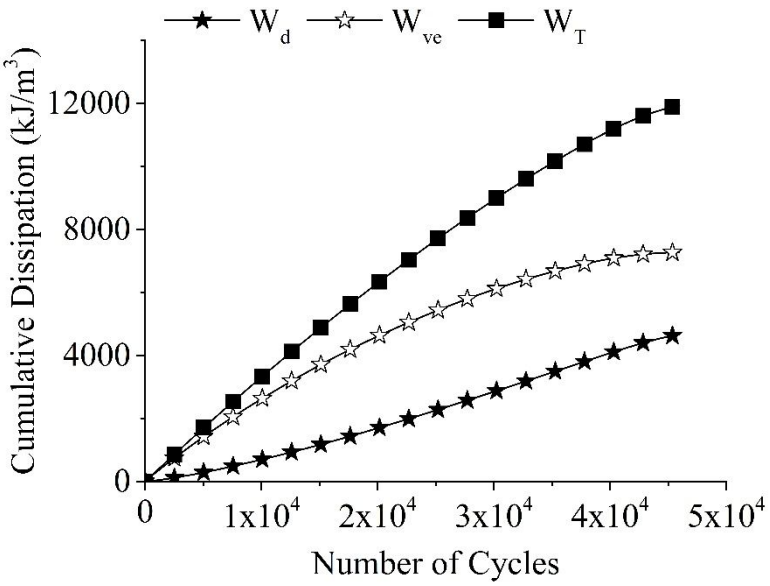

Fig. C.28: Cumulative viscoelastic, and damage dissipation using the methodology proposed by Varma et al. 2019 for VG30-WMA at 400 microstrain

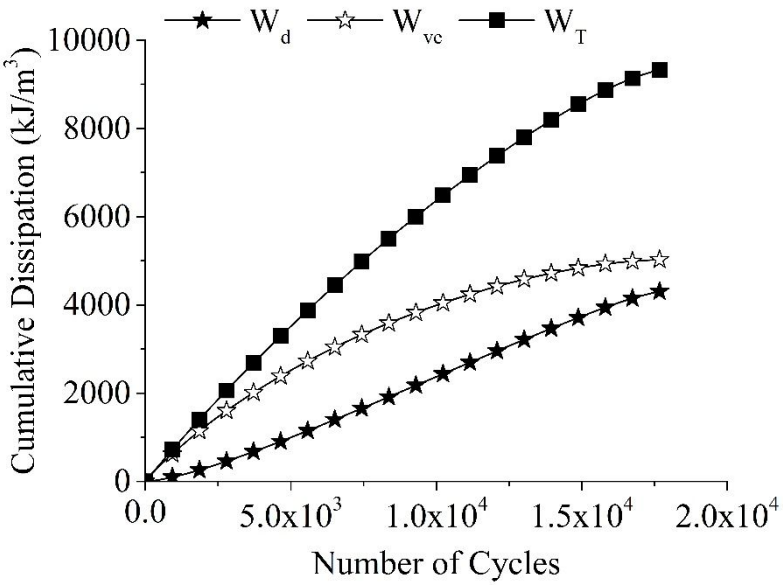

Fig. C.29: Cumulative viscoelastic, and damage dissipation using the methodology proposed by Varma et al. 2019 for VG30-WMA at 600 microstrain

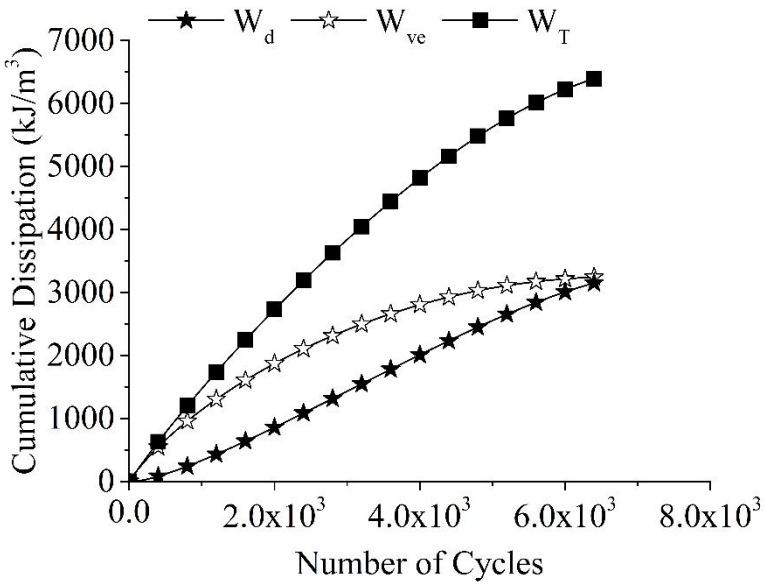

Fig. C.30: Cumulative viscoelastic, and damage dissipation using the methodology proposed by Varma et al. 2019 for VG30-WMA at 800 microstrain

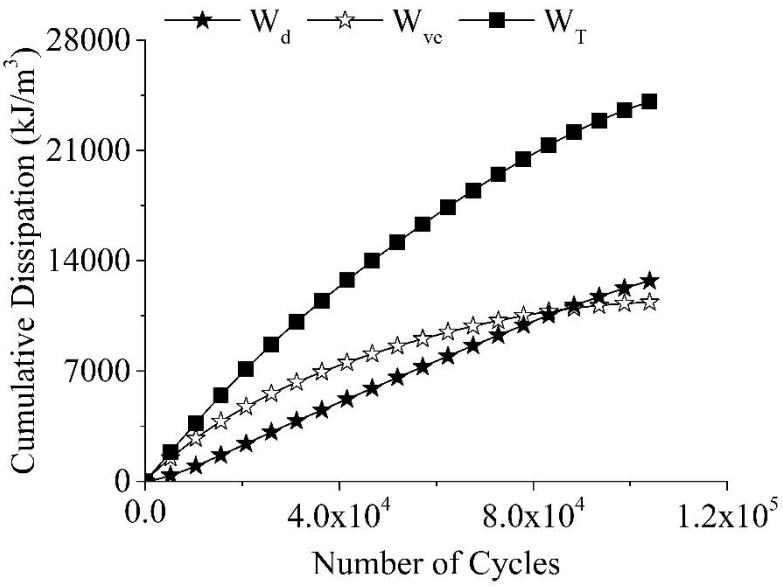

Fig. C.31: Cumulative viscoelastic, and damage dissipation using the methodology proposed by Varma et al. 2019 for VG30-L at 400 microstrain

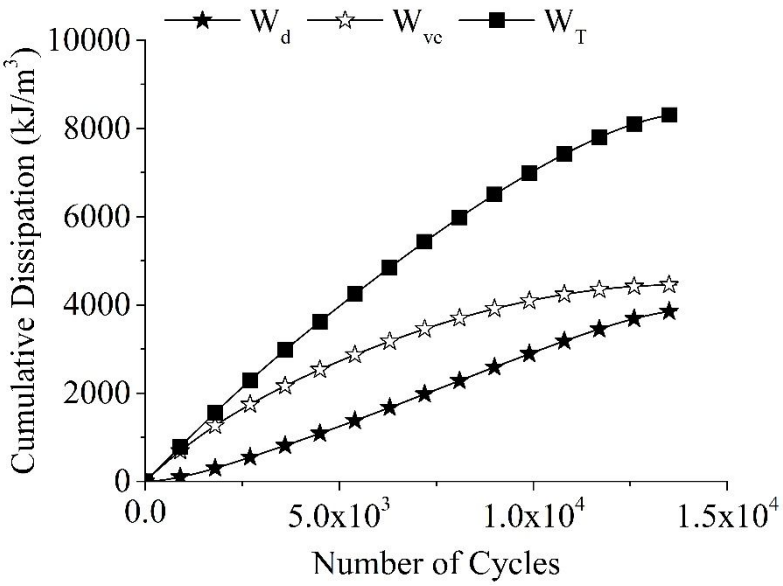

Fig. C.32: Cumulative viscoelastic, and damage dissipation using the methodology proposed by Varma et al. 2019 for VG30-L at 600 microstrain

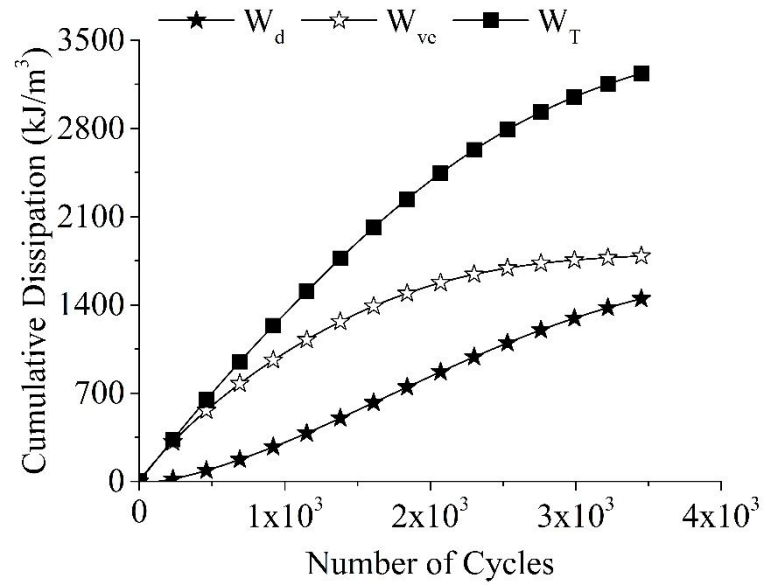

Fig. C.33: Cumulative viscoelastic, and damage dissipation using the methodology proposed by Varma et al. 2019 for VG30-L at 800 microstrain

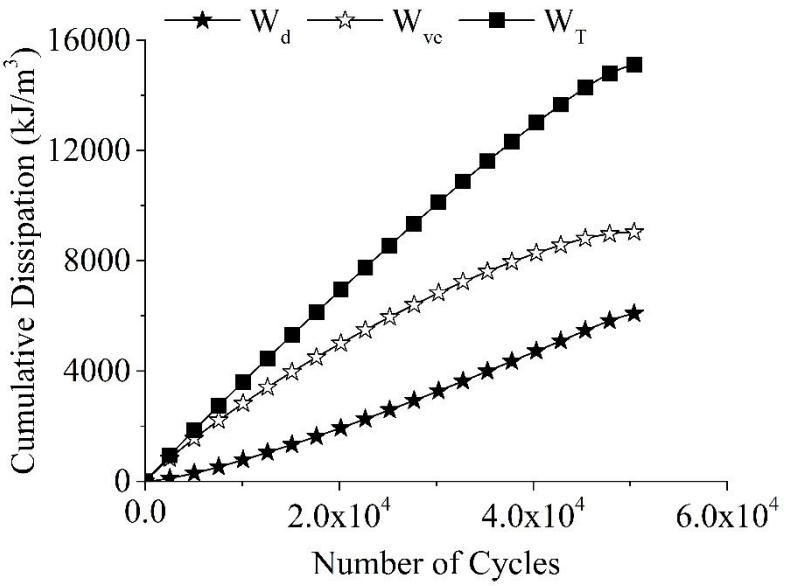

Fig. C.34: Cumulative viscoelastic, and damage dissipation using the methodology proposed by Varma et al. 2019 for VG30-WMA-L at 400 microstrain

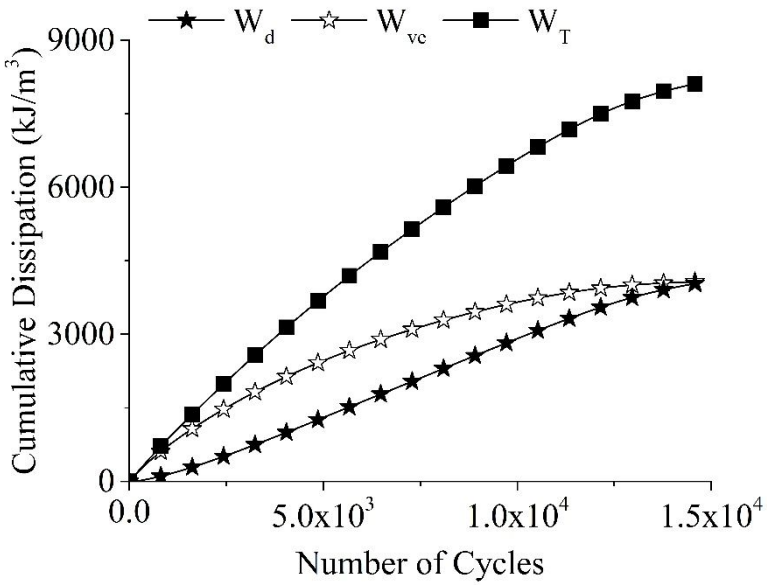

Fig. C.35: Cumulative viscoelastic, and damage dissipation using the methodology proposed by Varma et al. 2019 for VG30-WMA-L at 600 microstrain

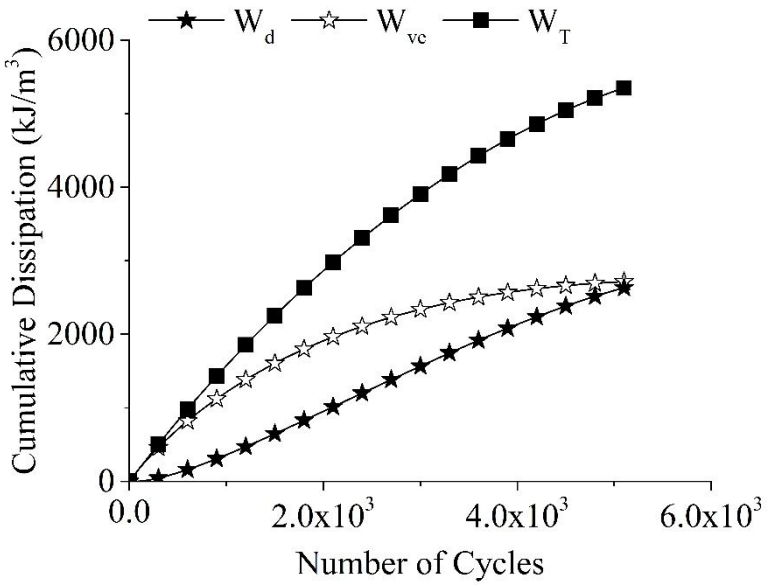

Fig. C.36: Cumulative viscoelastic, and damage dissipation using the methodology proposed by Varma et al. 2019 for VG30-WMA-L at 800 microstrain

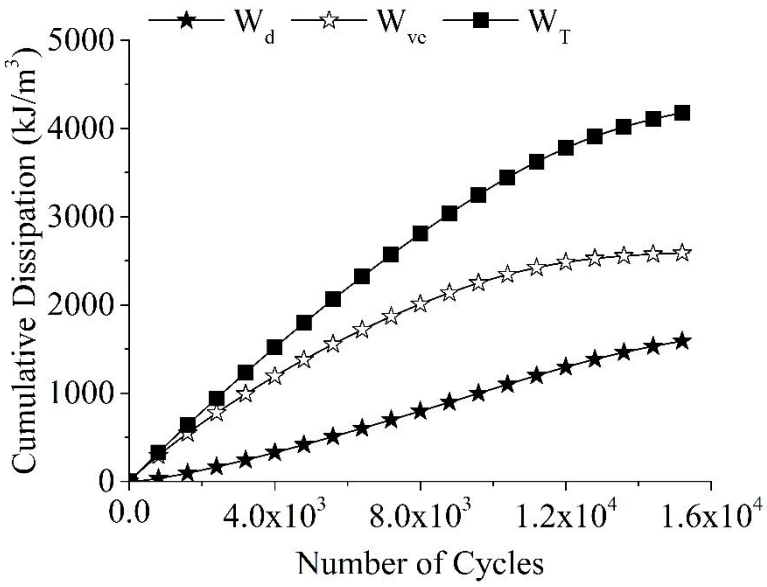

Fig. C.37: Cumulative viscoelastic, and damage dissipation using the methodology proposed by Varma et al. 2019 for VG30-MC at 400 microstrain

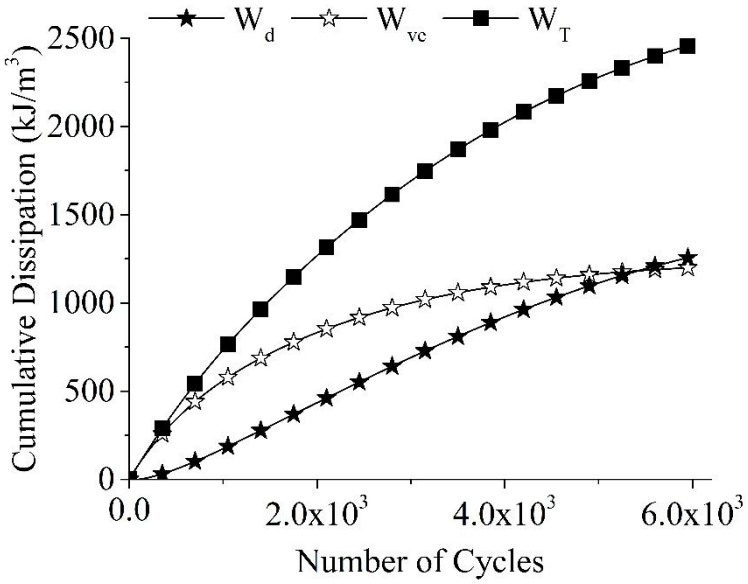

Fig. C.38: Cumulative viscoelastic, and damage dissipation using the methodology proposed by Varma et al. 2019 for VG30-MC at 600 microstrain

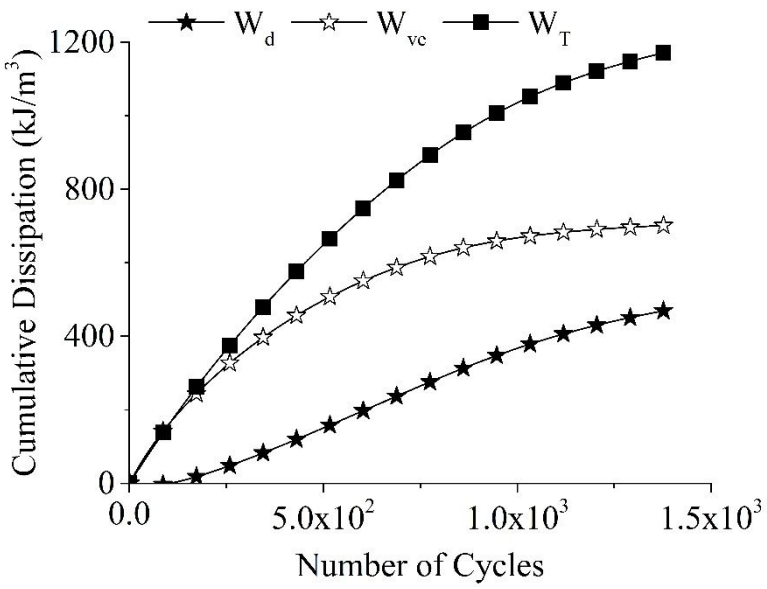

Fig. C.39: Cumulative viscoelastic, and damage dissipation using the methodology proposed by Varma et al. 2019 for VG30-MC at 800 microstrain

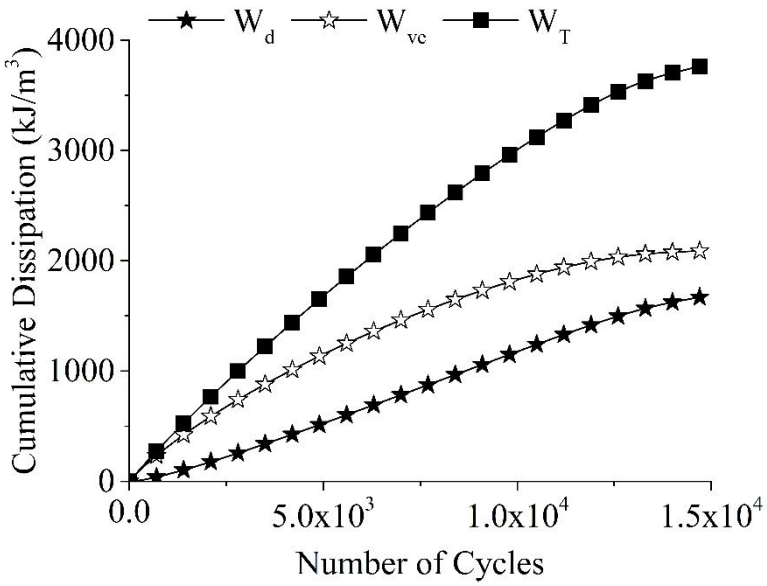

Fig. C.40: Cumulative viscoelastic, and damage dissipation using the methodology proposed by Varma et al. 2019 for VG30-WMA-MC at 400 microstrain

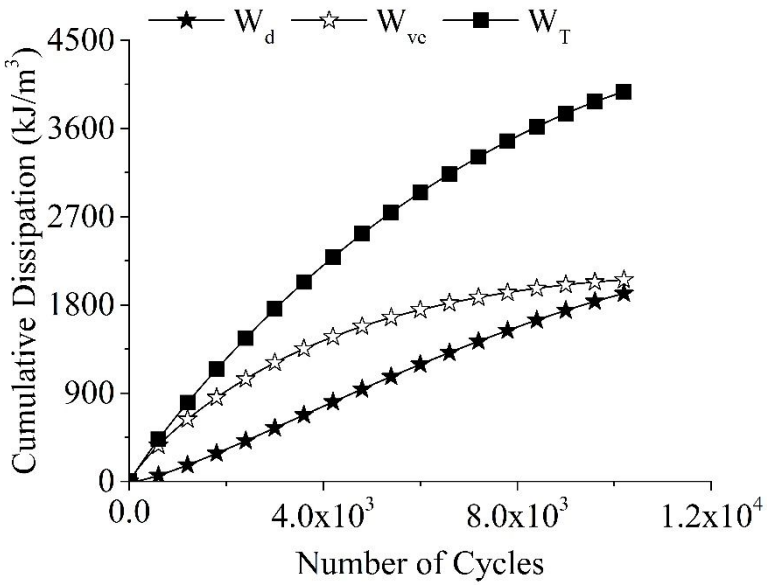

Fig. C.41: Cumulative viscoelastic, and damage dissipation using the methodology proposed by Varma et al. 2019 for VG30-WMA-MC at 600 microstrain

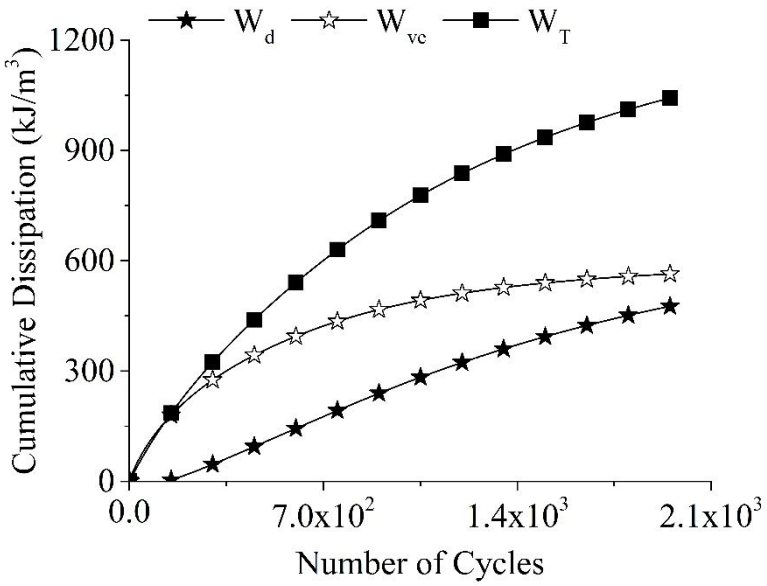

Fig. C.42: Cumulative viscoelastic, and damage dissipation using the methodology proposed by Varma et al. 2019 for VG30-WMA-MC at 800 microstrain

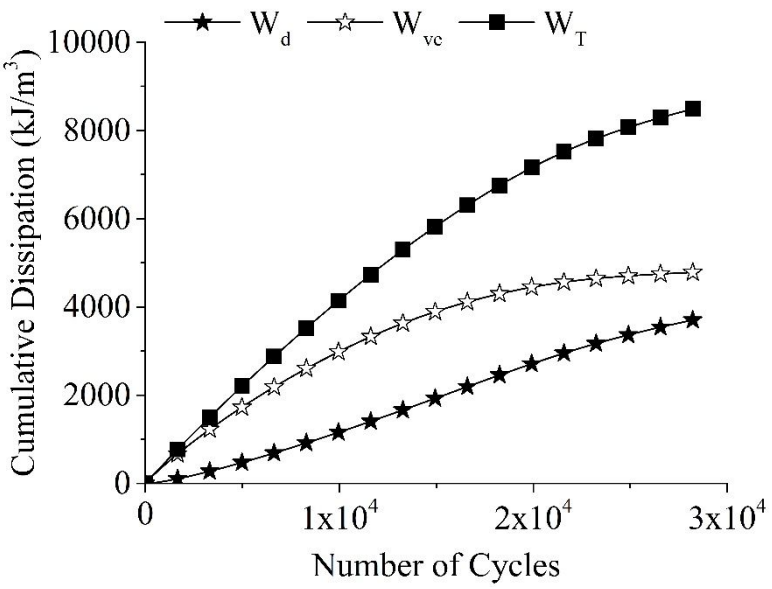

Fig. C.43: Cumulative viscoelastic, and damage dissipation using the methodology proposed by Varma et al. 2019 for VG30-L-MC at 400 microstrain

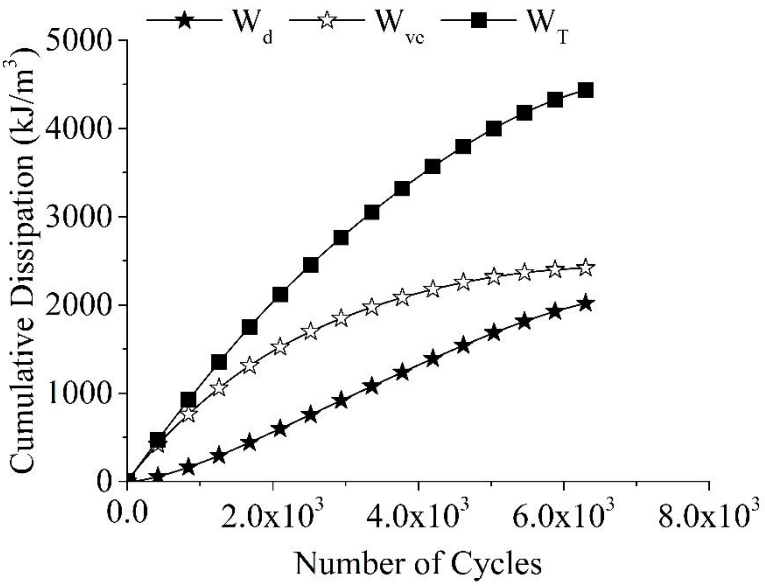

Fig. C.44: Cumulative viscoelastic, and damage dissipation using the methodology proposed by Varma et al. 2019 for VG30-L-MC at 600 microstrain

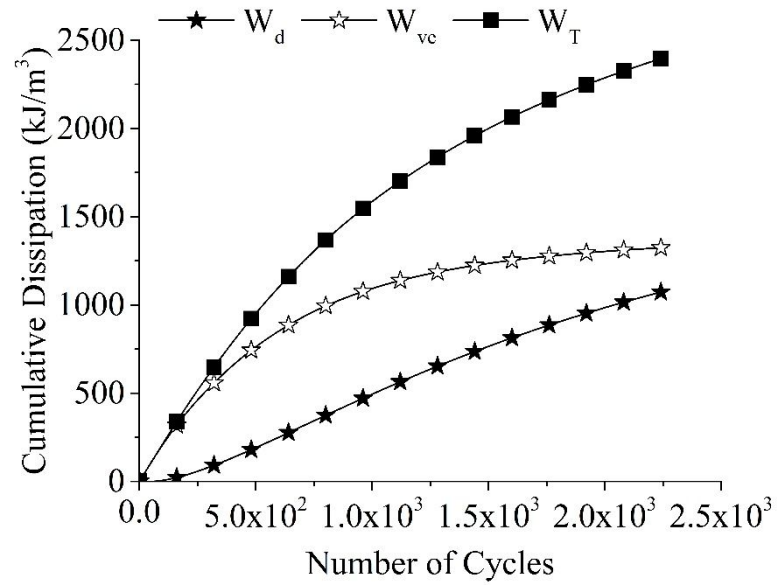

Fig. C.45: Cumulative viscoelastic, and damage dissipation using the methodology proposed by Varma et al. 2019 for VG30-L-MC at 800 microstrain

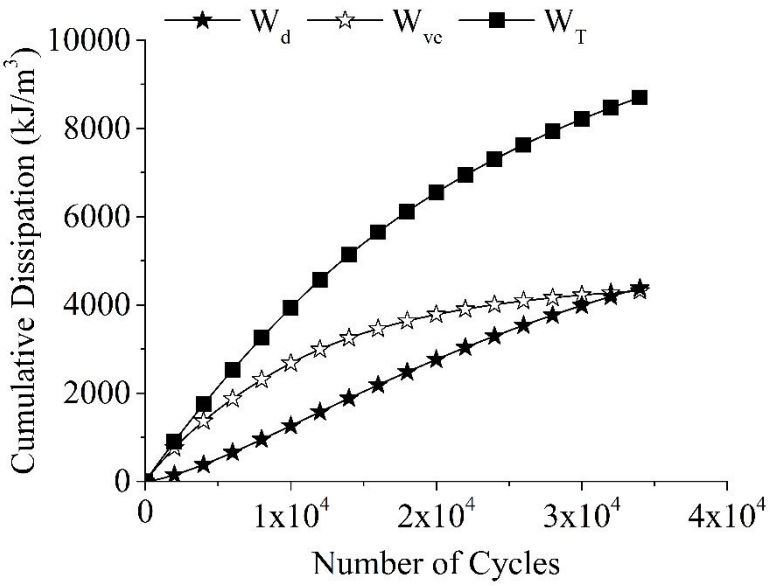

Fig. C.46: Cumulative viscoelastic, and damage dissipation using the methodology proposed by Varma et al. 2019 for VG30-WMA-L-MC at 400 microstrain

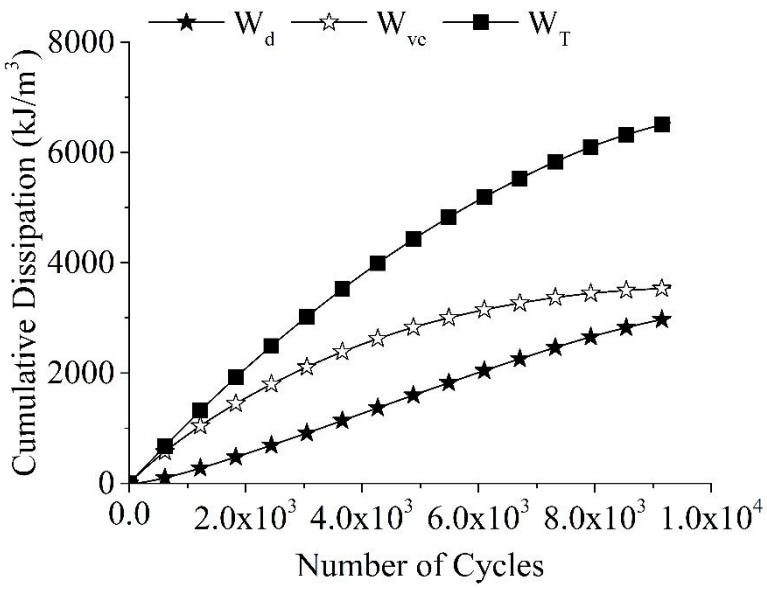

Fig. C.47: Cumulative viscoelastic, and damage dissipation using the methodology proposed by Varma et al. 2019 for VG30-WMA-L-MC at 600 microstrain

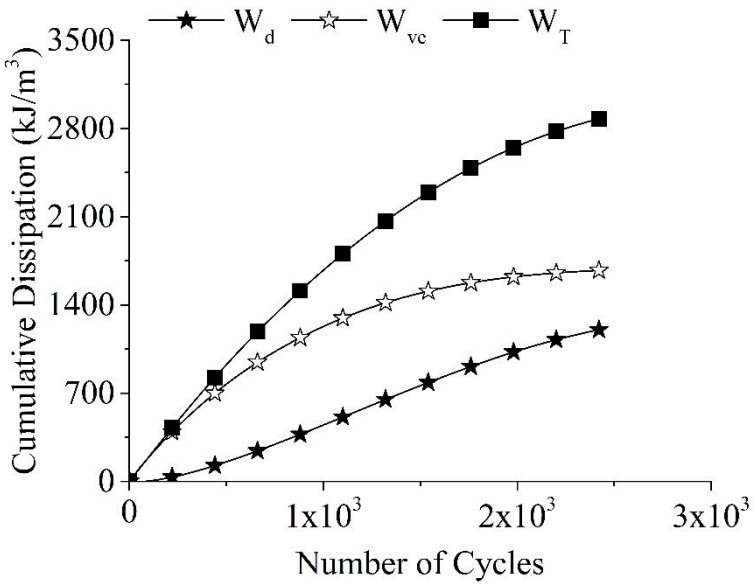

Fig. C.48: Cumulative viscoelastic, and damage dissipation using the methodology proposed by Varma et al. 2019 for VG30-WMA-L-MC at 800 microstrain

C.3. Viscoelastic Dissipation - Approach 3

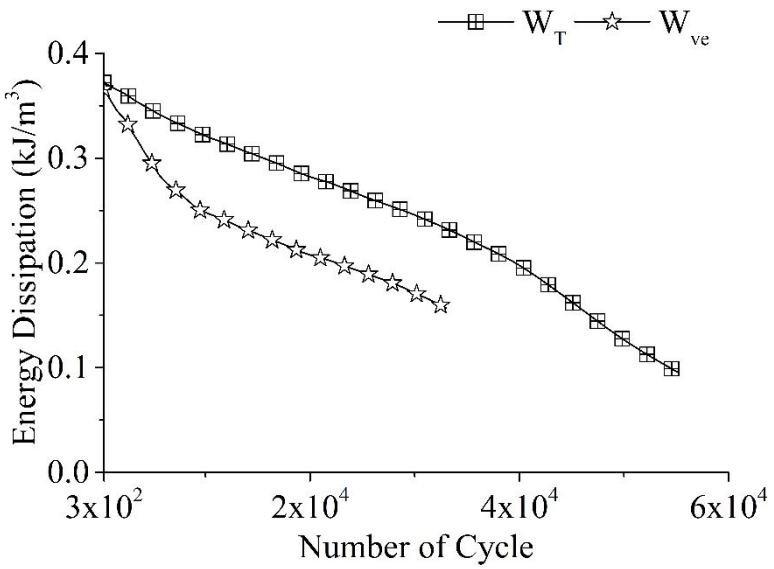

Fig. C.49: Evolution of W_T and W_{ve} calculated following Varma et al. 2017 for VG30 at 400 microstrain

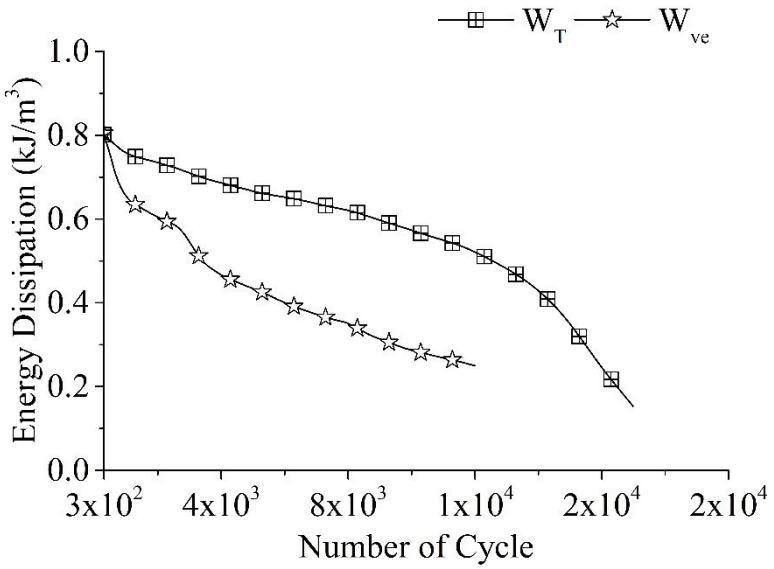

Fig. C.50: Evolution of W_T and W_{ve} calculated following Varma et al. 2017 for VG30 at 600 microstrain

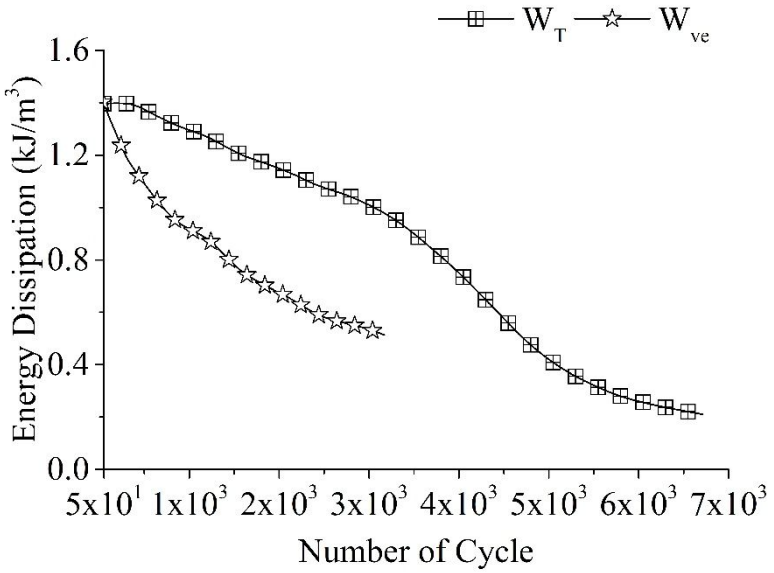

Fig. C.51: Evolution of W_T and W_{ve} calculated following Varma et al. 2017 for VG30 at 800 microstrain

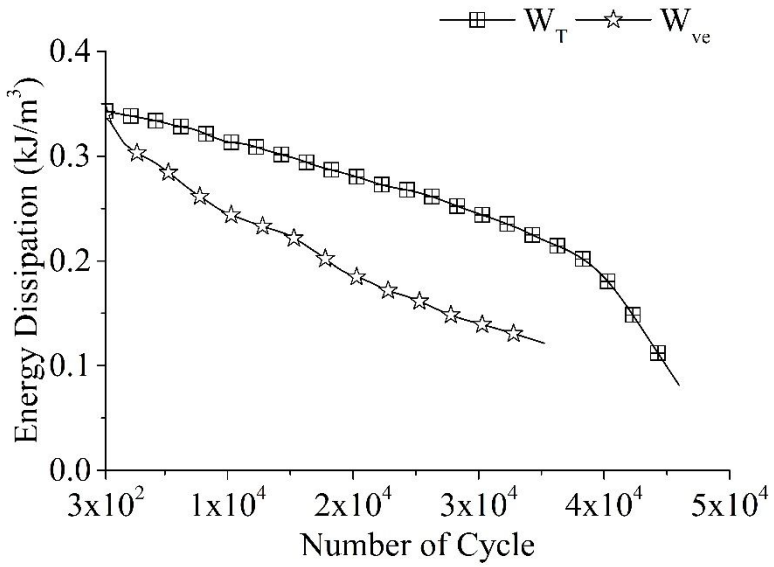

Fig. C.52: Evolution of W_T and W_{ve} calculated following Varma et al. 2017 for VG30-WMA at 400 microstrain

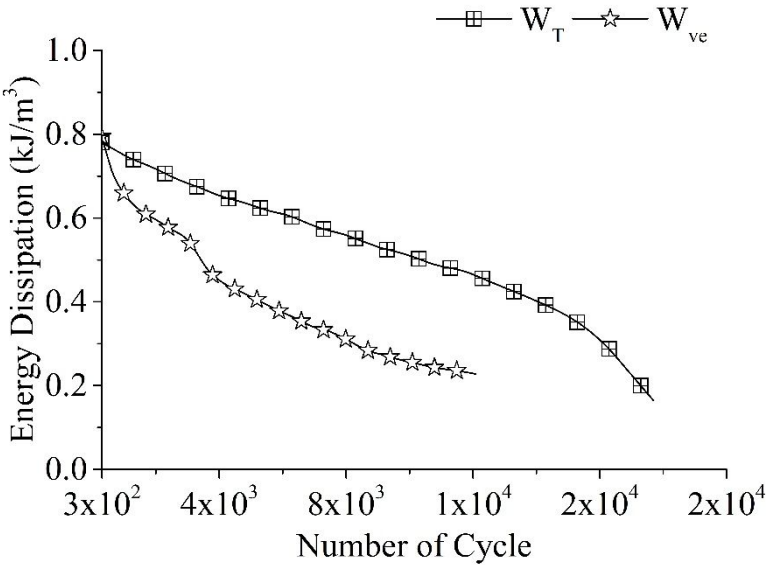

Fig. C.53: Evolution of W_T and W_{ve} calculated following Varma et al. 2017 for VG30-WMA at 600 microstrain

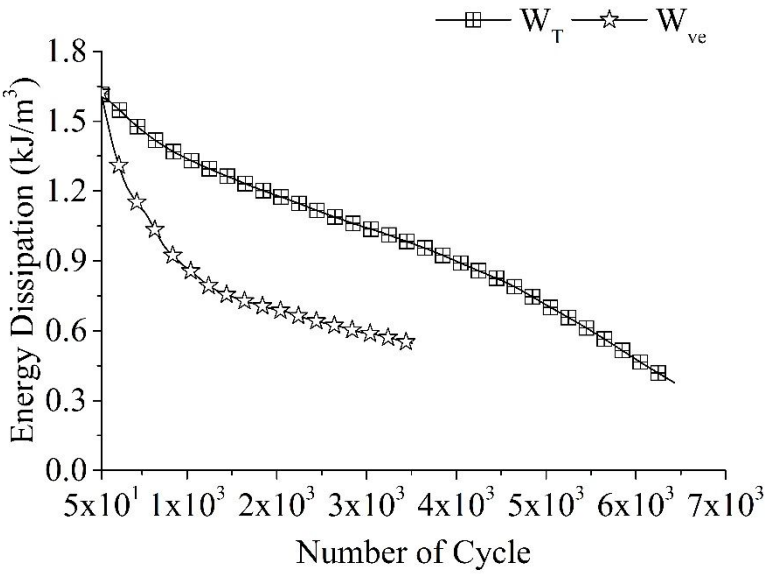

Fig. C.54: Evolution of W_T and W_{ve} calculated following Varma et al. 2017 for VG30-WMA at 800 microstrain

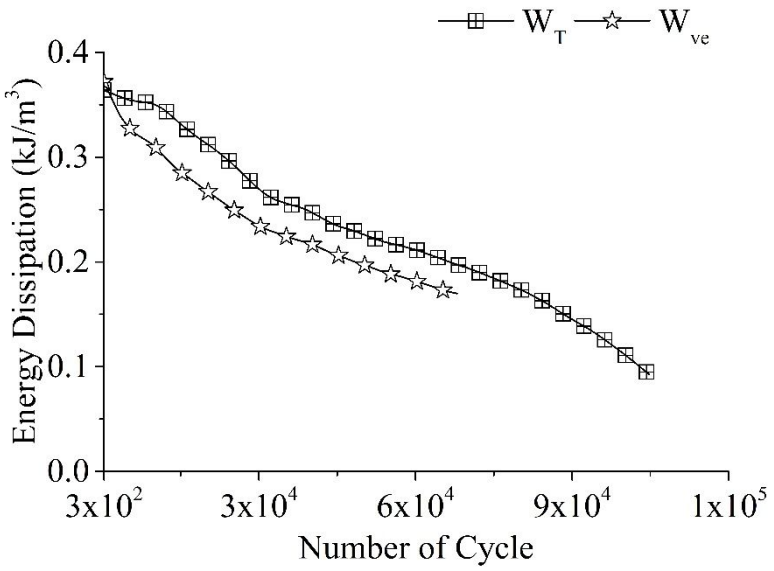

Fig. C.55: Evolution of W_T and W_{ve} calculated following Varma et al. 2017 for VG30-L at 400 microstrain

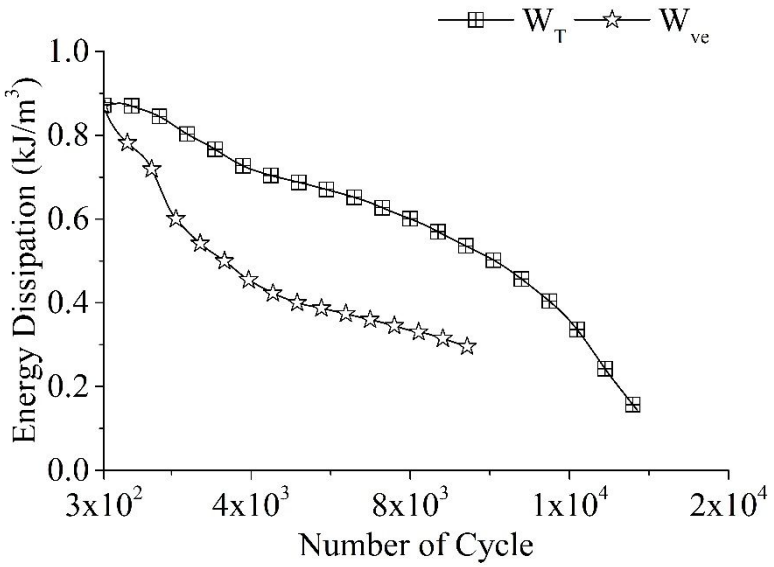

Fig. C.56: Evolution of W_T and W_{ve} calculated following Varma et al. 2017 for VG30-L at 600 microstrain

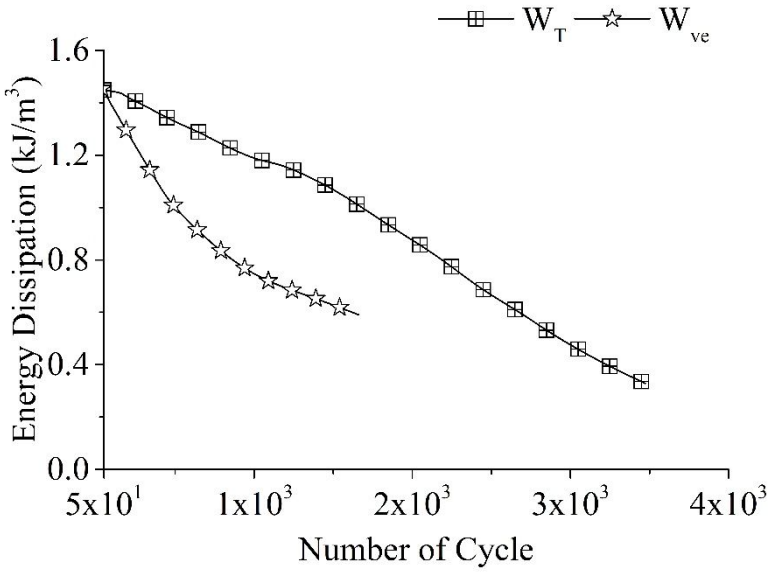

Fig. C.57: Evolution of W_T and W_{ve} calculated following Varma et al. 2017 for VG30-L at 800 microstrain

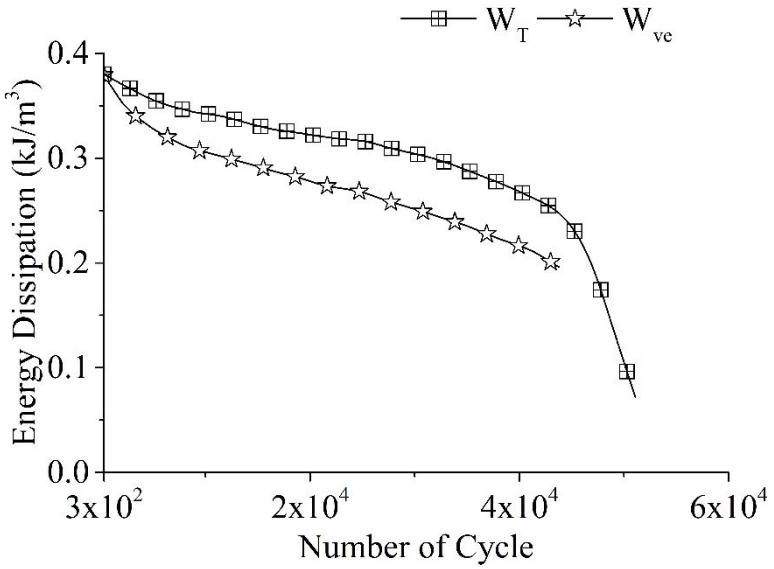

Fig. C.58: Evolution of W_T and W_{ve} calculated following Varma et al. 2017 for VG30-WMA-L at 400 microstrain

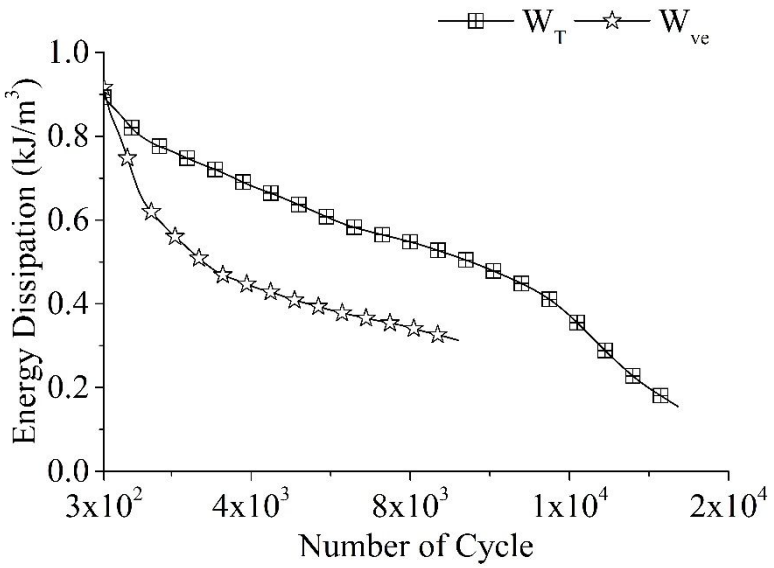

Fig. C.59: Evolution of W_T and W_{ve} calculated following Varma et al. 2017 for VG30-WMA-L at 600 microstrain

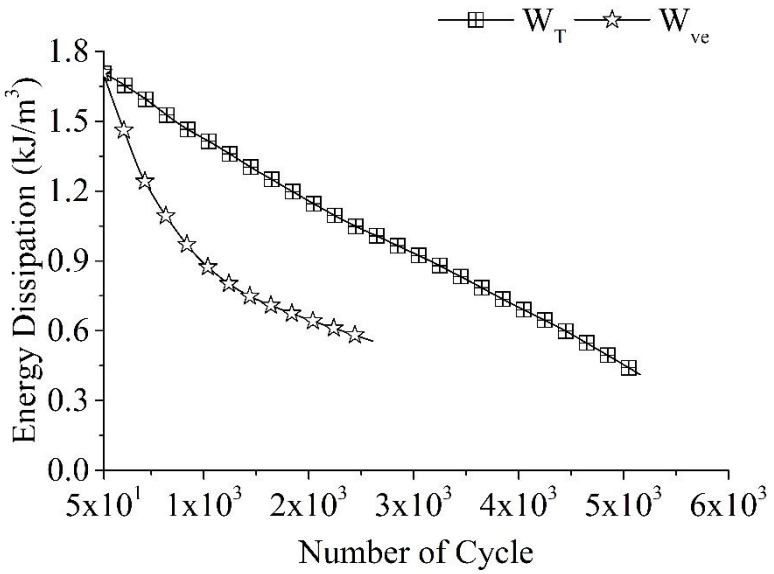

Fig. C.60: Evolution of W_T and W_{ve} calculated following Varma et al. 2017 for VG30-WMA-L at 800 microstrain

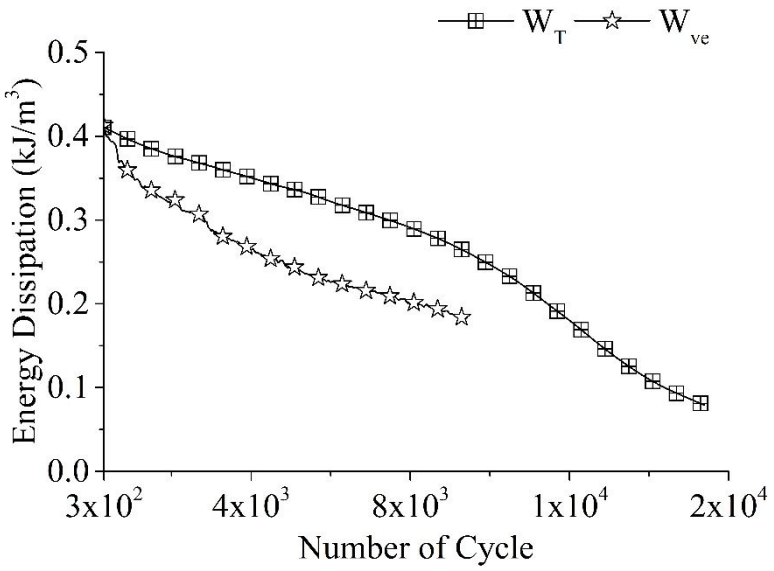

Fig. C.61: Evolution of W_T and W_{ve} calculated following Varma et al. 2017 for VG30-MC at 400 microstrain

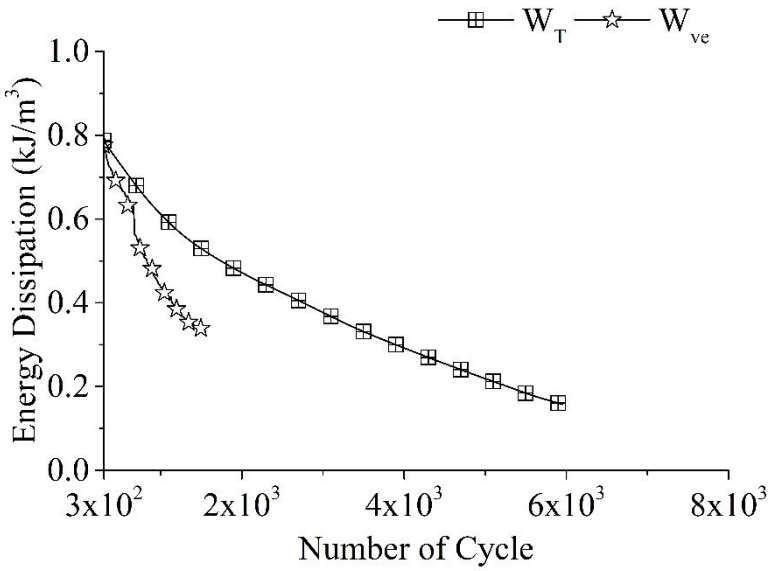

Fig. C.62: Evolution of W_T and W_{ve} calculated following Varma et al. 2017 for VG30-MC at 600 microstrain

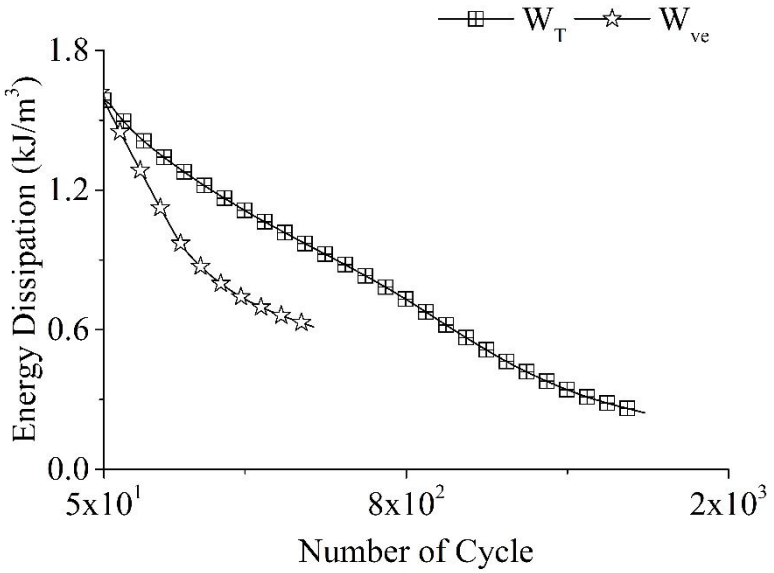

Fig. C.63: Evolution of W_T and W_{ve} calculated following Varma et al. 2017 for VG30-MC at 800 microstrain

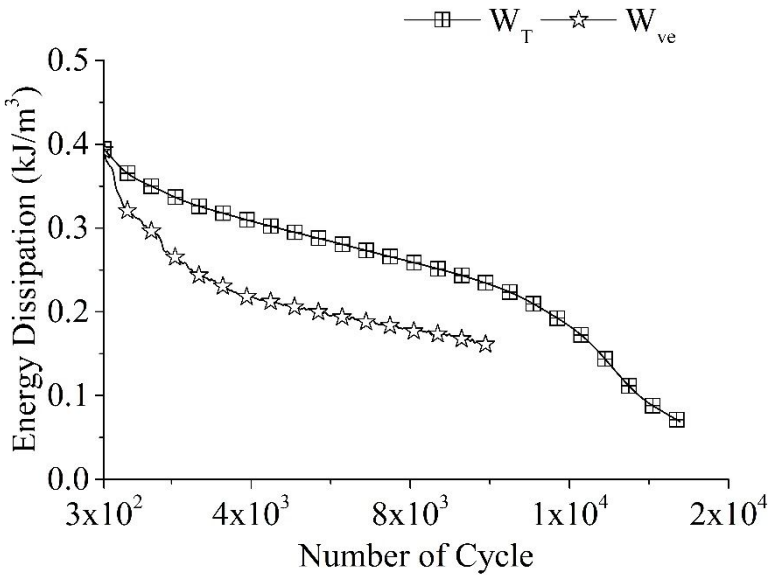

Fig. C.64: Evolution of W_T and W_{ve} calculated following Varma et al. 2017 for VG30-WMA-MC at 400 microstrain

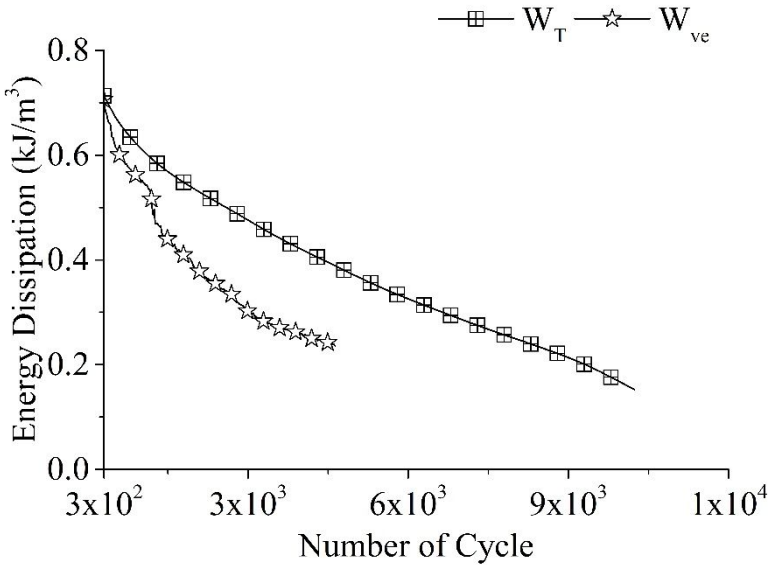

Fig. C.65: Evolution of W_T and W_{ve} calculated following Varma et al. 2017 for VG30-WMA-MC at 600 microstrain

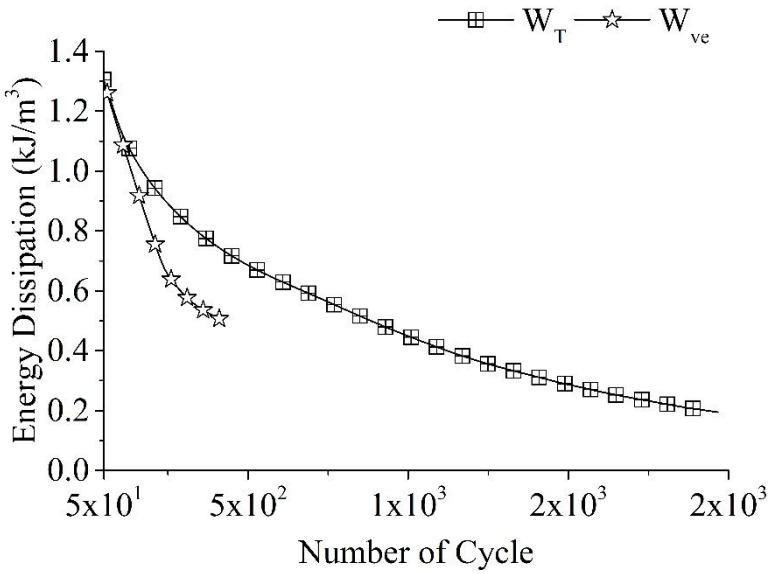

Fig. C.66: Evolution of W_T and W_{ve} calculated following Varma et al. 2017 for VG30-WMA-MC at 800 microstrain

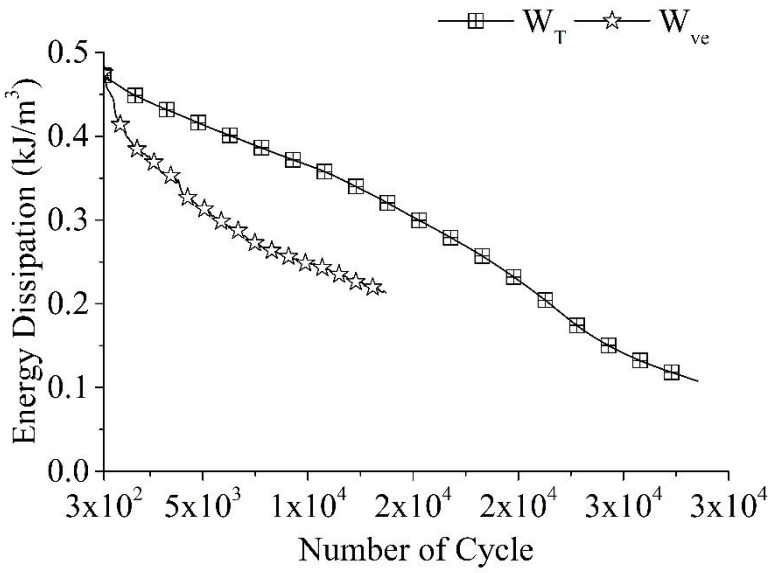

Fig. C.67: Evolution of W_T and W_{ve} calculated following Varma et al. 2017 for VG30-L-MC at 400 microstrain

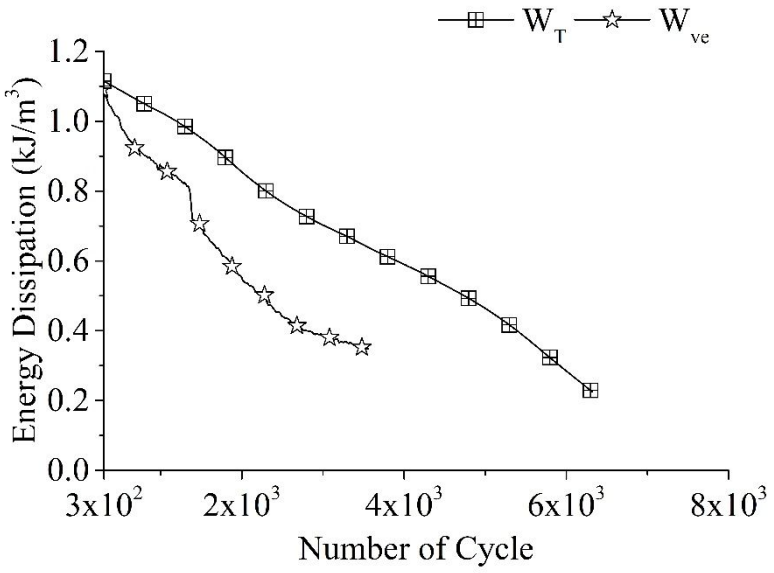

Fig. C.68: Evolution of W_T and W_{ve} calculated following Varma et al. 2017 for VG30-L-MC at 600 microstrain

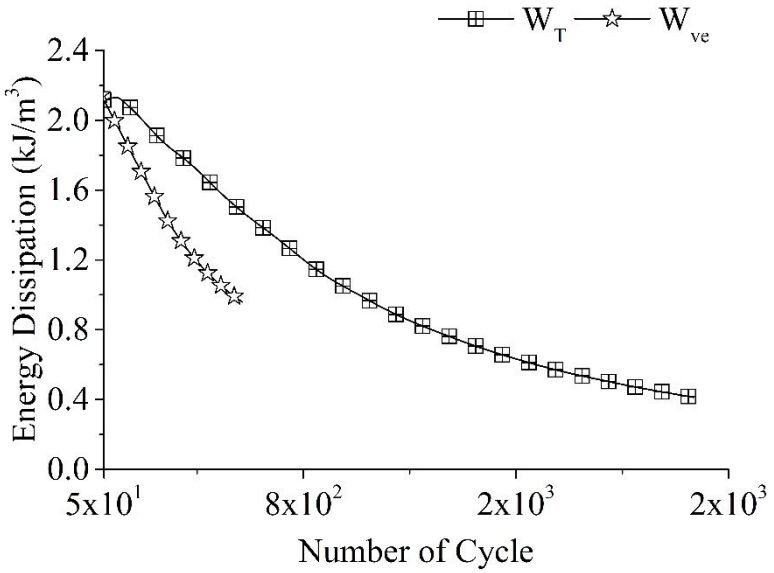

Fig. C.69: Evolution of W_T and W_{ve} calculated following Varma et al. 2017 for VG30-L-MC at 800 microstrain

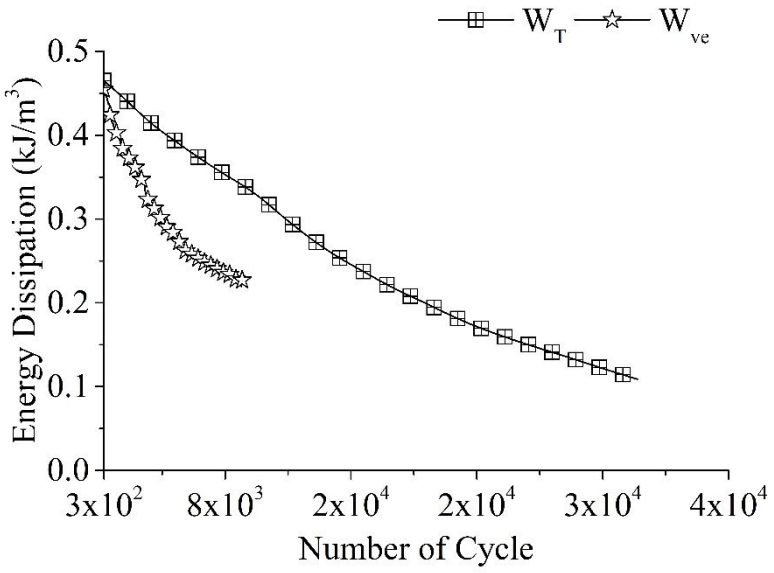

Fig. C.70: Evolution of W_T and W_{ve} calculated following Varma et al. 2017 for VG30-WMA-L-MC at 400 microstrain

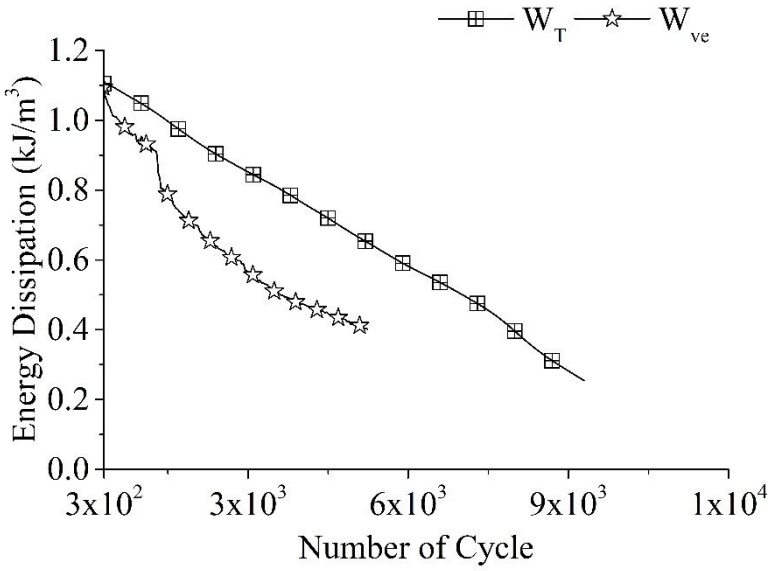

Fig. C.71: Evolution of W_T and W_{ve} calculated following Varma et al. 2017 for VG30-WMA-L-MC at 600 microstrain

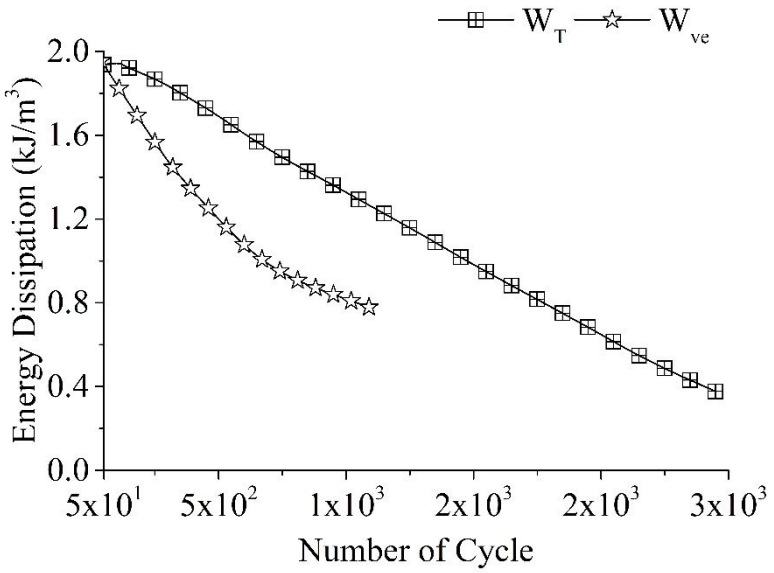

Fig. C.72: Evolution of W_T and W_{ve} calculated following Varma et al. 2017 for VG30-WMA-L-MC at 800 microstrain

REFERENCES

1. **AASHTO, M303**. (2014). "Standard specification for lime for asphalt mixtures." *American Association of State Highway and Transportation Officials*, Washington, D.C., USA.
2. **AASHTO, R30**. (2015). "Standard practice for mixture conditioning of hot mix asphalt." *American Association of State Highway and Transportation Officials*, Washington, D.C., USA.
3. **AASHTO, T219**. (2013). "Standard method of test for testing lime for chemical constituents and particle sizes." *American Association of State Highway and Transportation Officials*, Washington, D.C., USA.
4. **AASHTO, T283**. (2014). "Standard method of test for resistance of compacted asphalt mixtures to moisture-induced damage." *American Association of State Highway and Transportation Officials*, Washington, D.C., USA.
5. **AASHTO, T321**. (2014). "Method for determining the fatigue life of compacted hot-mix asphalt (HMA) subjected to repeated flexural bending." *American Association of State Highway and Transportation Officials*, Washington, D.C., USA.
6. **Ahmad, M., Mannan, U. A., Islam, M. R.,** and **Tarefder, R. A**. (2018). "Chemical and mechanical changes in asphalt binder due to moisture conditioning." *Road Materials and Pavement Design*, *19*(5), 1216-1229.
7. **Airey, G. D.,** and **Choi, Y. K**. (2002). "State of the art report on moisture sensitivity test methods for bituminous pavement materials." *Road Materials and Pavement Design*, 3(4), 355-372. https://doi.org/10.1080/14680629.2002.9689930
8. **Airey, G. D., Collop, A. C., Zoorob, S. E.,** and **Elliott, R. C**. (2008). "The influence of aggregate, filler and bitumen on asphalt mixture moisture damage." *Construction and building materials.*, 22(9), 2015-2024.
9. **Alatas, T.,** and **Ethem, M.K**. (2013). "The effects of using styrene-butadiene-styrene and fly ash together on the resistance to moisture-induced damage, permanent deformation and fatigue of hot mixture asphalt." *KSCE Journal of Civil Engineering,* 17(5), 1030-1039.
10. **Alavi, M., Hajj, E., Hanz, A.** and **Bahia, H**. (2013). "Evaluating Adhesion Properties and Moisture Damage Susceptibility of Warm-Mix Asphalts: Bitumen Bond Strength and Dynamic Modulus Ratio Tests." *Transportation Research Record: Journal of the Transportation Research Board*, 2295, 44-53.

11. **Al-Khateeb, G.,** and **Shenoy, A**. (2011). "A simple quantitative method for identification of failure due to fatigue damage." *International Journal of Damage Mechanics*, *20*, 3–21. https://doi.org/10.1177/1056789509343084.
12. **Amelian, S., Abtahi, S. M.,** and **Hejazi, S. M**. (2014). "Moisture susceptibility evaluation of asphalt mixes based on image analysis." *Construction and Building Materials*, *63*, 294-302.
13. **Apeagyei, A. K., Grenfell, J. R. A.,** and **Airey, G. D**. (2015). "Influence of aggregate absorption and diffusion properties on moisture damage in asphalt mixtures." *Road Materials and Pavement Design*, 16(sup1), 404-422. https://doi.org/10.1080/14680629.2015.1030827
14. **Arabani, M.,** and **Hamedi, Gh. H**. (2011). "Using the surface free energy method to evaluate the effects of polymeric aggregate treatment on moisture damage in hot-mix asphalt." *Journal of Materials in Civil Engineering*, 23(6), 802-811. https://doi.org/10.1061/(ASCE)MT.1943-5533.0000228
15. **Arambula, E., Caro, S.,** and **Masad, E**. (2010a). "Experimental measurement and numerical simulation of water vapor diffusion through asphalt pavement materials." *Journal of Materials in Civil Engineering*, 22(6), 588-598. https://doi.org/10.1061/(ASCE)MT.1943-5533.0000059
16. **Arambula, E., Garboczi, E. J., Masad, E.,** and **Kassem, E**. (2010b). "Numerical analysis of moisture vapor diffusion in asphalt mixtures using digital images." *Materials and Structures*, 43, 897-911. https://doi.org/10.1617/s11527-009-9554-3
17. **Arambula, E., Masad, E.,** and **Martin, A. E**. (2007). "Influence of air void distribution on the moisture susceptibility of asphalt mixes." *Journal of Materials in Civil Engineering*, 19(8), 655-664. https://doi.org/10.1061/(ASCE)0899-1561(2007)19:8(655)
18. **Asphalt Institute**. (2007). "Moisture sensitivity: Best practices to minimize moisture sensitivity in asphalt mixtures." *Asphalt Institute*, MS-24, Lexington, KY.
19. **Asphalt Institute**. (2014). "Mix Design Methods for Asphalt." *Asphalt Institute*, MS-02, Lexington, KY.
20. **ASTM D7981**. (2015). "Standard practice for compaction of prismatic asphalt specimens by means of the shear box compactor." *American Standard for Testing Materials*, West Conshohocken, PA, USA.
21. **ASTM, D4402**. (2015). "Standard test method for viscosity determination of asphalt at elevated temperatures using a rotational viscometer." *American Standard for Testing and Materials*, West Conshohocken, PA, USA.

22. **ASTM, D6857**. (2009). "Standard test method for maximum specific gravity and density of asphalt mixtures using automatic vacuum sealing method." *American Standard for Testing and Materials*, West Conshohocken, PA, USA.
23. **ASTM, D6931**. (2012). "Standard test method for indirect tensile strength of bituminous mixtures." *American Standard for Testing and Materials*, West Conshohocken, PA, USA.
24. **ASTM, D6931**. (2017). "Standard test method for indirect tensile strength of bituminous mixtures." *American Standard for Testing and Materials*, West Conshohocken, PA, USA.
25. **ASTM, D70**. (2009). "Standard Test Method for Density of Semi-Solid Bituminous Materials (Pycnometer Method)." *American Standard for Testing and Materials*, West Conshohocken, PA, USA.
26. **ASTM, D7460**. (2010). "Determining Fatigue Failure of Compacted Asphalt Concrete Subjected to Repeated Flexural Bending." *American Standard for Testing and Materials*, West Conshohocken, PA, USA.
27. **ASTM, D7870**. (2013). "Standard practice for moisture conditioning compacted asphalt mixture specimens by using hydrostatic pore pressure." *American Standard for Testing and Materials*, West Conshohocken, PA, USA.
28. **ASTM, D7981**. (2015). "Standard Practice for Compaction of Prismatic Asphalt Specimens by Means of the Shear Box Compactor." *American Standard for Testing and Materials*, West Conshohocken, PA, USA.
29. **Bahia, H.,** and **Ahmad, S**. (1999). "Evaluation and correlation of lab and field tensile strength ratio (TSR) procedures and values in assessing the stripping potential of asphalt mixes." *Technical Report: Wisconsin Department of Transportation*, University of Wisconsin, WI/SPR-10-99, Wisconsin, Madison.
30. **Bausano, J.,** and **Williams, R. C**. (2009). "Transitioning from AASHTO T283 to the simple performance test using moisture conditioning." *Journal of materials in civil engineering*, *21*(2), 73-82.
31. **Behiry, A.E.M**. (2012) "Laboratory evaluation of resistance to moisture damage in asphalt mixtures." *Ain Shams Engineering Journal,* 4, 351–363.
32. **Bhasin, A., Castelo Branco, V. T., Masad, E.,** and **Little, D. N**. (2009). "Quantitative comparison of energy methods to characterize fatigue in asphalt materials." *Journal of Materials in Civil Engineering*, *21*(2), 83-92.
33. **Bhasin, A., Little, D. N., Vasconcelos, K. L.,** and **Masad, E**. (2007). "Surface free energy to identify moisture sensitivity of materials for asphalt mixes." *Transportation Research Record: Journal of the Transportation Research Board*, *2001*(1), 37-45.

34. **Bonaquist, R**. (2011). “Mix design practices for warm mix asphalt.”, *Technical Report: Transportation Research Board-National Research Council*, NCHRP Report 691, Washington, D.C., USA.
35. **Boyes, A. J**. (2011). “Reducing moisture damage in asphalt mixes using recycled waste additives.” *Master of Science Thesis*, California Polytechnic State University, California.
36. **Brown, E. R., Kandhal, P. S.,** and **Zhang, J**. (2001). “Performance testing for hot mix asphalt.” *Technical Report*: *National Center for Asphalt Technology*, Auburn University, 01-05, Alabama.
37. **Button, J. W., Estakhri, C. K.,** and **Wimsatt, A. J**. (2007). “A synthesis of warm-mix asphalt.” *Texas Transportation Institute*, Report 5597-1, Texas, USA.
38. **Caputo, P., Abe, A. A., Loise, V., Porto, M., Calandra, P., Angelico, R.,** and **Rossi, C. O.** (2020). "The role of additives in warm mix asphalt technology: an insight into their mechanisms of improving an emerging technology." *Nanomaterials*, 10, 1202.
39. **Caro, A., Masad, E., Bhasin, A.,** and **Little, D. N**. (2008a). “Moisture susceptibility of asphalt mixtures, part 1: mechanisms.” *International Journal of Pavement Engineering*, 9(2), 81-98. https://doi.org/10.1080/10298430701792128
40. **Caro, A., Masad, E., Bhasin, A.,** and **Little, D. N**. (2008b). “Moisture susceptibility of asphalt mixtures, part 2: characterisation and modelling.” *International Journal of Pavement Engineering*, 9(2), 99-114. https://doi.org/10.1080/10298430701792144
41. **Carpenter, S. H., Ghuzlan, K. A.,** and **Shen, S**. (2003). “Fatigue endurance limit for highway and airport pavements.” *Transportation research record*, 1832(1), 131-138.
42. **Chakravarty, H.,** and **Sinha, S**. (2020). “Moisture damage of bituminous pavements and application of nanotechnology in its prevention.” *Journal of Materials in Civil Engineering*, 32(8), 03120003. https://doi.org/10.1061/(ASCE)MT.1943-5533.0003293
43. **Chen, J. S., Lin, K. Y.,** and **Young, S. Y**. (2004). “Effects of crack width and permeability on moisture-induced damage of pavements.” *Journal of Materials in Civil Engineering*, 16(3), 276-282. https://doi.org/10.1061/(ASCE)0899-1561(2004)16:3(276)
44. **Cheng, D., Little, D. N., Lytton, R.,** and **Holste, J. C**. (2003). “Moisture damage evaluation of asphalt mixtures by considering both moisture diffusion and repeated-load conditions.” *Transportation research record*, 1832(1), 42-49, Washington D.C.
45. **Cheng, J., Shen, J.** and **Xiao, F**. (2011). “Moisture susceptibility of warm-mix asphalt mixtures containing nanosized hydrated lime.” *Journal of Materials in Civil Engineering*, 23(11), 1552-1559.

46. **Cho, D. W.,** and **Kim, K**. (2010). "The mechanisms of moisture damage in asphalt pavement by applying chemistry aspects." *KSCE Journal of Civil Engineering*, *14*(3), 333-341.
47. **Das, P. K., Baaj, H., Kringos, N.,** and **Tighe, S**. (2015). "Coupling of oxidative ageing and moisture damage in asphalt mixtures." *Road Materials and Pavement Design*, 16(sup1), 265-279. https://doi.org/10.1080/14680629.2015.1030835
48. **Di Benedetto, H., Ashayer Soltani, A.,** and **Chaverot, P**. (1996). "Fatigue damage for bituminous mixtures: a pertinent approach." *Journal of the Association of Asphalt Paving Technologists*, 65, 142-152.
49. **Di Benedetto, H., De La Roche, C., Baaj, H., Pronk, A.,** and **Lundstrom, R**. (2004). "Fatigue of bituminous mixtures." *Materials and structures*, *37*(3), 202-216.
50. **Dijk, V. W**. (1975). Practical Fatigue Characterization of Bituminous Mixes. Proc., Association of Asphalt Paving Technologists, *Phoenix, Ariz., Vol. 44, Feb. 1975.*
51. **Elsayed, A.,** and **Lindly, J**. (1996). Estimating permeability of untreated roadway bases. *Transportation Research Record: Journal of the Transportation Research Board*, (1519), 11-18.
52. **EN: 12697-24** (2004). "Bituminous Mixtures –Test Methods for Hot Mix Asphalt – Resistance to Fatigue." *European Committee for standardization.*
53. **Epps, J. A.,** and **Monismith, C. L**. (1972). "Fatigue of Asphalt Concrete Mixtures—Summary of Existing Information." *Fatigue of Compacted Bituminous Aggregate Mixtures*, ASTM STP 508, 19-45.
54. **Epps, J. A., Sebaaly, P. E., Penaranda, J., Mather, M. R., McCann, M. B.,** and **Hand, A. J**. (2000). "Compatibility of a test for moisture-induced damage with Superpave volumetric mix design." *National Cooperative Highway Research Program*, Report No. 444, Washington, D.C.
55. **Federal Highway Administration**. (2021). U.S. Department of Transportation, <https://www.fhwa.dot.gov/pavement/asphalt/wma.cfm> (accessed 20 June 2021).
56. **Fitzgibbon, A., Pilu, M.,** and **Fisher, R. B**. (1999). "Direct least square fitting of ellipses." *IEEE Transactions on Pattern Analysis and Machine Intelligence*, 21(5), 476–480. https://doi.org/10.1109/34.765658.
57. **Ghabchi, R., Singh, D., Zaman, M.,** and **Tian, Q**. (2013). "Mechanistic evaluation of the effect of WMA additives on wettability and moisture susceptibility properties of asphalt mixes." *Journal of Testing and Evaluation*, 41(6), 933-942. https://doi.org/10.1520/JTE20120317

58. **Ghuzlan, K.A.** and **Carpenter, S.H**. (2000). "Energy-derived, Damage-Based Failure Criterion for Fatigue Testing." *Transportation Research Record: Journal of the Transportation Research Board*, 1723: 141149.
59. **Grenfell, J., Ahmad, N., Liu, Y., Apeagyei, A., Large, D.,** and **Airey, G**. (2014). "Assessing asphalt mixture moisture susceptibility through intrinsic adhesion, bitumen stripping and mechanical damage." *Road Materials and Pavement Design*, 15(1), 131-152.
60. **Gupta, R.,** and **Narayan, S. P. A.** (2016). "Estimation of viscous and fatigue dissipation of bituminous concrete in repeated loading tests." *Functional Pavement Design: Proceedings of the 4th Chinese-European Workshop*, 319-328, Delft, The Netherlands.
61. **Haggag, M., Mogawer, W.,** and **Bonaquist, R.** (2011). "Fatigue evaluation of warm-mix asphalt mixtures: Use of uniaxial, cyclic, direct tension compression test." *Transportation Research Record: Journal of the Transportation Research Board.*, 2208, 26-32.
62. **Hartman, A. M.,** and **Gilchrist, M. D.** (2004). "Evaluating four-point bend fatigue of asphalt mix using image analysis." *Journal of Materials in Civil Engineering*, 16(1), 60-68.
63. **Hartman, A. M.,** and **Gilchrist, M. D**. (2004). "Evaluating four-point bend fatigue of asphalt mix using image analysis." *Journal of materials in civil engineering*, *16*(1), 60-68.
64. **Harvey, J.,** and **Monismith, C. L**. (1993). "Effects of laboratory asphalt concrete specimen preparation variables on fatigue and permanent deformation test results using strategic highway research program a-003a proposed testing equipment." *Transportation Research Record*, 1417.
65. **Hasan, M. R. M., You, Z., Porter, D.,** and **Goh, S. W**. (2015). "Laboratory moisture susceptibility evaluation of WMA under possible field conditions." *Construction and Building Materials*, 101, 57-64. https://doi.org/10.1016/j.conbuildmat.2015.10.004
66. **Hesami, S., Roshani, H., Hamedi, G.,** and **Azarhoosh, A**. (2013). "Evaluate the mechanism of the effect of hydrated lime on moisture damage of warm mix asphalt." *Construction and Building Materials,* 47, 935–941.
67. **Hicks, R. G., Santucci, L.,** and **Aschenbrener, T**. (2003). "Moisture Sensitivity of Asphalt Pavements: Introduction and Seminar Objectives." *Transportation Research Record: Journal of the Transportation Research Board*, San Diego, California, 3-19.
68. **http://unfccc.int/2860.php**, accessed on February 11, 2017.
69. http://www.eapa.org/promo.php?c=202, accessed on February 11, 2017.
70. **https://pavementinteractive.org**, accessed on February 11, 2017.

71. **Huang, B., Shu, X.,** and **Tang, Y**. (2005b). "Comparison of semi-circular bending and indirect tensile strength tests for HMA mixtures." *Advances in Pavement Engineering*, Geo-Frontiers Congress, 1-12, Texas, United States.
72. **Huang, S. C., Robertson, R. E., Branthaver, J. F.,** and **Claine Petersen, J**. (2005a). "Impact of lime modification of asphalt and freeze–thaw cycling on the asphalt–aggregate interaction and moisture resistance to moisture damage." *Journal of materials in civil engineering*, *17*(6), 711-718.
73. **Hudson, W. R.,** and **Kennedy, T. W**. (1968). "An indirect tensile test for stabilized materials." *A Report of the Centre for Highway Research*, University of Texas, Austin, 98-1.
74. **Hung, A. M., Goodwin, A.,** and **Fini, E. H**. (2017). "Effects of water exposure on bitumen surface microstructure." *Construction and Building Materials*, 135, 682-688. https://doi.org/10.1016/j.conbuildmat.2017.01.002
75. **Hurley, G.C.** and **Prowell, B.D**. (2006). "Evaluation of Evotherm for use in warm mix asphalt." *NCAT Report 06-02*, National Center for Asphalt Technology, Auburn University, Alabama, USA.
76. **IPC Global**. (2011). "Universal testing software 015 - beam fatigue test." *IPC Global*, Victoria, Australia.
77. ***IPC Global***. (2016). "Servo-pneumatic four-point bend apparatus." *IPC Global,* Victoria, Australia.
78. **IRC.** (2009). "Specifications for Dense Graded Bituminous Mixes." *IRC 111,* Indian Roads Congress, New Delhi, India.
79. **IS: 73**. (2013). "Paving bitumen specification." *Bureau of Indian Standards, New Delhi, India*.
80. **Kakar, M. R., Hamzah, M. O., Akhtar, M. N.,** and **Woodward, D.** (2016). "Surface free energy and moisture susceptibility evaluation of asphalt binders modified with surfactant-based chemical additive." *Journal of Cleaner Production*, 112, 2342-2353.
81. **Kakar, M. R., Hamzah, M. O.,** and **Valentin, J**. (2015). "A review on moisture damages of hot and warm mix asphalt and related investigations." *Journal of Cleaner Production*, 99, 39-58. https://doi.org/10.1016/j.jclepro.2015.03.028
82. **Kandhal, P**. (1994). "Field and laboratory investigation of stripping in asphalt pavements: State of the art report." *Transportation Research Record*, 1454, 36-47, Washington, D.C.

83. **Kanitpong, K.** and **Bahia, U. H**. (2003). "Role of adhesion and thin film tackiness of asphalt binders in moisture damage of HMA." *Journal of Association of Asphalt Paving Technologists*, 72, 502- 528.
84. **Kanitpong, K.,** and **Bahia, H. U**. (2007). "Evaluation of HMA moisture damage in Wisconsin as it relates to pavement performance." *International Journal of Pavement Engineering*, *9*(1), 9-17.
85. **Kennedy, T. W.** and **Anagnos. J. N**. (1983). "Procedures for the Static and Repeated-Load Indirect Tensile Test." *Technical Report: Centre for Transportation Research*, University of Texas at Austin, FHWA/TX- 84/19, 183-14, Austin.
86. **Kennedy, T. W., Roberts, F. L., Lee, K. W.,** and **Anagnos, J. N**. (1982). "Texas freeze-thaw pedestal test for evaluating moisture susceptibility for asphalt mixtures." *Technical Report: Center for Transportation Research*, University of Texas at Austin, FHWA/TX-81/47+ 253-3, Austin.
87. **Khodaii, A., Nejad, F. M., Forough, S. A.,** and **Ahari, A, S**. (2013) "Investigating the Effects of Loading Frequency and Temperature on Moisture Sensitivity of SBS Modified Asphalt Mixtures" *Journal of Materials in Civil Engineering*, 1943-5533.
88. **Khosla, N. P., Birdsall, B. G.,** and **Kawaguchi, S**. (2000). "Evaluation of moisture susceptibility of asphalt mixtures: conventional and new methods." *Transportation Research Record*, *1728*(1), 43-51.
89. **Kim, Y. R.** and **Little, D. N**. (1989). "Evaluation of healing in asphalt concrete by means of the theory of nonlinear viscoelasticity." *Transportation Research Record*, 1228, 198-210.
90. **Kim, Y. R., Little, D. N.,** and **Lytton, R. L**. (2003). "Fatigue and healing characterization of asphalt mixtures." *Journal of Materials in Civil Engineering*, *15*(1), 75-83.
91. **Kringos, N**. (2007). "Modelling of combined physical–mechanical moisture-induced damage in asphaltic mixes." PhD dissertation, TU Delft, 2007, ISBN 9789090217659.
92. **Kringos, N.,** and **Scarpas, A**. (2005). "Raveling of asphaltic mixes due to water damage: computational identification of controlling parameters." *Transportation research record: journal of the transportation research board*, (1929), 79-87.
93. **Kringos, N.,** and **Scarpas, A**. (2008). "Physical and mechanical moisture susceptibility of asphaltic mixtures." *International Journal of Solids and Structures*, *45*(9), 2671-2685.
94. **Kringos, N., Azari, H.,** and **Scarpas. A**. (2009). "Identification of Parameters Related to Moisture Conditioning That Cause Variability in Modified Lottman Test." *Transportation*

Research Record: Journal of the Transportation Research Board, Transportation Research Board of the National Academies, 2127, 1-11, Washington, D.C.

95. **Kringos, N., Scarpas, A., Copeland, A.,** and **Youtcheff, J**. (2008b). "Modelling of combined physical-mechanical moisture-induced damage in asphaltic mixes, part-2: moisture susceptibility parameters." *International Journal of Pavement Engineering*, 9(2), 129-151. https://doi.org/10.1080/10298430701792227
96. **Kringos, N., Scarpas, T., Kasbergen, C.,** and **Selvadurai, P**. (2008a). "Modelling of combined physical-mechanical moisture-induced damage in asphaltic mixes, part-1: governing processes and formulations." *International Journal of Pavement Engineering*, 9(2), 115-128. https://doi.org/10.1080/10298430701792185
97. **Krishnan, J. M.** and **A. Veeraragavan**. (2016). "Development of warrants for modified binders." *Technical report: Interim report submitted to DST*, Government of India, IIT Madras.
98. **Krishnan, J. M.,** and **Rao, C. L**. (2000). "Mechanics of air voids reduction of asphalt concrete using mixture theory." *International Journal of Engineering Science*, *38*(12), 1331-1354.
99. **Krishnan, J. M.,** and **Rao, C. L**. (2001). "Permeability and bleeding of asphalt concrete using mixture theory." *International Journal of Engineering Science*, 39(6), 611-627. https://doi.org/10.1016/S0020-7225(00)00064-1
100. **Kuang, Y**. (2012). "Evaluation of Evotherm as a WMA technology compaction and anti-strip additive." *Graduate Theses and Dissertations*, 12370, Iowa State University, Ames, Iowa, USA.
101. **Lesueur, D.,** and **Little, D. N**. (1999). "Effect of hydrated lime on rheology, fracture, and aging of bitumen." *Transportation Research Record: Journal of the Transportation Research Board*, 1661, 93-105.
102. **Lesueur, D., Petit, J.,** and **Ritter, H**. (2013). "The mechanisms of hydrated lime modification of asphalt mixtures: a state-of-the-art review." *Road Materials and Pavement Design*, 14(1), 1-16. https://doi.org/10.1080/14680629.2012.743669
103. **Li, X., Wang, H., Zhang, C., Diab, A.,** and **You, Z.** (2016). "Characteristics of a surfactant produced warm mix asphalt binder and workability of the mixture." *Journal of Testing and Evaluation*, 6, 2219-2230.
104. **Lippert, D L., Sholar, G. A.,** and **Williams, A. A**. (2015). "State department of transportation moisture damage roundtable." *Transportation Research Record: Journal of*

the Transportation Research Board, Synopsis of a workshop, Transportation Research Circular, E-C198, Washington, D.C.

105. **Little, D. N.,** and **Jones, D. J**. (2003). "Moisture sensitivity of asphalt pavements: chemical and mechanical processes of moisture damage in hot-mix asphalt pavements." *Transportation Research Record: Journal of the Transportation Research Board*, 37 – 74, Washington, D.C.

106. **Little, D. N.,** and **Jones, D. R**. (2004). "Moisture sensitivity of asphalt pavements: Chemical and Mechanical Processes of Moisture Damage in Hot-Mix Asphalt Pavements", *Transportation Research Record: Journal of the Transportation Research Board*, 37 – 74, Washington, D.C.

107. **Little, D. N.,** and **Petersen, J. C**. (2005). "Unique effects of hydrated lime filler on the performance-related properties of asphalt cements: Physical and chemical interactions revisited." *Journal of Materials in Civil Engineering*, 17(2), 207-218. https://dx.doi.org/10.1061/(ASCE)0899-1561(2005)17:2(207)

108. **Little, D. N., Epps, J. A.,** and **Sebaaly, P. E**. (2006). "The benefits of hydrated lime in hot mix asphalt." *Technical Report: National Lime Association*, University of Nevada, Reno.

109. ***Lottman, R. P**. (1971). "*The moisture mechanism that causes asphalt stripping in asphaltic pavement mixtures*." Technical Report:* Engineering Experimental Station*, Final Report R-47, University of Idaho, Moscow.*

110. **Lottman, R. P**. (1978). "Predicting Moisture-Inducted Damage to Asphaltic Concrete." *Technical Report: Transportation Research Board-National Research Council*, NCHRP Report 192, Washington, DC.

111. **Lottman, R. P**. (1982). *"Laboratory test method for Predicting moisture-induced damage to asphalt concrete." Transportation Research Record*, *843, 88-95.*

112. **Lu, Q.,** and **Harvey, J. T**. (2006). "Evaluation of moisture sensitivity of hot mix asphalt by flexural beam fatigue test." *Asphalt Concrete: Simulation, Modeling, and Experimental Characterization*, R. Lytton Symposium on Mechanics of Flexible Pavements, 124-133, Louisiana, US.

113. **Lu, Q.,** and **Harvey, J. T**. (2008). "Inclusion of moisture effect in fatigue test for asphalt pavements." *Transportation and Development Innovative Best Practices,* 498-504.

114. **Luo, R., Huang, T., Zhang, D.,** and **Lytton, R. L**. (2017). "Water vapour diffusion in asphalt mixtures under different relative humidity differentials." *Construction and Building Materials*, 136, 126-138. https://doi.org/10.1016/j.conbuildmat.2017.01.034

115. **Mallick, R. B., Gould, J. S., Bhattacharjee, S., Regimand, A., James, L. H.,** and **Brown, E. R**. (2003). "Development of a rational procedure for evaluation of moisture susceptibility of asphalt paving mixes." *Transportation Research Record: Journal of the Transportation Research Board*, Washington, DC.

116. **Masad, E., Castelblanco, A.,** and **Birgisson, B**. (2006a). "Effects of air void size distribution, pore pressure, and bond energy on moisture damage." *Journal of Testing and Evaluation*, 34(1), 15-23. https://doi.org/10.1520/JTE13112

117. **Masad, E., Zollinger, C., Bulut, R., Little, D.,** and **Lytton, R**. (2006b). "Characterization of HMA moisture damage using surface energy and fracture properties." *Asphalt Paving Technology: Association of Asphalt Technologists-Proceedings of the Technical Sessions*, 75, 713-754.

118. **MATLAB** (2018). Version 9.4.0.813654 (R2018a).

119. **Matthews, J. M., Monismith, C. L.,** and **Craus, J**. (1993). "Investigation of laboratory fatigue testing procedures for asphalt aggregate mixtures." *Journal of Transportation Engineering*, *119*(4), 634-654.

120. **Monismith, C. L**. (1970). "Influence of shape, size, and surface texture on the stiffness and fatigue response of asphalt mixtures." *Highway Research Board*, 109, Columbia, United States.

121. **Morea, F., Marcozzi, R.,** and **Castano, G.** (2012). "Rheological properties of asphalt binders with chemical tensoactive additives used in warm mix asphalts (WMAs)." *Construction and Building Materials*, 29, 135-141.

122. **MoRTH**. (2013). "Specification for Road & Bridge Works", *Indian Roads Congress*, *New Delhi, India.*

123. **Pereira, R., Almeida-Costa, A., Duarte, C.,** and **Benta, A.** (2018). "Warm mix asphalt: chemical additives' effects on bitumen properties and limestone aggregates mixture compactibility." *International Journal of Pavement Research and Technology*, 11, 285-299.

124. **Pinkham, R. E., Cote, S. A., Mallick, R. B., Tao, M., Bradbury, R. L.,** and **Regimand, A**. (2012). "Use of moisture induced stress testing to evaluate stripping potential of hot mix asphalt (HMA)." *Technical Report*: *Maine Department of Transportation*, Worcester Polytechnic Institute, ME 12-08, Augusta, Maine.

125. **Prowell, B. D., Hurley, G. C.,** and **Crews, E**. (2007). "Field performance of warm-mix asphalt at national center for asphalt technology test track." *Transportation Research*

Record: Journal of the Transportation Research Board, 1998, 96-102. https://doi.org/10.3141/1998-12

126. **Rasouli, A., Kavussi, A., Jalili, M.,** and **Hossein, A**. (2018). "Evaluating the effect of laboratory aging on fatigue behavior of asphalt mixtures containing hydrated lime." *Construction and Building Materials*, 164, 655–662.

127. **Roja, K. L.,** and **Krishnan, J. M.** (2016). "Use of dissipated energy to quantify fatigue life of warm mix asphalt." *Functional Pavement Design: Proceedings of the 4th Chinese-European Workshop,* 239-247, Delft, The Netherlands.

128. **Roja, K. L.,** and **Krishnan, J. M**. (2016). "Use of Dissipated Energy to Quantify Fatigue Life of Warm Mix Asphalt." *Functional Pavement Design: Proceedings of the 4th Chinese-European Workshop,* 239-247, Delft, The Netherlands.

129. **Rowe, G. M.,** and **Bouldin, M. G**. (2000). *"*Improved techniques to evaluate the fatigue resistance of asphaltic mixtures*." 2nd Eurasphalt and Eurobitume Congress*, *Barcelona, Spain, 754–763.*

130. **Sanchez-Alonso, E., Vega-Zamanillo, A., Castro-Fresno, D.,** and **DelRio-Prat, M**. (2011). "Evaluation of compactability and mechanical properties of bituminous mixes with warm additives." *Construction and Building Materials*, 25, 2304-2311. https://doi.org/10.1016/ j.conbuildmat.2010.11.024

131. **Sasaki, I., Moriyoshi, A.,** and **Hachiya, Y**. (2006). "Water/gas permeability of bituminous mixtures and involvement in blistering phenomenon." *Journal of the Japan Petroleum Institute*,49(2), 57-64. https://doi.org/10.1627/jpi.49.57

132. **Sebaaly, P. E., Hajj, E. Y.,** and **Piratheepan, M**. (2015). "Evaluation of selected warm mix asphalt technologies." *Road Materials and Pavement Design*, 16(sup1), 475-486. https://doi.org/10.1080/14680629.2015.1030825

133. **Shatnawi, S., Nagarajaiah, M.,** and **Harvey, J**. (1995). "Moisture sensitivity evaluation of binder-aggregate mixtures." *Transportation research record*, *1492*, 71.

134. **Silva, H. M., J. R. Oliveira, J. Peralta,** and **S. E. Zoorob.** (2010). "Optimization of warm mix asphalts using different blends of binders and synthetic paraffin wax contents." *Construction and Building Materials*, 24 (9): 1621–1631.

135. **Soenen, H., Vansteenkiste, S.,** and **Maeijer, P. K. D**. (2020). "Fundamental approaches to predict moisture damage in asphalt mixtures: state-of-the-art review." *Infrastructures*, 5(2), 20. https://doi.org/10.3390/infrastructures5020020

136. **Solaimanian, M., Harvey, J., Tahmoressi, M.,** and **Tandon. V**. (2003). "Moisture Sensitivity of Asphalt Pavements: Test Methods to Predict Moisture Sensitivity of Hot-Mix

Asphalt Pavement." *Transportation Research Record: Journal of the Transportation Research Board*, 76-113, Washington, D.C.

137. **Solaimanian, M., Kennedy, T. W.,** and **Elmore, W. E**. (1993). "Long-term evaluation of stripping and moisture damage in asphalt pavements treated with lime and antistripping agents." *Technical Report: Center for Transportation Research*, Bureau of Engineering Research, FHWA/TX-94+1286-1F, University of Texas, Austin.

138. **Stuart, K., D**. (1990). "Moisture Damage in Asphalt Mixtures- A State-of-the-Art Report." *Transportation Research Record: Journal of the Transportation Research Board*, FHWA/RD-90-019, McLean, Virginia.

139. **Tangella, S. C. S. R., Craus, J., Deacon, J. A.,** and **Monismith, C. L. (1990).** "Summary report on fatigue response of asphalt mixtures." *TM-UCB-A-003A-89-3*, Institute of Transportation Studies, University of California, Berkeley, California, USA.

140. **Tarefder, R. A.,** and **Zaman, A. M**. (2009). "Nanoscale evaluation of moisture damage in polymer modified asphalts." *Journal of Materials in Civil Engineering*, *22*(7), 714-725.

141. **Tarefder, R.,** and **Ahmad, M**. (2015a). "Evaluating the relationship between permeability and moisture damage of asphalt concrete pavements." *Journal of Materials in Civil Engineering*, *27*(5), 04014172.

142. **Tarefder, R.,** and **Ahmad, M**. (2015b). "Evaluation of pore structure and its influence on permeability and moisture damage in asphalt concrete." *International Journal of Pavement Engineering*, 1–10.

143. **Tayebali, A. A., Rowe, G. M.,** and **Sousa, J. B**. (1992). "Fatigue response of asphalt-aggregate mixtures." *Journal of the Association of Asphalt Paving Technologists*, 61, 333-360.

144. **Taylor, M. A.,** and **Khosla, N. P**. (1983). "Stripping of asphalt pavements: State of the art." *Transportation Research Record*, 911, 150-158.

145. **Terrel, R. L.,** and **Al-Swaili, S**. (1994). "Water sensitivity of asphalt-aggregate mixes: test selection." *Technical Report*: *Strategic Highway Research Program*, National Research Council, SHRP-A-403, Washington, DC.

146. **Terrel, R. L.,** and **Saleh, A**., (1994). "Water sensitivity of asphalt-aggregate mixes: test selection." *Strategic Highway Research Program*, A-403, Washington, DC.

147. **Terrel, R.L.** and **J.W. Shute**. (1989). "Summary Report on Water Sensitivity." *Technical Report*: *Strategic Highway Research Program*, Oregon State University, SHRP-AIR-003, Corvallis, Oregon.

148. **Thaulow, S**., (1957). "Tensile Splitting Test and High Strength Concrete Test Cylinders." *Journal of the American Concrete Institute*, 28(7), 699-705.

149. **Vargas-Nordcbeck, A., Leiva-Villacorta, F., Aguiar-Moya, J. P.,** and **Loria-Salazar, L**. (2016). "Evaluating moisture susceptibility of asphalt concrete mixtures through simple performance tests." *Transportation Research Record*, 2575(1), 70-78.

150. **Varma, R. K., Narayan, S. P. A.,** and **Krishnan, J. M.** (2019). "Quantification of viscous and fatigue dissipation of asphalt concrete in four-point bending tests." *Journal of Materials in Civil Engineering*, 31(12), 04019285.

151. **Varma, R. K., Narayan, S. P. A.,** and **Krishnan, J. M**. (2019). "Quantification of viscous and fatigue dissipation of asphalt concrete in four-point bending tests." *Journal of Materials in Civil Engineering*, 31(12), 04019285. https://doi.org/10.1061/(ASCE)MT.1943-5533.0002938

152. **Varma, R. K., Padmarekha, A., Ravindran, P., Bahia, H. U.,** and **Krishnan, J. M**. (2017). "Evolution of energy dissipation during four-point bending of bituminous mixtures." *Road Materials and Pavement Design*, 18(sup2), 252-263. https://doi.org/10.1080/14680%20629.2017.1304252

153. **Varveri, A., Avgerinopoulos, S., Scarpas, A., Collop, A.,** and **Erkens, S**. (2014). "On the combined effect of moisture diffusion and cyclic pore pressure generation in asphalt concrete." *Transportation Research Record: Journal of the Transportation Research Board*, Washington, DC.

154. **Vasconcelos, K. L., Bhasin, A.,** and **Little, D. N**. (2010). "Measurement of water diffusion in asphalt binders using Fourier transform infrared-attenuated total reflectance." *Transportation Research Record: Journal of the Transportation Research Board*, 2179, 29-38. https://doi.org/10.3141/2179-04

155. **Vasconcelos, K. L., Bhasin, A., Little, D. N.,** and **Lytton, R. L**. (2011). "Experimental measurement of water diffusion through fine aggregate mixtures." *Journal of Materials in Civil Engineering*, 23(4), 445-452. https://doi.org/10.1061/(ASCE)MT.1943-5533.0000190

156. **West, R. C., Zhang, J.,** and **Cooley, A**. (2004). "Evaluation of the asphalt pavement analyzer for moisture sensitivity testing." *NCAT Report 04-04*, National Center for Asphalt Technology, Auburn University, Alabama, USA.

157. **Xiao, F., Jordan, J.,** and **Amirkhanian, S. N**. (2009). "Laboratory investigation of moisture damage in warm-mix asphalt containing moist aggregate." *Transportation*

Research Record: Journal of the Transportation Research Board, 2126, 115-124. https://doi.org/ 10.3141/2126-14

158. **Xiao, F., S. N. Amirkhanian, M. Karakouzian,** and **M. Khalili**. (2015). "Rheology evaluations of WMA binders using ultraviolet and PAV aging procedures." *Construction and Building Materials*, 79 (15): 56–64.

159. **Yang, B., Xu, H., Zhou, P.,** and **Tan, Y**. (2020). "Investigation of aggregate moisture content variation and its impact on pavement performance of WMA." *Construction and Building Materials*, 255, 119350. https://doi.org/10.1016/j.conbuildmat.2020.119350

160. **Yilmaz, A.,** and **Sargin, S**. (2012). "Water effect on deteriorations of asphalt pavements." *Journal of Science and Technology*, 2(1), 1-6.

161. **Yin, F., West, R. C., Director, P. E., Xie, Z., Taylor, A.,** and **Julian, G**. (2017). "Effects of loading rate and mix reheating on indirect tensile nflex factor and semi-circular bend j-integral test results to assess the cracking resistance of asphalt mixtures." *NCAT Report 17-09*, National Center for Asphalt Technology, Auburn University, Alabama, USA.

LIST OF PUBLICATIONS

1. **Vishal, U.**, and Chowdary, V. (2018). "Moisture conditioning process for large-sized prismatic straight beam specimens of bituminous concrete." *International Journal of Engineering and Advanced Technology*, 8(2C), 117-122.
2. **Vishal, U.**, Chowdary, V., Padmarekha, A., and Krishnan, J. M. (2020). "Influence of moisture damage on fatigue of warm mix and hot mix asphalt mixture." *Journal of Materials in Civil Engineering*, 32(9), 04020247. https://doi.org/10.1061/(ASCE)MT.2019420320-5%20533.0003321
3. **Vishal, U.**, Padmarekha, A., Chowdary, V., and Krishnan, J. M. (2021). "Effect of moisture on viscoelastic dissipation and dissipation due to damage in warm mix asphalt." Materials and Structures. (Under Review).